The University of Southern Queensland

USING A REMOTELY CONTROLLED PLATFORM TO ACQUIRE LOW-ALTITUDE IMAGERY FOR GRAIN CROP MAPPING

A Dissertation submitted by

Troy Arnold Jensen

B.Eng (DDIAE)
M.Eng (USQ)

For the award

Doctor of Philosophy

November 2008

Dedication

To my Mother, the motivation behind my education

Abstract

Agricultural crops exhibit within-field spatial variation. This variation partly results from relevant bio-physical and environmental factors that influence the crop during the growing season. The plant integrates the effects of nutrition, water, pests and disease, and displays the results in the foliage. Remote sensing techniques allow the foliage to be monitored and the crop status to be assessed.

While the use of conventional remote sensing systems has found many applications in agriculture, it is constrained by a number of issues and problems related to spatial resolution, repeat cycle, minimum area acquired, timeliness of data, etc. Thus, this research explores the potential of developing and assessing low-cost sensing technologies to overcome these limitations. The specific objectives were to: a) identify, evaluate, and analyse the different options for a low-cost low-altitude (LCLA) remote sensing system that has potential for precision agriculture, b) develop a LCLA remote sensing system that is appropriate for use in mapping selected crop attributes (i.e. grain protein, yield, maturity and crop type), and c) evaluate the accuracy of classification and prediction of the cereal crop attributes.

A low-cost sensor system was developed that incorporated two consumer digital still cameras. One camera captured the colour portion of the spectrum, while the other one (with the addition of a band-pass filter) captured the near infrared light. Both cameras were modified to be remotely triggered and externally powered. This sensor arrangement utilised 1.0 megapixel cameras in the earlier investigations and then 5.0 megapixel cameras in most recent missions. The sensors were equally well suited to mounting on a remotely controlled aircraft or suspended beneath a helium balloon.

Various approaches were taken to determine and evaluate the relationships between imagery and crop attributes. Statistical methods included the use of correlation and discriminant function analysis, along with partial least squares regression. Image analysis techniques included the use of both pixel-based (supervised approach) and object-orientated (multi-resolution segmentation) classifications.

The results showed that low-cost low-altitude remote sensing systems (incorporating consumer digital cameras with helium balloons or remotely controlled aircraft) have great capacity to quantify variability in cereal grain crops. Excellent relationships were found between the 'at-harvest' yield (R^2=0.902) and protein content (R^2=0.660) of wheat using a single image recorded at flowering. Partial least squares regression, using the cross-validated approach, produced a stronger relationship with a prediction accuracy of 94.2% for yield and 88.5% for protein. This relationship exceeded all other studies reported in the literature.

The same LCLA system has also accurately discriminated (using statistical methods) between: a) different nutrition levels in a wheat crop with 75.6% of the cases correctly classified, and b) between different cereal grain species (with differing nutrition levels) with 86.3% accuracy. These classification accuracies are comparable with, or exceeding other more expensive and/or complicated methods. Attempting to discriminate using image analysis procedures, the pixel-based methods yielded an overall accuracy of 65.9% when classifying cereal grain crop species comprising of nine classes. When merged to six classes, the accuracy improved to 82.1%. Using an object-orientated approach has improved the overall accuracy to 81.0% for the nine-category classification. This study also demonstrated LCLA's ability to assess the various growth stages of a barley crop prior to maturity with 83.5% of cases correctly classified.

This study concluded that it is feasible to accurately assess selected cereal grain crop attributes using low-cost consumer technologies. The accuracies achieved using this system were comparable with, or exceeded, other reported studies that used more complicated and expensive sampling systems. Further work is needed to continue refining the initial work on a fully autonomous unmanned aerial vehicle (UAV) started in the later part of this study, to extend the use of the LCLA system into broader scale applications.

Certification of Dissertation

I certify that the ideas, experimental work, results, analyses, software and conclusions reported in this dissertation are entirely my own effort, except where otherwise acknowledged. I also certify that the work is original and has not been previously submitted for any other award, except where otherwise acknowledged.

Signature of Candidate   Date

ENSORSEMENT

Signature of Supervisor   Date

Publications

Published International Journal

Jensen, TA, Apan, A, Young, F & Zeller, LC 2007, 'Detecting the attributes of a wheat crop using digital imagery acquired from a low-altitude platform', *Computers and Electronics in Agriculture*, vol. 59, no. 1-2, pp. 66-77.

Published Conference Proceedings

Hussain, A, Raine, SR, Henderson, CW & Jensen, TA 2008, 'Evaluation of a proximal vision data acquisition system for measuring spatial variability in lettuce growth', paper presented to Global Issues, Paddock Action - 14th Australian Agronomy Conference, Adelaide, Australia, 21-25 September 2008.

Jensen, TA, Apan, A, Young, F & Zeller, L 2005, 'Grain Crop Attributes Detected Using Digital Imagery Acquired from a Low-Altitude Helium balloon', paper presented to 5th European Conference on Precision Agriculture, Uppsala Sweden, 9-12 June 2005.

Jensen, TA 2004, 'Remote sensing – an innovative balloon platform', paper presented to 8th Annual Symposium on Precision Agriculture Research & Applications in Australasia, Sydney, Australia, 20 August 2004.

Jensen, TA, Apan, A, Young, F, Zeller, LC & Cleminson, K 2003, 'Assessing grain crop attributes using digital imagery acquired from a low-altitude remote controlled aircraft', paper presented to First Spatial Sciences Conference, Canberra, Australia, 22-27 September 2003.

Jensen, TA, Apan, A, Young, F & Zeller, LC 2002, 'Capturing of remotely sensed images to advance the use of yield maps and other spatial information to improve crop management and forecasting.' paper presented to 11th Australasian Remote Sensing and Photogrammetry Conference, Brisbane, Australia, 2-6 September 2002.

Popular Press

Alcorn, G 2004, 'The balloon goes up on crop monitoring', *Australian Grain*, vol. 14, no. 1, pp. 48-9.

Jensen, TA & Apan, A 2003, 'Small planes big plans', *Position Magazine*, vol. 7, pp. 75-67.

Acknowledgements

I thank my principal supervisor Associate Professor Armando Apan for his infinite wisdom, direction and motivation throughout this work. My associate supervisor, Associate Professor Frank Young, also provided valuable comments and suggestions.

Les Zeller has provided friendship, motivation, electronic skills, assistance in data collection and was also a great sounding board for ideas.

Ken Cleminson provided advice on things remotely controlled and access to his planes, as well as flying them, during the early development stages of this project.

Dr. Wayne Strong expounded his infinite agronomic wisdom to me when I needed assistance.

Ross and Jordie Milne kindly provided access to their plane, as well as in flying the craft in the later stages of the project.

To the ARCAA team from QUT for the use of their autonomous UAV during the final testing of my concept, my thanks.

My appreciation to the now defunct DPI&F Precision Agriculture team for the access to datasets and funds for this work that ran in parallel to their GRDC-funded projects.

Finally, to my wife Leath and children Xanthea, Lucinda and Harry who have been very patient and tolerant whilst I have been in the final stages of this thesis. I am sure they are looking forward to having a father and husband back with them again.

Table of Contents

List of Figures

List of Tables

Abbreviations

AGL .... Above ground level
AMSA .... Australian Maritime Safety Authority
ANOVA................. Analysis of variance
AOI .... Area-of-interest
ARCAA................. Australian Research Centre for Aerospace Automation
ASTER .... Advanced Spaceborne Thermal Emission and Reflectance Radiometer
B .... Blue
BSD .... Best separation distance
CASA.................... Civil Aviation Safety Authority
CCD...................... Charged couple device
CF......................... CompactFlash
CIR .... Colour infrared
CMOS................... Complementary metal–oxide semiconductor
DA .... Discriminant function analysis
DAS .... Days after sowing
DC .... Direct current
DGPS .... Differential GPS
DN .... Digital number
DPI&F................... Department of Primary Industries and Fisheries (Queensland)
DVI .... Difference Vegetation Index
G........................... Green
GCP...................... Ground control point
GIS .... Geographic information system
GLCM .... Grey level co-occurrence matrix
GNDVI .... Green Normalised Difference Vegetation Index
GPS...................... Global positioning system
GRDC................... Grains Research and Development Corporation
JPEG.................... Joint Photographic Experts Group
LCLA .... Low-cost low-altitude
LED .... Light emitting diode
ML .... Maximum likelihood
NASA.................... National Aeronautics and Space Administration
NDVI..................... Normalised Difference Vegetation Index
NiMH .... Nickel-metal hydride
NIR .... Near infrared
NIRB..................... Near infrared detected with the blue sensor
NIRG .... Near infrared detected with the green sensor

NIRR..................... Near infrared detected with the red sensor

NOTAM .... Notice to airmen

PA......................... Precision agriculture

PCI .... Peripheral component interconnect

PCMCIA .... Personal Computer Memory Card International Association

PLS....................... Partial least squares

PPR .... Plant pigment ratio

PSRI .... Plant Senescence Vegetation Index

QUT...................... Queensland University of Technology

R........................... Red

RCA...................... Remotely controlled aircraft

RGB...................... Red-green-blue

RMS .... Root mean squared

RMSEP................. Root mean squared error of prediction

RTK .... Real-time kinematic

RVI .... Red Ratio Vegetation Index

SIPI....................... Structure insensitive pigment index

SLR .... Single lens reflex

SSCM .... Site-specific crop management

TARMAC .... Toowoomba Amateur Radio Model Club

TM .... Thematic mapper

UAV .... Unmanned aerial vehicle

UQG .... University of Queensland Gatton

US .... United States

USQ...................... University of Southern Queensland

UV .... Ultra violet

VRT .... Variable rate-application technology

VMC .... Visual meteorological conditions

Chapter 1

Introduction

1.1 Background

The ability to measure yield (tonnes / hectare), and more recently the quality (% protein), of cereal crops has lead to an increased understanding of the causes of the spatial variations within a production unit (Jensen *et al.* 2001a). The main drawback of the current technology is that the quantity and quality information, being obtained as the crop is harvested, can only be used retrospectively, and thus cannot be used to rectify deficiencies encountered during the growing season or plan niche harvesting strategies for consistent quality segregation.

If the crop is the best indicator of its own environment (Legg & Stafford 1998), then a "*sensing system that can tap into what the crop is 'saying'*" (Stafford 2000, p. 270) will aid in the understanding of the variability within the cropping system. "*Remotely sensed images…can provide information about crop growth and spatial variations within fields*" (NRC 1997, p. 37) and these images can show the spatial and spectral variations (at the time the images were captured) resulting from soil and crop characteristics.

Remote sensing has been described as "*the practice of deriving information using images acquired from an overhead perspective, using electromagnetic radiation that is emitted or reflected from the earth's surface*" (Campbell 2002, p. 6). Remotely sensed multispectral imagery can significantly improve the quality and reduce the cost, of site characterisation and monitoring (Wright *et al.* 2003). Such remotely sensed images can be sourced from satellite, aerial and ground based platforms.

Considerable research has been conducted using satellite imagery to observe cropping areas. Such research includes matching multi-temporal yield and image data (Layrol *et al.* 2000), predicting wheat grain yield and protein content (Liu *et al.* 2006), spectral discrimination and separability analysis using ASTER imagery (Apan *et al.* 2002), and leaf area index estimations using Landsat TM (Price & Bausch 1995). Despite the advantages, satellite remote sensing has well known limitations including timeliness, cloud cover, cost, poor spatial resolution (Zhang *et al.* 2002) and a fixed schedule of coverage that may not allow specific events to be captured (Wright *et al.* 2003). The usefulness of satellite data is further limited when evaluating small areas of interest and small objects.

One of the oldest and most widely applied forms of remote sensing are images captured from aerial platforms (Wright *et al.* 2003). Examples of research conducted using aerial imagery to evaluate cropping systems include the following: monitoring growth and identifying crop stress in kenaf (Cook *et al.* 1999); investigating crop stress in cotton (Roth 1993) and peanuts (Wright & Mills 2002); and predicting grain yield (Staggenborg & Taylor 2000) and cotton lint yield (Vellidis *et al.* 2004). Airborne sensors offer much greater flexibility than satellite platforms by being able to operate under clouds and having a much finer spatial resolution (Lamb & Brown 2001). When the area imaged per flight is large, the cost per hectare is relatively inexpensive (Godwin *et al.* 2003a). Conversely, when the area imaged per flight is small, the cost increases dramatically. Aerial imagery is still costly when dedicated ‘mobilisation’ of the aircraft is required, especially for remote localities and repeated data acquisition needs.

Alternatively, cameras mounted on an unmanned aerial platform have greater utility with the potential to provide cheaper and repetitive information. This will enable farmers to make improved in-season management decisions about their crop, particularly for small areas.

1.2 Research Problem and its Significance

The recent ability to measure quantity (yield), and more recently, quality (protein) parameters of cereal crops, has sparked interests in determining the causes for variations within a production unit. Knowledge of within-field spatial variability, be it due to nutrition, soil moisture, compaction or pestilence, will allow better crop management to maximise financial returns and in promoting sound environmental practices. However, the main drawback of this yield and protein monitoring technology is that the quantity and quality information is only available as the crop is being harvested or afterwards, and cannot be applied to rectify deficiencies encountered during the growing season of the crop. Hence, this information can only be used retrospectively, and / or to aid with management planning for future crops.

Remotely sensed images have the potential to detect and map variations in crop condition. However, commercially available remote sensing platforms are often limited by their spatial, temporal and spectral resolutions, and the cost of the imagery is a major concern when dealing with small production areas. Thus, there is a need for a system that has the ability to frequently capture images, has high spatial resolution, and covers the spectral range under investigation. The system should also be cost-effective. An unmanned aerial platform with a suitable sensor could provide the needed management information in a timely fashion, as well as satisfying the technical (spatial, temporal and spectral) and costing criteria. The research conducted in this thesis investigated that possibility.

1.3 Research Objectives

The goal of this research was to investigate the potential of detecting variations within a growing crop with imagery acquired by a low-cost unmanned aerial platform.

To achieve this goal, the research formed the hypothesis: *" 'Off-the-shelf' consumer camera technologies and low-cost low-altitude platforms can provide selected sets of information appropriate for use in precision agriculture."*

This hypothesis was tested by addressing the following specific objectives:

1. To identify, evaluate and analyse the different options for a low-cost low-altitude (LCLA) remote sensing system that has potential for precision agriculture;
2. To develop a LCLA remote sensing system that is appropriate for use in mapping selected crop attributes; and
3. To evaluate the accuracy of classification and prediction of cereal crop attributes (protein, yield, maturity and crop type) using the LCLA remote sensing system.

1.4 Context, Scope and Delimitation of the Study

The work detailed in this thesis ran in parallel with three research projects conducted by the Department of Primary Industries and Fisheries (DPI&F) Queensland, Australia for the Grains Research and Development Corporation (GRDC) from 1998-2006. These three projects were:

- DAQ434 "*Strategies to apply yield maps to identify and correct yield limiting factors for northern cereal crops*";
- DAQ 528 "*Predicting grain quality with yield and protein maps and remotely sensed imagery*"; and
- DAQ00067 "*Eye in the sky to revolutionise northern crop production*".

The purpose of these three projects were to interpret site-specific information (yield maps) by developing strategies that would systematically identify production-limiting factors as probable causes for observed variation in grain yield. During the implementation of these projects, it became obvious that monitoring crop yield provides only part of the agronomic story for grain crops. The understanding would be greatly enhanced if the grain quality, with protein being the primary measure, of the crop being harvested was considered. Mapping these two features (i.e. yield and protein) of a cereal crop enables inferences to be drawn regarding two of the most common production-limiting factors for Australian wheat / barley crops: namely water and nitrogen supply.

Satellite and aerial images capture site-specific information that could similarly enhance crop management, provided that the spectral information is closely correlated with crop yield or grain protein or both. With the capability to monitor grain protein at harvest still under development, it was hoped that spectral data from remotely sensed images could provide the means of identifying areas in cereal crops of high and / or low grain protein. This ability to identify differing areas would be invaluable for harvesting selected areas of similar grain protein. As premiums are paid for the higher protein contents in wheat and for the lower protein contents in barley, the return from a crop could be maximised through segregation.

An equally valuable use for this information would be improved forecasting of grain classification for marketing advantage. These prospective applications of remotely sensed imagery enable information to be used predictively (before harvesting) rather than retrospectively (after harvesting), as is the case with the interpretation of yield maps.

Conventional aerial and satellite imagery had limitations (especially in the northern region of Australia) that became evident during the course of the above mentioned three projects. Being in control of a system that was low-cost, portable, easy to deploy and able to be utilised on a regular basis, was attractive and prompted the research and development that constitutes this thesis.

During the development of the low-cost low-altitude remote sensing system, it became evident that the system had application to more than just protein and yield investigations. The system was evaluated over many and varied data collection missions. These included: spatial variability assessments in pineapple crops, quantifying the areas of high moisture content in a cattle feedlot, checking irrigation uniformity and growth rates in a cotton and lettuce crop and looking at the wear patterns and turf growth on football fields. This thesis, however, concentrated on the application of low-cost low-altitude remotely sensed imagery to cereal crop production. In addition to yield and protein investigations, crop type and maturity discrimination were also evaluated as part of this thesis.

1.5 Organisation of the Thesis

This thesis is organised into seven chapters and this is represented schematically in Figure 1.1.

The *First Chapter* presents the background to the research and development that was carried out as part of this thesis and also poses the research problem and sets out the objectives.

The *Second Chapter* reviews the two areas of knowledge that are pertinent to this study: remote sensing and precision agriculture. The use of spatial data layers in precision agriculture is discussed along with the potential of remote sensing to provide additional in-crop information to aid in management decisions. Existing remote sensing systems and their uses are reviewed. Furthermore, digital imaging technologies and their applicability to low-cost remote sensing systems are investigated.

Chapter Three describes the preliminary investigations that were conducted to evaluate the various components that would be required of a low-cost low-altitude (LCLA) remote sensing system. These investigations covered both the selection of the platform and the sensor system.

Chapter Four and *Chapter Five* cover the development of the LCLA system and the steps taken to collect real-world data using the system. Crop mapping investigations were carried out to map grain yield, protein and crop maturity, and to discriminate between various cereal crop types.

The *Sixth Chapter* covers the various statistical, image analysis and geographic information system based assessments that were undertaken to quantify the performance of the LCLA remote sensing system and how well it compares to existing technologies and techniques. Lastly, the *Final Chapter* covers the conclusions and recommendations for future work.

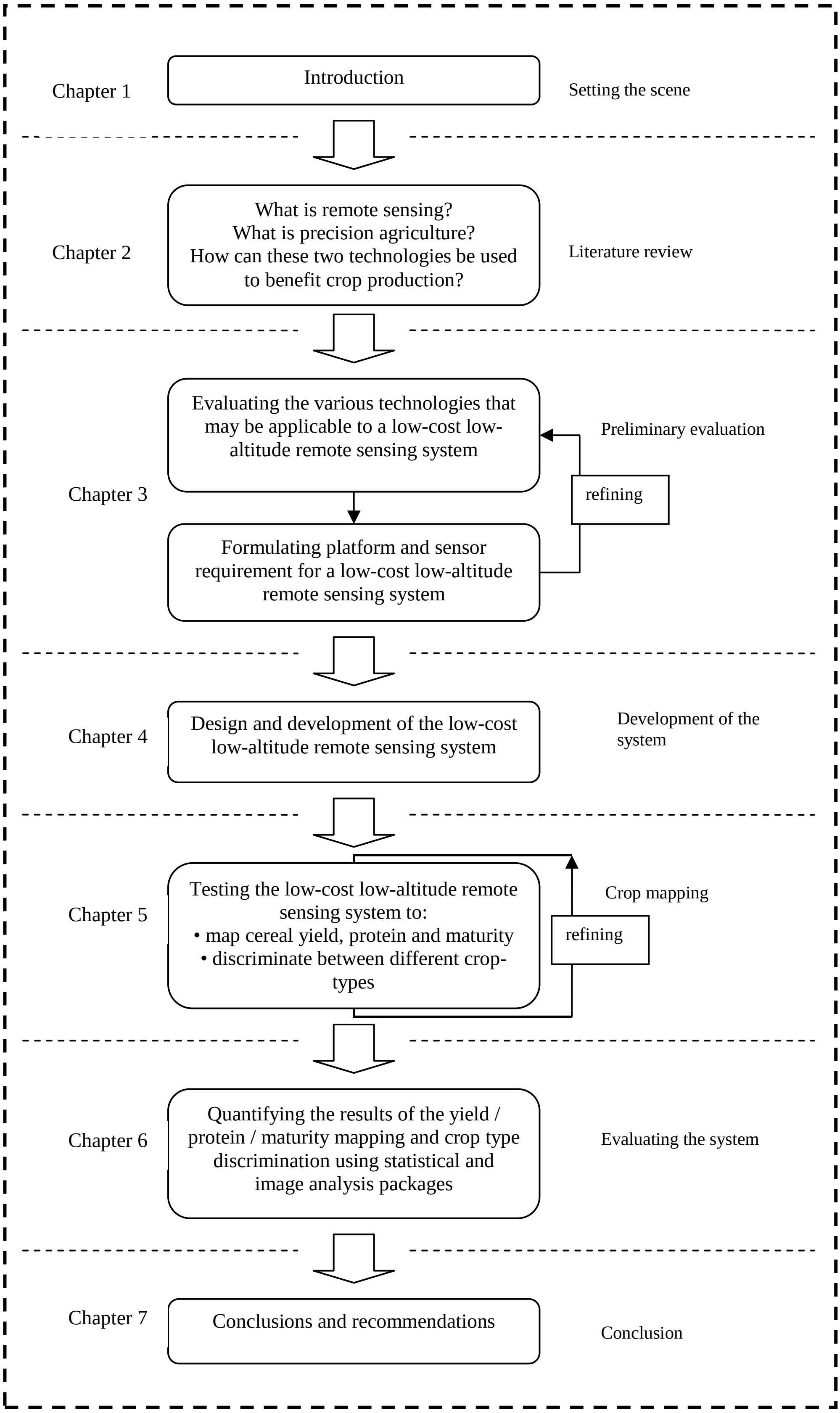

Figure 1.1 The schematic layout of this thesis.

Chapter 2

Literature Review: Precision Agriculture and Remote Sensing

In the first chapter, the potential of a low-cost low-altitude (LCLA) remote sensing system was postulated. This second chapter reviewed the potential for the use of such a system in an agricultural perspective. This review considers both the niche for a LCLA remote sensing system in precision agriculture applications, as well as the relevant sciences and technologies of remote sensing.

2.1 Precision Agriculture

Parameters related to crop production are known to vary across a field. This within-field spatial variability has been know for centuries (Stafford 2000), with yield variations (Fairfield Smith 1938) and soil conditions / characteristics (Keen & Haines 1925) being mapped as far back as the early 20th Century. Prior to the mechanisation of farming that occurred in the latter half of last century, the size of production units were very small and delineated by natural boundaries, such as water courses and change of soil types (Stafford 2000). This small field size enabled farmers to vary the treatments manually.

As the mechanisation and intensive production on farms increased—made possible by the increased size of agricultural tractors—the ability to take into account within-field spatial variability in these larger production units was lost. For ease of management in applying inputs, these fields were generally treated uniformly.

As field sizes have continued to grow (e.g. Australian grain farms have increased in size by almost 60 % in the last 25 years, to average just under 2000 ha (ABARE 2006)) by amalgamating these smaller land parcels, so has the potential for within-field variability. Significant spatial variation in crop parameters has been documented to occur within fields (Cook & Bramley 1998; Godwin *et al.* 2003b; Stafford *et al.* 1996). This variation is often attributed to differences in plant available water due to rainfall distribution and changes in soil properties (Oliver *et al.* 2006; Rodriguez *et al.* 2005), although other management factors such as compaction (Jensen *et al.* 2001b) and fertility (Delin *et al.* 2005) can also contribute to the variation.

With the development of technologies such as global positioning systems (GPS) and the ability of machinery to differentially apply inputs, it is becoming more feasible to treat areas of the field differently to compensate for the variation, similar to the earlier half of last century, albeit, minus the fences.

Precision agriculture attempts to measure this spatial variability in order to manage it. Variation is a feature of all farming systems, particularly in grain cropping systems, and includes:

- Soils–colour, texture, soil depth, nutrition, compaction;
- Topography–contour, slope, aspect, elevation;
- Crop growth–emergence, vigour, disease, phenology, yield, protein;
- Weeds–species, density, distribution;
- Pests and diseases; and
- Moisture supply–passage of storm rain, run-off events, fallow management.

In addition to spatial variability, there is variability over time (either within a season or from season to season), or temporal variability. These variabilities influences both crop potential and crop performance (Thylen *et al.* 1999). Crop potential (a function of soil properties and seasonal conditions) influences a grower’s management decisions on inputs (amount and timing). Crop performance (yield and quality) determines the return on investment (profit). If a higher fertiliser rate is applied to target a high crop potential and the season does not finish well, grain quality penalties may be incurred. Alternatively, if too low an application rate is applied in a good year, production penalties may be incurred (Kelly *et al.* 2004). In both of these cases, profit will be reduced.

By measuring variation, the farmer is in a better position to manage it. Available management options might include (Jochinke *et al.* 2007):

- Invest–increase the production potential by overcoming the constraints to production (e.g. soil amelioration, claying or liming);
- Vary–manage according to its current production potential by adjusting the spatial distribution of inputs (e.g. seed, fertiliser and other inputs); and
- Remove–the costs of management may be too high, and an equally viable outcome might be to stop production on these poor areas.

2.1.1 Definition and Components

Definitions

Many definitions of Precision Agriculture (PA) exist and there are many different ideas of what PA should encompass. One such definition is (NRC 1997, p. 17):

> *"Precision agriculture is a management strategy that uses information technologies to bring data from multiple sources to bear on decisions associated with crop production."*

While the above definition raises important information dimensions, it fails to emphasise the basic premise of PA—the management of spatial and temporal variability. This variability is better incorporated in the following definition which comes from the US House of Representatives (US 1997):

> *"Precision Agriculture—an integrated information- and production- based farming system that is designed to increase long-term, site specific and whole farm production efficiencies, productivity, and profitability while minimizing unintended impacts on wildlife and the environment."*

The bill expands on this definition and explains that this will be achieved by:

- Combining agricultural sciences, agricultural inputs and practices, agronomic production databases, and precision agriculture technologies to efficiently manage agronomic and livestock production systems;
- Gathering on-farm information pertaining to the variation and interaction of site-specific spatial and temporal factors affecting crop and livestock production;
- Integrating such information with appropriate data derived from field scouting, remote sensing, and other precision agriculture technologies in a timely manner in order to facilitate on-farm decision making; or
- Using such information to prescribe and deliver site-specific application of agricultural inputs and management practices in agricultural production systems.

As the focus of this study is on cereal grain, the livestock and other components of PA (listed above) will not be considered.

The particular form of PA that relates to crop management (Whelan 2007) is often termed Site-Specific Crop Management (SSCM) and is defined as:

> *"A form of PA whereby decisions on resource application and agronomic practices are improved to better match soil and crop requirements as they vary in the field."*

This crop-focused definition narrows the PA philosophy of timely management of variation down to its implementation in cropping systems. It relies on matching resource application and agronomic practices with the variation in soil attributes and crop requirements across a field. This implies a 'differential' treatment of field variation rather than 'uniform' treatment that underlies traditional agricultural management systems. SSCM should be part of a holistic management approach rather than a simple application of technology and should be absorbed into the current farming system—for nothing can replace good agronomy and appropriate crop management.

PA or SSCM can be thought of as a circular process or wheel (see Figure 2.1):

- Firstly, monitoring or measuring;
- Next, mapping;
- From maps, decision making; and
- Finally, these decisions lead to new or altered actions, which are then monitored, and the cycle continues.

At the heart of this system is the spatial referencing (GPS) that occurs with each action or process.

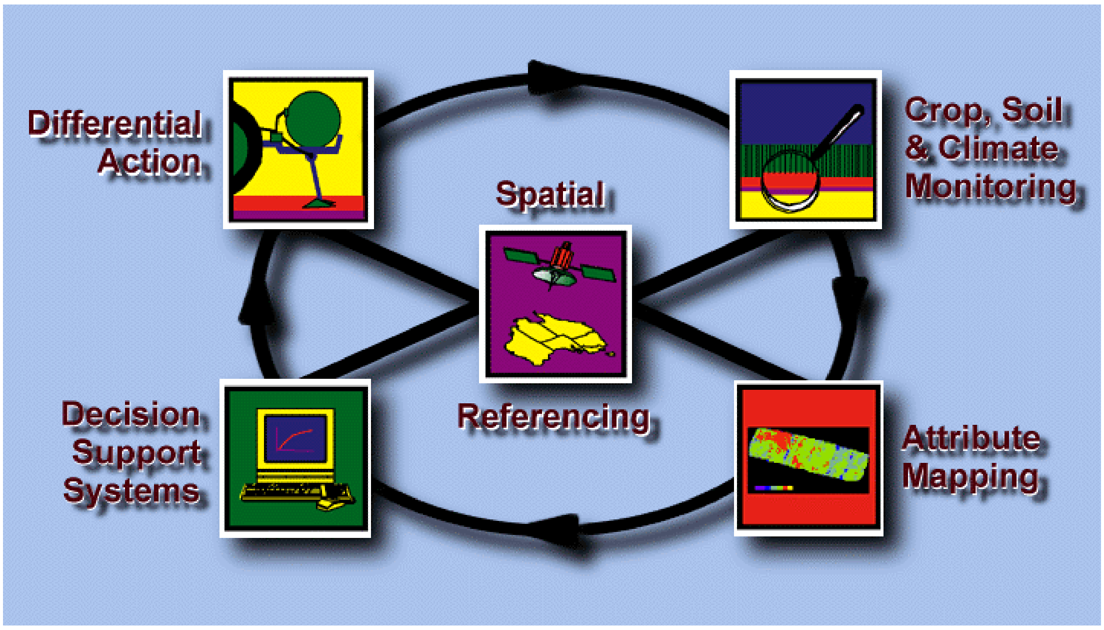

Figure 2.1 The precision agriculture wheel (McBratney & Whelan 2001).

For the use of PA to be justified, there are several criteria that must be satisfied (Plant 2001):

- That significant within-field spatial variability exists and that influences yield and quality;
- The causes of the variability can be determined and quantified; and
- Modifying management practises based on this variability increases profit and decreases environmental impact.

The variability that is evident can change from one part of the field to another (spatial) and from one year to the next (temporal) (Blackmore *et al.* 2003; Joernsgaard & Halmoe 2003). In one year, a particular part of the field can be the highest yielding and in the following year it can be the lowest yielding. The quality and quantity of crop variability is driven by:

- Field variability due to aspect, slope, elevation;
- Soil variability due to soil fertility; physical properties (density, texture, mechanical strength, moisture content, electrical conductivity), chemical properties (pH, organic matter, salinity, cation exchange capacity, plant available water content, hydraulic conductivity), and soil depth; and
- Crop variability due to nutrients, water, chlorophyll content, as well as weeds, disease, insects, wind, hail and frost.

Enabling Technologies

The current ability of PA to take into account the variability mentioned above would not have been possible without a revolutionary development in technologies (Stafford 2000) and having several of these technologies converge (Zhang *et al.* 2002) to provide the data to drive the system. These technologies (i.e. computing capacity, GPS, geographic information system (GIS), sensors, automatic control and remote sensing) will be looked at separately.

Computing

Many technologies support precision agriculture, but none is more important than computers (Pierce & Nowak 1999). PA requires the acquisition, management, analysis and output of large amounts of spatial and temporal data, that would not be possible without the use of computers.

Spatial Referencing

In order to produce a map of variability from a field, it is necessary to quantify the variation with the locations from which it was taken (Cook & Bramley 1998). This is the spatial referencing component of Figure 2.1 and is made possible by the use of satellite navigation systems, of which the US Global Positioning Systems (GPS) is the prominent one. Each system consists of a space segment that comprises a constellation of dedicated satellites, a ground control segment that monitors, manoeuvres and updates the satellites, and a user segment that calculates ground position (Krüger *et al.* 1994).

The required accuracy of the GPS depends on the operation being considered, with the following levels of accuracy being recommended (Stafford 1996): 30 m for variable fertiliser application, 10 m for yield mapping, 1 m for variable herbicide application, 10 cm for spray overlap / row crop planting and 5 cm for seed bed forming. The higher accuracies are achievable with differentially corrected GPS and the decimetre-level accuracies achievable with real-time kinematic (RTK) GPS (Schmidt *et al.* 2003).

Information Management

Once soil, crop and environmental information has been captured (with spatial referencing), it needs to be stored, statistically analysed and interpreted before management decisions can be made. An information management system such as a geographic information system (GIS) can be employed to meet these requirements. A GIS is an information system capable of integrating, storing, editing, analysing, sharing, and displaying geographically referenced information (Pierce & Nowak 1999).

Because precision agriculture is concerned with spatial and temporal variability, and because it is information-based and decision-focused, it is the spatial analysis capabilities of GIS that enable precision agriculture (Pierce & Nowak 1999). The GIS is the brain of the precision farming system (Clark & McGuckin 1996).

Production Mapping

Significant within-field variability exists in factors that influence crop yield (Plant 2001). This variability occurs over most, if not all, production areas. The variation is usually a result of multiple factors, such as soil moisture, soil characteristics, compaction, pests, diseases, weeds or the supply of nutrients. The complexity of the inter-relation of these factors make understanding the yield variability difficult (Sudduth *et al.* 1996). In the northern grain-growing region of eastern Australia however, moisture and nutrient limitations, particularly nitrogen, commonly affect crop production (Jensen *et al.* 2001a). These two variables are also expected to contribute to substantial within-field variations where there appears to be little or no soil variation.

Crop yield is an integrator of the many varying crop and soil parameters (Borgelt & Sudduth 1992) and is measured by integrating several sensor and information sources including grain flow rate, moisture content, forward velocity and grain harvester position. This integrated system is commonly referred to as a yield monitor, which allows yield maps to be produced (Reitz & Kutzbach 1996; Stafford *et al.* 1996).

The yield as a parameter only provides part of the explanation of what is occurring in the field. If this and other contributing data is correlated with grain quality, our understanding of the soil fertility status is significantly improved (Strong & Holford 1997).

To quantify the yield–protein relationship, numerous methods have been adopted: grain heads have been collected prior to harvest (Stafford 1999); samples taken from the auger as it discharges into the grain bin (Reyns *et al.* 1999); and an apparatus developed to accurately sub-sample a field (Jensen *et al.* 2001a). This apparatus was utilised and a protein map produced that, when combined with the yield map, gave a much clearer understanding of the determining factors in the crop production. Sites could now be identified where nitrogen (N) supply was likely to have limited crop yield (Kelly *et al.* 2004).

The protein content of grain is a good measure of quality, but measuring grain protein spatially continues to be a difficult task. Protein monitors are under development, but not commercially available (Thylén *et al.* 2002; Zhang *et al.* 2002) and the prototype units that are being used are having problems with the stability of calibrations (Jensen *et al.* 2005; Taylor *et al.* 2005) .

Attribute Sensors

Sensors are devices that respond to a physical stimulus. With computers to record the sensor’s output, a GPS to measure position, and a GIS to map and analyse the data, any output can be mapped at a very fine scale. Sensors are critical to the success of the development of PA for three important reasons: sensors have fixed cost, can sample at very small scales of space and time, and facilitate repeated measures (Pierce & Nowak 1999).

Sensors can be in contact or remote, ground based or space based, and direct or indirect. Sensors have been developed to measure machinery, soil, plants, pests, atmospheric properties, and water. Sensors are also capable of detecting the phenomena of motion, sound, pressure, strain, heat, light, and magnetism. These measurements relating to properties such as reflectance, resistance, absorbance, capacitance, and conductance (Pierce & Nowak 1999). Sensors are needed to provide the site-specific data that is the foundation of the PA system (Hummel *et al.* 1996).

Remote sensing, the detection and measurement of photons of differing energies emanating from distant object (Frazier *et al.* 1997), comprises one such group of sensors and will be further investigated later in this chapter.

Variable rate application technology (VRT)

Having determined that there is variability within the production area and within a crop, the next step in the PA cycle is to determine what has caused the variability and to try to remedy the situation. Depending on what attributes (e.g. topography, soil type, drainage, soil test results, rainfall, chemical / fertiliser application rates and yield) have been mapped will determine what parameters can be investigated to diagnose the variability. This diagnosis can be undertaken in a GIS which adds the spatial context to generate prescription maps. In turn, these maps enable controllers to automatically adjust the parameter.

If a single influencing factor has been identified and if this factor can be adjusted continuously, then some form of VRT can be employed (Plant 2001). Such parameters as seeding rate (Beavers *et al.* 2008), fungicide (Dammer *et al.* 2008), herbicide (Qiu *et al.* 1998), liquid fertiliser (Yang 2001), nitrogen (Zhao *et al.* 2007) and irrigation (Perry *et al.* 2003), have been varied to match the condition in each part of the field.

2.1.2 Purpose and Benefits

The benefits that precision agricultural technologies offer, as detailed by Cook *et al.* (2000), include enhanced likelihood of profit, product of consistent quality, and reduced risk to the environment. PA also provides farmers and agronomists with the capacity to monitor conditions across the entire field and / or farm. This ability to quantify parameters aids in the understanding of the variability within fields, and can enhance decisions on crop selection, agronomic management and / or alternative land uses. Such analysis may also identify physical or chemical constraints that are easily managed with appropriate treatments. PA can also provide the tools to assess whether the treatments have had a positive or negative impact on financial returns.

2.1.3 Limitations and Opportunities of Precision Agriculture

Yield monitors have been commercially available for use on combine harvesters since the mid 1990s. Although this has allowed grain growers to collect yield maps over a multiple of years, the difficulty in the interpretation of the results has limited the uptake of this precision agricultural technology both in Australia and overseas. In Chapter 1, it was indicated that the Department of Primary Industries and Fisheries (DPI&F) received project funding (1998–2006) from the Grains Research and Development Corporation (GRDC). The aim of this research was to identify and correct yield limiting factors. During this research, it became obvious that monitoring yield provided only part of the agronomic story. The understanding would be greatly enhanced if the quality—with protein being the primary measure—of the crop were considered.

As the yield and protein maps were generated with at-harvest data, the information could only be used retrospectively (after harvesting) to make management decisions about subsequent crops, with no capacity to make pro-active decisions about the existing crop. In order to make management decisions during the growing season of the crop, it was hoped that spectral data from remotely sensed images could provide the means of identifying the variability in cereal crops. The desire to provide a low-cost imaging system, with appropriate spectral / spatial / temporal resolution that can discern differing crop parameters and crop types, was spawned, resulting in the research detailed in this dissertation.

2.2 Remote Sensing

Remote sensing is the science and art of obtaining information about an object, area or phenomenon through the analysis of data acquired by a device that is not in contact with the subject under investigation (Lillesand *et al.* 2004).

2.2.1 Basic Concepts

Human Vision

The human visual system can detect the range of light spectrum from about 400 nm (violet) to about 700 nm (red) (Lillesand *et al.* 2004) and perceives this range of frequencies as a smoothly varying rainbow of colours. This range of light frequencies is called the visible portion of the light spectrum, as it is detectable by the human eye.

The human eye has a lens and iris diaphragm (see Figure 2.2) which serve similar functions to the corresponding features of a camera. Light reaching the eye passes through the pupil and is focused onto the retina by the lens (Mather 2004). The retina has the ability to separately sense three different portions of the spectrum, and are concentrated around the eye's fovea. These peak sensitivities are identified as red (580 nm), green (540 nm) and blue (450 nm)—the primary colours.

Our perception of which colour we are seeing is determined by which combination of sensors are excited and by how much. This is known as the trichromatic theory of colour vision or additive colour mixing. When the three types of sensors in the retina receive differing stimulation, colour is perceived, however when they are stimulated equally, white light is perceived (see Figure 2.3). Like the human eye, colour televisions, computer monitors and charged coupled devices (CCD) operate on the principle of additive colour mixing

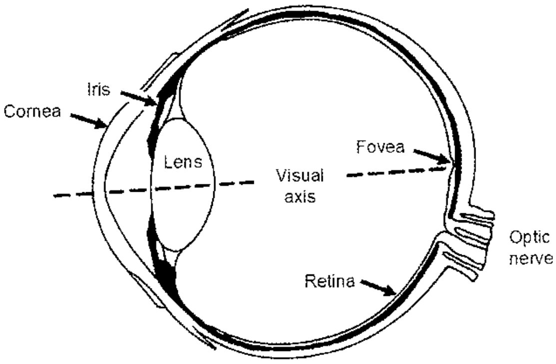

Figure 2.2 A simplified cross-section of the human eye (Mather 2004).

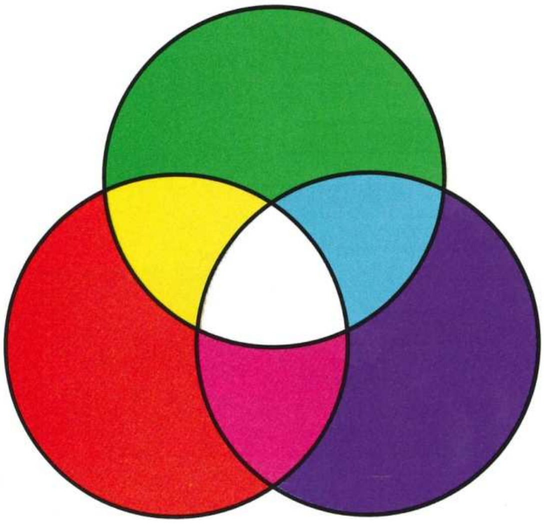

Figure 2.3 Trichromatic theory of colour vision (Jensen 2007).

The Electromagnetic Spectrum

Remote sensing involves the irradiative interaction of light with the objects of interest (Thorp & Tian 2004). The function of the sensor in remote sensing is very similar to that of the human eye, which detects a form of electromagnetic radiation. The visible light, along with other forms ranging for radio waves through to gamma rays (see Figure 2.4) are collectively grouped, according to wavelength, in the electromagnetic spectrum (Lillesand *et al.* 2004).

All matter reflects, absorbs, penetrates and emits electro-magnetic radiation in a unique way and are said to have differing spectral reflectance in the electromagnetic spectrum, of which several are displayed in Figure 2.5. The signature of healthy vegetation is significantly different to that of dry vegetation, water etc.

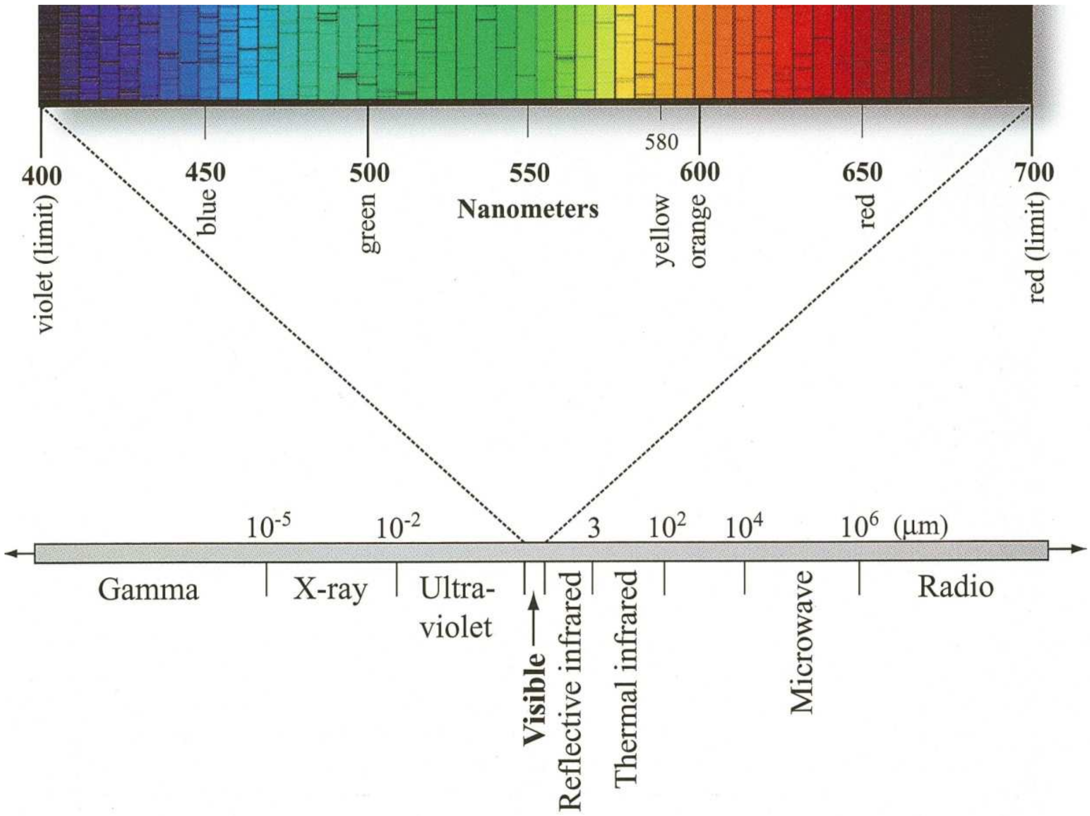

Figure 2.4 The visible portion and other components of the electromagnetic spectrum (Jensen 2007).

Interaction of Light with Plant Leaves

When electro-magnetic energy is incident on any given earth surface feature, three fundamental energy interactions with the feature are possible (Lillesand *et al.* 2004):

- Reflected–what is bounced off (and detected by our eyes);
- Absorbed– used in chemical processes (e.g. photosynthesis or warming); and
- Transmitted–ready to be reflected, absorbed or transmitted by another surface.

As radiation in the visible portion of the spectrum falls on a healthy leaf, the chlorophyll—contained in the chloroplast—strongly absorbs energy in the wavelengths centred at about 450 and 670 nm (Lillesand *et al.* 2004). The energy in the green portion of the visible spectrum is not absorbed, therefore reflected resulting in the bump in the green line at 550 nm in Figure 2.5, and the reason that we perceive healthy plants as green.

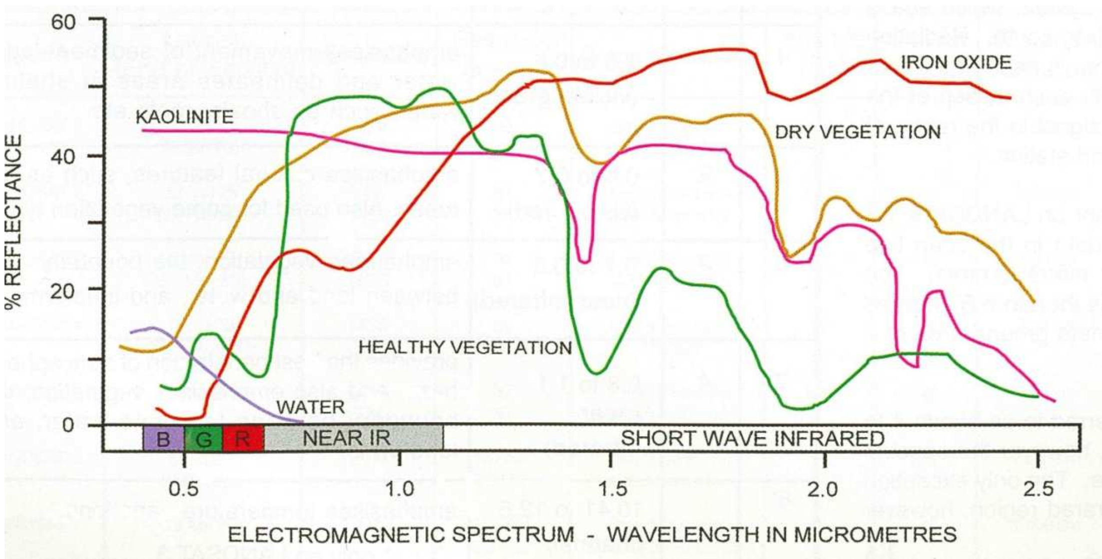

Figure 2.5 Spectral reflectance curves for natural features in the range 400–2500 nm (Geoimage 2005).

At the upper end of the visible spectrum, the absorption by chlorophyll begins to decline and reflectance rises sharply (Campbell 2002). In the range from 700–1300 nm, a plant leaf typically reflects 40–50 % of the energy incident on it, with most of the remaining energy being transmitted. Reflectance in this range results primarily from the internal structure of the plant leaf. Because this structure is highly variable between species, reflectance measurements in this range often permit discrimination between species, even if they appear the same in the visible portion of the spectrum (Lillesand *et al.* 2004).

As a plant matures—or is subject to stress caused by disease, insect attack, water or nutrition shortage—the spectral characteristics of the leaf changes and this happens more or less simultaneously in both the visible and near infrared regions (Campbell 2002). However, changes in the near infrared reflectance are often more noticeable.

2.2.2 Methods of Remote Sensing

A remote sensing system consists of two major components: the *sensor* or device that is used to detect and record information from the target, and the *platform* or vehicle which moves the sensor over the target area. There are varying degrees of sophistication of these systems from a simple system (such as the first recorded aerial photograph taken by Gaspard Felix Tournachon from his balloon in 1858) to the most complex hyperspectral space-borne system (such as the current Hyperion instrument onboard NASA's EO1 earth observing satellite).

As the primary focus of this research is the agricultural application of remote sensing, the literature review will focus on this topic. However, techniques or technologies that have been used for other purposes but have application to agriculture, will also be included. Specific agricultural examples will be included at the end of each subsection.

Platforms

Satellite

The application of satellites as a remote sensing platform commenced with NASA's *Corona* orbital satellite reconnaissance program in the late 1950s. Mission 9009 returned to earth on 18 August 1960 with the first images of earth captured from space (cited in Jensen 2007). This mission was later followed by dedicated remote sensing satellites such as the launch of LandSat in 1972. Many satellite remote sensing systems have since been (and continued to be) put into space. Recent high resolution satellite launches—IKONOS (1999), QuickBird (2001) and OrbView (2003)—have reduced the spatial resolution down to 0.61 m. The spatial, spectral, and temporal resolutions of some of the higher and moderate resolution remote sensing satellites are summarised in Table 2.1.

Table 2.1 Imaging properties of some remote sensing satellites.

Satellite	**Revisit** (days)	**Sensor/Band**	**Spectral range** (micrometers)	**Resolution** (m)	**Swath width** (km)	**Quantisation** (bits)
ASTER	16	VNIR				
		1	0.52-0.60			
		2	0.63-0.69	15	60	8
		3	0.76-0.86			
		SWIR				
		4	1.60-1.70			
		5	2.14-2.18			
		6	2.18-2.22	30	60	8
		7	2.23-2.28			
		8	2.29-2.36			
		9	2.36-2.43			
		TIR				
		10	8.12-8.47			
		11	8.47-8.82			
		12	8.92-9.27	90	60	12
		13	10.25-10.95			
		14	10.95-11.65			
Ikonos	3.5-5	Panchromatic				
		1	0.45-0.90	1	11	11
		Multispectral				
		1	0.45-0.53			
		2	0.52-0.61	4	11	11
		3	0.64-0.72			
		4	0.77-0.88			
IRS	5	Panchromatic				
		1	0.50-0.75	5.4	63-70	6
		LISS-III				
		2	0.52-0.59			
		3	0.62-0.68	23.5	141	7
		4	0.77-0.86			
		5	1.55-1.70	70.5	148	7
		WiFS				
		3	0.62-0.68	188	728-812	7
		4	0.77-0.85			
Landsat 1,2,3	18	MSS				
		4	0.50-0.60			
		5	0.60-0.70	80	183	8
		6	0.70-0.80			
		7	0.80-1.10			

Continued….

Table 2.1 (continued) Imaging properties of some higher resolution satellites.

Satellite	**Revisit** (days)	**Sensor/Band**	**Spectral range** (micrometers)	**Resolution** (m)	**Swath width** (km)	**Quantisation** (bits)
Landsat 4,5	16	MSS (as above)				
		TM				
		1	0.45-0.52	30	183	8
		2	0.52-0.60			
		3	0.63-0.69			
		4	0.76-0.90			
		5	1.55-1.76			
		6	10.42-12.50	120	183	8
		7	2.08-2.35	30	183	8
Landsat 7	16	TM (as above)				
		ETM+				
		6	as above	60	183	8
		8 (Pan)	0.52-0.90	15	183	8
QuickBird	1-3.5	Panchromatic				
		1	0.45-0.90	0.61	16.5	11
		Multispectral				
		1	0.45-0.52	2.44	16.5	11
		2	0.52-0.60			
		3	0.63-0.69			
		4	0.76-0.90			
SPOT 1,2 & 3	1-4	Panchromatic				
		1	0.50-0.73	10	60	8
		Multispectral				
		1	0.50-0.59	20	60	8
		2	0.61-0.68			
		3	0.78-0.89			
SPOT 4	1-4	Panchromatic				
		1	0.61-0.68	10	60	8
		Multispectral				
		1	0.50-0.59	20	60	8
		2	0.61-0.68			
		3	0.78-0.89			
		4	1.58-1.75			
SPOT 5	1-4	Panchromatic				
		1	0.48-0.71	5	60	8
		Multispectral				
		1	0.50-0.59	10	60	8
		2	0.61-0.68			
		3	0.78-0.89			
		4	1.58-1.75	20	60	8

The applications to which this satellite remotely sensed data have been put are numerous. Some of the applications described by Lillesand *et al* (2004) include the following: land use / land, geologic and soil mapping; applications in agriculture, forestry, rangeland, water resource, urban and regional planning, wildlife ecology and archaeological; and environmental and natural disaster assessments. Some specific examples include: a) policing the illegal use of underground water (Allan 1982); b) estimation of ground cover (Maas & Rajan 2008); c) discrimination of different grasses (Price *et al.* 2002); d) quantifying land use / land cover in African rainforest (Thenkabail *et al.* 2004); e) mapping leaf area index (Chen *et al.* 2002); f) detecting sugarcane "orange rust" disease (Apan *et al.* 2004); and g) predicting cereal yields (Enclona *et al.* 2004; Willis *et al.* 1998).

Inhabited Aerial Vehicles

The modern discipline of remote sensing arose with the parallel development of photography and of flight. The earliest systems were generally lighter-than-air with the balloonist Gaspard Felix Tournachon (*alias* Nadar) taking photographs of Paris from his balloon in 1858 and George R. Lawrence using kites to take shots of San Francisco after the earthquake in 1906 (Jensen 2007).

The first heavier-than-air systems involved the use of carrier pigeons (with attached cameras—the system patented by Julius Neubronner in 1903). The invention of the aircraft provided a more reliable platform with L.P. Bonvillain accompanying Wilbur Wright and taking a motion picture over Camp d'Auvours, France in 1908 (Jensen 2007).

The combination of aircraft and photography was utilised by the military to perform photo-reconnaissance roles. During World War I, trenches were mapped and troop movements and stockpiled arms monitored. These techniques were refined during World War II with photo-reconnaissance playing a vital role in military intelligence, monitoring troop build-ups and identifying V2 rocket facilities. The Cold War brought about specialist photo-reconnaissance aircraft (the U2) to undertake the collection of information.

Modern uses of aircraft as a remote sensing platform are numerous and the applications are vast. The array of applications includes the following: terrain analysis (Bhanu *et al.* 1997); quantifying leaf area index, nitrogen concentration, and photosynthetic efficiency in vegetation (Boegh *et al.* 2002); archaeological prospecting (Brivio *et al.* 2000); mapping of small areas shanty towns (Mason *et al.* 1997); detection of landscape features (water, snow, fire, vegetation and soil) (Price 1998) and vegetation condition (Nixon *et al.* 1985).

Even though medium-sized aircraft are currently used for the vast majority of airborne remote sensing (Dare 2005), many researchers have been experimenting with innovative methods of recording data utilising small aircraft, with the motivation for these experiments being budget driven. Platforms do not have to be sophisticated with ultralight aircraft (Clevers 1988; Hunt Jr *et al.* 2003) and powered parasail (Moran *et al.* 2003) utilised as remote sensing platforms.

Uninhabited Aerial Vehicles

This experimentation with inhabited small aircraft has also lead to the evaluation of uninhabited aerial vehicles (UAV) as a suitable low-cost platform for remote sensing.

> *Blimps, kites and balloons* have been used in several applications to: a) map spatial variability between and within agricultural (rice and soybean) fields (Inoue *et al.* 2000) and to assess crop N status (Jia *et al.* 2004); b) monitor gully erosion (Ries & Marzolff 2003) and changes in land surface conditions (Baker *et al.* 2004); c) determine coverage of pecan tree crowns to predict evapotranspiration (Wang *et al.* 2007); d) measure gas flux (Vierling *et al.* 2006); e) map periglacial geomorphology (Boike & Yoshikawa 2003); f) detect weeds (Lamb & Brown 2001; Richardson *et al.* 1985); and g) detect changes in ecological systems (Murden & Risenhoover 2000).
>
> *Remotely controlled helicopters* have also been used to map crop status (Sugiura *et al.* 2005), monitor rangelands (Rango *et al.* 2006), detect damages from hurricanes (Murphy *et al.* 2008), and as an alternative to satellite remote sensing in developing countries (Swain *et al.* 2007).

Advances in microelectronics, micro sensors and telecommunications have given *remotely controlled aircraft* (or UAVs) an enormous potential in a wide variety of scenarios. Several applications to which UAVs have been applied include: a) pipeline inspections (Hausamann *et al.* 2005); b) detecting coffee ripeness (Furfaro *et al.* 2007); c) sampling air for dust (Espinar & Wiese 2006) and spores (Schmale III *et al.* 2008); d) monitoring climatic conditions in hurricanes (Murphy *et al.* 2008); e) performing search and rescue missions (Goodrich *et al.* 2008); f) monitoring rangeland condition (Hardin & Jackson 2005); g) detecting cotton response to irrigation and crop residue (Sullivan *et al.* 2007); h) detection and monitoring of marine mammals (Schoonmaker *et al.* 2008); i) monitoring archaeological sites (Hinckley & Walker 1993); and j) surveillance of borders and coasts, fire detection, and search and rescue (Martínez-Val & Hernández 1999).

Proximal or Ground-based

Proximal or ground-based systems can be used in several ways: gain an insight into the spectral reflectance characteristics of selected materials, calibrate remote sensor data, and provide unique spectral data for improved information extraction using multispectral and hyperspectral remote sensing data (Jensen 2007).

Studies have used ground-based remote sensing to quantify lettuce head area (Hussain *et al.* 2008), to detect changes in gully erosion (Baker *et al.* 2004), to detect and map weeds (Yang *et al.* 2002), to predict grain yield in maize by the use of active sensors (Inman *et al.* 2007), and to monitor crop canopy conditions as a real-time method of variable-rate N applications (Jørgensen & Jørgensen 2007).

Sensors

Sensors play an important role in the spectral resolution of the image and are the devices that detect the changes in the subject being viewed. Sensors can be either multispectral or hyperspectral with both types being utilised by proximal, aerial and satellite remote sensing systems. Details for some of the various satellites based sensors are given in table 2.1, with multispectral and hyperspectral sensors being discussed in the following section.

Multispectral

The procedure demonstrated in 1861 by the Scottish Physicist James Maxwell, of photographing a bow of multicoloured ribbon multiple times using different coloured filters (red, green and blue and yellow) (cited in Jensen 2007), was a very early multispectral sensor. Since the time of Maxwell, video and digital imaging systems have become a versatile remote sensing tool.

Airborne video and digital still imagery has the advantages of relatively low cost, as well as real-time or near-real-time availability of imagery for visual assessment and computer image processing. These sensors have the ability to obtain data in very narrow spectral bands (by the use of band-pass filters) in the visible to mid-infrared regions (Everitt *et al.* 1995; Mausel *et al.* 1992) of the electromagnetic spectrum and are generally limited to between 4 and 12 spectral bands of information (Jensen 2007). The bands are generally centred on 440 nm (blue), 550 nm (green), 650 nm (red) and 770 nm (NIR) with the bandwidth from 10–20 nm (Lamb 2000; Lévesque & King 1999; Yang *et al.* 2000). This remote sensing method has been used increasingly in precision agriculture and natural resource management to detect and assess crop growth and yield variability (Gopalapillai & Tian 1999; Yang & Anderson 1999; Yang & Anderson 2000; Yang *et al.* 2000)

The type of information collected by multispectral sensors depends on the application. Such sensors have been used in the following: a) monitor and map variability in vegetation canopies based on changes in their spectral signatures (Lamb 2000); b) perform within-field qualitative assessments of agricultural crops (Blackmer *et al.* 1996); c) detect crop stress (Pearson *et al.* 1994); d) estimate sorghum yield (Yang & Anderson 2000) and kenaf production and crop stress (Cook *et al.* 1999); e) map variable growing conditions and yields of cotton, sorghum and corn (Yang *et al.* 2001); f) assess vegetation condition (Nixon *et al.* 1985); and g) distinguish weeds (Richardson *et al.* 1985).

Hyperspectral

Multispectral sensors have limitations in providing accurate estimates of biophysical and yield characteristics of agricultural crops (Thenkabail *et al.* 2002) and crop type or species identification (Asner *et al.* 2000). Limitations such as these have led to an increasing interest in the narrow-waveband hyperspectral sensors. Hyperspectral imaging systems typically acquire data in hundreds, or even thousands of spectral bands.

Examples of hyperspectral sensors include:

- Airborne Visible / Infrared Imaging (details at http://aviris.jpl.nasa.gov/)–has 224 bands in the region from 400–2500 nm (bands spaced 10 nm apart). It has the capability of collecting image data in very narrow and contiguous spectral bands throughout the visible, NIR and mid-infrared regions.
- Hyperion (on-board NASA's EO1 spacecraft, details at http://eo1.gsfc.nasa.gov/)–provides a high resolution hyperspectral imager capable of resolving 220 spectral bands (from 0.4 to 2.5 µm) with a 30 meter spatial resolution. The instrument images a 7.5 km by 100 km land area per image and provides detailed spectral mapping across all 220 channels.
- ASD FieldSpec 3 (details at http://www.asdi.com/) (proximal)–collects samples every 1.4 nm over the 350–1050 nm and every 2 nm over the 1000–2500 nm range.

With so many bands of information (variables) and so few readings in comparison, analysing information from hyperspectral data requires the use of sophisticated digital image processing software (Jensen 2007) to reduce the dimensionality of the data to a manageable degree. Such sensors have been evaluated for use in precision agriculture (Deguise *et al.* 1998; Willis *et al.* 1998), and used to explain variability and to classify African rainforests (Thenkabail *et al.* 2004).

These sensors are expensive to purchase and operate, are generally large and require a full-sized aircraft to house the instrument (except for the handheld sensors). As a result, these expensive devices are have not been extensively used in commercial agriculture, and are hence beyond the scope of this research.

Vegetation Indices

Vegetation indices—a dimensionless, radiometric measure that indicates relative abundance and activity of green vegetation (Jensen 2007)—is formed from combinations of several spectral. These values are added, divided, or multiplied in a manner designed to yield a single value that indicates the amount or vigour of vegetation within a pixel (Campbell 2002). These indices theoretically provide values that are more highly correlated to plant parameters (e.g. leaf area index, biomass or vegetative cover) than the raw reflectance measurements (Wanjura & Hatfield 1986). Some of the common vegetation indices, with application to multispectral data, are summarised in Table 2.2.

Table 2.2 Potential vegetation indices that can be calculated with multispectral remotely sensed data.

Name	**Abbreviation**	**Formulae**	**Reference**
Red Ratio Vegetation Index	RVI	$\frac{NIR}{R}$	(Jordan 1969)
Normalised Difference Vegetation Index	NDVI	$\frac{(NIR - R)}{(NIR + R)}$	(Rouse *et al.* 1974)
Difference Vegetation Index	DVI	$NIR - R$	(Tucker 1979)
Soil Adjusted Vegetation Index	SAVI	$\frac{(NIR - R)}{(NIR + R + L)}\ (1 + L)$	(Huete 1988)
Green Normalised Difference Vegetation Index	GNDVI	$\frac{(NIR - G)}{(NIR + G)}$	(Gitelson *et al.* 1996)
Plant Nitrogen Spectral Index	PNSI	$\frac{(NIR + R)}{(NIR - R)}$	(Stone *et al.* 1996)
Plant Senescence Reflectance Index	PSRI	$\frac{(R - G)}{NIR}$	(Merzlyak *et al.* 1999)
Enhanced Vegetation Index	EVI	$2.5\ \frac{(NIR - R)}{(NIR + (6R - 7.5B) + 1)}$	(Huete *et al.* 2002)
Green Ratio Vegetation Index	GVI	$\frac{NIR}{G}$	(Xue *et al.* 2004)
Red Green Normalised Difference Index	RGNDI	$\frac{(R - G)}{(R + G)}$	(Li *et al.* 2008)
Red Green Vegetation Index	RGVI	$\frac{R}{G}$	(Li *et al.* 2008)

2.2.3 Problems and Limitations of Using Existing Remote Sensing Systems in Precision Agriculture

Remote sensing offers a non-invasive method of acquiring a bird’s-eye view of vegetation. In order to successfully detect and map vegetation attributes, there must be suitable differences in spectral reflectance of the vegetation types and the sensor have the appropriate resolution to detect the differences (Lamb & Brown 2001)

The required spatial resolution of any imagery will depend on whether the target is characterised by continuous change or whether the variation occurs in discrete patches. The former case requires considerably higher spatial resolution than the latter. Obviously, a spatial resolution comparable in size to the expected size of the variability is a good starting point (Atkinson & Curran 1997).

Satellite Systems

Satellite systems have limitations, some of which were detailed by Zhang *et al.*(2002) and include: a) a set repeat cycle that may not allow a specific event to be captured; b) the limited extent of the area of interest; c) the cost of the data; d) poor spatial resolution; and e) the time take to access imagery from the supplier. As the growth and management of agricultural crops are dictated by local weather conditions (Atkinson & Curran 1997), cloud cover can have an impact on the satellite remote sensing opportunities. For example, in SE Queensland, Australia, during the peak winter growing months of August to October, the mean number of clear days are 15.8 14.5 and 12.2, respectively, for “Dalby Post Office” (Site number: 041023, Latitude: -27.18° Longitude: 151.26 °E, Elevation: 344 m) (BOM 2008). This possibility of cloud requires a high-scheduling flexibility for any monitoring system (Lamb 2000).

Piloted Airborne Systems

Airborne sensors offer much greater flexibility than satellite platforms and have overcome some of these problems. They are able to operate under clouds and having a much finer spatial resolution (Lamb & Brown 2001). The cost of the imagery is still of concern and a number of people have been working on reducing the cost of the sensors (Everitt *et al.* 1995). However, the operating cost remains high due to the cost of commissioning the aircraft especially when a dedicated ‘mobilisation’ of the aircraft is required (refer Chapter 1.1). This is particularly true for remote localities and repeated data acquisition needs.

Remotely-Controlled Aerial Platforms

Remote-control helicopters (refer section 2.2.2) were used to generate maps of crop status (Sugiura *et al.* 2005), while model aircraft were used as the platform to remotely sensed crop biomass and nitrogen status (Hunt Jr. *et al.* 2005). Additionally, a high-altitude unmanned aerial vehicle was used to monitor crop ripeness and weeds in a coffee plantation (Herwitz *et al.* 2004). However, these systems are expensive: helicopters are worth tens of thousands while the high-altitude UAVs are worth millions of dollars. These costs make the use of advanced remotely-controlled aerial platforms prohibitive for most agricultural applications.

2.2.4 Technologies for Use in a Low-Cost Low-Altitude Remote Sensing Systems

Platforms

There have been several occurrences of low-altitude aerial platforms being reported as research tools to collect imagery. A cable-supported and helium balloon platform has been used to record temporal changes in surficial environments (Baker *et al.* 2004). Kites and balloons were used to map periglacial geomorphology in Alaska (Boike & Yoshikawa 2003). Blimps have been used to map spatial variability between and within agricultural (rice and soybean) fields (Inoue *et al.* 2000) and to monitor gully erosion (Ries & Marzolff 2003). Remote-control helicopters were used to generate maps of crop status (refer 2.2.2) and model aircraft were used as the platform to remotely sense crop biomass and nitrogen status (Hunt Jr. *et al.* 2005). Additionally, a high-altitude unmanned aerial vehicle was used to monitor crop ripeness and weeds in a coffee plantation (Herwitz *et al.* 2004).

Sensor Technologies

Many studies have used photographic film as a remote sensing medium (Blackmer *et al.* 1996; Brooner & Simonett 1971; Hinckley & Walker 1993). However, with the advent of digital cameras, many researchers are comparing the two media. The transition to digital environment is inevitable (Light 1996) as processing film takes time, it needs to be scanned and the target cannot be confirmed. Digital sensors have better geometric stability, there is no film deterioration, better radiometric quality, greater quantum efficiency, and wider spectral sensitivity range (King *et al.* 1994).

Thus, digital sensors are becoming a viable alternative to small-format analogue cameras (Mason *et al.* 1997). Digital camera technology has changed tremendously in the last decade, and prices plummeted as quickly as performance has increased (Lamb & Brown 2001). Although digital cameras have been used on aerial platforms since the early 1990s (Everitt *et al.* 1995), recent technological developments in sensor and navigational systems offer new innovative applications for tactical level farming.

Operating Principles of Digital / Video Cameras

The charged couple device (CCD), the imaging sensor in most digital and video cameras, is a collection of tiny light-sensitive diodes, which convert photons (light) into electrons (electrical charge). These diodes are called photosites. The photosites on a CCD respond only to light intensity, not to colour. The brighter the light that hits a single photosite, the greater the electrical charge that will accumulate at that site. The accumulated charge of each photosite in the image is transported across the chip and read at one corner of the array. An analogue-to-digital converter turns each pixels' value into a digital value (Lillesand *et al.* 2004).

Unfortunately, each photosite is "colour blind" and only keeps track of the total intensity of the light that strikes its surface. In order to get a full colour image, most sensors use filtering to look at the light in its three primary colours. Once all three colours have been recorded, they can be added together to create the full spectrum of colours that we are accustomed to seeing on computer monitors and colour printers.

There are several ways of recording the three colours in a digital camera:

1. The highest quality cameras use three separate sensors, each with a different filter over it. Light is directed to the different sensors by placing a beam splitter in the camera (Herwitz *et al.* 2004).
2. A second method is to rotate a series of red, blue and green filters in front of a single sensor (Lévesque & King 1999). The sensor records three separate images in rapid succession, however the three images are not taken at precisely the same moment requiring both the camera and the target of the photo to remain stationary for all three readings. This is not practical for most mobile photographic application.
3. A more economical and practical method, and used on most digital cameras, is to record the three primary colours from a single image by permanently placing a filter over each individual photosite (Lillesand *et al.* 2004). By breaking up the sensor into a variety of red, blue and green pixels, it is possible to get suitable information in the general vicinity of each sensor to make very accurate estimate about the true colour at that location.

The most common pattern of filters is the Bayer filter pattern (see Figure 2.6). This pattern alternates a row of red and green filters with a row of blue and green filters. The pixels are not evenly divided—there are as many green pixels as there are blue and red combined. As the human eye is not equally sensitive to all three colours, it is necessary to include more information from the green pixels in order to create an image that the eye will perceive as a "true colour".

The advantages of this method are that only one sensor is required, and all the colour information (red, green and blue) is recorded at the same moment. It means that the camera can be smaller, cheaper, and useful in a wider variety of situations.

CCDs are sensitive not only to visible light, but also to infrared light. If the infrared was not filtered out, it would become part of the RGB data and therefore become visible in the resulting pictures. This means that the photos taken would look different to that perceived by the human eye. To overcome this problem, a blue filter is placed in-front of the CCD to greatly reduce the infrared seen by the CCD, thereby making the CCD behave much more like the human eye.

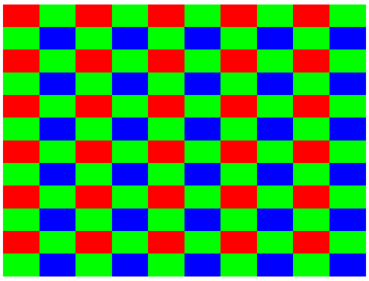

Figure 2.6 Bayer filter pattern.

Resolution

The amount of detail that the camera can capture is called the resolution, and it is measured in pixels. The more pixels the camera has, the more detail it can capture.

Compression

It takes a lot of memory to store digital photos. For example, the Kodak CX7525 (a 5.0 Megapixel camera) can store 204 images on a 128 MB SD card when set on “good” image size (1496 x 1122), 118 images when set on “better” image size (2048 x 1536), and only 79 images when set on “best” image size (2560 x 1920) (Kodak 2004). Almost all digital cameras use some sort of data compression to make the files smaller. There are two features of digital images that make compression possible: repetition and irrelevancy (Nice *et al.* 2006).

> *Repetition*–certain patterns developing in the colours in the image. For example, if the sky takes up 30 percent of the photograph, some shades of blue are going to be repeated over and over again. Compression routines take advantage of patterns that repeat and there is no loss of information as the image can be reconstructed exactly as it was recorded. Unfortunately, the files size may only be reduced by 50 %, and sometimes not even close to that level.

Irrelevancy–recording more information than is easily detected by the human eye. Compression routines take advantage of this fact in order to throw away some of the more meaningless data. Smaller files are achieved by excluding more data, with most offering various levels of resolution. Lower resolution means more compression. Some cameras include the option to store images with no compression at all ("CCD raw mode") for the very best quality.

2.3 Summary

There are numerous satellites that can provide remotely sensed imagery (e.g. Landsat, SPOT, IKONOS and ASTER). These platforms have spatial resolutions varying from 30 m to less than 1 m, and with revisit times from 16 days to 1 day (if off-nadir capacity is programmed). However, these systems have limitations for precision agricultural applications, particularly where the extent of the area-of-interest is not large (< 100 ha) and where the scale of the variation being investigated is small. Clouds and cloud cover are also an issue in being able to image data when required.

Aerial imagery acquisitions resolve some of these issues as it has finer spatial resolution and ability to be captured on demand. However, this system also creates other problems. The cost of imagery is very high when a dedicated mobilisation of the aircraft is required and there is the issue of availability of the plane and sensor, particularly when sourced from interstate where long transit distances are involved.

Several studies have shown that low-altitude platforms (e.g. kites, balloons, blimp and remotely controlled aircraft) have the capacity to be used as an alternative platform for observing various phenomena. This study focused on the potential of detecting and mapping grain crop attributes using digital imagery acquired from a low-altitude platform.

Chapter 3

Preliminary Evaluation and Assessment of Sensor and Platform Systems

Existing remote sensing imaging systems have limitations that include availability, timeliness and cost (Chapter 2); those of particular importance when the area-of-interest is small (< 10 ha) and when the required resolution is high (sub-metre pixel resolution). This chapter investigates the suitability of alternative readily-available consumer imaging technologies, in combination with low-altitude platforms, to capture selected attributes of agricultural crops.

3.1 Potential Systems

The potential imaging system has two components: the *sensor* system and the *platform* on which it is deployed. Preliminary studies were conducted to investigate the suitability of using a low-altitude unmanned aerial vehicle (platform) and consumer imaging technologies (sensor) as an appropriate remote sensing system for mapping grain crop attributes.

3.1.1 Platform

There is a range of potential low-altitude unmanned aerial vehicles (UAVs) that could be utilised as the platform for the low-cost low-altitude remote sensing system. Such platforms could include blimps, balloons, kites and remotely controlled model airplanes and helicopters.

Low-altitude unmanned platforms are variable in their specifications with no single kind of platform being ideal for all types of low-altitude remote sensing. Key issues are cost, safety, operator expertise, and quality of imagery for a particular project or application. These factors were weighed on a case-by-case basis in order to select the optimum platform for a given low-altitude remote sensing mission. A summary of this evaluation is shown in Table 3.1. For example, where the area to be imaged is small, and ease of deployment and operation is the primary consideration, balloons / blimps provide the ideal platform. However, where the area to be imaged is large, and pilots are available, fixed wing aircraft are the preferred choice.

Brief Review of Unmanned Aerial Vehicle (UAV) Applications

Although there have been numerous applications of UAVs as a remote sensing tool (see Table 3.2 for a range of studies) some have utilised high altitude and / or high cost sensors. As the focus of this research was to develop a low-cost low altitude (LCLA) remote system for use in agricultural applications, these parameters were further investigated.

Of the applications listed in Table 3.2, several systems have direct application to the LCLA remote sensing system. These were reviewed in more detail below:

1. A UAV was used to acquire low-altitude high-resolution imagery for resource management (Quilter & Anderson 2000). The UAV was based on a remotely controlled model airplane (RCA) with 2.5 m wingspan that could fly up to 300 m above ground level. The sensor used was a 35 mm film camera with a single vertical image covering a ground area ranging from 75 m^2 up to 6.5 hectares, depending on camera lens and flying height. The system was utilised to document the effectiveness of riparian restoration, to monitor impact of all-terrain vehicles on vegetation, and to evaluate range management techniques. The total reported cost of the system (UAV, engine, radio controls, and camera) was approximately US$1000 as well as 100+ hours of labour to build the UAV. As this study was undertaken in the year 2000, the advent of much better resolution digital cameras and the production of “nearly-ready-to-fly” models could have changed this scenario.

Table 3.1 Comparison of various UAV platform types to perform LCLA remote sensing applications in agriculture (☼☼☼☼☼ indicates high compliance, ☼ indicates no or low compliance)*.

Requirement	Platform				
	Kite	**Balloon / blimp**	**Fixed wing (electric)**	**Fixed wing (internal combustion)**	**Helicopter**
Low speed, low altitude flight	☼☼☼☼☼	☼☼☼☼☼	☼☼☼	☼☼☼	☼☼☼☼☼
Low purchase cost	☼☼☼☼☼	☼☼☼☼☼	☼☼☼	☼☼☼	☼
Autonomous flight capability	☼	☼	☼☼☼☼☼	☼☼☼☼☼	☼
Applicability to small plot work	☼☼☼☼☼	☼☼☼☼☼	☼☼☼	☼☼☼	☼☼☼☼☼
Applicability to broadacre agriculture	☼	☼	☼☼☼☼☼	☼☼☼☼☼	☼☼
Ease of launch	☼☼☼☼☼	☼☼☼☼☼	☼☼	☼☼	☼☼
Payload to weight ratio	☼☼	☼☼	☼☼☼	☼☼☼☼☼	☼☼☼☼☼
Low vibration	☼☼☼☼☼	☼☼☼☼☼	☼☼☼	☼☼☼	☼
Low operating cost	☼	☼☼	☼☼☼☼☼	☼☼☼	☼☼☼
Simplicity of operation	☼☼☼☼☼	☼☼☼☼☼	☼☼☼	☼☼	☼
Hover capability	☼☼☼☼☼	☼☼☼☼☼	☼	☼	☼☼☼☼☼
Endurance	☼☼☼	☼☼☼☼☼	☼☼☼	☼☼☼☼☼	☼☼☼
Portability in station wagon	☼☼☼☼☼	☼☼☼☼☼	☼☼☼☼☼	☼☼☼☼☼	☼☼☼☼☼
Low Deployment time	☼☼☼	☼☼☼	☼☼☼	☼☼☼	☼☼☼
Ease of repair	☼☼☼☼☼	☼☼☼☼☼	☼☼☼	☼☼☼	☼
Level of manpower required	☼	☼	☼☼☼	☼☼☼	☼☼☼
Directability	☼	☼	☼☼☼☼☼	☼☼☼	☼☼☼
Safety considerations	☼	☼	☼☼	☼☼☼	☼☼☼☼☼

* assessed by the author from available information.

Table 3.2 Some applications of UAVs in remote sensing.

Mission objective	**Platform**	**Sensor**	**Reference**
inspecting pipelines	RCA	synthetic aperture radar	(Hausamann *et al.* 2005)
detecting coffee ripeness	RCA	multispectral camera	(Furfaro *et al.* 2007; Herwitz *et al.* 2004; Johnson *et al.* 2004)
sampling air for dust	RCA	dust sampler	(Espinar & Wiese 2006)
managing golf courses	kite	digital camera	(Aber *et al.* 2003)
researching hurricanes	helicopter/RCA	video camera	(Murphy *et al.* 2008)
mapping crop status	helicopter	3 CCD camera	(Sugiura *et al.* 2005)
monitoring rangeland	RCA	35 mm camera	(Quilter & Anderson 2000; Rango *et al.* 2006)
maping spatial variability between and within agricultural (rice and soybean) fields	blimp	4 camera multi-spectral sensor	(Inoue *et al.* 2000)
assessing crop N status	balloon	35 mm camera	(Jia *et al.* 2004)
monitoring gully erosion	blimp	35 mm camera	(Ries & Marzolff 2003)
detecting changes in land surface conditions	balloon	digital camera	(Baker *et al.* 2004)
determining coverage of pecan tree crowns to predict evapotranspiration	balloon	digital camera	(Wang *et al.* 2007)
measuring gas flux	blimp	hyperspectral, thermal and video camera	(Vierling *et al.* 2006)
mapping periglacial geomorphology	kite and balloon	film camera	(Boike & Yoshikawa 2003)
detecting changes in ecological systems	blimp	2 film SLR cameras	(Murden & Risenhoover 2000)
monitor rangelands	helicopter/RCA	digital camera	(Rango *et al.* 2006)
providing an alternative to satellite RS in developing countries	helicopter	high resolution cameras	(Swain *et al.* 2007)
detecting spores	RCA	spore sampler	(Schmale III *et al.* 2008)
performing search and rescue missions	RCA	video camera	(Goodrich *et al.* 2008)
monitoring rangeland condition	RCA	35 mm camera	(Hardin & Jackson 2005)
detecting cotton response to irrigation and crop residue	RCA	thermal infrared	(Sullivan *et al.* 2007)
detecting and monitoring of marine mammals	RCA	4 camera multispectral sensor	(Schoonmaker *et al.* 2008)
monitoring archaeological sites	RCA	film camera	(Hinckley & Walker 1993)
providing surveillance of borders and coasts, fire detection, and search and rescue	RCA	TV, photographic and thermal camera	(Martínez-Val & Hernández 1999)
evaluating drip irrigation trials	RCA	digital camera	(Simpson *et al.* 2003)

2. A 2.5 m wingspan electric powered model aircraft, with consumer digital still cameras (Nikon Coolpix 800), was used in a study (Stombaugh *et al.* 2003) to investigate crop vigour and plant densities. The system utilised a video downlink to aid the ground crew in positioning the UAV. The digital camera was triggered via a servo that utilised an unused channel on the radio equipment. The entire system cost was less than US$1500.
3. A helium-filled blimp (6.4 m long x 2 m in diameter) was used to acquire low-altitude aerial images that was used to monitor rangeland vegetation (Murden & Risenhoover 2000). The imaging system consisted of 2 x 35 mm still cameras and monochrome charged couple device (CCD) camera used for positioning. The blimp, which was able to collect images from 122 m above the ground, had a total cost of US$6500. It was a good compromise between ground-based methods of data collection and fixed-wing or satellite remote sensing.
4. A specially designed hot-air blimp was used in geomorphic and vegetation investigations in Spain (Ries & Marzolff 2003). The system utilised a blimp (10 m long with a volume of 100 m^3) that was manoeuvred via a ground tether. The propane burner and camera system are operated by radio control from the ground. The blimp flew up to 400 m high and could lift a payload of 6 kg. The cost of the fully equipped, custom-built hot-air blimp system was approximately $12,000; the dual-camera system and radio control apparatus cost $1500 and $600 respectively. A minimum of four people are necessary for ground operation of the system. Dual *Pentax* cameras were utilised for simultaneous photographs of the same ground area, with one camera loaded with normal colour film, and the other with colour-infrared film.
5. Large kites have been used to suspend film and digital cameras to capture large-scale high-resolution images in the colour and near infrared (NIR) for golf course management (Aber *et al.* 2003). The cameras are lifted 50–150 m above the surface to provide information for managers to visualise and evaluate the condition of the golf course and the consequences of management practices. Kite aerial photography is a means to acquire relatively low-cost imagery compared to manned (airplane or helicopter) methods.

3.1.2 Sensor System

The potential technologies that can be utilised as the sensor for this research included video and still camera in both analogue and digital forms. On reviewing the literature, these technologies, in various configurations and combinations, have been successfully used as remote sensing tools on conventional aircraft, low-altitude platforms and proximal sensing.

> *Aircraft* based sensors include the use of the following systems: Kodak monochrome 1.4 megapixel digital cameras with rotating filters to detect forest damage caused by mining (Lévesque & King 1999); a 35 mm camera using colour infrared (CIR) film to predict grain-yield variability (Staggenborg & Taylor 2000); and a 4 CCD video sensing system that has been used to monitor crop emergence, canopy vigour and biomass (Lamb 2000).
>
> The use of sensors on *low-altitude* platforms include a video transmission system used to position a UAV over a target to acquire digital camera images of drip irrigation trials (Simpson *et al.* 2003). In addition, two single lens reflex (SLR) (1 x colour and 1 x NIR) cameras position under a blimp to monitor gully erosion (Ries & Marzolff 2003).
>
> The *proximal* remote sensing configurations include the use of a dual video camera system (with narrow bandpass filters to capture red and NIR) to measure the area covered by green growing plants (Baron *et al.* 2002). This study used a frame-grabber to capture images from the video stream. In another study to estimate vegetation cover, a webcam was used to frame the image collected by a digital still camera (Zhou & Robson 2001). This system was mounted on a 5.2 m high mast.

As the initial intention was to mount the sensing system onto a small unmanned aerial vehicle, the size and weight of the payload was the major limiting factor. The technologies that were reviewed in the literature that had potential to be adopted included the board video, 35 mm film and digital cameras. The weight limitation of the proposed system precluded the multiple video camera systems that have been used in conventional aircraft.

3.2 Requirements for a LCLA System for Precision Agriculture

Within the context of this research, there are numerous considerations to be evaluated to determine the suitability of a low-cost low-altitude (LCLA) remote sensing system for use in agriculture. The deployment and crop considerations, legislative requirements, and cost will be considered.

3.2.1 Deployment Considerations

Given the objectives of this research, the following parameters were considered important in the evaluation of the LCLA remote sensing system:

Functionality: The system should be able to acquire aerial images with coverage of at least 3 ha and a minimum spatial (pixel) resolution of 0.5 m.

Portability: The platform should be easily transportable to and from target areas. The platform had to fit into a utility vehicle or full-sized station wagon or similar. If assembly and disassembly was required to reduce the size, this had to be accomplished by one operator in no more than 10-15 minutes using only basic tools.

Simplicity: The system should be very simple to operate and maintain. The system should be made of readily available materials and components that can be easily repaired or replaced in the event of minor damage or failure.

Robustness: The system should be able to undertake multiple deployments and handle the environmental parameters (e.g. long grass, rough roads and trees) found in the close proximity to agricultural fields. As the sensing equipment is usually the most delicate and expensive items onboard the platform, the platform design had to provide ample protection for this equipment.

3.2.2 Crop Considerations

Remote sensing offers a non-invasive method of viewing crops. Lamb and Brown (2001) suggested that for successful mapping of vegetation, there are two main requirements: a) suitable differences in spectral reflectance or texture exist in the subject matter, and b) the remote sensing instrument has appropriate spatial and spectral resolution to detect such differences.

As this research is principally focused on mapping crop parameters (quantity, quality and maturity) and on discriminating between different crop types, the emphasis in this study has been placed on winter cereal crops where these parameters are of interest to make informed management decisions.

3.2.3 Legislative Requirements

The regulations covering civilian aviation in Australia are extensively set out by the Civil Aviation Safety Authority (CASA) in the *Civil Aviation Safety Regulations Act of 1998* (CASA 2003). The use of unmanned aerial vehicles falls within this category, and the particular areas of the regulations that deal with UAVs are contained in "*PART 10–Unmanned aircraft and rocket*". Other recommendations are available in the CASA Advisory Circular "*AC 101-1 Unmanned aircraft and rockets–unmanned aerial vehicle (UAV) operations, design specification, maintenance and training of human resources.*" These regulations cover all forms of UAV platforms including tethered balloons and kites, unmanned free balloons, and UAV systems. Sections of the regulations that cover the activities undertaken in this research have been summarised below.

A large UAV means any of the following:

(a) An unmanned airship with an envelope capacity greater than 100 cubic metres;
(b) An unmanned powered parachute with a launch mass greater than 150 kilograms;
(c) An unmanned aeroplane with a launch mass greater than 150 kilograms;
(d) An unmanned rotorcraft with a launch mass greater than 100 kilograms;
(e) An unmanned powered lift device with a launch mass greater than 100 kilograms.

A micro UAV means a UAV with a gross weight of 100 grams or less.
And a small UAV means a UAV that is neither a large UAV nor a micro UAV.
UAV means unmanned aircraft, other than a balloon or a kite.

For the purposes of this research, the UAV systems utilised will fall under the "small" category detailed above. The use of balloons will be covered in a later section. A summary of the operating regulations for a "small" UAV system are detailed below.

Operation near people

(1) A person must not operate a UAV within 30 metres of a person who is not directly associated with the operation of the UAV.
(2) Subregulation (1) does not apply in relation to a person who stands behind the UAV while it is taking off.
(3) Subregulation (1) also does not prevent the operation of a UAV airship within 30 metres of a person if the airship approaches no closer to the person than 10 metres horizontally and 30 feet vertically.

Where small UAVs may be operated

A person may operate a small UAV outside an approved area only if:

(a) Where the UAV is operated above 400 feet above ground level (AGL), the operator has CASA's approval to do so; and
(b) The UAV stays clear of populous areas.

The "approved area" mentioned in the above section is further defined as follows:

Approval of areas for operation of unmanned aircraft or rockets

(1) A person may apply to CASA for the approval of an area as an area for the operation of:

(a) Unmanned aircraft generally, or a particular class of unmanned aircraft; or
(b) Rockets.

(2) For paragraph (1) (a), the classes of unmanned aircraft are:

(a) Tethered balloons and kites;
(b) Unmanned free balloons;
(c) UAVs;
(d) Model aircraft.

(3) In considering whether to approve an area for any of those purposes, CASA must take into account the likely effect on the safety of air navigation of the operation of unmanned aircraft in, or the launching of rockets in or over, the area.

(4) An approval has effect from the time written notice of it is given to the applicant, or a later day or day and time stated in the approval.
(5) An approval may be expressed to have effect for a particular period (including a period of less than 1 day), or indefinitely.
(6) CASA may impose conditions on the approval in the interests of the safety of air navigation.
(7) If CASA approves an area under subregulation (1), it must publish details of the approval (including any condition) in a notice-to-airmen (NOTAM) or on an aeronautical chart.
(8) CASA may revoke the approval of an area, or change the conditions that apply to such an approval, in the interests of the safety of air navigation

The following section summarises further legal information relating to issues such as airspace restrictions, maximum operating heights, dropping or discharging of objects and weather and day limitations.

Maximum operating height
A person may operate an unmanned aircraft at above 400 feet AGL only:
(a) In an area approved under the regulation as an area for the operation of unmanned aircraft of the same class as the aircraft concerned, and in accordance with any conditions of the approval; or
(b) As otherwise permitted by this Part.

Dropping or discharging of things
A person must not cause a thing to be dropped or discharged from an unmanned aircraft in a way that creates a hazard to another aircraft, a person, or property.

Weather and day limitations
A person may operate an unmanned aircraft:
(a) In or into cloud; or
(b) At night; or
(c) In conditions other than visual meteorological conditions (VMC);
Only if permitted by another provision of this Part, or in accordance with an air traffic control direction.

All of these legal requirements are written specifically for Australian airspace and should be considered accordingly.

3.2.4 Costs

With the potential to provide agronomists and farm advisers with a tool to enable them to view crop attributes from above, the total capital cost of the system would need to be less than AUD$2000 in order to make it an attractive alternative to other forms of remote sensing. There should also be no substantial operating costs.

3.3 Preliminary Deployment and Assessment of a Sensor and Platform System

Several missions were undertaken in this study to evaluate the various components of the system. Details of these missions are listed in Table 3.3.

Table 3.3 The missions undertaken as part of the preliminary investigation.

Mission #	Date	Location	Platform	Sensor and description
1	June 2001	"TARMAC" Vale View -27.673°, 151.911°	Zephyr UAV	Single analogue video camera (resolution 500 x 500 pixels), video footage transmitted to ground and recorded on digital video camera, later used frame grabbing software to convert to still (*.jpg) that could be used later. Required 2 missions: one to capture colour, another to capture IR (IR using Hoya R72 filter). Problems with 'noise' in video footage and directionality of transmission signal. Showed potential; images captured of trees, sorghum crop, road etc.
2	July 2001	Clifton -27.934°, 151.908°	Zephyr UAV	Same system as mission #1, with targets, wheat crop
3	18 Mar 2003	"TARMAC" Vale View -27.673°, 151.911°	Magic UAV	Single Kodak DC3200 (1 megapixel colour still camera) in plane rather than video camera, images stored to onboard card, sorghum crop, many images collected
4	21 Mar 2003	UQ, Gatton -27.569°, 152.337°	Magic UAV	Same system as mission #3, with water and nutrition stress, 2 missions, one to capture colour (lots of useful images) another to capture IR. Not many images collected as blurry, shutter speeds too slow. (Camera needs to be modified to make more sensitive to IR)
5	6 June 2003	Toowoomba -27.535°, 151.932°	Camera on ground	Used Canon Powershot G2 (high end point and shoot) that gives camera parameters when images taken. Hence could gauge the effect of putting the Hoya R72 filter in front.

3.3.1 Platform System

During this preliminary investigation, relationships were formed with members of the 'Toowoomba Amateur Radio Model Aircraft Club' (TARMAC) who were interested in expanding the application of their hobby (i.e. flying remotely controlled aircraft) into a real-world situation. As a result, there were numerous aircraft on which to mount sensors and pilots to fly them. With this access to remotely controlled aircraft, particular emphasis was placed on this form of low-altitude unmanned platform, and the majority of testing conducted used this method.

Commissioning of the UAV

Radio controlled model aircraft had been used as an aerial platform to provide very low-cost very high-resolution imagery (Hardin & Jackson 2005; Quilter & Anderson 2000; Simpson *et al.* 2003). The aircraft to be utilised as remote sensing platforms were based on the selection criteria detailed in previous studies (Hardin & Jackson 2005; Hunt Jr. *et al.* 2005), namely, stability in wind, takeoff / landing requirements, carrying capacity and slow flight capability.

Hobbyist unmanned aerial vehicles were used during the preliminary evaluation. These radio-controlled aircraft were controlled remotely, with a hand-held transmitter and a receiver within the aircraft. The receiver controlled the corresponding servos that moved the control surfaces (rudder, ailerons, elevators and throttle) based on the position of joysticks on the transmitter, which in turn moved the plane.

Radio control electronics have three essential elements. The *transmitter* is the controller and has control sticks and switches at the users' finger tips. The *receiver* is mounted in the model and receives and processes the signal from the transmitter, translating it into signals that are sent to the *servos*. The number of servos installed in a model determines the number of channels that the radio must accommodate.

Several differing airframes were utilised in the testing of the unmanned aerial vehicle, however the radio control equipment (minimum of 6 channels and operating on the 36 MHz band) was common in all tests. The general minimum requirement of the airframe was a) a high-wing cabin-design (for stable slow flight), and b) balsa wood construction (ease of repairs) with a 2 m wingspan (to provide sufficient lift). A platform of this size needs to be powered by at least a 10 cc 4-stroke glow fuel (methanol) motor minimum (or equivalent) to carry a payload of approximately 0.75 kg (digital camera with associated batteries).

One of the major obstacles in utilising a UAV as a platform is the limitation in the payload that can be carried, as the larger the aircraft, the larger the payload. Larger model aircraft have inherent obstacles including transportation (wings larger than 2.2 m are difficult to fit into a standard station wagon) and require longer take-off and landing areas. However, larger aircraft are inherently more stable and less responsive (take longer to react to flying changes), hence easier to fly and easier to locate in the sky and judge the direction of travel.

Photographs of the various airframes are included in the sensor discussion sections following. An example of such an airframe, the unmanned aerial vehicle utilised on Mission #4, is shown in Figure 3.1.

Figure 3.1 The 'Magic' UAV and the 36 MHz radio control gear used at UQG (Mission #4).

3.3.2 Sensor System

Analogue Video Camera

With the reduction in cost, miniaturisation, and increase in the resolution of charged couple devices (CCDs), it is now possible to incorporate several of these devices into a single sensor that can be deployed on a remotely controlled aircraft. The literature showed that it is possible to use board video camera with transmitters, on-board a UAV, to transmit footage to the ground where it is stored on a VHS video tape (Simpson *et al.* 2003). Frame grabbing software could also be used to extract images to be analysed (Baron *et al.* 2002).

Based on these previous studies, miniature surveillance video cameras were initially chosen as the sensing system. An analogue video system (consisting a camera, transmitter and receiver) was purchased from OzSpy (details at http://www.ozspy.com.au). The specifications of the camera are detailed in Table 3.4. The video signal (1 volt peak-to-peak) from the video camera was relayed to the ground using a low power (10 mW) miniature video transmitter operating at 2.4 GHz. A video receiver, operating at the same frequency, was used on the ground to receive the signal. The information received was displayed and / or recorded on a tape in a *Sony Digital8 Handycam* video camera using the analogue input channel. The video transmitting and receiving components are shown in Figure 3.2 and the monitoring and recording system is shown in Figure 3.3. The initial test aircraft is shown in Figure 3.4.

Table 3.4 Black and white video camera specifications.

Pickup element	1/3" Sony B&W CCD image sensor
Number of pixels	512 (h) x 582 (w)
Resolution	400 TV lines
Minimum illumination	0.1 Lux /F2.0
S/N ratio	More than 48dB
Electronic shutter	1/50 to 1/100,000 sec
Lens	F5.5/F3.5
Lens angle	92°
Power consumption	120 mA
Dimensions	42 x 42 mm
Power	12 V
Weight	15 g

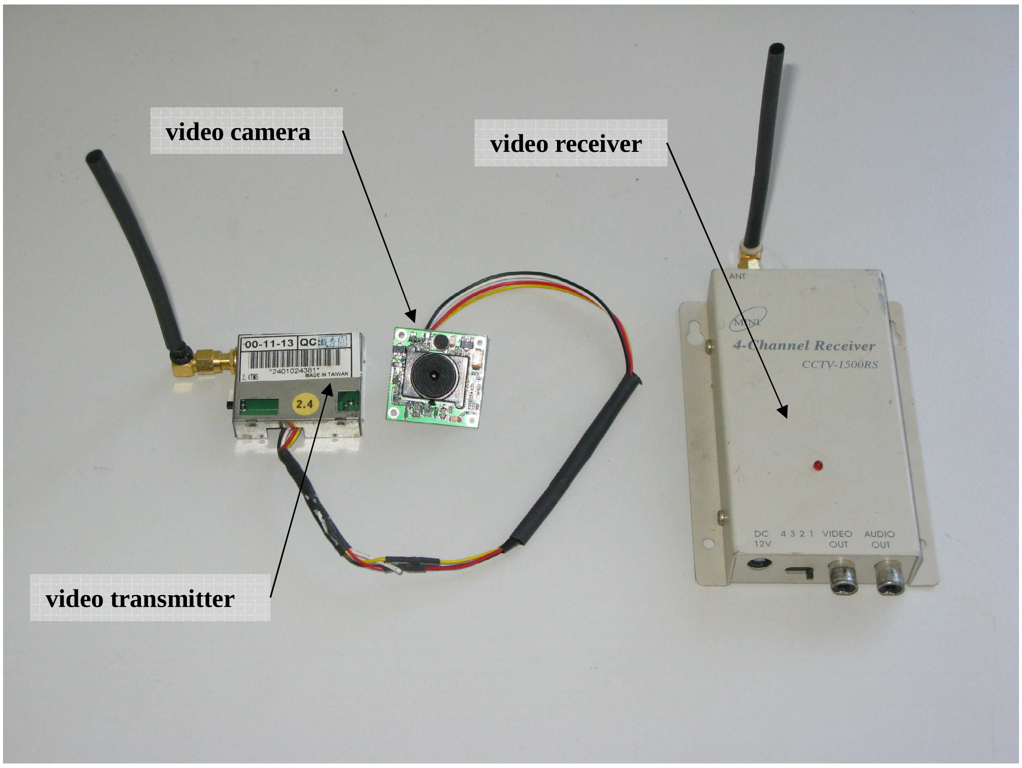

Figure 3.2 The components of the 2.4 GHz surveillance video system–transmitter (left), camera (middle) and receiver (right).

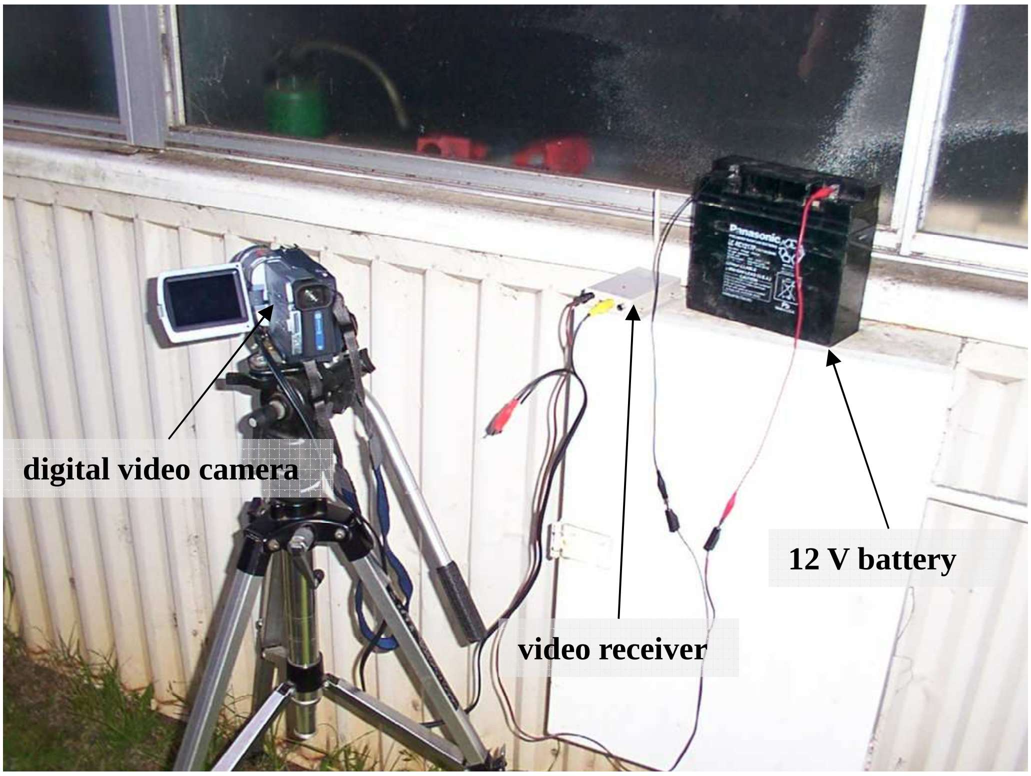

Figure 3.3 The analogue video stream is intercepted by the video receiver and recorded on the digital video recorder. The 12 V battery is powering the video receiver.

Figure 3.4 The ‘Zephyr’ UAV with wing removed (left), radio control gear (middle) and starter box containing fuel and battery charger (right) prior to deployment.

The testing was conducted with one monochrome camera and 2.4 GHz video transmitter (to transmit the footage to the ground) mounted on the ‘Zephyr’ UAV (Mission #1). The UAV was of a high wing construction utilising a 10 cc glow methanol motor and a 1.8 m wing. An auxiliary 12 V sealed lead-acid battery was also installed on the aircraft to supply power to the video transmission system. The video footage being transmitted to the ground was intercepted with a video receiver, and this analogue data stream was viewed and stored on the digital video camera. The position of the video camera and the UAV configuration is shown in Figure 3.5.

Figure 3.5 The ‘Zephyr’ UAV showing the hole for the mini video camera in the underside of the fuselage (between the two white strips).

The video footage was transferred from the digital video camera to a computer via a peripheral component interconnect (PCI) image capture card and Pinnacle Systems *‘Pinnacle Studio DV Version 7’* software (details at http://www.pinnaclesys.com/). The specifications and requirements of the software are given in Table 3.5. This software allowed images to be viewed ‘frame-by-frame’, with the most appropriate images being ‘frame-grabbed’ and stored on the hard drive of the computer. An example of such an image is shown in Figure 3.6.

Table 3.5 Specifications and computer requirements for Studio DV Version 7.

Hardware	Internal PCI
Capture resolution	720 x 576 (PAL)
Video format	DV
Analogue input	No
Analogue output	No
DV input	Yes
DV output	Yes
Operating system	Win 98SE / ME / 2000
30 min video	0.2 GB–6.5 GB
Minimum system requirements	PII 300 Mhz, 64 MB Ram, 80 Mb disk space

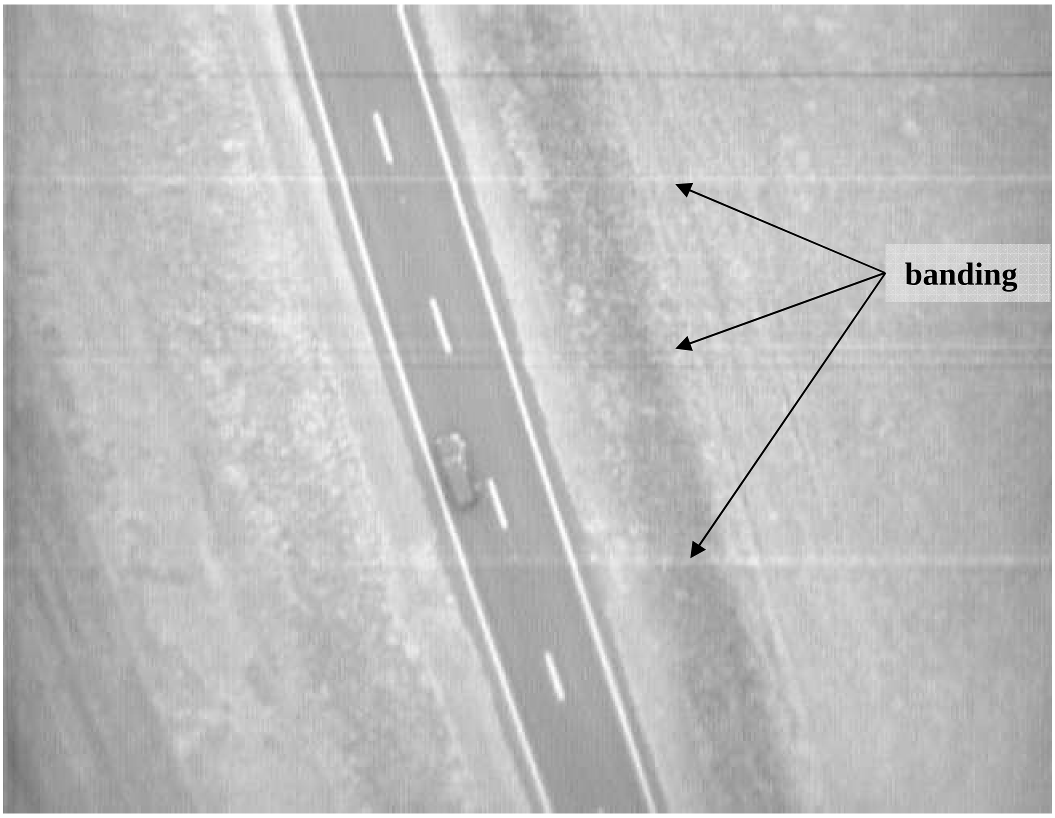

Figure 3.6 A frame-grabbed image showing a car driving along a dual carriage-way (note the banding in the image) acquired during Mission #1.

The colour portion of the spectrum provide useful information, however, the best relationships between imagery and green vegetation are found in the near infrared (Inoue *et al.* 2000). Numerous studies have used monochrome video cameras to record NIR information (Everitt *et al.* 1995; Inoue *et al.* 2000; Pearson *et al.* 1994).

Although the specifications were not available for the board video camera used in the preliminary evaluation, reviewing spectral responses for other published CCD imagers (such as the KODAK KAI-0340(Kodak 2008)) indicated that both colour and monochrome CCDs are sensitive to the NIR portion of the spectrum (see Figure 3.7).

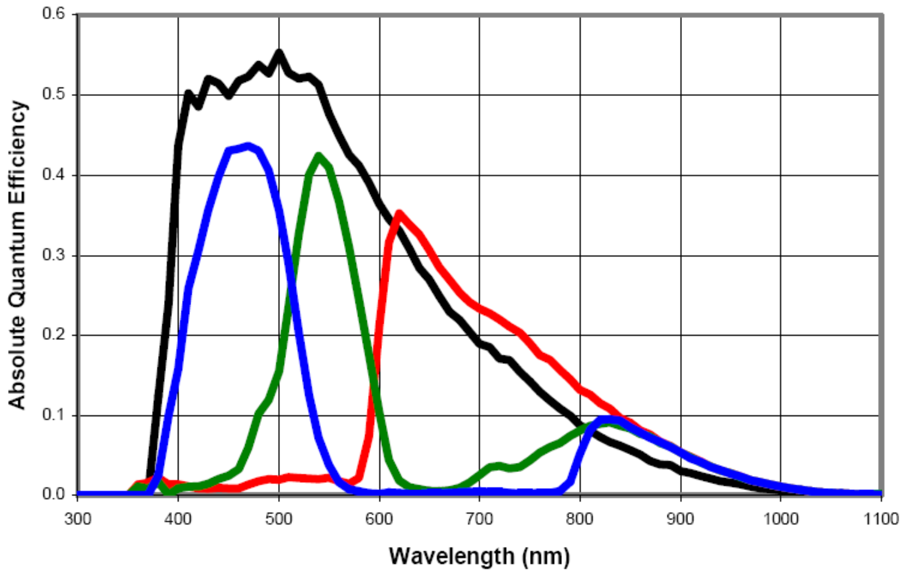

Figure 3.7 The spectral response for the Kodak KAI-0340 (Kodak 2008) showing the response for the monochrome sensor in black and that of the blue / green / red sensors in the corresponding colours.

In order to ensure that only the near-infrared light was incident on the CCD, narrow bandpass filters have been used (Baron *et al.* 2002), such as the Kodak Wratten 25 (Quilter & Anderson 2001) and Wratten 88a filters (Wright *et al.* 2003). In this study, the visible portion of the spectrum was excluded by placing a Hoya R72 filter (HOYA 2005) in front of the lens. Specifications of the R72 are shown in Figure 3.8. The R72 has a slight transmittance in the deep visible red just below the 700 nm visible-infrared boundary, 50% transmission at 720 nm and more than 90% transmittance over the 800–2200 nm range. An example of an NIR image obtained with the miniature video camera and Hoya R72 filter is shown in Figure 3.9 (note the high reflectance of trees in the centre of the image).

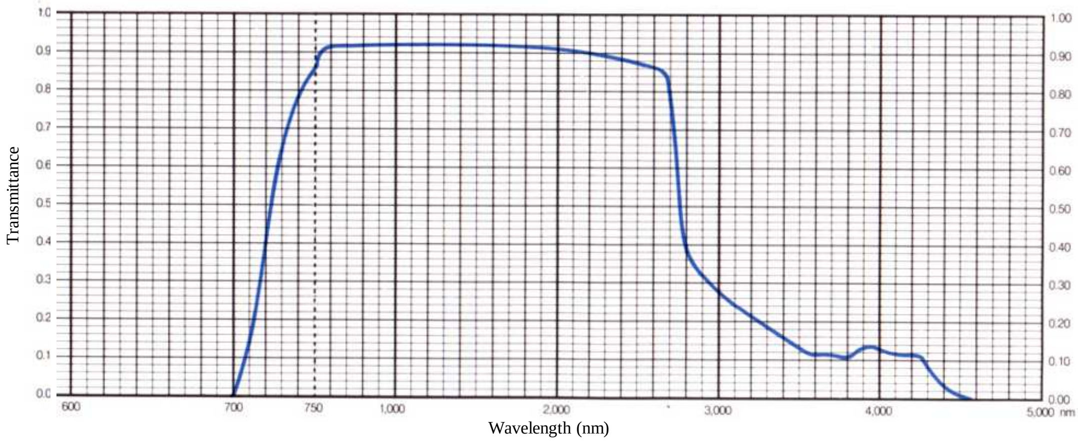

Figure 3.8 Transmittance of the Hoya R72 filter for the various wavelengths of light.

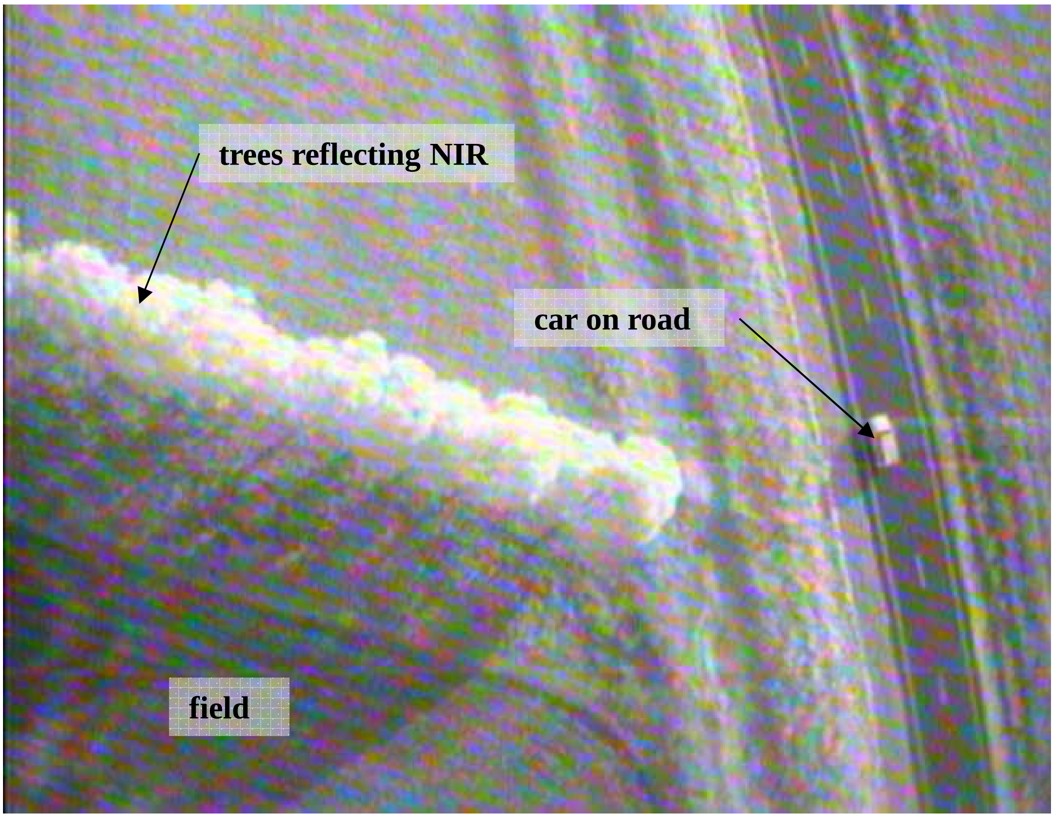

Figure 3.9 An NIR image collected with the video camera-frame grabber setup on Mission #1 (note the bright signature of the row of trees through the centre of the image).

With the successful capture of the monochrome and NIR images, initial plans were to follow other studies (Escobar *et al.* 1998) that had multiple cameras (possibly 6–10) with a specific narrow bandpass filter on each camera to give multispectral results. With the video footage containing 25 frames per second, a multiplexer was tested where 3–4 frames were recorded from each of 4 cameras with a 2–3 frame gap between successive camera images. Within a one second time-gap, several usable frames could be captured from each camera, representing nearly simultaneous image acquisition. This system had the potential to provide a light-weight multi-spectral sensor system.

As can be seen from the sample images (Figures 3.6 and 3.9), the resolution was not high (approximately 400 lines from the 512 x 582 pixels sensor). In order to get reasonable image resolution, the UAV had to be flown reasonably close to the ground, making the image coverage low. Noise was also evident in the images, possibly due to the directionality of the signal and electrical interference. There was also the issue of the large size of the video files once downloaded onto the computer– 30 minutes of video footage used in excess of 2 Gb of hard-disk space. For the above-mentioned reasons, this proposed system was not pursued past the evaluation phase.

35 mm Film Camera

Numerous studies have used 35 mm cameras to capture remotely sensed imagery (Quilter & Anderson 2001; Scharf & Lory 2000) as this is a mature technology. In other studies, researchers have commented that analogue (film) cameras were more economical than digital cameras (Light 1996), however this was in 1996 when digital cameras were at their infancy. As arrays have become larger and storage capacity becomes more affordable, digital cameras have become the preferred method (Wright *et al.* 2003) of capturing NIR and colour information. Film is problematical due to a) the care needed in handling the film and cost, b) inconsistency with developing, c) errors during scanning, and d) the need for a second camera if colour images are also required.

Such 35 mm systems were reviewed and an example of a low-cost remote sensing system that had been installed in a UAV (Spies, S 2002 pers. comm., 2 July) is shown in Figure 3.10. After considering the above problems, as well as the limitations on weight / space and the number of images able to be collected (a maximum of 36 exposures on colour and NIR film), this study did not pursue the 35 mm camera system.

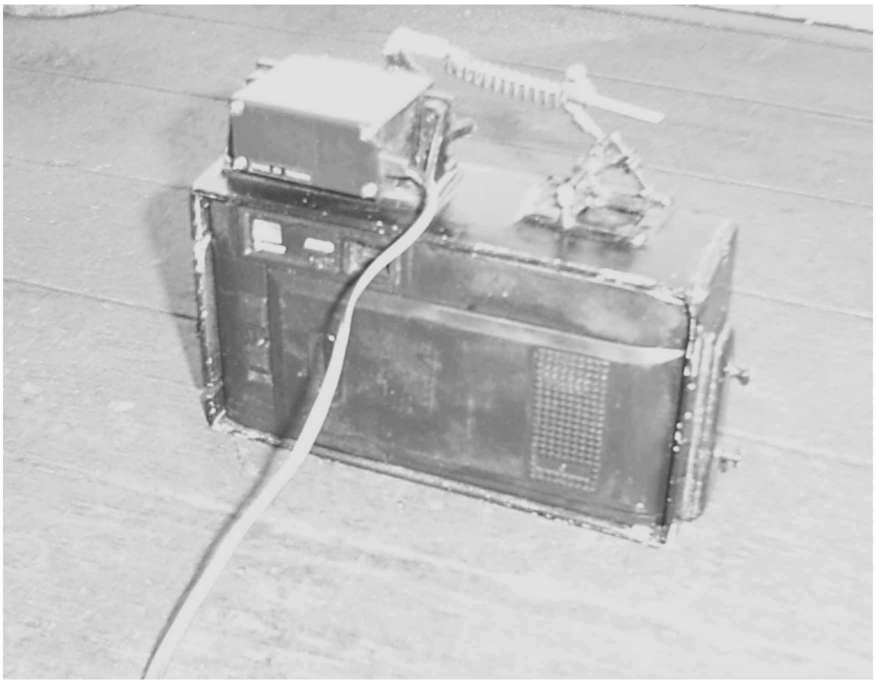

Figure 3.10 A 35 mm instamatic camera, installed in a mounting frame and utilising a servo to depress the shutter button, that was used to take images from a UAV.

Digital Camera

Digital cameras have been utilised in a number of remote sensing applications (also refer section 2.2.2): monitor informal townships (Mason *et al.* 1997), develop large scale elevation models (King *et al.* 1994), investigate the light environment beneath the forest canopy (Chapman 2007), detect changes in dynamic surficial environments (Baker *et al.* 2004), quantify lettuce head area (Hussain *et al.* 2008) and detect and map weeds (Yang *et al.* 2002).

Digital sensors are becoming a viable and reliable alternative to small-format analogue cameras (Mason *et al.* 1997) as they are compact, can cover the crop spectral range, and enable immediate reviewing of images. Digital cameras were thus reviewed with the intention of mounting such a camera on the unmanned aerial platform. In order to determine the minimum requirements of a sensor to suit this application, the low-end of the resolution range (approximately 1 megapixel in

2003), was targeted. The Kodak DC3200 (Eastman Kodak Company, Rochester, New York, USA) was chosen for its simplicity and ease of use, robustness, ability to mount a servo to depress shutter release button, and capacity to be powered by AA batteries (commonly available and easy to replace in the field). An image of the chosen camera is given in Figure 3.11 and its specifications are provided in Table 3.6.

In the initial configuration, the camera utilised its own internal batteries, with the images being stored to the 64 Mb CompactFlash card in the camera. The camera was initially attached to the underside of a UAV using rubber bands (see Figure 3.12).

Figure 3.11 The Kodak DC3200 digital camera.

Table 3.6 The specifications of the Kodak DC3200 digital still camera.

CCD Resolution		1,344 x 971 = 1.31 millions of pixels (total number of pixels)
Picture Resolution	**Best/ Better**	1,152 x 864 = 995,328 pixels
	Good	576 x 432 = 248,832 pixels
Colour		24-bit, millions of colors
Picture File Format		JPEG
Picture Storage	**Internal**	2 MB flash memory
	External	ATA-compatible CompactFlash card
Viewfinder		Virtual image
ASA/ISO Sensitivity		100
Flash Range		1.5 to 2.4 m
Lens	**Type**	Optical quality glass
	Maximum Aperture	F/3.6
	Focal Length	39 mm (equivalent to 35 mm camera) 5.4 mm (actual)
	Focus Distance (fixed)	0.6 m to infinity
Power	**Batteries**	(4) AA size 1.5-volt alkaline or AA size 1.2-volt Ni-MH rechargeable
Dimensions	**Width**	113 mm
	Depth	53 mm
	Height	81 mm
Weight		215 g without batteries

Figure 3.12 The single DC3200 camera attached to the underside of the 1.4 m wingspan 'Magic' UAV.

Image acquisition was initiated by activating a switch on the radio control and using this spare channel to activate a rotary servo to depress the shutter release button on top of the camera (see Figure 3.13). Servos are hobbyist remote control devices typically employed in radio-controlled models, where they are used to provide actuation for various mechanical systems such as the steering of a motor car, the flaps on an aeroplane, or the rudder of a boat. Radio control servos are composed of a direct current (DC) motor mechanically linked to a potentiometer. Pulse-width modulation signals, which are sent to the servo from the radio control gear, are translated into position commands by electronics inside the servo. When the servo is commanded to rotate, the DC motor is powered until the potentiometer reaches the value corresponding to the commanded position.

Images were captured with the above mentioned system on the 18th March 2003 (Mission #3) using the 'Magic' UAV (powered by an 8 cc glow methanol motor). In less than 30 minutes flying time, over 100 images were collected and a selection is shown as Figures 3.14–16. Figure 3.14 is an image taken from approximately 300 m above ground level and show the contoured layout of the cultivation, a dry creek bed and a dry dam. More detail is shown in Figure 3.15 as it was taken from a lower altitude (approximately 120 m above ground level). The influence of the tree line on the growing crop is clearly visible, as are the headlands and the greater biomass due to more fertile soil. The tree line in this image is the same as captured by the video system in Figure 3.9.

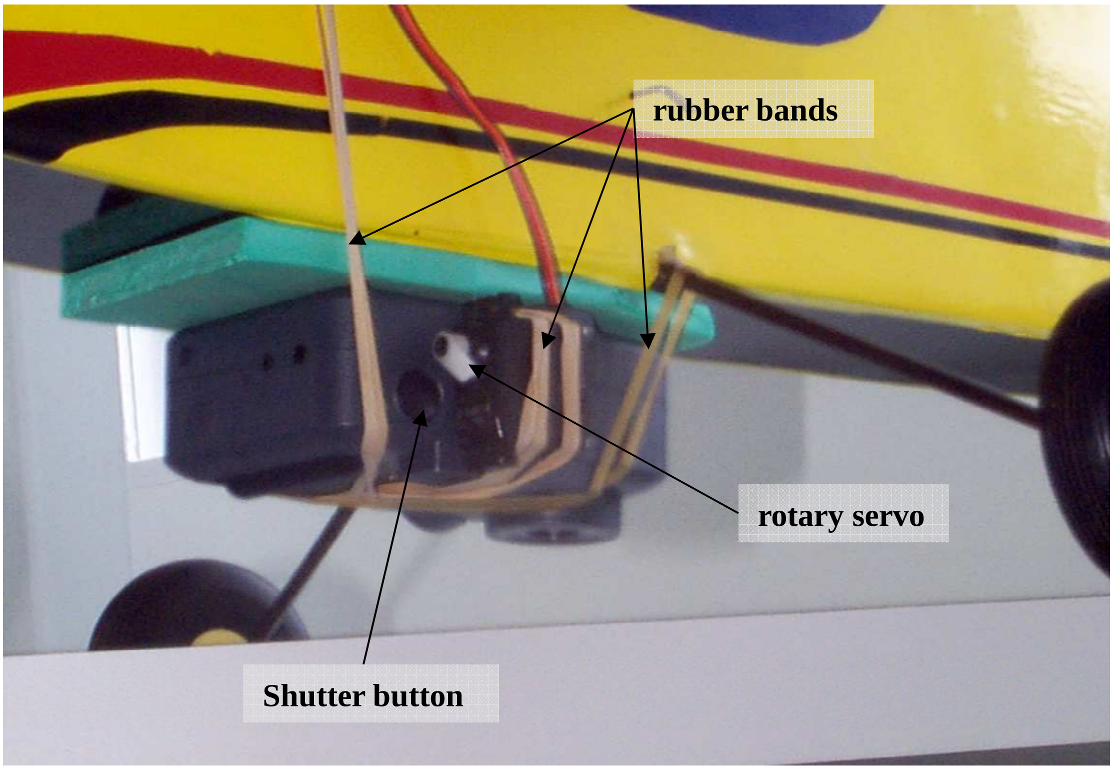

Figure 3.13 The DC3200 mounted underneath the UAV (note the rotary servo to depress the shutter release button).

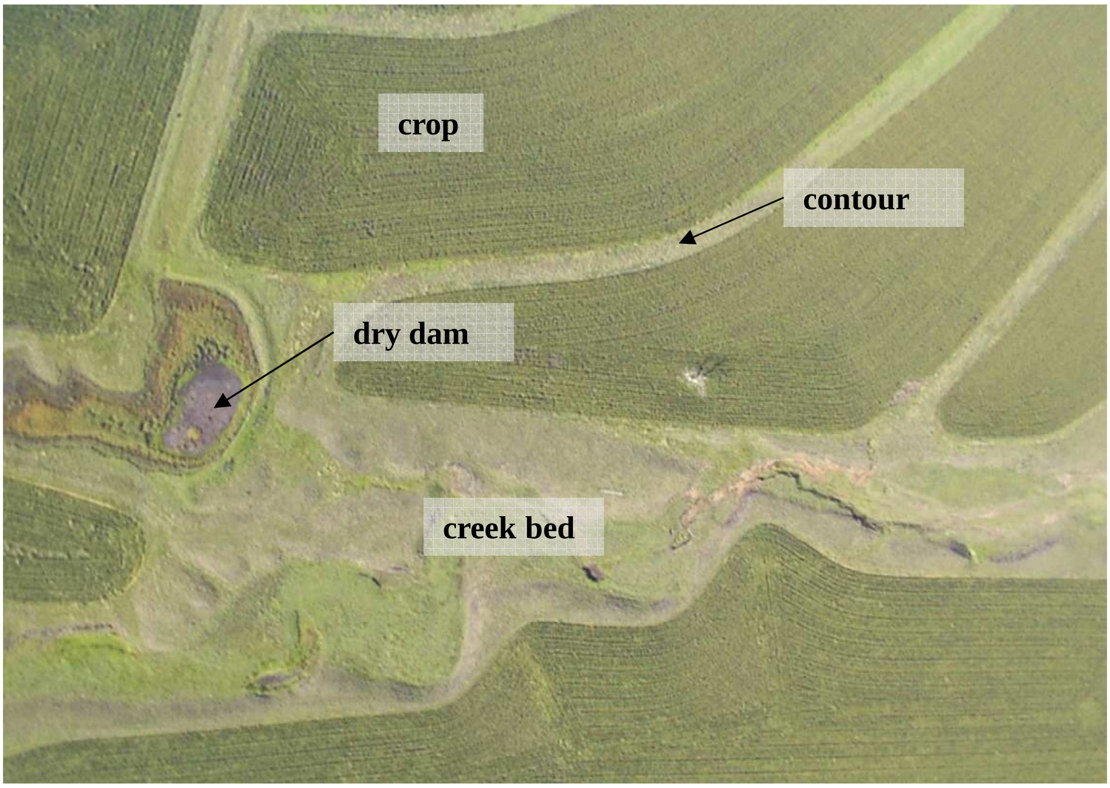

Figure 3.14 An image capture on Mission #3 showing the layout of the land.

Figure 3.15 More detailed information captured during Mission #3.

With the plane at an even lower altitude (approximately 50 m), individual plants can be clearly distinguished (Figure 3.16), as can planting misses, seed germination problems, weeds, grass areas, variation in topography and drainage directions. This test provided a proof-of-concept that off-the-shelf digital still camera can acquire images that have suitable spectral and spatial resolution to detect variations in crop parameters. Furthermore, it is robust, easy to use and relatively inexpensive. Further investigations were warranted.

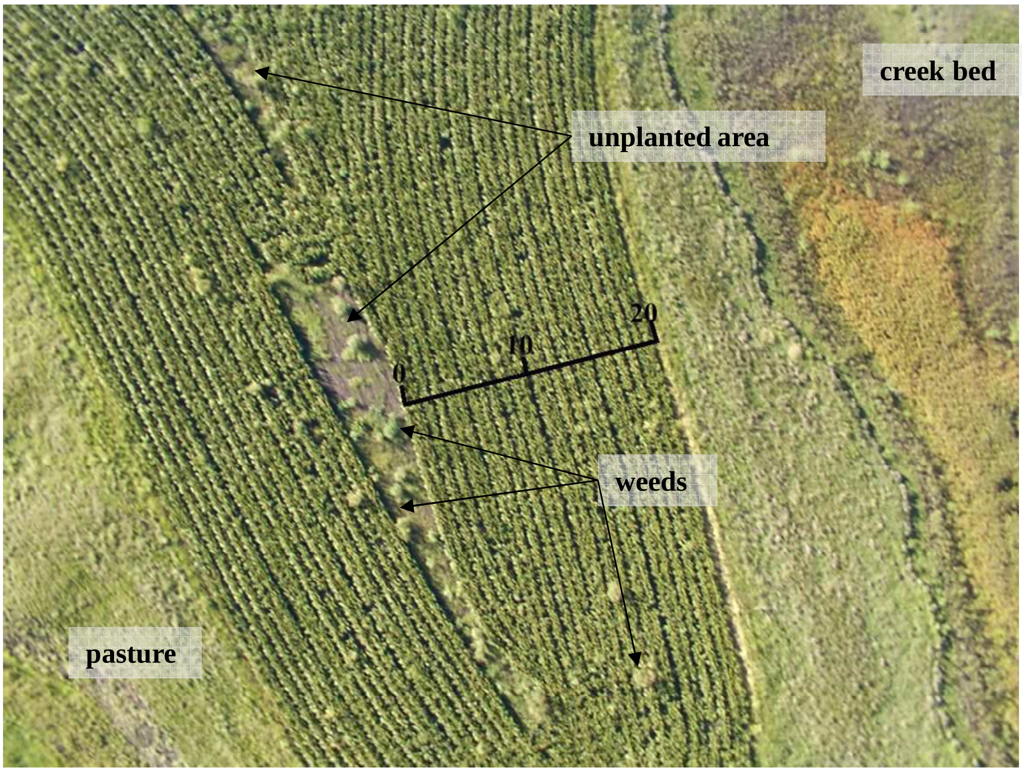

Figure 3.16 A low-level image collected during Mission #3.

Testing the DC3200's Sensitivity to NIR

Studies have indicated that most colour CCD imagers are sensitive to NIR light (Dean *et al.* 2000), as displayed in Figure 3.7. The DC3200 was not only able to capture colour information, but with the addition of the Hoya R72 filter (used previously with the board video camera), can also record the NIR information. Static images taken of a tree (see Figure 3.17) showed the level of information that can be captured in both the colour and the NIR using the DC3200 camera. Note the higher reflection values for all photosynthetic material in the image.

The concept of collecting colour and NIR images from the aerial platform was tested at a trial site at Gatton (Mission #4). Two flights were required as follows: a) the first flight to capture the colour images, and b) a second flight, with Hoya R72 in front of the lens, to capture the NIR images. Images were successfully captured on both missions. The colour images showed good detail with differing crop maturities, the effects of weeds and the presence of natural (power lines, fallow) and artificial features (car, ground control points), all being evident in Figure 3.18.

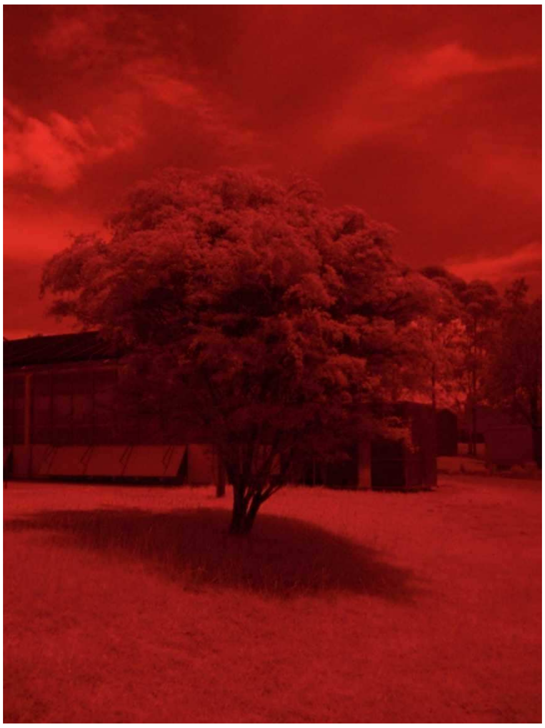

Figure 3.17 A photo of a tree in standard colour mode (left) and with a Hoya 'R72' filter placed in front of the camera (IR mode, right).

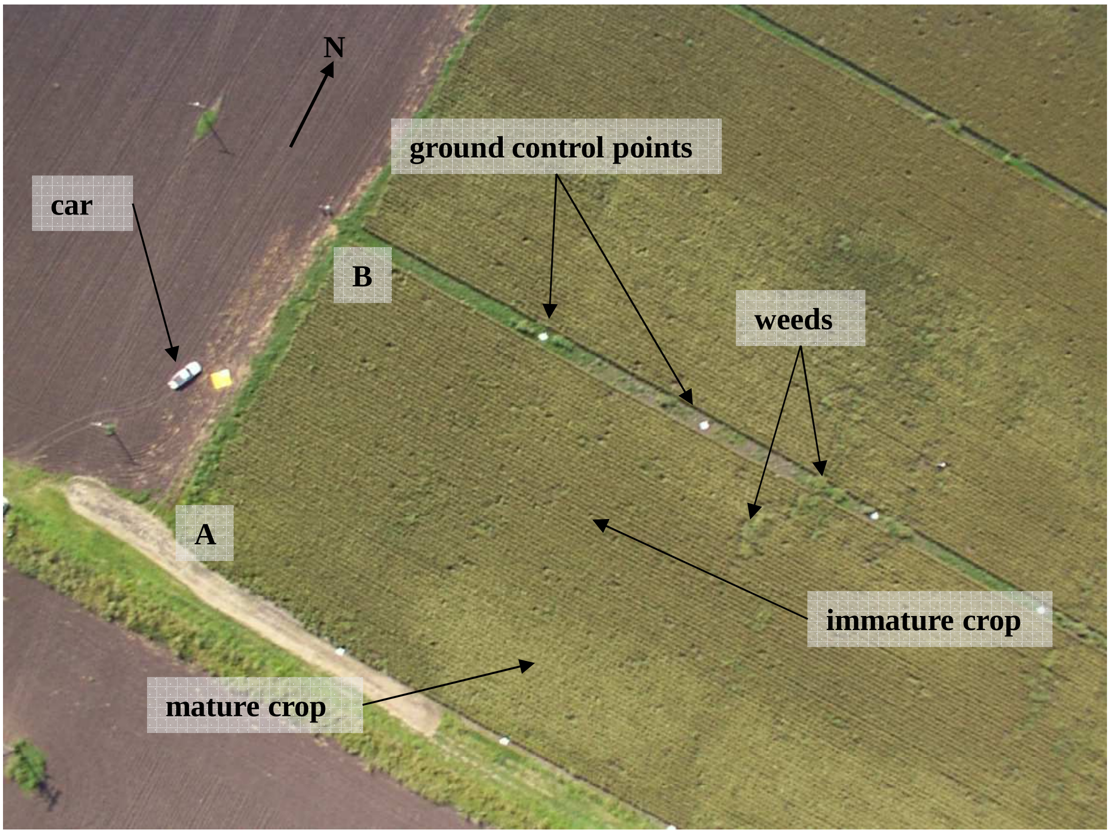

Figure 3.18 Features of the Gatton trial site (Mission #4), 21st March 2003.

In contrast to the colour images, the NIR images were very dark. The image shown in Figure 3.19 has been lightened using the image processing package Microsoft PhotoEditor to compensate for the low exposure resulting from the use of the Hoya R72. The blur evident in this image, and the darkness of the original image, resulted from insufficient light entering the camera and due to the speed of the aircraft. The camera tried to compensate for the lack of light by decreasing the shutter speed (hence the blur) to make a correct exposure. To overcome this problem, the sensitivity of the camera to NIR light had to be improved.

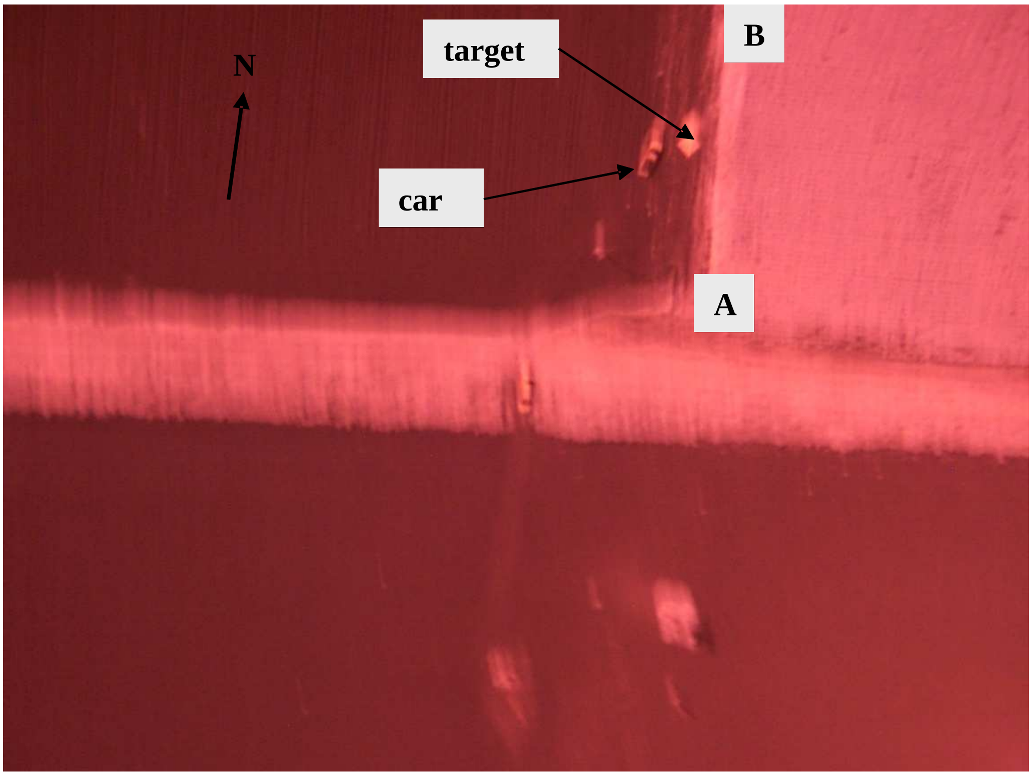

Figure 3.19 The NIR image of the same corner of the field as in Figure 3.18 (Note the location of the car and points A & B both images).

Effects of using the Hoya R72 on Standard Camera Operations

As the DC3200 camera only offered basic functionality, no camera settings were recorded with the images. An investigation was conducted to determine the effect of the Hoya R72 filter by using a more expensive camera with greater functionality (in this case a Canon PowerShot G2—camera specifications given in Table 3.7). Images were captured of the same subject, with and without the Hoya R72 filter being positioned in front of the lens. The resulting images are shown as Figure 3.20 (the

NIR image on the left with the colour on the right). The colour image was recorded 15 s after the NIR image with the camera set to automatic mode, where it controlled the exposure settings.

Table 3.7 The specifications of the Canon PowerShot G2 .

Effective pixels	Approx. 4-million-pixels		
Image sensor	1/1.8 inch CCD Approx. 4.1-million-pixels (total)		
Lens	7 (W) - 21 (T) mm (35mm film equivalent : 34 - 102 mm)		
	F2.0 (W) - F2.5 (T)		
Digital zoom	Up to approx. 3.6 times (Up to approximately 11 times in combination with the optical zoom)		
Optical viewfinder	Real-image optical zoom viewfinder		
	Field of view approx. 84 %		
LCD monitor	1.8 inch, low-temperature polycrystalline silicon TFT color LCD		
	Field of view 100 %		
Autofocus method	TTL autofocus (continuous or single)		
	Focus lock and Manual focus are available		
Focusing points	Switchable (Center or 3 selectable positions)		
Focusing range	Normal AF :	70 cm - infinity	
	Macro AF :	6 cm (W)/ 20 cm (T) - 70 cm	
	Manual focus :	6 cm (W)/ 20 cm (T) - infinity	
Shutter	Mechanical shutter + electronic shutter, 15 - 1/1000 sec		
Exposure control method	Program AE, Shutter-priority AE, Aperture-priority AE or Manual exposure control		
	AE lock is available		
Sensitivity	Auto, ISO 50, ISO 100, ISO 200 and ISO 400 equivalent		
White balance	TTL auto white balance, pre-set white balance (available settings: Daylight, Cloudy, Tungsten, Fluorescent, Fluorescent H or Flash) or Custom white balance		
Built-in flash	Flash range :	70 cm - 4.5 m (2.3 ft. - 14.8 ft.) (W)	
		70 cm - 3.6 m (2.3 ft. - 11.8 ft.) (T)	
		(When sensitivity is set to ISO 100 equivalent)	
Self-timer	Activates shutter after a 10-sec. delay		
Storage media	CompactFlash™ (CF) card (Type I and Type II)		
File format	Design rule for Camera File system, DPOF-compliant		
Image recording format	Still images :	JPEG or RAW	
	Movies :	AVI (Image data: Motion JPEG, Audio data: WAVE [monaural])	
JPEG compression	Super fine, Fine or Normal		
Number of recording pixels	Still images :	Large :	2272 x 1704 pixels
		Medium 1 :	1600 x 1200 pixels
		Medium 2 :	1024 x 768 pixels
		Small :	640 x 480 pixels
	Movies :	320 x 240 pixels	
		160 x 120 pixels	
		Approx. 15 frames/second	
Interface	Universal Serial Bus (USB), Audio/Video Output (NTSC or PAL selectable, monaural audio)		
Power Source	Rechargeable Lithium-ion battery (type: BP-511)		
Dimensions	121 (w) x 77 (h) x 64 (d) mm		
Weight	Approx. 425 g (camera body only)		

Figure 3.20 Image of tree with Hoya R72 filter (left) and in normal mode (right), (Mission #5).

There is no visual evidence of blur in the images in Figure 3.20 where the images were taken from the ground in a stationary and stable position. There is high reflection of NIR light from the foliage of the eucalypt tree and high absorption of NIR light by the blue sky.

To quantify the effects of the use of the Hoya R72, the properties for the images displayed in Figure 3.20 were viewed in the camera's image managing software (Canon Utilities ZoomBrowser EX 6.0). The properties are shown in Figure 3.21 with the NIR on the left and the colour on the right. The brightness histogram (green rectangle) and shooting information (blue oval) for each image are indicated in Figure 3.21. The effect of the Hoya R72 filter was to make the image proportionally darker (the shift to the left in the histogram, indicated by the green box) and to slow the shutter speed from 1/200th of a second in the standard colour image down to a quarter of a second for the NIR. The aperture also increased from an f5.6 in the NIR to an f2.0 in the colour.

It is assumed that the effect of the Hoya R72 on the DC3200 is similar to that of the G2 camera, and hence the reason why the wider aperture and slower shutter speed were required by the camera to make a correct exposure, as in Figure 3.19. This automatic camera compensation for the low light levels present when using the Hoya R72 would explain the dark and blurred images captured during the NIR image testing and the image shown in Figure 3.19.

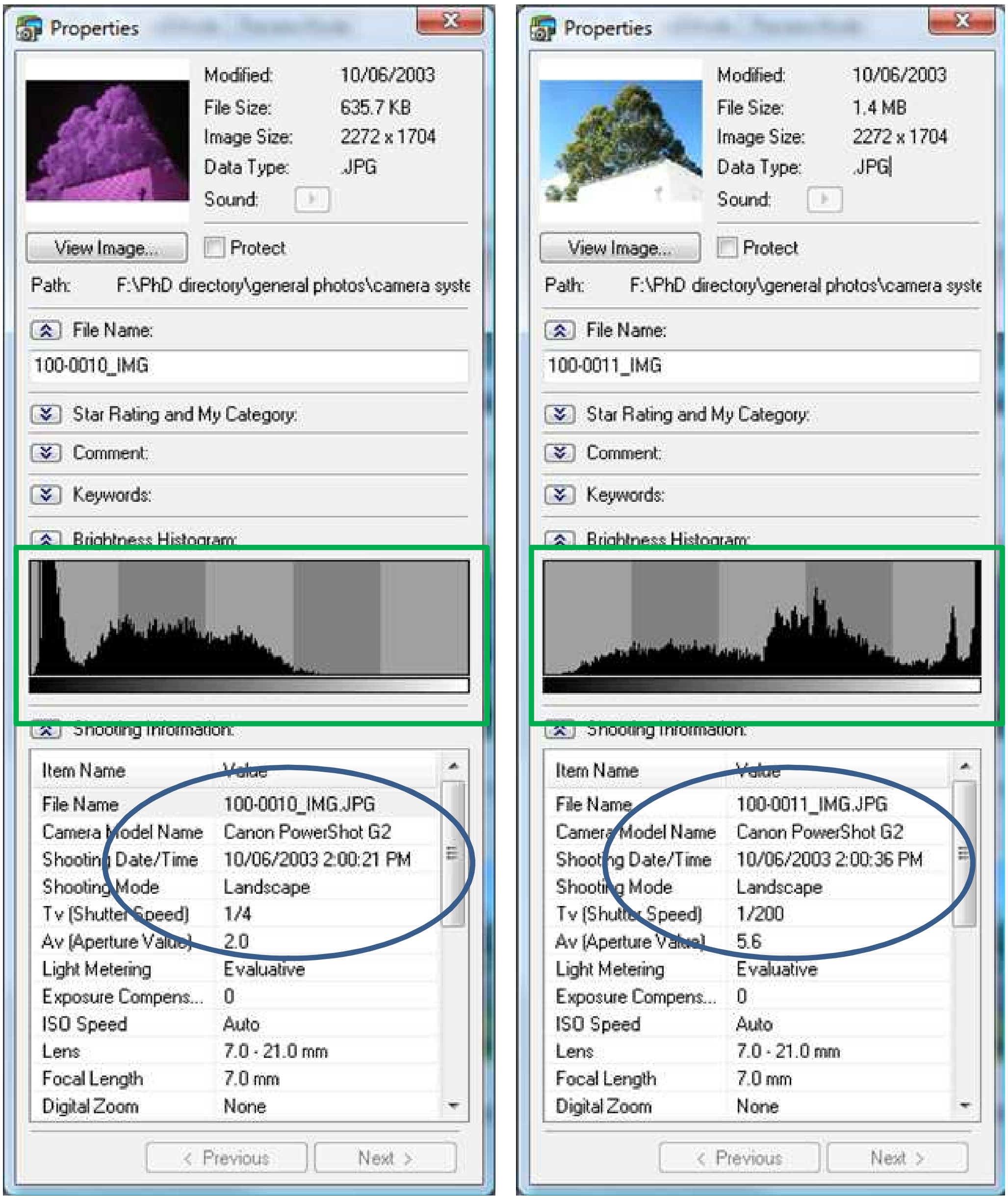

Figure 3.21 The camera settings when taking the images in Figure 3.20.

The charged couple device (CCD) has a degree of sensitivity in the NIR (refer section 3.2.2 and Figure 3.7). Digital cameras are used to record images that correspond with what is perceived by the human eye. As the human eye is not sensitive to NIR, digital cameras have been modified to decrease the sensitivity to NIR, and thus better represent the capabilities of the human eye. Hence, a NIR blocking filter is placed in front of the CCD to give the most acceptable colour representation. Details of how it is possible to remove this filter to increase sensitivity to NIR is provided on the internet (Wooten 2003). To investigate the enhanced spectral response that could be expected from removing the NIR blocking filter from the Kodak DC3200 camera, specifications for other published sensors were reviewed. One such example is shown in Figure 3.22. Note the enhance sensitivity, particularly in the NIR region, by removing the NIR blocking filter.

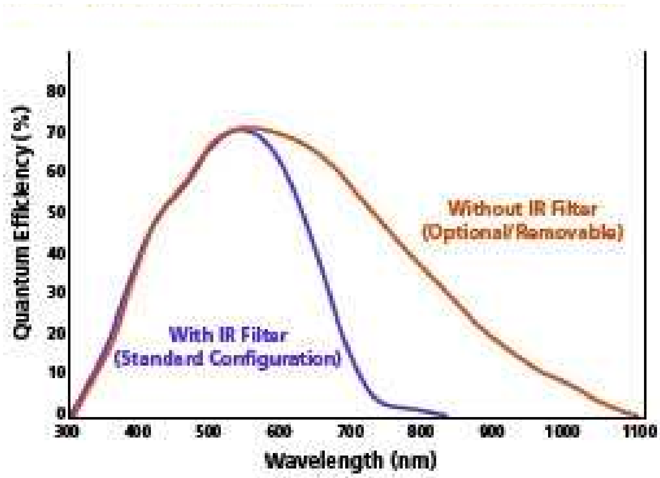

Figure 3.22 Spectral response with and without IR cut-out (Vaytek 2003)

With IR Cut-Out Filter Removed from DC3200

The procedure of removing the ‘blue’ NIR cut-out filter (shown in Figure 3.23) was performed on the DC3200. The removal of the filter and replacing it with clear glass (so that the optical path was unaltered) was undertaken by camera repair technicians, who also configured the cameras for electronic (remote) activation and external powering. With these modifications, the operations of the cameras were then checked to ensure the manufacturer’s operating tolerances were maintained.

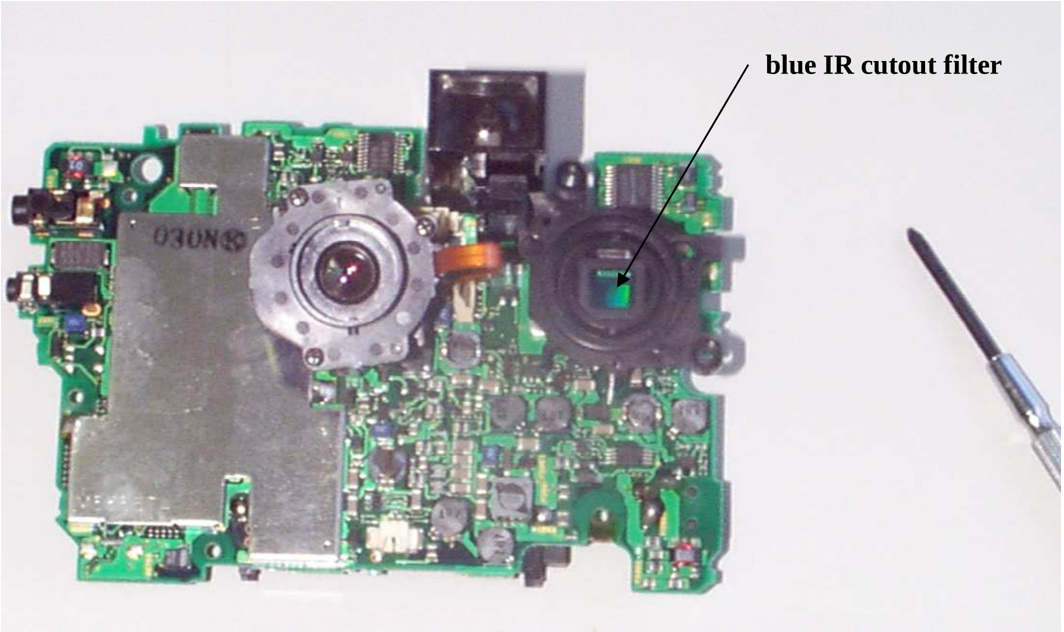

Figure 3.23 The DC 3200 pulled apart showing the 'blue' IR cut-out filter.

Electronically Triggering the Camera

Using the servo to depress the shutter-release button was not an accurate and repeatable method of initiating image acquisition due to the several seconds delay resident in servo rotation and the difficulty of attaching the servo to the camera. Also, relying on the pilot of the UAV to initiate image acquisition distracted them from their primary objective—flying the UAV. Rather than using the servo to physically depress the shutter button, the output to the servo was investigated as a potential method of electronically activating the camera.

A separate 2-channel radio control system (*HiTech* brand, operating at 29 MHz), operating independently of the avionics system, was accessed with the intention of using one of the servo outputs to control the image acquisition. This required an additional receiver on the aircraft.

The receiver output from the 29 MHz radio control system was tested in the laboratory (see Figure 3.24) and was a typical servo output, i.e. 50 Hz square wave. The initial approach was to detect the change in pulse width (achieved by moving the throttle / rudder stick) to initiate image capture. As the 2-channel radio equipment was low-cost, the output was relatively noisy (Figure 3.25). Rather than trying to measure the pulse width (to detect a change), it proved simpler to consider the presence and absence of signal, achieved by disconnecting and reconnecting power via a normally closed push button switch. To monitor the signal, a complementary metal-oxide semiconductor (CMOS) re-triggerable monostable was used as a missing pulse detector, which then triggered a second monostable (one shot) to produce a single pulse. A transistor circuit provided the necessary current to operate the relay that triggered the camera. If and when the first monostable failed to receive a pulse from the receiver within 100 ms, resulting from the button being pressed on the transmitter, the image acquisition sequence would be initiated and an image recorded on the camera.

Figure 3.24 Testing the output of the 29 MHz 2 channel radio control transmitter.

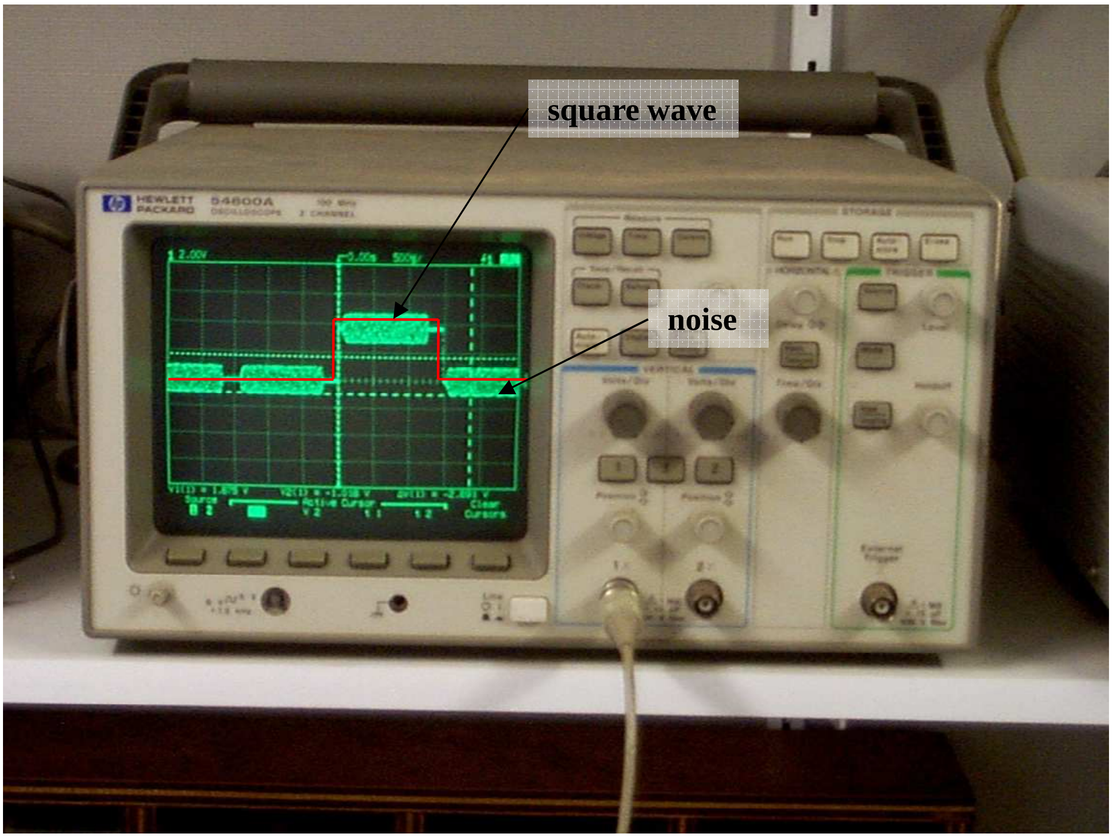

Figure 3.25 The change in the output signal from the receiver when the throttle / rudder stick was moved. The output was noisy, making it difficult to measure.

3.4 Conclusions

This chapter has shown that remotely controlled aircraft have the capacity to provide a stable platform that the average hobbyist has the skills and ability to fly. Off-the-shelf digital cameras can acquire useful images when there is sufficient light to make an acceptable exposure. The same digital cameras can be remotely triggered using a low-cost remote control equipment that is independent of the flight control that has no extra imposition on the pilot. This functionality is achievable with relatively inexpensive equipment with the total cost less than the targeted maximum of $2000. Such a system is also small enough to meet the size requirement (i.e. can be carried in a station wagon) with standard hobbyist size model planes still having ample capacity to lift the sensors, hence meeting all the platform requirements.

In order to fully utilise digital cameras as a low-cost low-altitude (LCLA) remote sensing system on these platforms, further development is needed to allow the simultaneous capture of images in the colour and near infrared portion of the spectrum. This will allow the continued development and the integration of the total system.

Chapter 4

Developing a Low-Cost Low-Altitude Remote Sensing System

The previous chapter presented a preliminary investigation and evaluation of the various components that had potential for a low-cost imaging system. Chapter 4 builds on that research and details the development of the low-cost low-altitude (LCLA) remote sensing system for use in capturing selected attributes of agricultural crops.

4.1 The Case for the Two-Camera System

4.1.1 Justification for Adoption

The case has already been made in Chapter 3 for a two-camera remote sensing system to overcome the problems of making two separate flights with the remotely controlled aircraft (RCA) in order to capture the colour and near infrared information. As the inherent proximity to obstacles and the dynamics of the flight associated with the take-off and landing of unmanned aerial vehicles (UAV) make these the most likely phases for which an incident to occur (Clothier, R. 2008, pers. comm., 14 October), halving the number of flights much reduces the crash risk. These two activities (i.e. take-off and landing) also place the highest demand on operators, with reports showing that most accidents attributed to human-error occur during these activities. Additionally, from an image analysis perspective, there is also the desire to capture the colour / near infrared images simultaneously. This can overcome lighting and altitude differences, as well as to ensure the same coverage of the subject area and the same sequencing of the images collected.

4.1.2 Specifications for the Improved System

In addition to the desired specification detailed in the deployment considerations (Chapter 3.2.1), the LCLA remote sensing system should be capable of meeting the spectral, spatial and temporal requirements of a system to capture information for agriculture. These requirements include; decimetre pixel resolution, the ability to record information for the colour and near infrared portion of the spectrum, and a temporal resolution to allow daily captures if required. Furthermore, the system should allow images to be downloaded and interrogated immediately upon the platform returning to ground to ensure the coverage of the target area.

4.1.3 Missions Undertaken with the LCLA Remote Sensing System

The missions undertaken during the development and deployment of the LCLA (2-camera) remote sensing system are documented in Table 4.1.

4.2 Development of the Data Acquisition System

The data acquisition system has two components: the sensor system and the platform on which it is deployed. The development of the platform and sensor system will be detailed separately.

Table 4.1 Missions with the LCLA remote sensing system

Mission #	Date	Location	Platform	Sensor and Description
7	3 June 2003	Toowoomba -27.535º, 151.932º	Cameras out car window	Testing of 2-camera system, remote triggering and with IR blocking filter removed from one camera to increase sensitivity in the IR.
8	12 June 2003	"TARMAC" Vale View -27.672º, 151.911º	Hannibal UAV	Testing of the 2-camera system described above, but from an aerial platform.
9	14 June 2003	"Argyle" Macalister -26.996º, 151.032º	He balloon	Real-world testing of the 2-camera system. No experienced UAV pilot, hence use of helium balloon. Crop at a very early stage. Tried again at later growth stage.
10	1 Aug 2003	"Argyle" Macalister -26.996º, 151.032º	Hannibal UAV	Same field as in previous test. Problems encountered with cameras powering-down due to inactivity, resulting in differing number of images on each camera.
11	2 Sept 2003	"Colonsay" Cecil Plains -27.501º, 151.392º	He balloon	2-camera sensor modified to overcome power-down issue. Nutrition trial with 0–120 kg/ha N applied. Many useful images collected and processed. Single tether line.
12	3 Oct 2003	Suncorp Stadium Brisbane -27.465º, 153.009º	He balloon	Sensor as above. Looked for difference in grass reflectance. Due to conditions, sensor thrashed around, camera mount broke and sensors hit the ground.
13	14 Oct 2003	"Colonsay" Cecil Plains -27.501º, 151.392º	He balloon	Sensor as above. Modified tether-line attachment resulting in more control. Lots of images collected and data analysed. Paper published in *Computers and Electronics in Agriculture* 2007
14	28 Jan 2004	Sandalwood feedlot, Bowenville -27.072º, 151.522º	He balloon	System as above, but with dual tether lines for added stability. Quantified wet areas in cattle feedlot and linked to odour generation.
15	3 Feb 2004	Kingsthorpe -27.551º, 151.777º	He balloon	System as above. Investigated ability of the system to map weed infestations, Undergraduate study at USQ.
16	12 Feb 2004	ANZ Stadium Brisbane -27.558º, 153.062º	He balloon	System as above. Looked for difference in grass reflectance and correlated with turf traction results.
17	3 Mar 2004	Postle St Toowoomba -27.618º, 151.917º	He balloon	System as above. Hail damage assessment. Undergraduate study at USQ.
18	22 Aug 2004	Wamuran Sunshine Coast -27.033º, 152.864º	He balloon	System as above. Quantified spatial distribution of pineapples.
19	12 Aug 2004	Nindigully Western Qld -28.476º, 148.724º	He balloon	System as above. Species trial with crop at early stage of growth. Conditions very windy and resulted in cameras being dislodged and hitting ground.
20	13 Sept 2004	Nindigully -28.476º, 148.724º	He balloon	2nd attempt at acquisition. Crop near to flowering. Useful images obtained, processed and analysed.
21	4 Oct 2004	"Tullona" Croppa Ck, NSW	He balloon	System as above. Very windy conditions. Due to large distance travelled, image acquisition attempted. Wind was that strong that both tether lines broke and ***balloon along with sensor was lost.***

…continued next page

…continued from previous page

22	20 June 2005	Wamuran Sunshine Coast -27.033º, 152.864º	10 m mast	A single DC3200 camera, positioned atop a 10 m mast, was used to image pineapples. Camera was powered and triggered by a cable that ran to the ground.
23	20 Aug 2005	"Daybreak" Dalby -27.254º, 151.283º	Milne UAV	Test flight of new 5 megapixel 2-camera sensor that was installed in a purpose built UAV.
24	4 Oct 2005	"Lundavra" Goondiwindi -28.056º, 150.087º	Milne UAV	System as above. Wheat / barley variety trial. Planned compared to Specterra aerial imagery. Unfortunately too late in growing season for relationships to be determined. However, crop maturity assessment undertaken.
25	18 Apr 2006	"Macquarie Downs" Leyburn -27.922º, 151.563º	Milne UAV	System as above. Images acquired of irrigated cotton that was near to picking. Investigated ability to detect nodes above cracked-boll.
26	29 Mar 2007	"Daneene" Dalby -27.230º, 151.168º	Milne UAV	System as above. Investigated nodes above cracked-boll in cotton due to various irrigation regimes. Unfortunately, no yield monitor data as planned. No further processing.
27	29 Apr 2007	DPI Gatton Research Station -27.545º, 152.332º	He balloon	Sensor as above, but He balloon utilised as platform. Imagery of lettuce under various fertiliser regimes. Showed good potential as an agronomic tool. More data to be collected later in the year
28	17 Aug – 8 Oct 2007	DPI Gatton Research Station -27.545º, 152.332º	10 m mast	Sensor as above, however mounted atop 10 m mast. Imagery of lettuce under various irrigation regimes. Several acquisitions performed during the growing season. Compared to other agronomic data collected. Paper in proceedings of the *14th Australian Agronomy Conference,* 2008.
29	5 Mar 2008	Watts Bridge Aerodrome -27.098º, 152.460º	QUT Boomerang UAV	Tested autopilot and the ability to autonomously trigger sensor when over waypoints. Sensor modified to be triggered by autopilot.

4.2.1 Platform

As presented in the preliminary evaluation of the system (Chapter 3), extensive use was made of hobbyist remotely-controlled aircraft. This use of remotely controlled aircraft, as the platform on which to deploy the sensor, continued during the development of the LCLA system. However, there were some instances where remote-controlled aircraft and / or experienced pilots were not available, or the site was not appropriate for aircraft use. Alternative platform configurations were evaluated and the same sensor system could be deployed underneath a helium balloon or mounted on top of a 10 m mast. The skill level needed to fly a helium balloon or to use a mast was much reduced compared to that of a remotely controlled aircraft and, depending on the target area, made this system a viable alternative.

Remotely controlled aircraft

Various remotely controlled aircraft were utilised as a platform for the LCLA remote sensing system. In each case, the aircraft was flown by an experienced operator with a second person (with separate radio control gear) acting as the image acquisition officer. In this development phase, the sensor was mounted underneath the fuselage of the aircraft and latex rubber bands were utilised to attach the sensor. This form of attachment also allowed for easy removal of the sensor system (refer Figure 3.12).

The system has continued to develop and has also been installed inside the aircraft (see section 4.2.3). The final configuration (a purpose built pod attached under the fuselage) will be discussed in section 5.4.3.

Balloon

A balloon platform was used on missions where the deployment of unmanned aerial vehicles (UAV) was not possible due to either the equipment being inoperable (due to mishaps), the pilot was unavailable, or the location or size of the target area did not suit the use of UAVs. A 1.7 m diameter latex balloon, inflated with balloon-grade helium, provided sufficient lift to carry in excess of 1.0 kg of payload.

This platform was controlled by tether-lines that were attached to the balloon, with the sensor being suspended underneath. The tether-lines were played out until the desired height for recording an image was reached. This height was controlled by viewing the video downlink footage. The balloon was retrieved by winding in the tether-lines and the images downloaded and viewed on a laptop computer whilst at location.

The details of this balloon platform system are given in the 'Systems Deployment' section 5.2.2.

4.2.2 1.0 Megapixel Digital Camera Sensor System

During the preliminary evaluation of the sensor system, the capabilities of the DC3200 camera were determined (refer section 3.3.2). With the DC3200's proven ability to capture near infrared information, along with its simplicity, ease of use and robustness, the use of this camera continued during the development phase. In order to provide a colour and near infrared sensor system, a 2-camera system was developed.

The multispectral sensor system (see Figure 4.1) consisted of two Kodak DC3200 digital cameras (1.0 megapixel), a small (25 mm x 25 mm) black-and-white analogue video camera and transmitter (used for positioning), two 6-volt battery packs, a radio controlled receiver, and a small printed circuit board.

Powering the 2-camera system

Two DC3200 cameras, which had been modified to be triggered remotely and to increase the sensitivity to the near infrared, were incorporated into the 2-camera system shown in Figure 4.1. The cameras were mounted in a balsawood frame to minimise the overall weight of the system. Each camera was powered with a separate 5-cell AA NiMH battery pack (6 volt direct current). Due to the 12 volt direct current requirement of the video camera and transmitter, the pack was also connected in series to meet this requirement. This also shared the power load between the two battery packs.

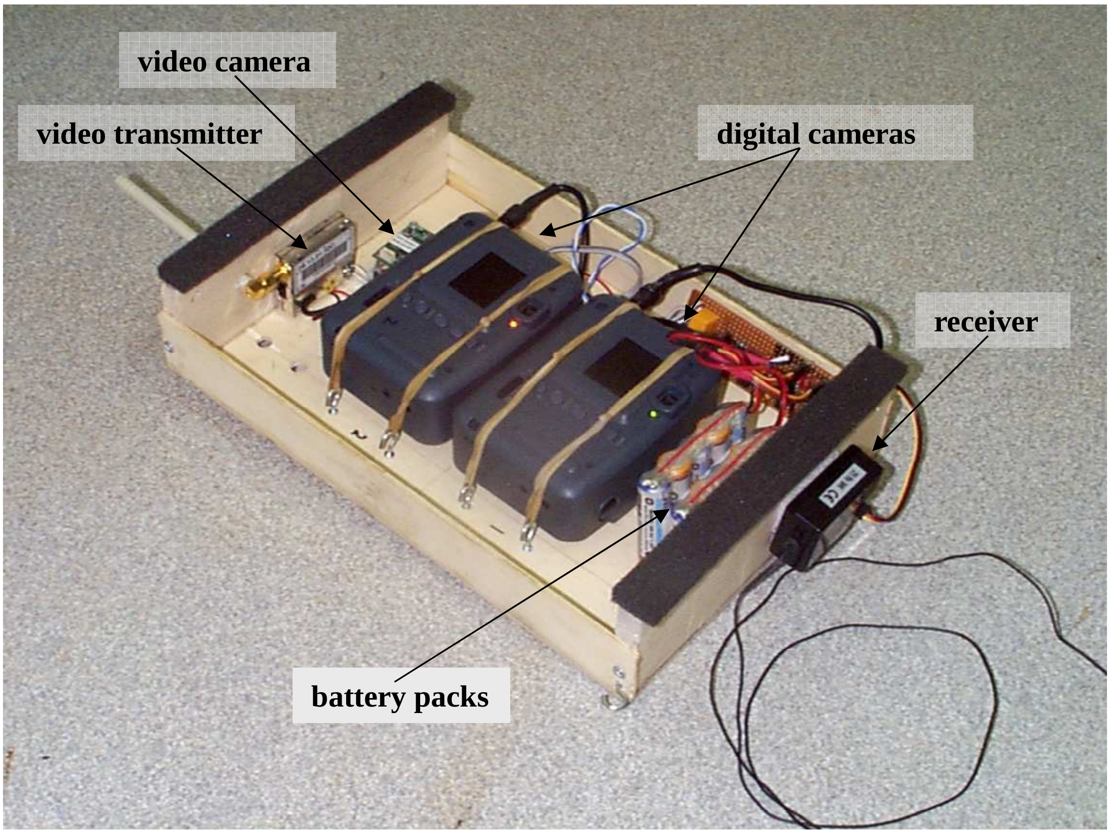

Figure 4.1 The 2-camera sensor system.

Triggering the 2-camera system

The method used to trigger the 2-camera system once again used the signal from a spare channel on the radio control equipment. As with the system described in section 3.3.2, the signal was monitored by using a CMOS re-triggerable monostable as a missing pulse detector. This in turn triggered a second monostable (one shot) to produce a single pulse. A transistor circuit was used to provide the necessary current to operate a double-pole double-throw relay to activate the camera. The use of this type of relay allowed complete electrical isolation between the digital cameras. If the first monostable failed to receive a pulse within 100 ms from the receiver, resultant from the button being pressed on the transmitter, the acquisition sequence would be initiated to capture an image. The data was stored to the 64 Mb CompactFlash card inserted into each camera.

On the completion of the mission, the two CompactFlash cards were removed from the cameras and each inserted into a Personal Computer Memory Card International Association (PCMCIA) picture card adapter that was in-turn inserted into a PCMCIA Type II slot on a laptop computer. This enabled both the colour and the near-infrared images to be viewed and checked for consistency and coverage of the target area.

Ground-based testing

On 3 June 2003, the sensing system was initially tested by driving a vehicle around a semi-rural area collecting images with the sensor directed out the open car window. Images were acquired with the vehicle travelling at approximately 17 m/s (60 kph) in order to investigate the effects of motion blur that would be encountered when mounted on the aircraft. By mistake, both cameras had been modified to increase the sensitivity to near infrared (NIR). In this test, one camera was used to capture NIR images (with the use of the Hoya R72 filter) with the other camera capturing a colour-near infrared (CIR) composite.

Image was taken approximately every 30 s, with a total of 66 images captured on each camera. As can be seen from Figure 4.2, the cameras captured fine detail of near objects (the wire pattern in the fence—approximately 10 m away) and far objects (vegetation). Although this was not the preferred configuration, it however indicated that by removing the IR cutout filter, the sensitivity of the DC3200 was increased and the problems with blurring of images (due to a combination of high aperture and slow shutter speed) eliminated.

Following this testing and the subsequent aerial testing at ‘TARMAC’, the colour-near infrared composite camera was replaced with a partially modified (only for remote triggering) conventional colour camera. The second ‘NIR sensitive’ camera was kept as a spare. All further testing was conducted with the two camera sensor that consisted of one colour and one NIR camera.

Figure 4.2 The image pair, with the NIR (top) and CIR image (bottom), taken out of the car window at 60 kph.

Aerial testing

‘TARMAC’

The sensor was test-flown on 12 June 2003 mounted on the ‘Hannibal’ UAV at the ‘Toowoomba Amateur Radio Model Aircraft Club’ (TARMAC) flying field. The installation of the sensor under the UAV is shown in Figure 4.3. This particular UAV was chosen from several other platforms based on the parameters of slow stable flight, large fuselage and ability to carry the additional payload (due to the 2-camera sensor). The UAV was powered by a 25 cc methanol glow motor, which combined with the 2.5 m wingspan, provided ample lift to mobilise the sensor.

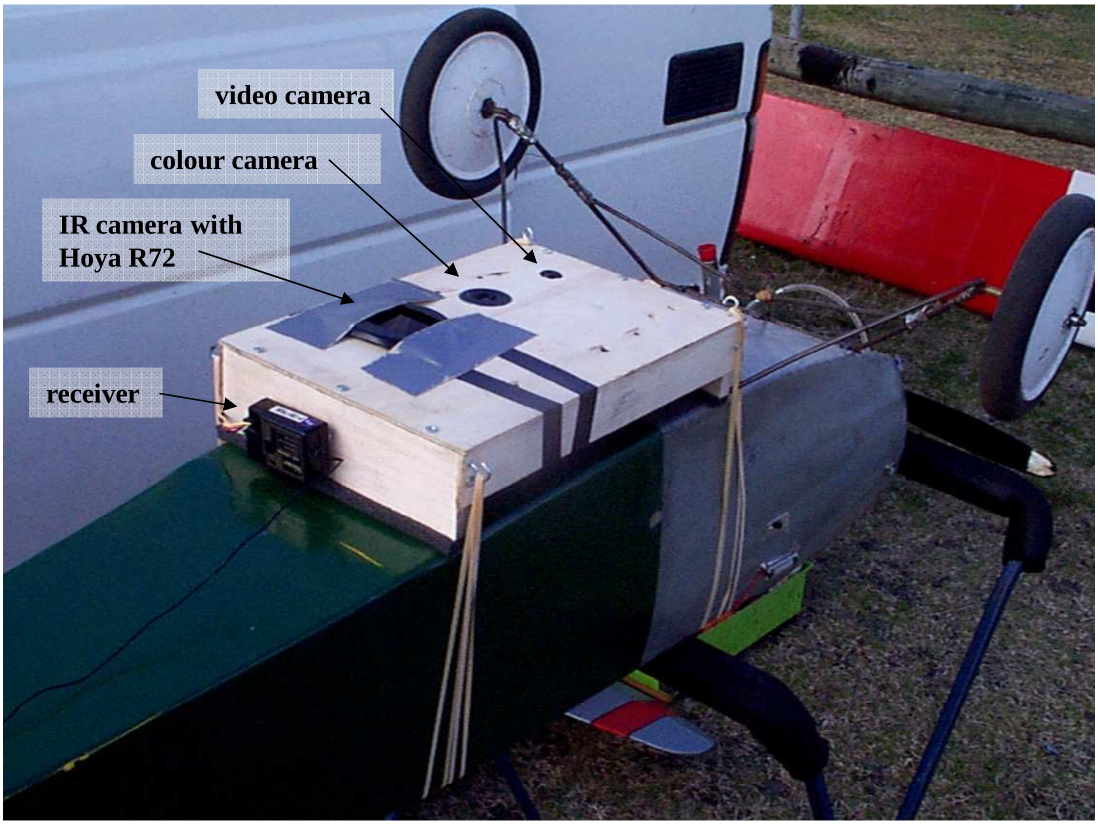

Figure 4.3 The sensor installed under the ‘Hannibal’ UAV at the TARMAC test, 12 June 2003.

Images were taken throughout the flight whenever the aircraft was over areas-of-interest, which included natural and man-made features around the flying field. This allowed 20 images to be recorded on each camera during the 15 minute flight. An example of a matched pair of images collected on this mission is displayed as Figure

4.4. The images taken (in NIR and CIR) show surprising detail of a house being constructed (centre of image), surrounding vegetation (top left of image) and dirt being stockpiled (centre left of image).

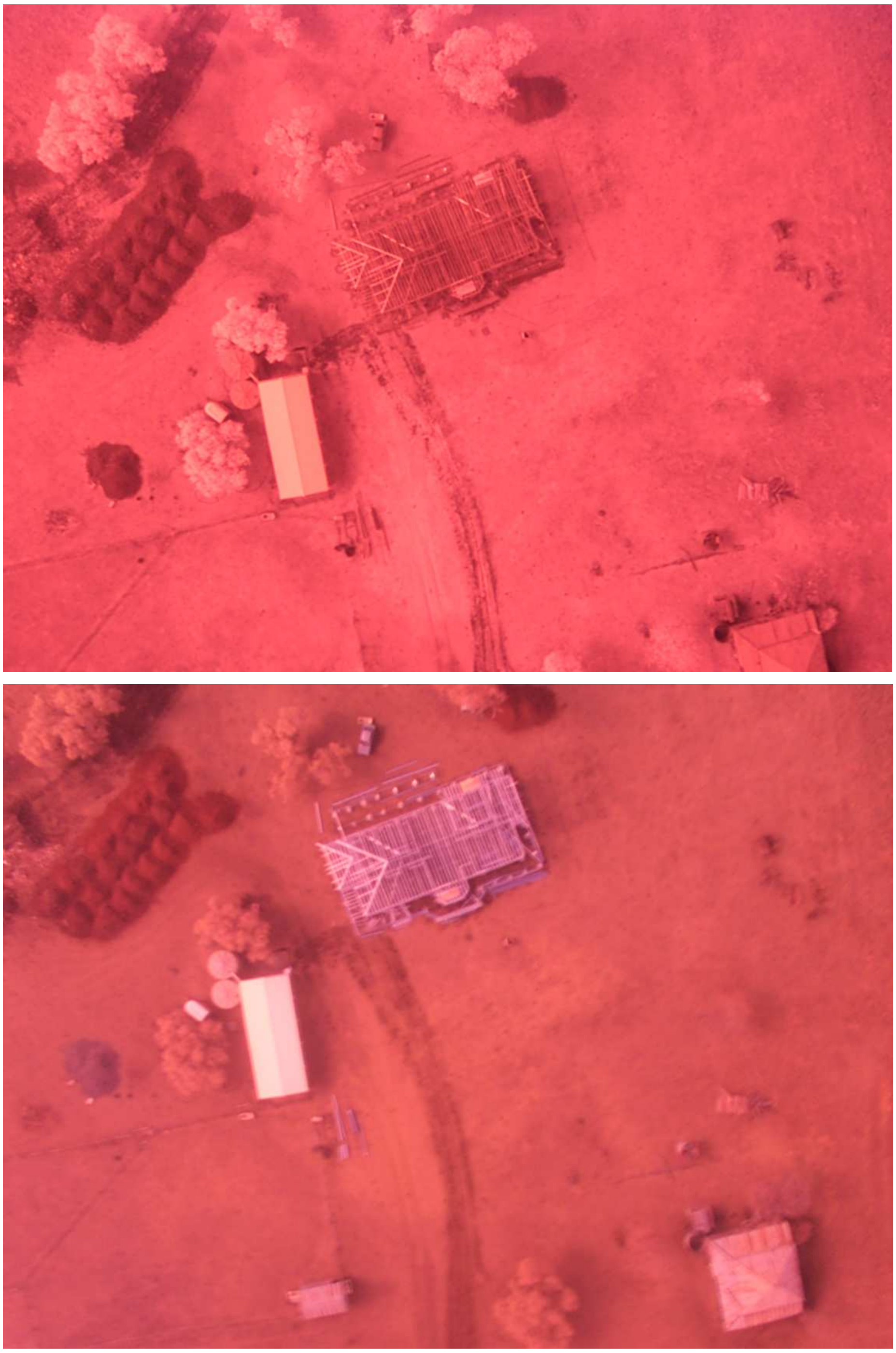

Figure 4.4 Simultaneous images captured from a UAV, utilising a Hoya R72 filter (top) and the CIR (bottom).

The system performed to expectation in this trial. To fully test the utility of this system configuration, a mission was planned over a real-world situation—a winter cereal cropping area at ‘Argyle’.

‘Argyle’

To test the sensor in a real world situation, images were collected over a 40 ha wheat field at ‘Argyle’, Macalister, about 100 km W of Toowoomba, using the 2-camera system. Rather than having two NIR cameras as in the previous two sets of images, a ‘normal’ colour camera was substituted for the CIR camera. Images were collected from this field on two separate occasions.

On 14 June 2003, the 2-camera sensor was suspended underneath a 1.7 m (7 ft) latex balloon filled with helium (He) gas (see Figure 4.5). The balloon was tied-off using a piece of cotton twine (visible in Figure 4.5). The sensor was attached to the twine using four equal length pieces of nylon fishing line. The single tether-line was attached to the system at the junction of the nylon fishing line and the cotton twine. The tether-line and the receiver antenna have been labelled in Figure 4.5. This configuration was utilised as the UAV pilot was unavailable to fly the plane on this occasion. During the mission, 25 images were captured on each camera. However, the pairing of the images was inconsistent due to several colour images not having a corresponding NIR image and *vice versa*. An example of a corresponding pair of images collected is shown as Figure 4.6.

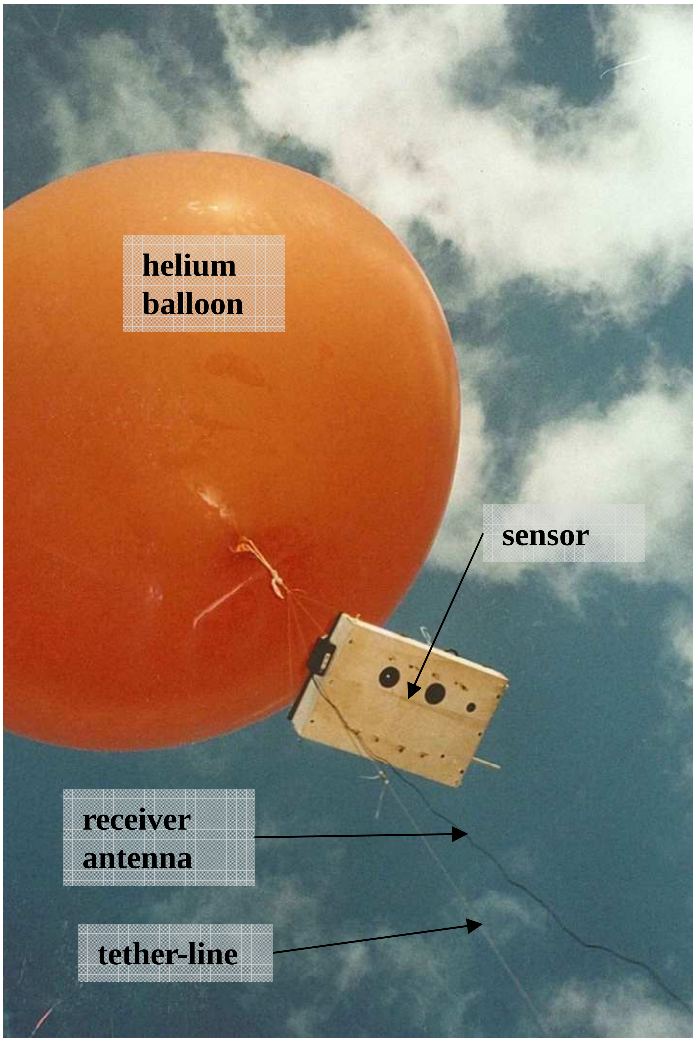

Figure 4.5 The sensor installed underneath the helium balloon, 14 June 2003.

As the wheat crop was at a very early growth stage (pre-tillering), indicated by the reflectance from the soil and displayed in high resolution images collected closer to the ground, little information could be used from this mission. The mission was, however, a test of the use of the sensor system suspended underneath the helium balloon. This method of deployment of the sensor required no flying experience, had less risk (compared to take-off and landing of the aircraft) and provided a stable platform (weather dependent). When using the He balloon system, a slight breeze was beneficial when acquiring images as it raked the system over at an angle allowing the sensor to swing underneath the tether line. A second mission was planned for a month later when the crop was more advanced.

Figure 4.6 The colour (top) and NIR (bottom) image collected from the helium balloon at Argyle, 14 June 2003.

The second mission occurred on 1 August 2003 and utilised the 'Hannibal' UAV as the platform (see Figure 4.7). The UAV, prior to take-off, is shown in Figure 4.8. To make the identification and orientation of images easier, images were only acquired when over target and flying in one direction. Although 60 colour images were successfully captured over the area-of-interest, no infrared images were recorded from the flight—only during the pre-flight taxiing period. This had not been encountered on other missions and appeared to be a powering issue with the cameras. On the previous missions, images were acquired at a comparatively high frequency (an image every 30–60 s). On the current mission, there was several minutes delay from the point of being readied for take-off, until the system was over target and ready to acquire images.

Figure 4.7 The 2-camera sensor installed under the 'Hannibal' UAV during the 'Argyle' mission, 1 August 2003.

Figure 4.8 The 'Hannibal' UAV ready for take-off, 1 August 2003.

Following this mission, an investigation into the operation of the cameras showed that after a duration of inactivity, the cameras would power down. This duration was 2 min 20 sec for the NIR and 2 min 40 sec for the colour camera. This powered-down state prevented the cameras from being able to be triggered remotely, resulting in images not being collected. The frequency of attempted image acquisition was sufficient to ensure the colour camera’s operation, however, it was not frequent enough to ensure the continued operation of the NIR camera. This resulted in no useful NIR images collected from this mission.

Overcoming the problem of cameras timing-out

To overcome the above mentioned issues of one or both cameras failing to trigger, a feedback and re-initialisation system was developed. The system monitored the condition of each camera at each image request to ensure successful image acquisition. The system, based on a micro-controller, two photo-transistors, and two relays, detected the state of the light emitting diode (LED) on the rear of the camera that indicated the operational state of the cameras. The LED has three states:

1. LED is continuously energised—camera is ready for image acquisition,
2. LED is intermittently energised (at a frequency of approximately 1 Hz)—camera is processing and storing an image, and
3. LED is not energised—camera is not powered, the memory is full, or some other problem.

A photo-transistor was positioned over this LED on each camera and a micro-controller used to monitor the state of each LED, and hence the camera readiness. The additional electronics associated with this micro-controller were installed on an electronic prototyping board, along with the double-pole double-throw relays described at the start of section 4.2.2. If the micro-controller encountered a problem (i.e. anything other than a ready signal), power would be disconnected from both digital cameras and the video camera for four seconds. This provided a visual feedback to the operator (via a break in video transmission) that the cameras were not functioning in the normal mode of operation. This disconnection of power allowed the cameras to power down and reboot ready for the next image acquisition and ensured matching images from the pair of cameras. The refined and modified 2-camera sensor is shown in Figure 4.9.

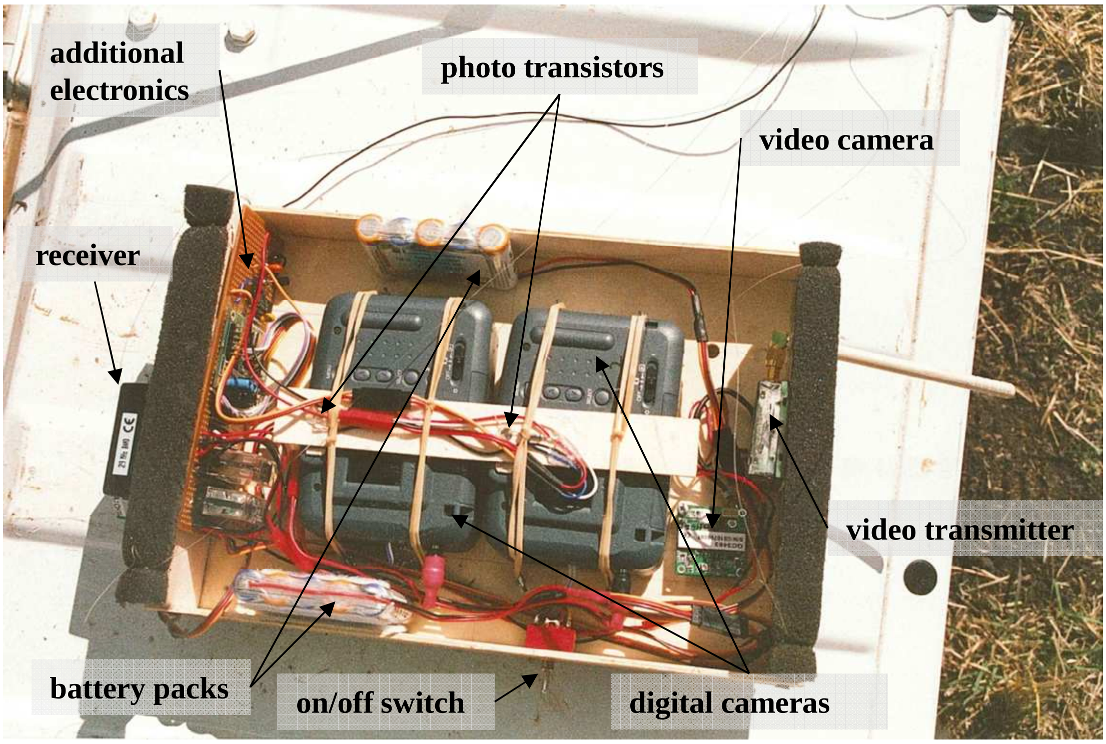

Figure 4.9 The 2-camera sensor with camera-status detection.

The images captured were stored to the 64 Mb CompactFlash™ card inserted into each camera. The video camera transmitted footage to the ground to aid in positioning with the receiver being used to trigger the cameras to initiate image acquisition. One camera records the visible wavelengths (approximately 400–700 nm) and the other camera captures the near-infrared information (700–1050 nm). The total weight of the system was 1.0 kg. It had a run time of two hours and could store 200 images (each image approximately 300 KB) per camera.

Data collection events

Imaging events that coincided with extensive agronomic evaluations were conducted at '*Colonsay*' in 2003 and at '*Nindigully*' in 2004. The data collected from these two sites was extensively analysed and will be discussed in the following chapters. An additional site at '*Tullona*' was also imaged in 2004, however during the mission, both tether-lines to the helium balloon broke and the sensor and platform were lost, preventing a retrieval of sensed data.

In order to regain the ability to capture LCLA remotely sensed data, the system needed to be replaced. As the DC3200 cameras were superseded and no longer available, an opportunity existed to upgrade the system with newer and higher resolution sensors. Section 4.2.3 details this development with the results discussed in section 5.4.1.

4.2.3 5.0 Megapixel Digital Camera Sensor System

The camera technician who originally modified the DC3200 cameras was consulted regarding current camera models that would meet the requirements for a LCLA remote sensing system. These requirements included: compact and low weight, ability to be remotely triggered, and most importantly, sensitivity to near-infrared light (once the NIR cutout filter is removed). The Kodak Easyshare CX7525 (see Figure 4.10) Digital Zoom Camera (Eastman Kodak Company, Rochester NY) was recommended and the details of this camera are included in Table 4.3.

Figure 4.10 The Kodak CX7525 digital zoom camera.

Table 4.2 The specifications for the Kodak CX7525 digital camera.

Standard Features	
CCD resolution	1/2.5 inch type (5.36 M total pixels)
Image resolution	5.0 MP (2560 x 1920 pixels)
Picture quality	5.0 MP - best
	4.4 MP - best 3:2
	3.1 MP - better
	1.7 MP - good
Zoom	15X total zoom
	3X optical zoom -- 5.6-16.8 mm (35 mm equivalent: 34-102 mm)
	5X advanced digital zoom
Aperture	f/2.7-5.2 (wide); f/4.6-8.7 (tele)
Shutter speed	1/2 - 1/1400 seconds
Display	4 cm indoor/outdoor color display
Performance Features	
Burst mode	2.4 fps, up to 5 pictures
Click to capture	0.6 seconds
Shot to shot	1.3 seconds
Movie mode	continuous MPEG-4 video with audio capture/playback
Movie image resolution	VGA (640 x 480 pixels) at 13 fps
	QVGA (320 x 240 pixels) at 20 fps
Movie file format	Still: JPEG/EXIF v2.21; Movie: QuickTime MOV (MPEG-4 compression)
Auto focus	TTL-AF, multi-zone, center-zone
Focus distance	Standard - 60 cm to infinity
	Landscape - 10 m to infinity
	Close-up wide - 13-70 cm
	Close-up tele - 22-70 cm
ISO equivalent	80-160 (automatic) and 80, 100, 200, 400 (manual)
White balance	auto, daylight, tungsten, fluorescent
Light metering method	TTL-AE, selectable: multi-pattern, center-weighted, center spot
Exposure control	programmed AE
Long time exposure	0.7-4 seconds
Ease of Use Features	
Flash range	wide - 0.6-3.6 m ; tele - 0.6-2.1 m
Auto-orientation	auto picture-rotation
Storage	16 MB internal memorySD/MMC card expansion slot
Self-timer	10 seconds
Additional Features	
Power options	2 AA KODAK MAX Digital Camera Batteries; 2 AA lithium or Ni-MH batteries or 1 CRV3 lithium battery; 3 volt DC
Weight	without batteries - 178 g
Dimensions	103 (w) x 65 (h) x 38 (d) mm

Two of the CX7525 cameras were purchased and modified to be remotely triggered (see Figure 4.11). The NIR cut-out filter of one camera was removed and replaced with clear glass to improve the sensitivity to near-infrared light (as was performed on the DC3200 cameras, refer section 3.3.2). Table 4.3 compares the improved features of the CX7525 to those of the DC3200.

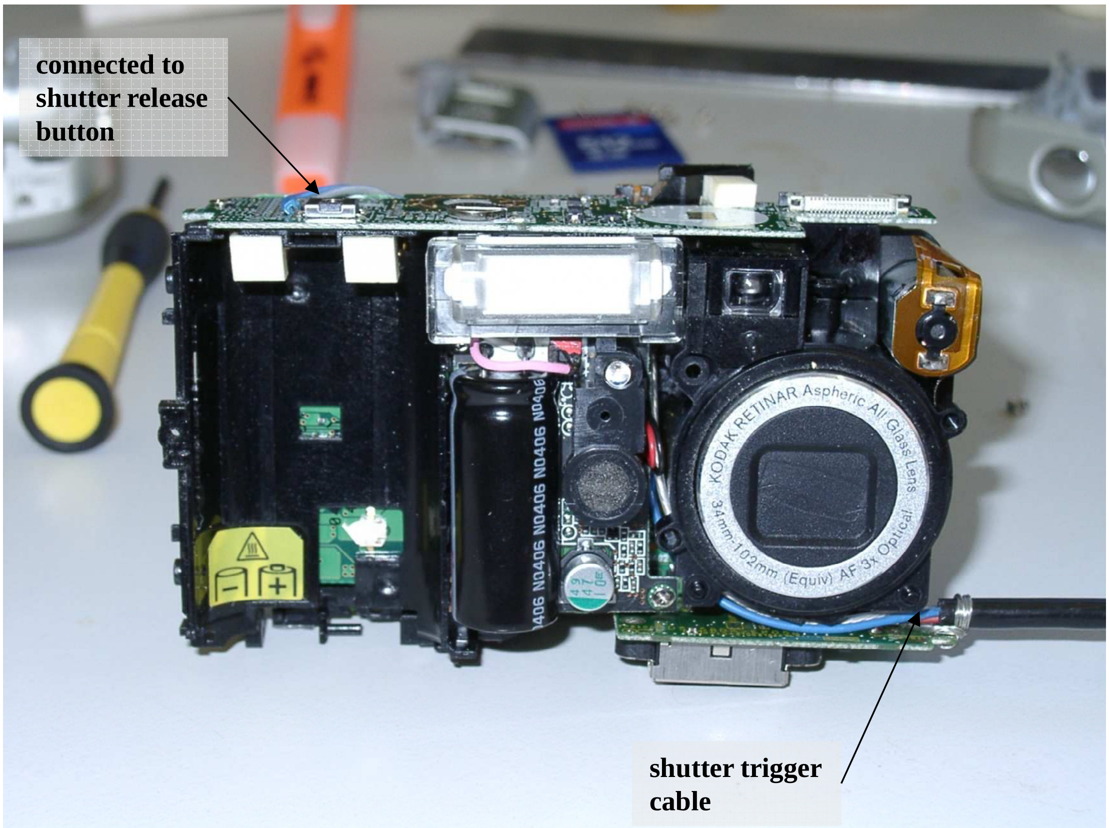

Figure 4.11 The CX7525 that has been modified to increase sensitivity to near-infrared light and to enable electronic triggering.

Table 4.3 Comparison between the DC3200 and CX7525 digital cameras.

Feature	DC3200	CX7525
CCD sensor	1152 x 864 = 1.0 Megapixel	2160 x 1920 = 5.0 Megapixel
Power	4 x AA	2 x AA
Image storage	CompactFlash	Secure Digital
Dimensions	113 (w) x 53 (d) x 81 (h) mm	103 (w) x 38 (d) x 65(h) mm
Weight	215 g without batteries	178 g without batteries

Not only was the CX7525 smaller and lighter than the DC3200, it also had a greater resolution and required two less batteries to power it. In storing the images, it also recorded the image details (i.e. time taken—helpful for sequencing images) and cameras settings (i.e. F-stop, exposure time, focal length and program mode). In addition, the CX7525 was able to be continuously energised by pulsing the pre-release on the shutter. With the camera set on the ‘Best’ setting, the Joint Photographic Experts Group (JPEG) compressed images varied in size from 400–900 Kb depending on the subject. The larger images required larger data cards, thus 512 Mb cards were utilised for this study.

A 2-camera sensor configuration, similar to that used with the DC3200 cameras, was developed and is shown in Figure 4.12. Rather than the low-end 29 MHz radio control equipment, as used with the DC3200 (detailed in section 3.3.2), higher performance 36 MHz equipment was utilised. As with all radio control equipment, the output was a 50 Hz square wave (a pulse every 20 ms) with a pulse width of 0.9–2.1 ms, depending on the position of the radio control stick. The output of the 36 MHz equipment was much cleaner than that of the 29 MHz equipment and was monitored by the use of a micro-controller (PICAXE-08, details at http://www.picaxe.co.uk). The logic in the programmable chip was used to monitor the pulse width on the designated channel of the radio equipment.

When image acquisition was initiated (by ‘flicking-up’ the elevator stick) the changed pulse width was detected and determined to be greater than a pre-programmed value (1.6 ms) resulting in a pulse being output from the PICAXE to trigger the cameras. In order to prevent the cameras going to sleep (one of the problems encountered with the DC3200s) a pulse of 2 s duration was sent every 25 s to the pre-shutter-release of the cameras to keep the cameras awake. As with the DC3200s, the cameras were mounted in balsa frame.

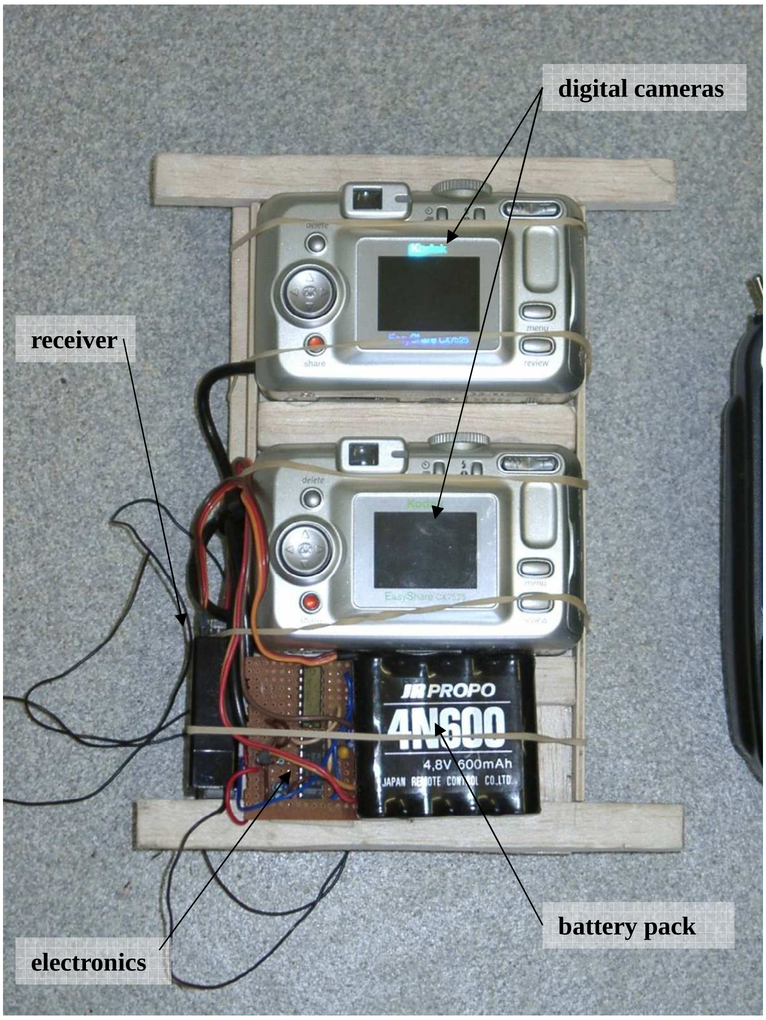

Figure 4.12 The 2-camera sensor utilising the CX7525 cameras (top view).

As the lens extends from the camera when powered, adapters were machined to accommodate this extension. The adapters were also used to securely attach the 58 mm diameter ‘Hoya R72’ filter for the NIR-sensitive cameras and the ‘Fotar ultra-violet (UV)’ filter for the colour camera (see Figure 4.13). The UV filter had no affect on the sensitivity of the colour camera and was used primarily to keep foreign objects off the camera lens and to making cleaning easier.

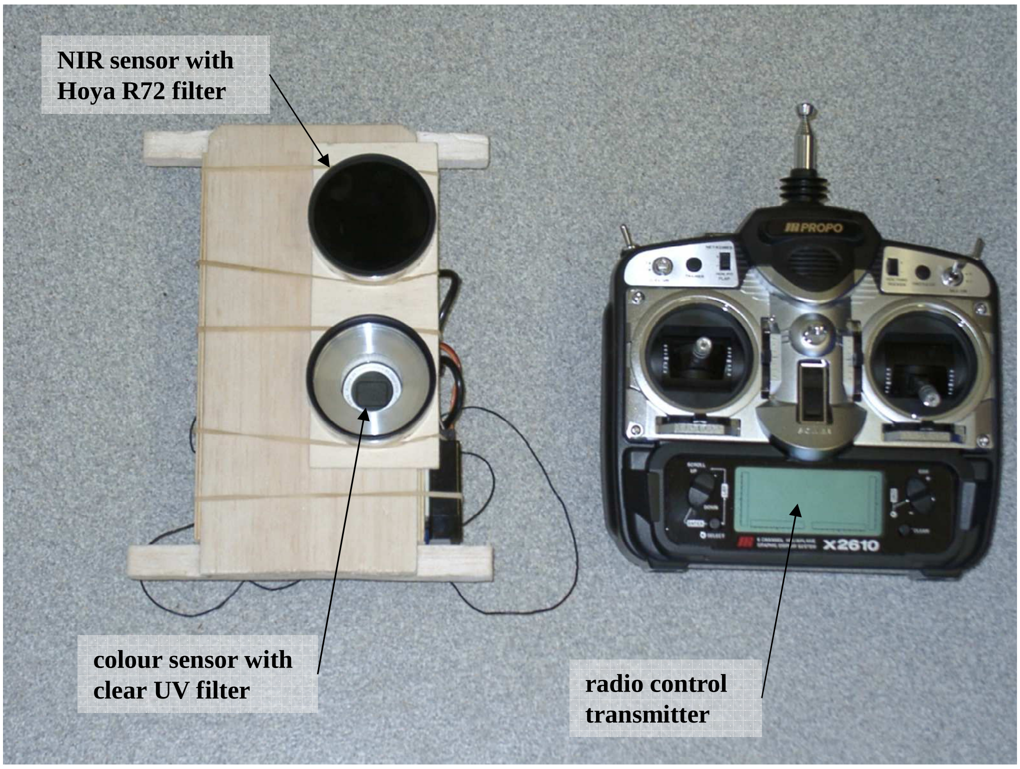

Figure 4.13 The underside view of the 2-camera sensor and the radio control transmitter.

Aerial testing

The sensor (mounted on the 'Milne' UAV) was test flown on 20 September 2005 at 'Daybreak' Dalby. The installation of the sensor in the UAV is shown in Figure 4.14 and the UAV prior to take-off in Figure 4.15. This particular UAV was specifically constructed as a low-cost low-altitude remote sensing platform by Milne Industries, Dalby. The UAV, a shoulder wing monoplane, was designed for slow stable flight, with a fuselage of sufficient size to carry the additional payload (courtesy of the 2-camera sensor). The UAV was powered by a 35 cc methanol glow motor, which combined with the 2.5 m 'Clark Y' lifting section wing, provide ample lift to mobilise the sensor and plane (gross mass 10 kg). The UAV was also equipped with a video camera downlink (to aid in positioning) and a live telemetry system. The telemetry system provided ground staff with 10 s updates of the platforms airspeed, engine condition, altitude and heading.

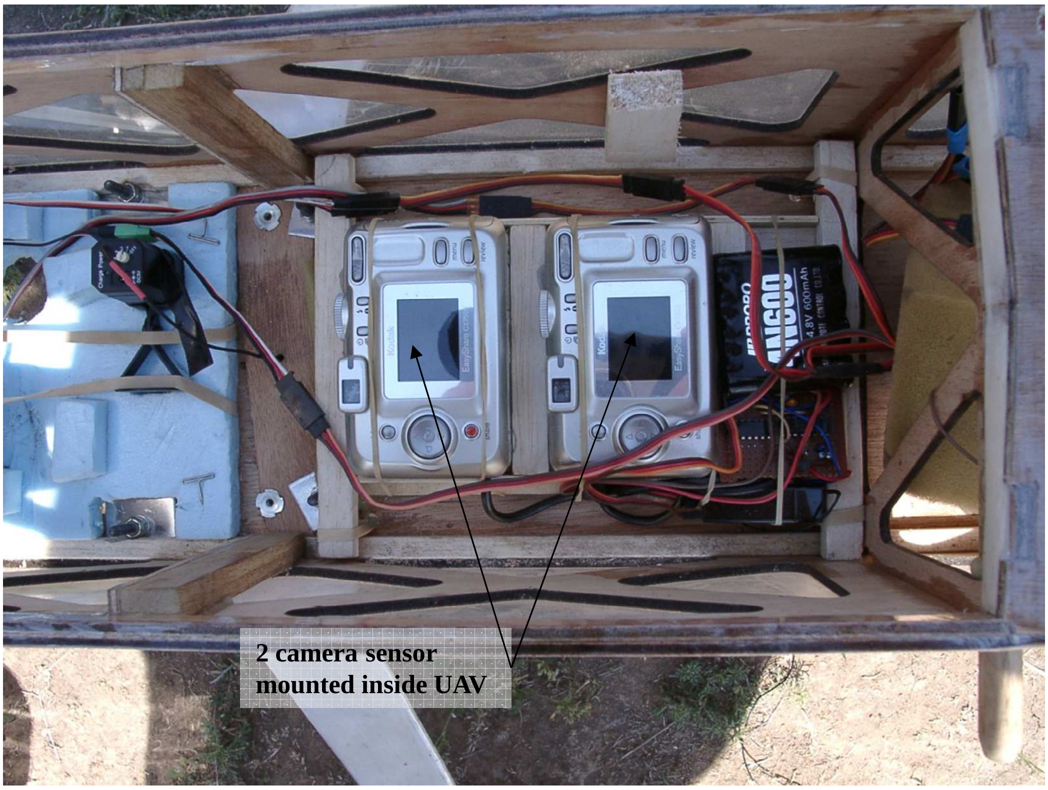

Figure 4.14 The CX7525 2-camera sensor installed in the ‘Milne’ UAV.

Figure 4.15 The ‘Milne’ UAV being prepared for takeoff, 20 September 2005.

Two separate missions were conducted on this day. The first mission was to collect some images and to check that the sensor system was functioning as expected, while the second mission was intended to acquire images. Over a 25 minute window, 100 images were collected on both the colour and the near-infrared cameras. Images were taken throughout each flight whenever the aircraft was over areas-of-interest, such as natural and man-made features. An example of a matched pair of images collected on this mission is displayed as Figure 4.16 (near-infrared) and Figure 4.17 (colour). The high reflectance in the NIR of the green grass and the trees in the orchard / around the residence is clearly visible in Figure 4.16. The complete absorbance of the NIR light by the pool is evident in the centre bottom of the images. The green grass, trees and infrastructure around the residence are also clearly shown in the colour image (Figure 4.17).

Figure 4.16 The near-infrared image collected on the 'Daybreak' mission, 20 September 2005.

Figure 4.17 The matching colour image for Figure 4.16.

Data collection events

This 5 megapixel low-cost low-altitude sensing system has since been used on numerous other occasions with two of these having application to precision agriculture in crops:

- The first application was a continuation of investigations into cereal crops with the configuration used at ‘Lundavra’ to acquire images over a wheat variety trial on 4 October 2005 (Mission #24), and
- Finally, a trial was conducted, with researchers from the Australian Research Centre for Aerospace Automation (ARCAA) - Queensland University of Technology (QUT) (Mission #29), on the ability of UAV autopilot to accurately trigger the 2-camera sensor when at a desired location.

One of the limitations of the existing system was that a great number of images look alike and unless a large number of natural features or artificial targets are present at the location, it was hard to identify and orientate the images. This situation was overcome on the second application mentioned above. On this mission, images were automatically obtained at predetermined locations by a UAV being controlled by an autopilot. The 5.0 megapixel sensor system was used to capture the images.

The two advances–the use of the 5.0 megapixel sensors and the use of the autopilot— are discussed in Chapter 5.4 and the results discussed in Chapter 6.4.

4.2.4 Tasking and Deployment

Site considerations

In order to have the best opportunity of quantifying the parameters being investigated, sufficient within-field spatial variability should exist in that parameter in the target area. Best management practises should also be employed to ensure that this variability is not masked by other parameters such as poor nutrition, poor pest management or compaction. In order to overcome some of these limitations, controlled traffic farming enterprises were used wherever possible. In addition, to aid in the analysis and understanding of the results, other agronomic datasets were collected, whenever possible.

Deployment checklist

The set of procedures detailed in Table 4.4 was reviewed prior to every mission to capture LCLA remotely sensed imagery in an attempt to ensure the success of the activity. This includes the initial acquisition and any follow-up missions.

Table 4.4 Deployment checklist for completion before each mission.

Operational Procedures	
Weather conditions conducive to imagery collection	☐
Crop at appropriate stage of growth	☐
Permission of landowner	☐
Pre-mission planning (wind direction and direction of strips)	☐
Good agronomic practises undertaken (i.e. so weeds etc. do not hinder associations)	☐
Sensor (camera)	
Spare batteries and batteries in camera charged and unit working correctly	☐
Appropriate filters selected	☐
Video down link working	☐
Image storage sufficient for area to be covered	☐
Access to picture card adaptor	☐
Sufficient space on laptop hard disc to store images	☐
Laptop batteries charged and appropriate cables / adapters to download images	☐
Height of image capture determined by ground pixel resolution required	☐
Platform (plane)	
Access to experienced remote control aircraft operator	☐
Take off and landing areas identified, emergency landing area also identified.	☐
Visually inspect aircraft for damage in transit.	☐
Fuelled up	☐
Radio communications batteries charged and working	☐
CASA approval if near airstrip	☐
Check each control surface on the aircraft moves freely and in the correct sense	☐
Let engine warm-up and check pick-up from idle to full power is satisfactory	☐
Under full power, recheck all flying controls	☐
Platform (balloon)	
Sufficient consumables (He gas and latex balloons)	☐
Check integrity of tether lines	☐
Double check attachments of all equipment	☐
Ground Control	
If images to be georeferenced, DGPS required. Check operation of GPS.	☐
Are there sufficient natural features in image able to be used for georeferencing (e.g. End of paddock, trees, roads etc.)?	☐
If insufficient natural features, insert man-made features	☐
Ensure good field notes to easily identify location of GCP in image	☐

4.2.5 Costings for the LCLA System

The minimal requirements for a LCLA remote sensing system are detailed below. The components are split into sensor and platform, with each being detailed separately.

Sensor

When the original 1.0 megapixel digital cameras were purchased in 2001, they cost the same as the 5.0 megapixel cameras purchased in 2005.

2 x Modified camera including batteries and memory card @ $400 ea	800
1 x Hoya R72 filter	50
Total (capital cost)	$850

Platform

The various costing for the components that constitute the platform are listed below.

Helium Balloon	
1.7 m diameter latex balloon	40
Helium gas to fill	200
Total (per mission)	$240
Hobbyist Remotely Controlled Aircraft	
Nearly ready to fly 1/6th scale model (2.3 m wingspan) kit	330
90 size (0.9 cubic inch) 2 stroke glow motor	300
6 channel radio	400
Total (capital cost)	$1030
Autonomous UAV	
A platform and radio equipment similar to above	1500
Autopilot (minimum $3000, as tested approximately $8000)	>3000
Total (capital cost)	>$4500

The operating cost ranges from approximately $10 (depending on flying time) to cover the fuel used by the UAV to $240 / mission for the He balloon platform (the gas and balloon are consumables). However, there is no capital expenditure for the balloon platform and ranges from $1000 upwards, depending on the sophistication of the UAV. Low-cost low-altitude remote sensing can be performed for under AUD$2000. However, if a fully autonomous system is preferred, the expense will be in excess of AUD$5500. Note price current in 2007.

4.3 Conclusions

This chapter detailed the development of the two components that make up the LCLA remote sensing system—the sensor and the platform.

The 1.7 m diameter helium balloon platform provided enough lift to mobilise the sensor system. The ability to position the balloon over the target, at varying heights, with no flying skills, made for a valuable imaging tool. If the mission did not suit the use of helium balloon, hobbyist remotely controlled aircraft were also utilised as the platform with purpose built UAV utilised on the latest missions.

The 1.0 megapixel cameras provided good information and set the minimum resolution requirement for a LCLA remote sensing system. However, using 5.0 megapixel cameras resulted in a halving of the pixel size for the same height of image acquisition, or keeping the same pixel size and acquiring the images from a greater height. This increased the extent of the images and proved the better alternative.

The evaluations undertaken during the development of the LCLA remote sensing system indicated that it had the potential to meet the spectral, spatial, temporal and cost prerequisites detailed in Chapter 1. Very fine levels of detail could be detected by the system and the portion of the spectrum covered by sensor provided information that would be useful to agriculture. The NIR bands provided good differentiation between crop and soil allowing planting misses and overlaps to be detected in a cropping field. In addition, lawn, pasture and different tree species are all spectrally discernable.

Both the UAV and the helium balloon had the capacity to be used on a regular basis. All of this was achieved with modified low-cost consumer digital cameras and readily available platforms (hobbyist remotely controlled aircraft or helium balloon), with the skill level to fly the RCA higher than that of the balloon. This can all be achieved for under AUD$2000.

In order to evaluate the application of the LCLA remote sensing system, testing and mapping of cereal crops was required. The materials and methods undertaken to perform these tasks were detailed in Chapter 5, while the analysis and discussion of the results were detailed in Chapter 6.

Chapter 5

Crop Mapping Methods using the LCLA System

Preliminary testing of the low-cost low-altitude (LCLA) remote sensing system indicated the system possessed appropriate spatial, spectral and temporal resolutions for use in precision agricultural studies. This chapter describes the methods used in evaluating the classification and prediction accuracies, when mapping cereal crop attributes, to confirm the applicability and usefulness of the LCLA remote sensing system.

5.1 Introduction

The methods used in the evaluation of the LCLA remote sensing system that is appropriate for use in precision agriculture comprises the following sections:

a) Selection of trial sites and auxiliary data layers;
b) Deployment of the system for data collection ;
c) Extraction of information (using image processing, statistical analysis and geographic information systems) from the images acquired from the LCLA remote sensing system to:
    - Map grain yield, protein and maturity, and
    - Discriminate different crop types;
d) Evaluation of the unmanned aerial vehicle (UAV) autopilot for use in a LCLA remote sensing system.

The methods undertaken to analyse the acquired images are shown in Figure 5.1.

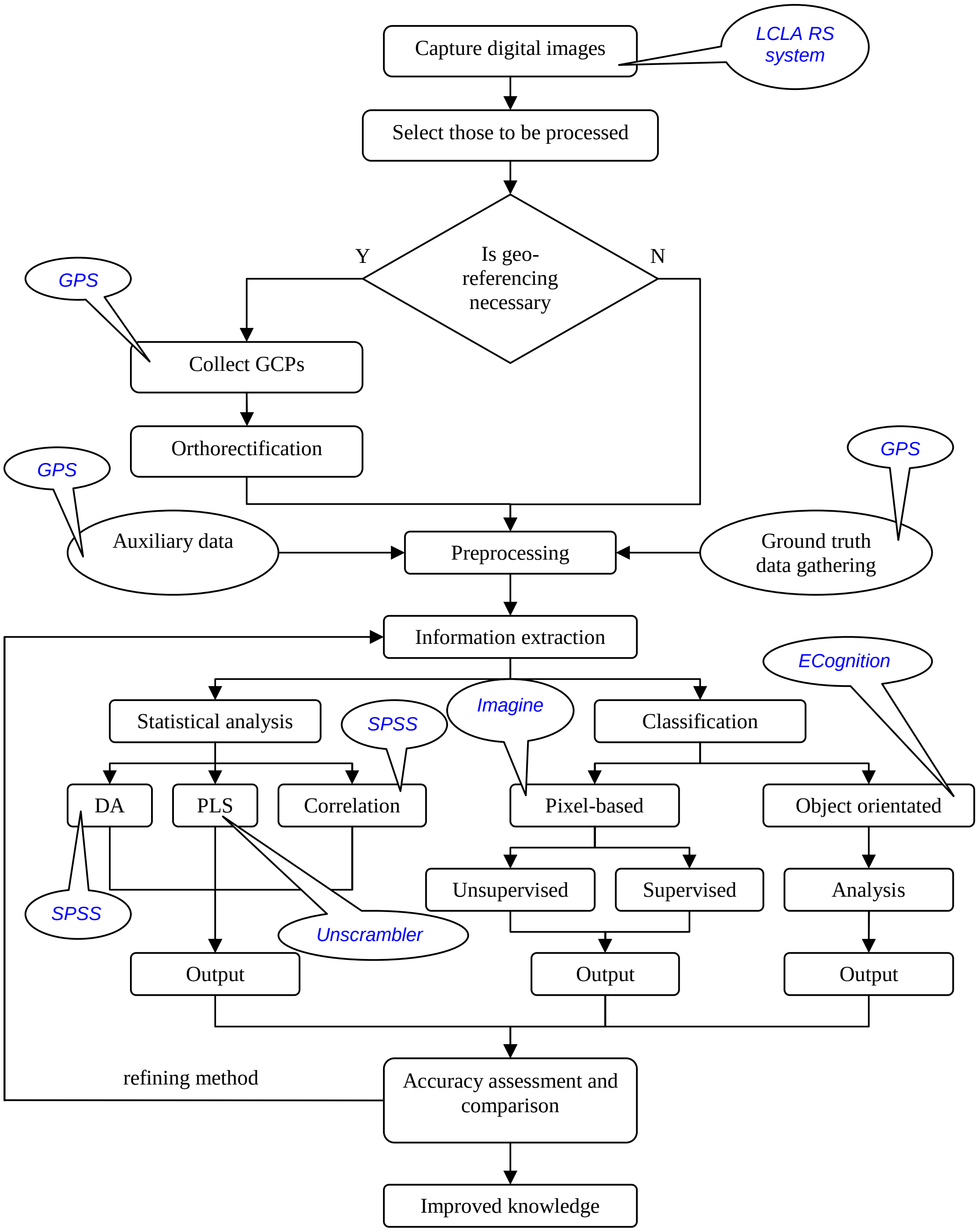

Figure 5.1 The sequences for digital image analysis adopted in this research.

5.2 Grain Yield and Protein Mapping

5.2.1 Study Area

The study area was located at the 'Colonsay' fertiliser trial site, in the Cecil Plains district of south-eastern Queensland (-27.501º, 151.392º), Australia (see Figure 5.2). This site was established to monitor the long-term effects of varying nutrient applications with fertiliser treatments being imposed at this location since 1985. The soil at the site is described as a deep self-mulching black vertosol (Isbell 1996) described as a Waco soil series (Harris *et al.* 1999).

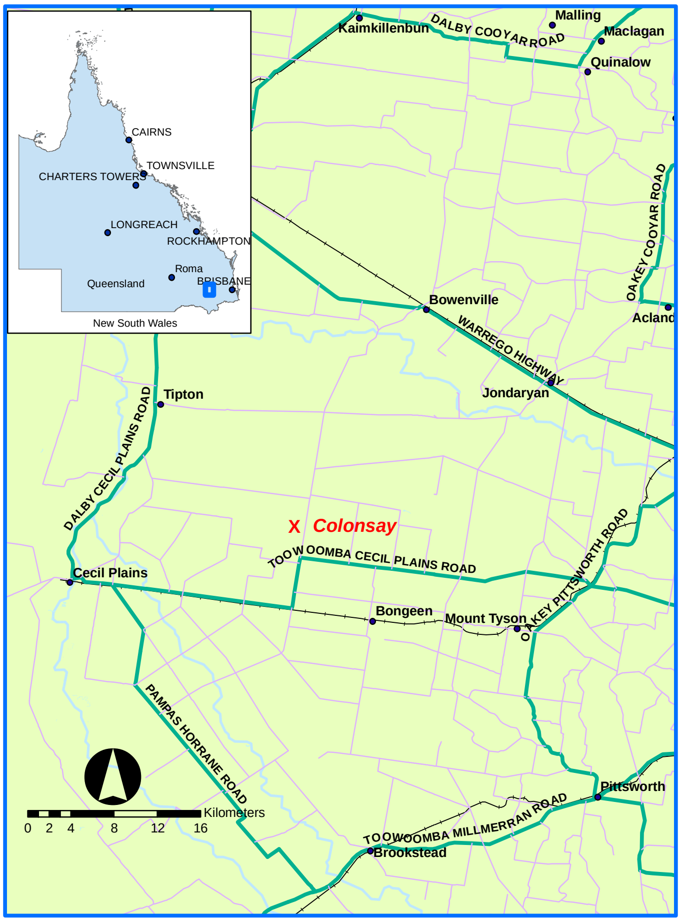

Figure 5.2 Location of the Colonsay trial in the Central Darling Downs region of Queensland.

Cereal wheat (*Triticum aestivum* cv. Strzelecki) was sown on 13 June 2003 into plots that received varying rates of nitrogen (N), phosphorus (P), and sulphur (S) fertiliser. The crop row spacing was 250 mm. Two experiments were operating concurrently, an N x P experiment and an S experiment. There were 20 treatments with three replicates in a split plot experimental design (see Figure 5.3). The split plot was to allow the N fertiliser to be applied pre-plant and at sowing. This pre-plant application was not possible in 2003, so both sub-plots were treated the same, with the N being side-dressed with the seed at sowing. Each sub-plot is 2.5 m wide and 50 m in length. The N x P experiment consisted of a combination of 4 N rates (0, 40, 80 and 120 kg/ha) and 4 P rates (0, 5, 10 and 20 kg/ha) applied with the seed at sowing. The N was applied as urea (46% N) and P as triple super-phosphate (20.7% P).

As the fertiliser rate for each plot had not been varied since the treatments were imposed in 1985, there was a diverse range of nutrition levels retained in this trial that could be used for comparison and evaluation purposes (refer to Figures 5.4, 5.5 and 5.6). Figure 5.4 shows a close-up oblique photo taken from the ground of several rows of plants in both a low and in a high nutrition plot. Figure 5.5, a close to ground aerial shot shows a close-up of five plots with nutrition levels ranging from low to high, while Figure 5.6 shows an overhead view of a majority of the trial site, both acquired from the LCLA system.

The starting moisture (immediately prior to planting in 2003) was uniform across all plots tested. Pre-plant available N rates varied from between 1.0 kg/ha, where no fertiliser was applied, to over 150 kg/ha being available at the high (120 kg/ha) nutrition plots. Plots of plant available water and plant available N are shown in Figures 5.7 and 5.8. Depending on the season, maintenance levels for crop production in this region and on this soil type ranged between 40–60 kg/ha for N and between 5–8 kg/ha for P. This is evident by depletion of N in subsoil layers (below 30cm) with the lower (0 kg/ha) rate, break even with the 40 kg/ha rate and accumulation with the higher (80 and 120 kg/ha) N application rates. Had the rainfall in the preceding season not been below average, these dryland crops may have needed a higher annual N rate (greater than 40–60 kg/ha) to maintain supply.

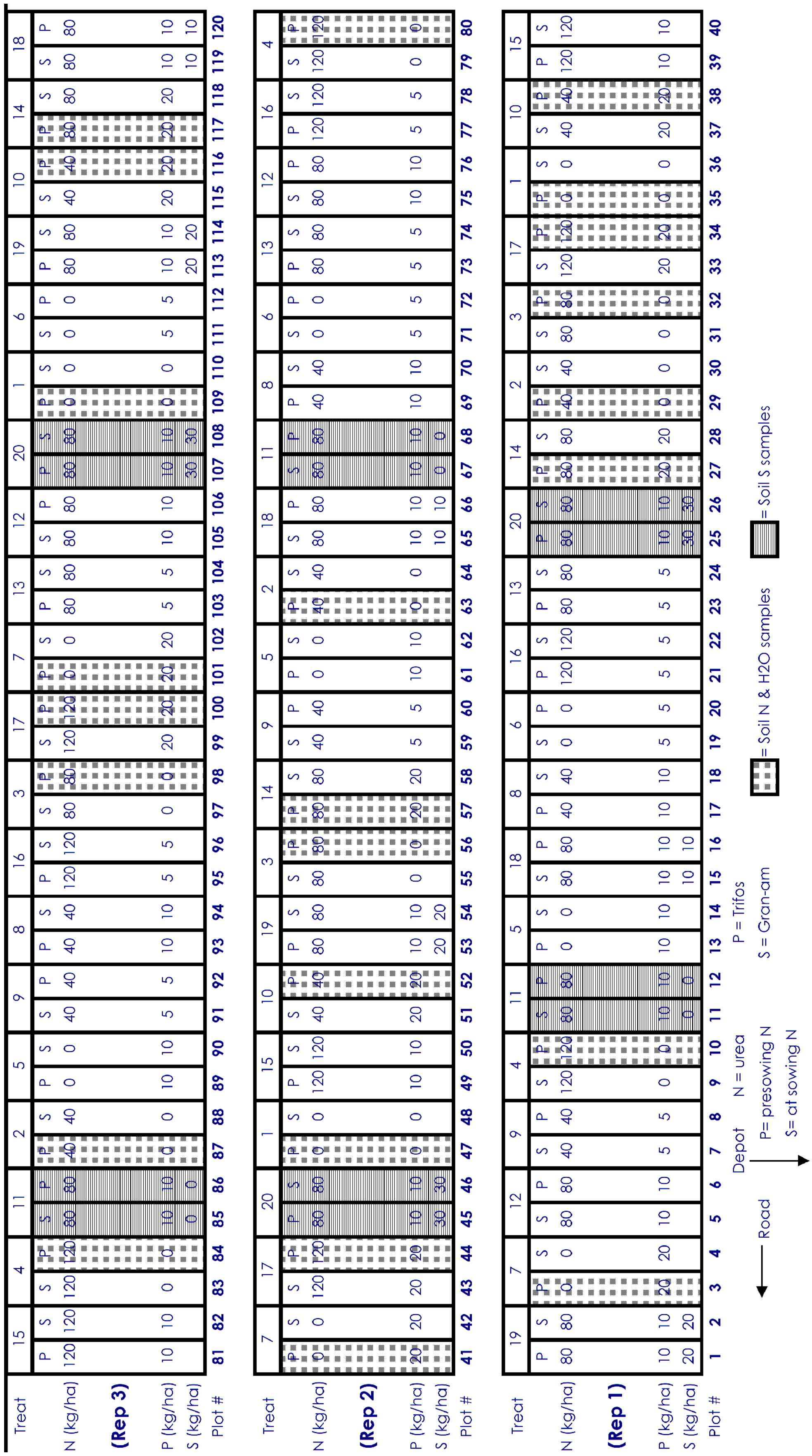

Figure 5.3 Schematic layout of 'Colonsay' site for 2003.

Figure 5.4 Example of a plot with low nutrition levels (left) and high nutrition levels (right).

Figure 5.5 The range of nutrition levels in adjacent plots as captured by the LCLA remote sensing system.

Figure 5.6 The range of nutrition levels evident in two-thirds of the trial site as captured by the LCLA remote sensing system.

A large range of agronomic measurements was taken at this site on which public and private research was being conducted. Some of these measurements included the following: the amount of fertiliser applied, plant cut information (chemical analysis, tiller number and leaf area index) during the growing season, soil analysis at planting (nutritional information, water content) and harvest parameters (yield and protein content). The analysis conducted as part of this research focused on the relationship between these ‘at-harvest’ parameters and imagery.

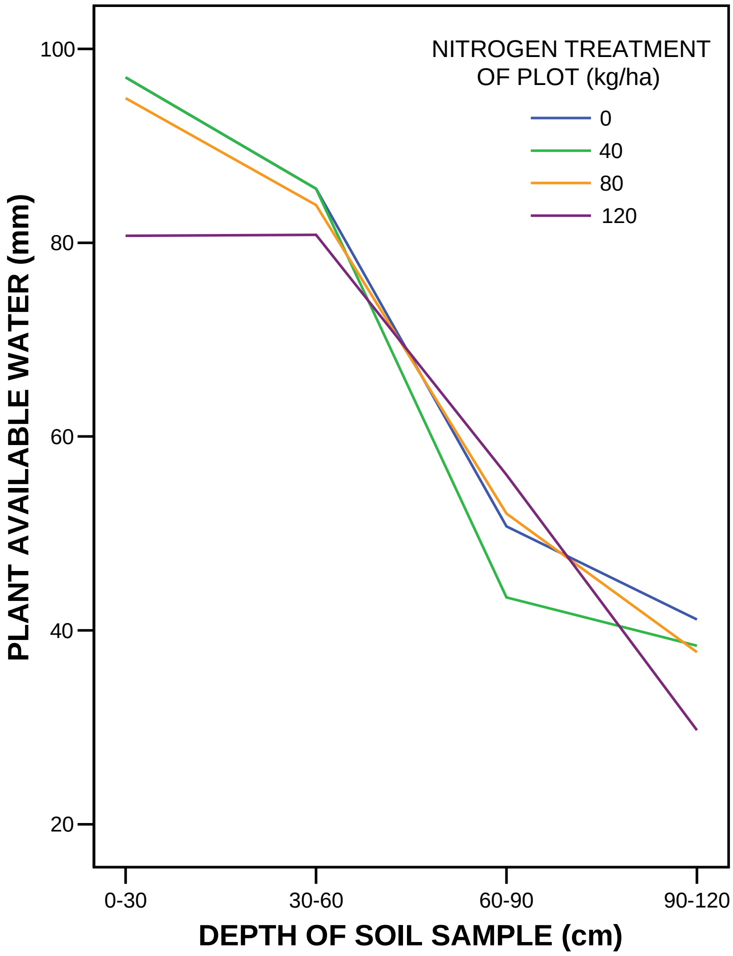

Figure 5.7 The range of plant available water contents for the various soil depths across the range of nitrogen treatment plots, immediately prior to planting in 2003.

The crop was machine-harvested at 155 days after sowing (DAS). The grain was weighed and a sub-sample taken for further analysis. Moisture and protein were determined from this sub-sample using the routine methods of near infrared (NIR) spectroscopy and Kjeldahl digest (Reyns *et al.* 2001; Wang *et al.* 2004). The values of grain yield and protein were thus an average of the whole plot, and were corrected to the Australian industry wheat standard of 12% (Kelly *et al.* 2004).

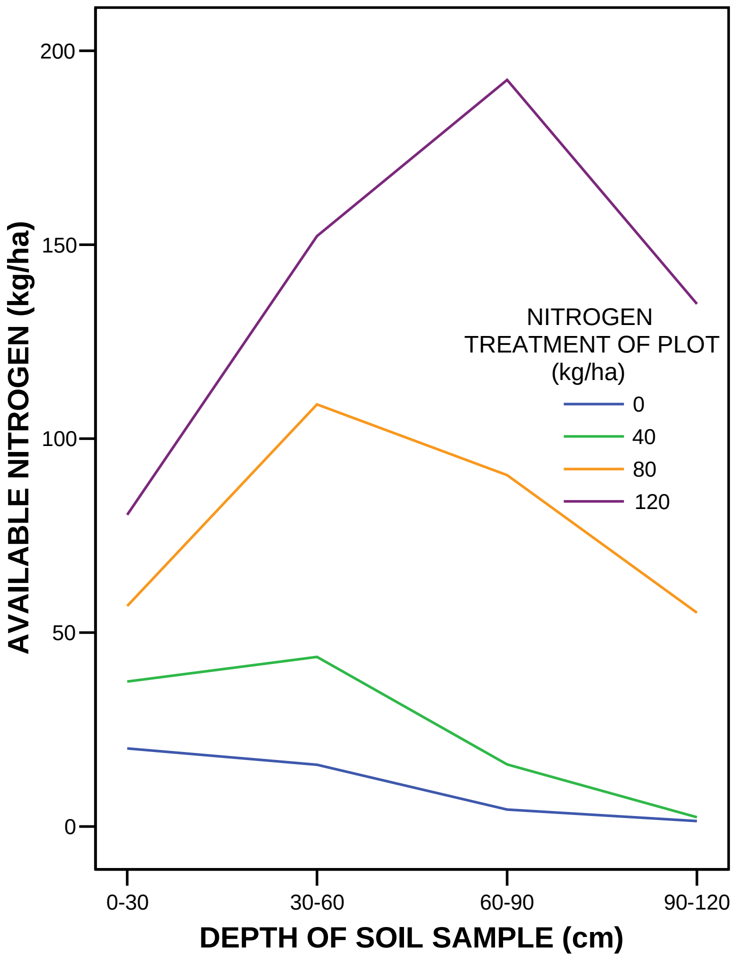

Figure 5.8 The range of available nitrogen for the various soil depths across the range of nitrogen treatment plots, immediately prior to planting in 2003.

5.2.2 System Deployment

The LCLA system was deployed at the 'Colonsay' site on two separate occasions (2 September and 14 October 2003) during the growing season of the wheat crop. On both occasions, the system was deployed below a 1.7 m (72 inch) diameter 'Prestige' latex balloon (manufactured by Tilco International Inc, St-Jean, Quebec, Canada) that was inflated with balloon-grade helium (containing 97% He – details at http://www.boc.com.au/) to provide sufficient lift to carry the 1.0 kg sensor. The balloon was tied off with a soft cotton string (the process being undertaken at a football stadium in Figure 5.9). What differed between the September and October imaging dates was the attachment of the sensor to the balloon and tether-line.

Figure 5.9 Tieing-off the inflated latex balloon with soft cotton string.

Deployment 2 September 2003

The system (see Figure 5.10) utilised the 2-camera sensor detailed in section 4.2.2. In order to suspend the sensor below the balloon, a doubled-up length of cotton twine was looped over the twisted neck of the balloon before it was doubled back on itself and tied. Both the tether-line and four even lengths of nylon fishing line, which were secured to each corner of the sensor, were attached to the twine. The sensor hung under the force of gravity below the balloon.

On the day of image acquisition, 2 September 2003 (81 DAS), there were a few scattered clouds and a gentle to light breeze blowing. The balloon was deployed by playing out the tether-line by releasing the brake on the Alvey® sidecast fishing reel.

The sensor system was positioned above the area of interest by viewing the video footage (that was being transmitted from the sensor system to a receiver and monitor on the ground) and adjusting the tether-line accordingly. The majority of the trial site was in view with the sensor positioned at approximately 400 m (derived from the lens geometry and ground pixel resolution) above ground level. A total of 75 images were acquired with each camera in the hour either side of solar noon.

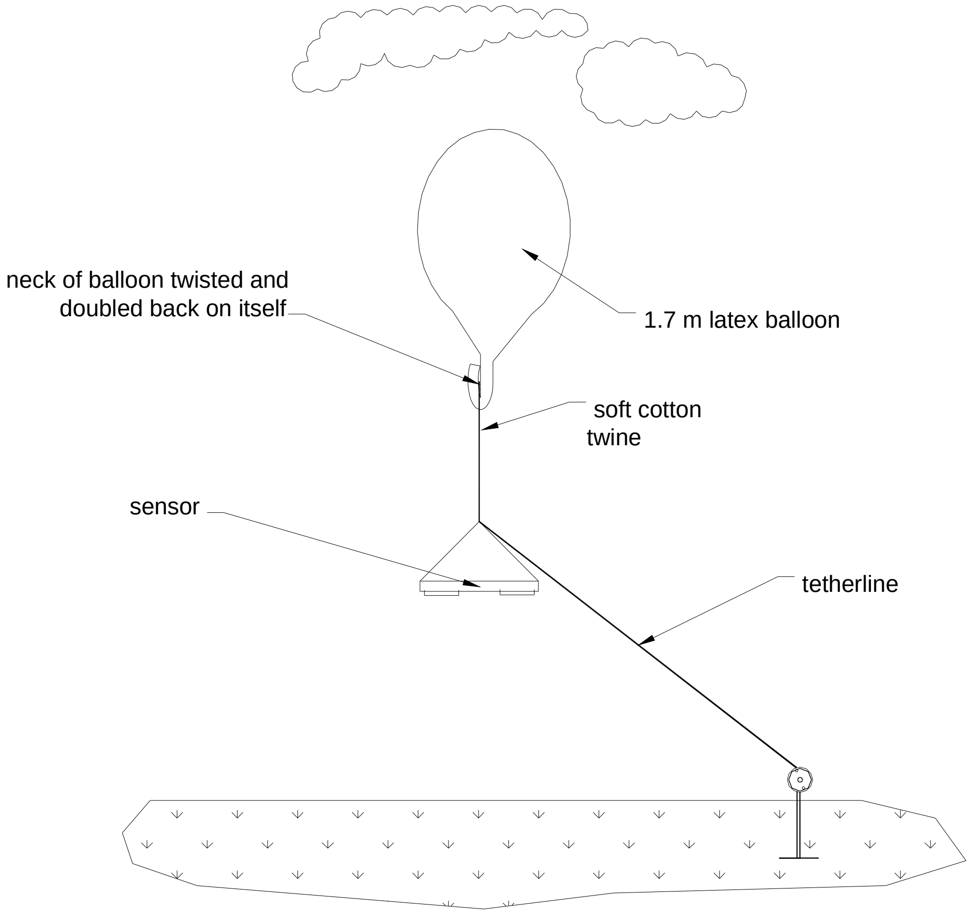

Figure 5.10 A schematic representation of the sensor as deployed on 2 September 2003.

Due to the gentle breeze, the sensor was generally positioned directly overhead, resulting in the tether-line contacting and interfering with the suspended sensor. This contact caused the sensor to rotate uncontrollably. When the captured images were reviewed on the ground, this rotation resulted in blurring of a large number of the images. The system is shown prior to deployment in Figure 5.11 and airborne in Figure 5.12.

Figure 5.11 Preparing for sensor deployment at 'Colonsay'.

Figure 5.12 The sensor is airborne.

Although some of the images were blurred, several image pairs (see Figures 5.13 and 5.14) show the potential of the system if the amount of movement of the sensor could be reduced. These images collected were not analysed due to the motion blur and because they were collected quite early in the growing season.

Figure 5.13 Colour image of the NW corner of the trial site.

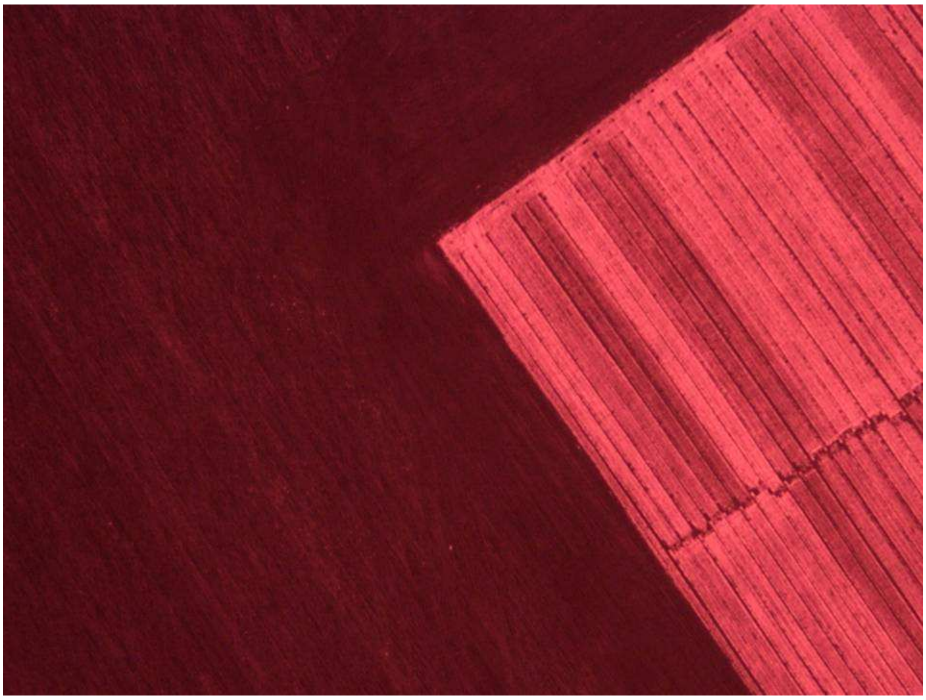

Figure 5.14 The NIR image that matches with the colour image shown in Figure 5.13.

Deployment on 14 October 2003

On the second image acquisition at the trial site, the rotation / motion of the sensor had been reduced. As with the previous acquisition, soft cotton twine was looped over the twisted neck of the balloon. Rather than attaching the balloon directly to the four nylon lines, it was hooked onto 2 x 25 kg breaking strain *'Halco Supa Snap Trace'* wires (details at http://www.halcotackle.com/) that were fixed to a stabilising frame. The frame was constructed of balsa wood and served to attach the tether-line to the balloon. The frame also provided a location where the sensor was suspended and could hang under the force of gravity. To stop the sensor from rotating freely beneath the frame, the rotation was restricted to ± 15° by the use of a slack light nylon line that was treaded through the sensor and attached to the two stabiliser arms.

Also attached to each stabiliser arm was a trace wire (25 kg breaking strain). A single tether-line (25 kg breaking strain nylon fishing line), was attached to the joined trace wires. This configuration is shown schematically in Figure 5.15 and prior to deployment (at a football stadium) in Figure 5.16. Depending on the wind direction and sensor orientation, there were some instances where the tether-line and trace wires were visible in the acquired images, as in Figure 5.17 (left hand corner).

The day of image acquisition, 14 October 2003 (123 DAS), had clear skies and only a light breeze blowing. The balloon was deployed by playing out the tether-line by releasing the brake on the Alvey® sidecast fishing reel. As the line was run out, the person controlling the line moved into the wind so as to position the sensor above the trial site. The sensor was again positioned at 400 m (as in the September acquisition) to cover the site and approximately 200 images were acquired with each camera in the hour either side of solar noon.

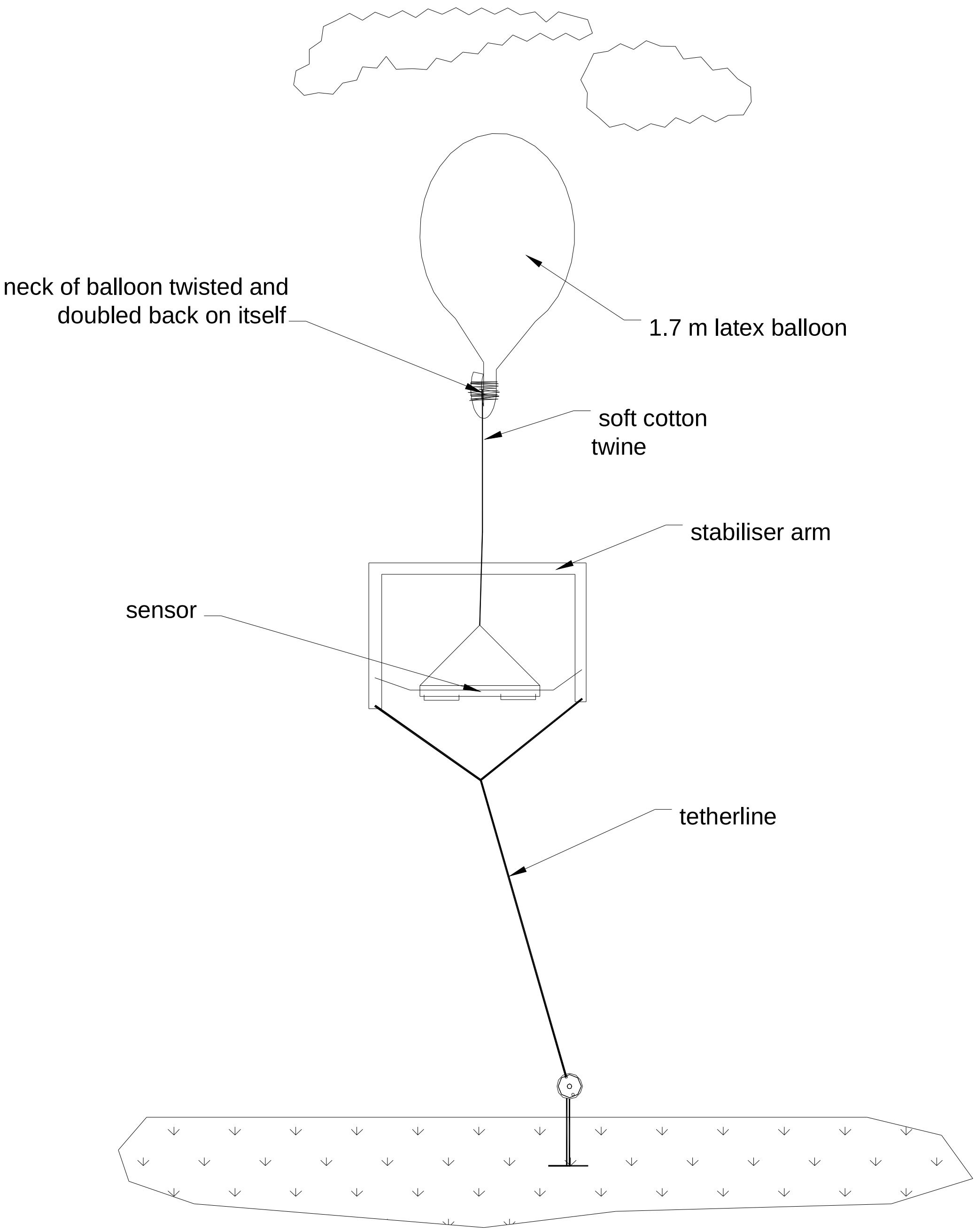

Figure 5.15 A schematic representation of the sensor as deployed on 14 October 2003.

Figure 5.16 The balloon attached to the stabilising frame with the sensor suspended underneath prior to deployment at a football stadium.

5.2.3 Image Processing and Analysis

On both image acquisition events, the images captured during the deployment were stored on the memory cards in each of the cameras. The images were viewed using the procedures detailed in section 4.2.2 to ensure sensor operation and that images were acquired from across the entire trial site. The images were later transferred to a desktop computer for analysis. One of these images is shown in Figure 5.17.

Figure 5.17 The colour image that was further processed.

A total of 29 global positioning system (GPS) locations were recorded throughout the trial site (see Figure 5.18), to be used in later analysis. Locations such as corner of trial block, missing rows, corner post etc. were identified and position recorded using a Compac Aero 2130 (Windows CE based) pocket computer that was running FieldRover II GIS software (SST 2000). The pocket computer was connected to the CSI LGBX Pro (details at http://www.csi-dgps.com/) differential GPS receiver, receiving the differential correction from the Australian Maritime Safety Authority (AMSA–details at http://www.amsa.gov.au/) guidance beacon (located in Brisbane – 294 kHz frequency). In order to obtain the best possible GPS fix, locations were only logged when the age of the differential correction was less than three seconds and more than six satellites were used to provide the solution, thus providing the sub-metre accuracy.

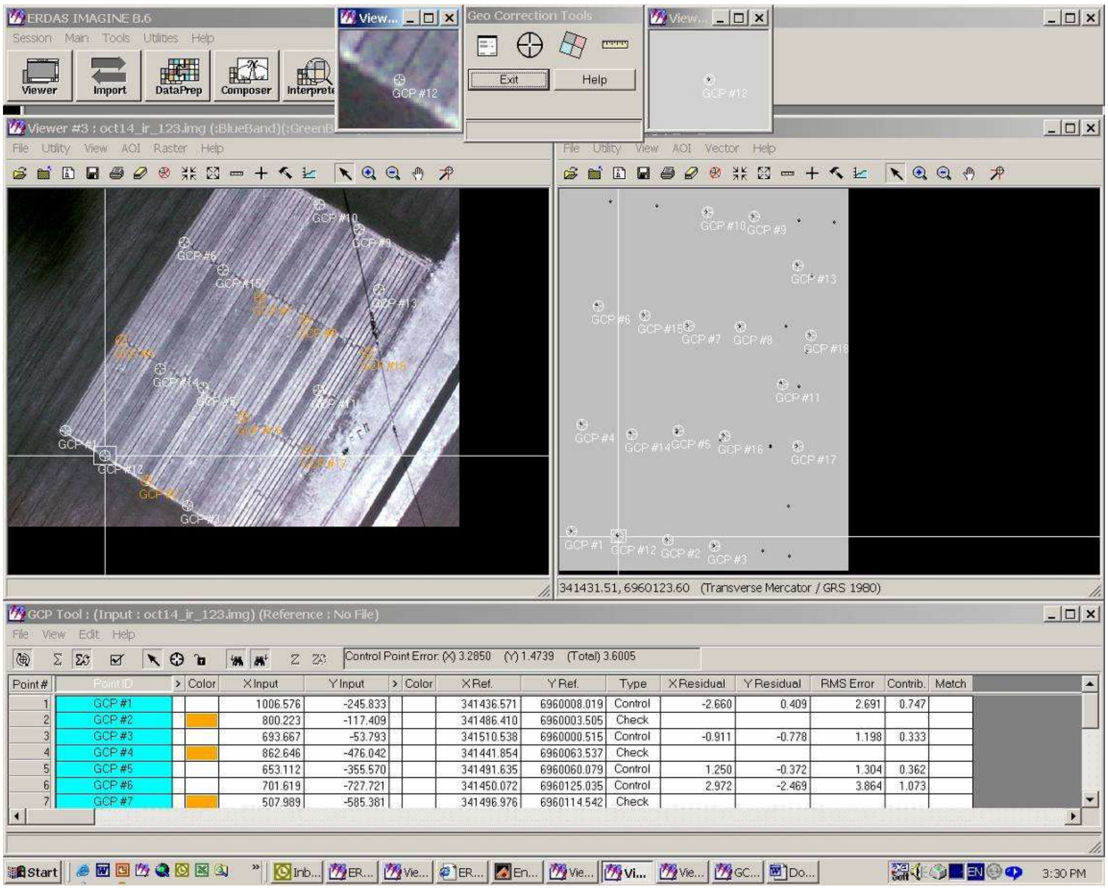

Figure 5.18 The ground control points used to geo-reference the image.

An ESRI shapefile of the GPS locations was exported from the FieldRover II (SST 2000) software and imported into ERDAS Imagine 8.6 (ERDAS 2002), the software that was used to perform the image analysis. The images that were transferred to the desktop computer were scrutinised in an image-viewing package for trial site coverage, clarity and compatibility between the colour and infrared images. The most appropriate images were chosen to be imported into the image analysis software.

The NIR image was chosen for geo-referencing due to the relatively clearer definition in the image. The green growing crop was clearly defined from the soil and stubble due to the fact that chlorophyll is extremely reflective of NIR and that soil / stubble is not. Geo-referencing was performed using 17 of the 29 locations that were recorded with the differentially corrected GPS at the time of image acquisition. Locations that were outside of the image extent or not able to be clearly defined in the image were not used. The geometric correction, using a polynomial model of the second order, was performed using 8 check points, and 9 control points. This resulted in a root mean squared (RMS) error (total) of 20.3 pixels. Using the nearest neighbour resampling method gave an output cell size of 0.25 m and hence an RMS error of 5.07 m. This was much greater than the accuracy of the differential GPS, and with the plots only being 2.0 m wide, could have resulted in there being a misalignment of over two and a half plots. This was not acceptable.

The procedures were reviewed and it was found that during conversion from the proprietary format in Field Rover software to the shapefile format, two significant figures were lost from the longitude and three significant figures were lost from the latitude. This was rectified by importing the proprietary files into Microsoft Excel and manipulating the data and saving as a text file. This *.txt file was imported in ArcView 3.1 (ESRI, Redlands CA USA) and saved as a shapefile. The shapefile was accessed and the geometric correction was redone: this time using 18 GPS locations. The control point error (using 7 points) was reduced to 3.60 with an output cell size of 0.248 m, equating to an RMS error of 0.895 m. This error was comparable to the sub metre accuracy of the differential GPS and was considered acceptable.

The colour image was registered to the already geo-referenced NIR image (described above) using the image-to-image registration function of the software. Using 24 ground control points (GCP) selected from throughout the image, the control point error (seven points) was 0.958, with an output cell size of 0.254 m using nearest neighbour resampling (see Figure 5.19).

Several attempts were made to use this spatial information (GPS location points and georeferenced images) to register the images collected on 2 September. Firstly, a 2 September near-infrared image was registered to the geo-rectified 14 October near-infrared image. This resulted in a control point error of 1.7 m. Using the swipe feature of the analysis software, the extent of this error was highlighted. The road was positioned a full road width out and there was overlap in the plots. In an attempt to improve this error, the same NIR image was registered to the ground control points collected on 14 October. The control point error increased to over 2.0 m.

The clearly defined features evident in the 14 October ground control point collection were not as evident in the image from 2 September. This may have been due to differential crop growth and mowing around the periphery of the plots. This made the selection of GCP more ambiguous and resulted in the increased error of registration. These ambiguous features, as well as the blurring in the images caused by the sensor rotation, hindered the image-to-image registration. Thus, analysis efforts were concentrated on 14 October acquired images.

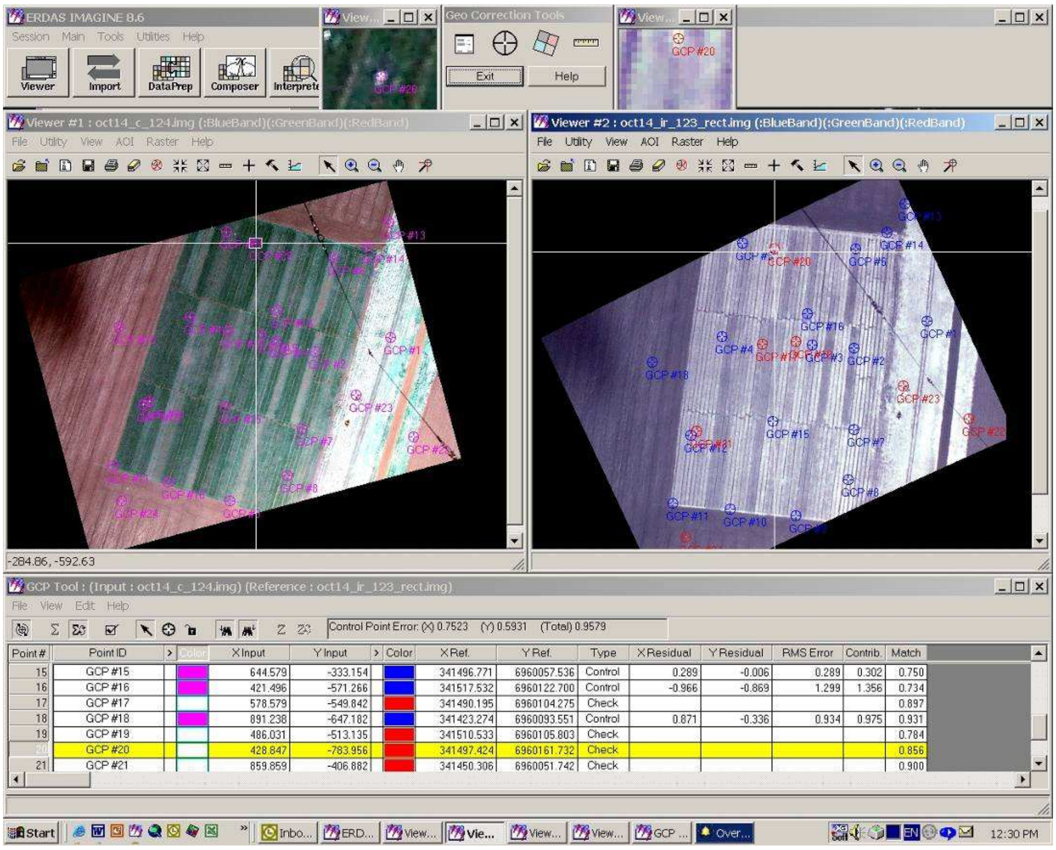

Figure 5.19 Ground control points chosen to register the colour to the NIR image.

With the colour image registered to the NIR image, the process of extracting pixel values was undertaken by defining areas of interest (AOI). No radiometric rectifications were performed on the images with the raw digital number (DN) values being exported to be analysed. This is the same process as used in other studies using digital cameras as an image acquisition tool (Staggenborg & Taylor 2000; Yang *et al.* 2000). Initially, the whole treatment (containing two adjacent plots) was defined. The whole treatment plots were compared with six ‘5x5 kernels’ randomly defined at uniform areas within the trial (see Figure 5.20).

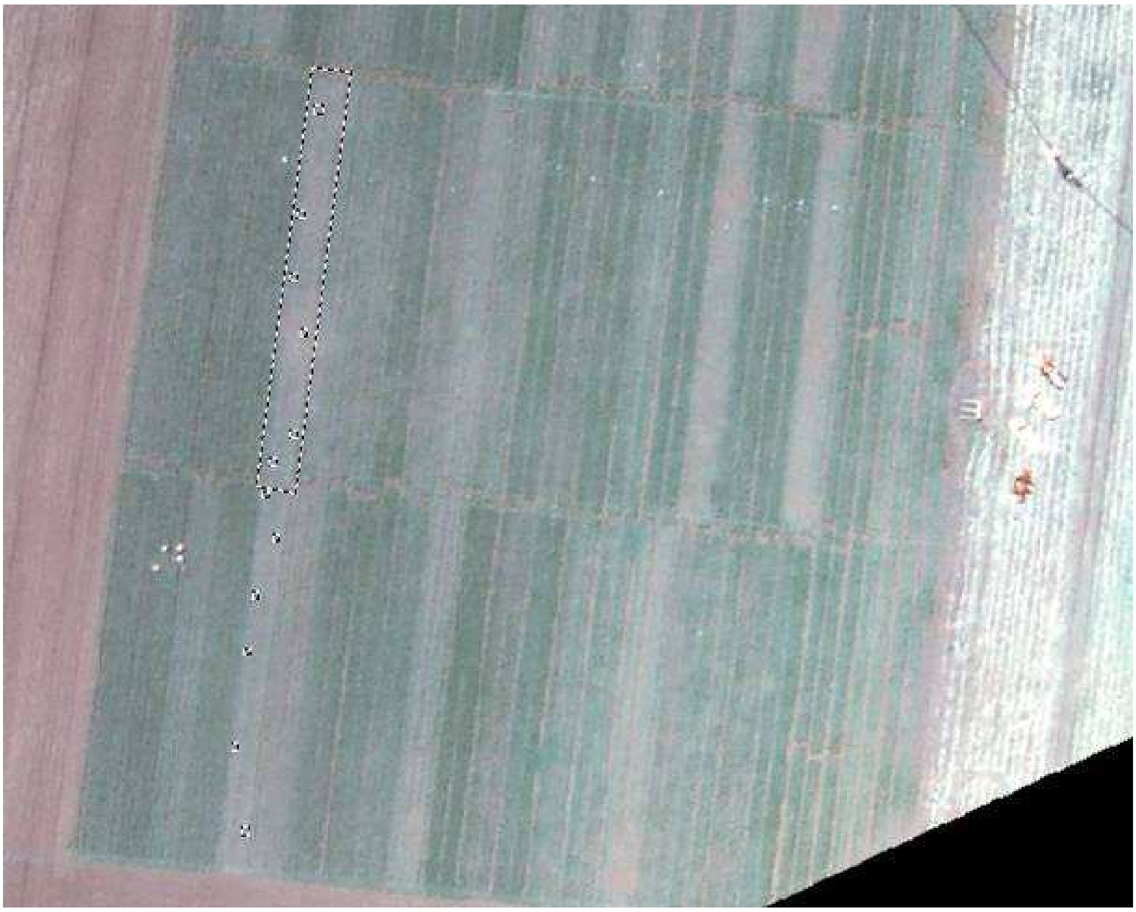

Figure 5.20 Selecting the areas of interest for the whole treatment and the ‘5x5 kernel’ study.

The box-plot results of the AOI study are shown in Figure 5.21. The outliers are shown as “o” (values between 1.5 and 3.0 box lengths from the upper or lower edge of the box), with the extreme cases (those with values more than 3.0 box lengths from the upper or lower edge of the box) are displayed as a “*”. The box length is the inter-quartile range.

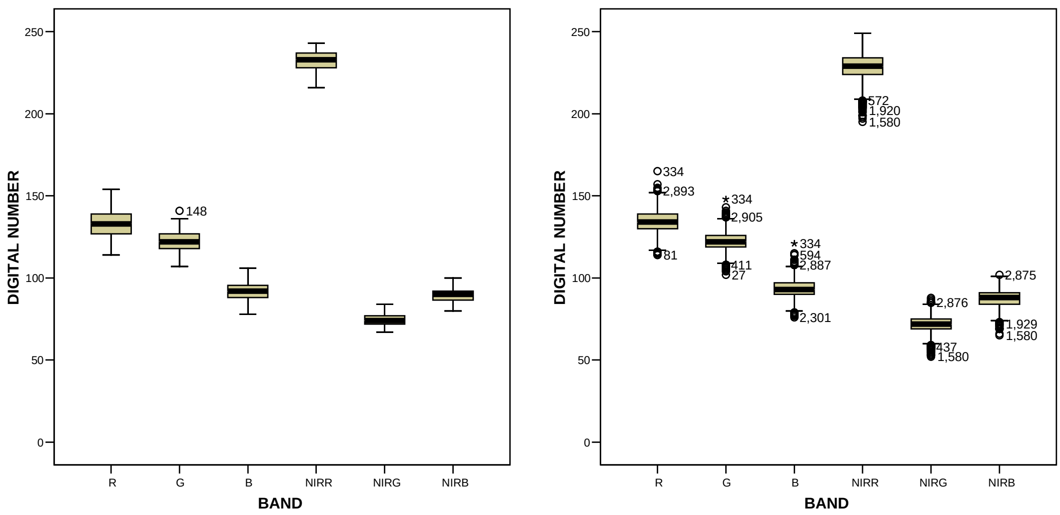

Figure 5.21 Box-plots of the digital numbers for the various bands*, selected using the ‘5 x 5’ kernel (left) and whole plot (right) AOIs (subplots 45 and 46).

*Colour camera (R-red sensor, G-green, B-Blue), NIR camera (NIRR-red sensor, NIRG-green, NIRB-blue)

Graphically, there is very little difference between each method. Reviewing the summary statistics indicated that although the ranges were greater in the ‘whole’ plot, the differences in averages between the two selection methods ranged from less than 0.1 % for the green sensor in the colour camera to just less than 4.0 % for the green sensor in the NIR camera (NIRG). As the ‘whole’ plot consisted of two identical plots side by side, treating each individually added statistical rigour. A two-pixel buffer around each plot also reduced the number of mixed pixels and this was the method utilised for further analysis (see Figure 5.22). This method of analysis was in line with the primary interest of this investigation, the crop attributes of yield and protein, which were measured for the whole plot.

The pixel values (DN) for the whole plot (except for a two-pixel buffer around the edge of the plot and around any other anomaly encountered) were extracted. This resulted in an average of 1300 pixels that were exported for each plot. Box-plot examples showing band values for a 0, 40, 80 and 120 kg/ha of applied nitrogen are shown in Figures 5.23 and 5.24. The average values for each of the 120 plots were formulated into a table on which statistical analysis could be conducted.

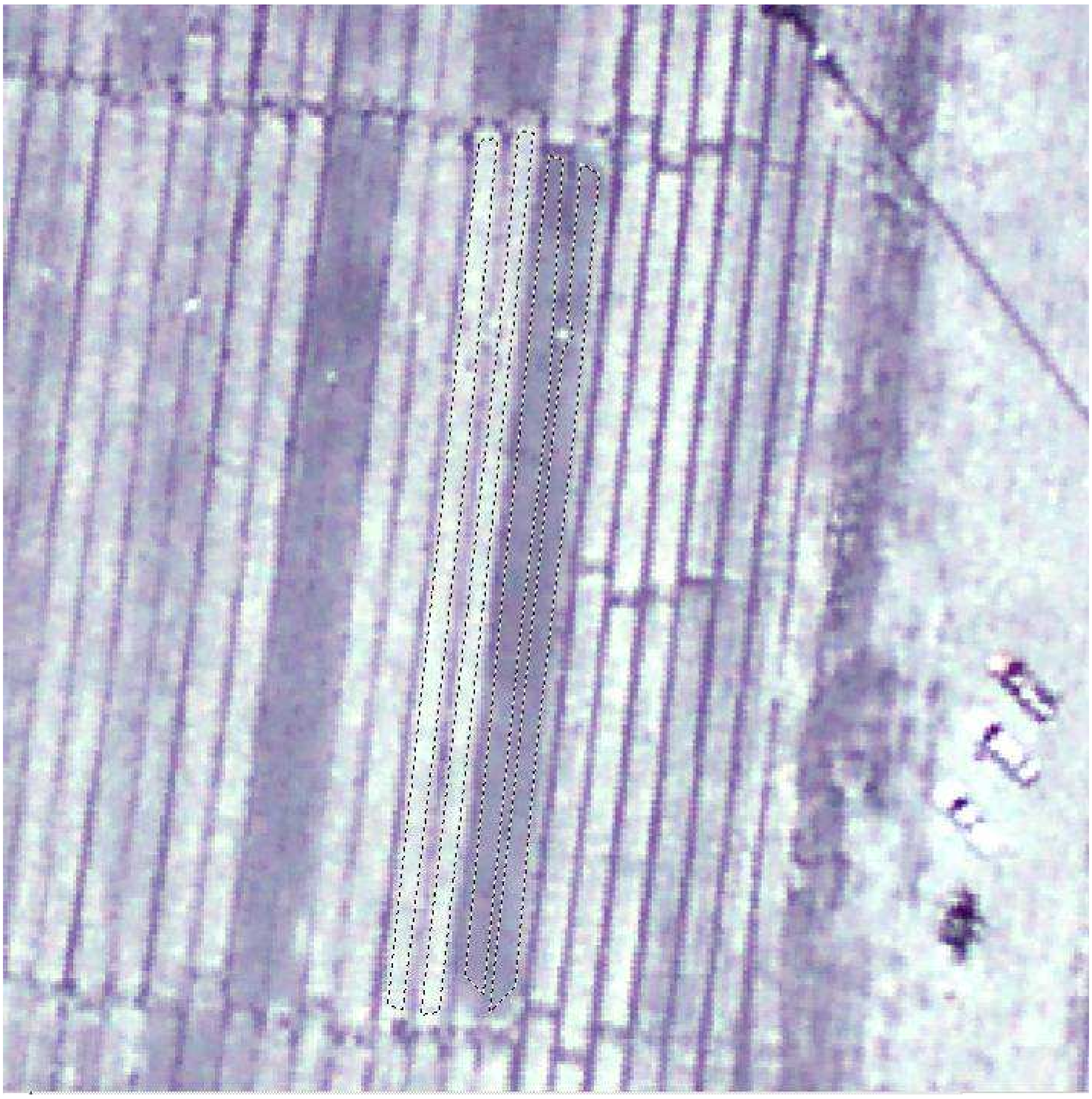

Figure 5.22 Selecting the area of interests (AOIs) for each of the plots (note the two pixel margin around each plot).

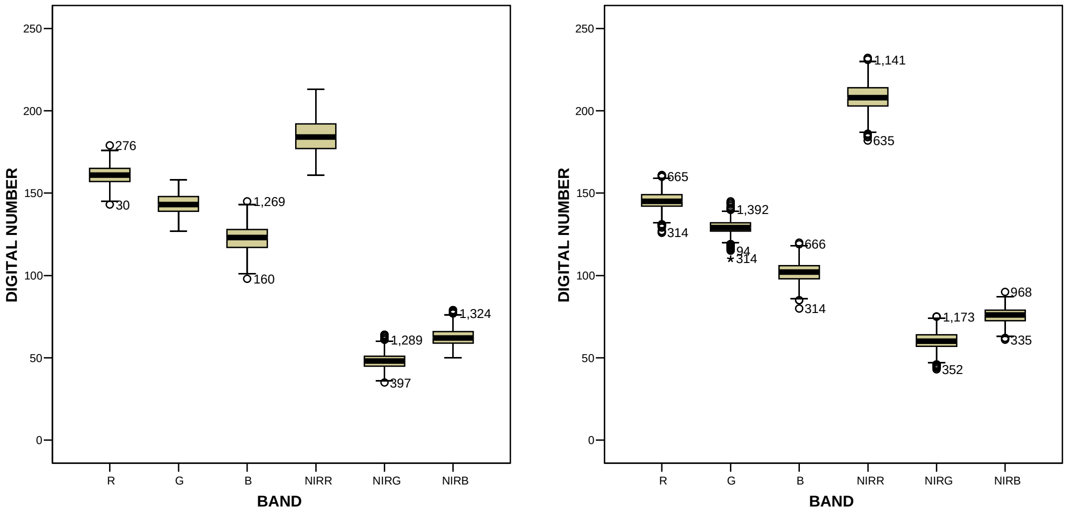

Figure 5.23 Box-plot of the digital numbers for all six bands for plot 41 (0 kg/ha N applied–left) and plot 51 (40 kg/ha N applied–right).

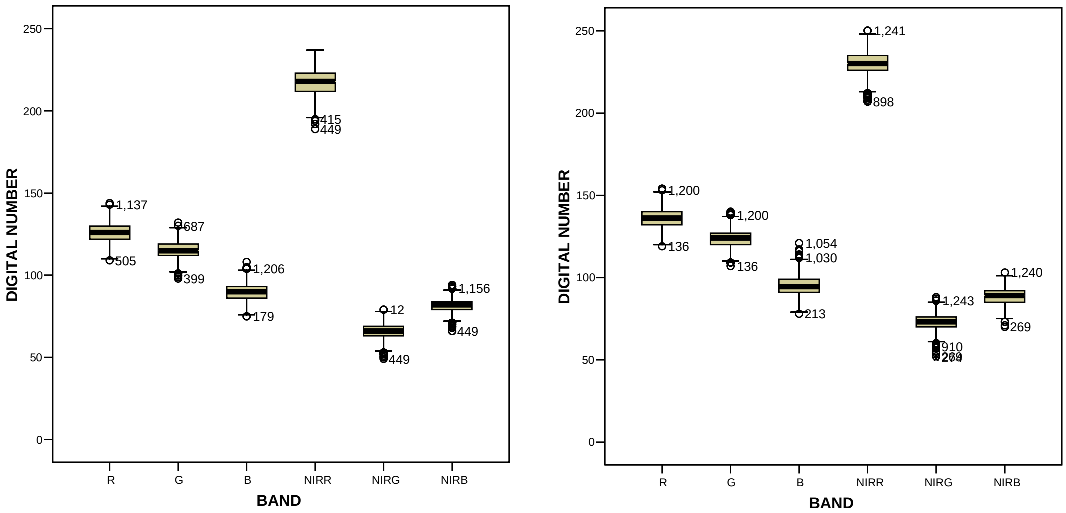

Figure 5.24 Box-plot of the digital numbers for all six bands for plot 57 (80 kg/ha N applied–left) and plot 43 (120 kg/ha N applied–right).

5.2.4 Statistical Analysis

The statistical analysis included correlation and discriminant function analysis using SPSS for Windows® Version 12.0.1 (SPSS 2003) and partial least squares regression using Unscrambler 9.1 (CAMO 2004). The correlation analysis and partial least squares regression were performed on the raw digital camera bands and the vegetation indices that could be derived using these bands. The discriminant function analysis (DA) was performed on the raw camera bands.

Correlation analysis estimates the coefficients of the linear equation that best predicts the value of the dependant variable and measures the strength of the relationship between the two variables (SPSS 2003). This procedure was used to investigate relationships between the bands and indices obtained with the LCLA remote sensing system and crop parameters (yield and protein).

Discriminant function analysis (DA) is a technique for combining independent variables into a new variable, on which each case in the study gets a score. This new variable, known as a discriminant function, is constructed in such a way that the score separates and/or discriminates among other cases in the different categories of the dependent variable (Kinnear & Gray 2004). A statistic called *Wilks' lambda* is use to test the efficacy of the discriminant function in producing significant differences among the target groups. The smaller the Wilks' Lambda, the more important the independent variable is to the discriminant function.

In SPSS there are two types of discriminant analysis: direct and stepwise. In direct DA, all variables are entered into the equation at once. With stepwise DA, statistical criteria alone determine the order of entry. The later procedure selects variables for inclusion within each step, however, before choosing a new variable to include, it checks to see if all of the variables previously selected remain significant (Johnson 1998). The stepwise DA is the most generally used (Kinnear & Gray 2004), especially where the number of variables is large (Johnson 1998).

When there are only two groups on which to perform a stepwise DA, there is just one discriminant function. However, with more than two groups, there can be several functions. It is unusual for more than the first three discriminant functions to be statistically robust, with the first function providing the best means of predicting group membership. Later functions may or may not contribute reliably to the prediction process (Kinnear & Gray 2004).

Stepwise DA was performed to quantify the ability of the sensor to accurately discriminate between the various fertiliser regimes present at this site, and has been used elsewhere to: a) evaluate nitrogen status in wheat (Filella *et al.* 1995) and in corn (Strachan *et al.* 2002), b) discriminate weeds (Piron *et al.* 2008), and c) provide an objective means of defining the minimal set of parameter necessary to evaluate malting quality in barley (Gianinetti *et al.* 2005).

Partial least squares regression (PLS) was implemented to assess the predictive power of the relationship between grain yield / protein and imagery values. PLS regression is a bilinear modelling method for relating the variations in one or several response variables (Y-variables) to the variations of several predictors (X-variables), with explanatory or predictive purposes (Esbensen 2002). Unlike the classical multiple regression technique, PLS performs particularly well when the various X-variables have high correlation (which is often the case for multispectral data). Information in the original X-data is projected onto a small number of underlying ("latent") variables called PLS components.

Aside from the raw imagery data, the set of derived vegetation indices was also calculated and analysed using the full cross-validation (leave-one-out) technique. The root mean squared error of prediction (RMSEP) was calculated, which gave the measurement of the average difference between predicted and measured response values. It can be interpreted as the average prediction error, expressed in the same unit as the original response value (CAMO 2004). The RMSEP values between datasets can be compared to determine which PLS regression model is better than others. The statistical procedures undertaken will be expanded on and the results discussed in Chapter 6.2.

5.3 Crop Type Discrimination and Mapping

5.3.1 Study Area

The study area was located at ‘Dunkerry South’, a farming systems trial site, near Nindigully (approximately 400 km WSW of Brisbane) in south-western Queensland (-28.476º, 148.724º), Australia (see Figure 5.25). During the 2004 winter crop season, various plots within the trial were planted with cereal wheat (*Triticum spp* cv. Baxter), barley (*Hordeum spp*. cv. Mackay), canola (*Brassica rapa* cv. Hyola 43), chickpeas (*Cicer arietinum* cv. Jimbour) and faba beans (*Vicia faba minor* cv. Fiord). Areas of the trial site (see Figure 5.26) were also set-aside for lucerne, grain legumes and medics. These however, were not present when the images were acquired, as they had failed during the growing season.

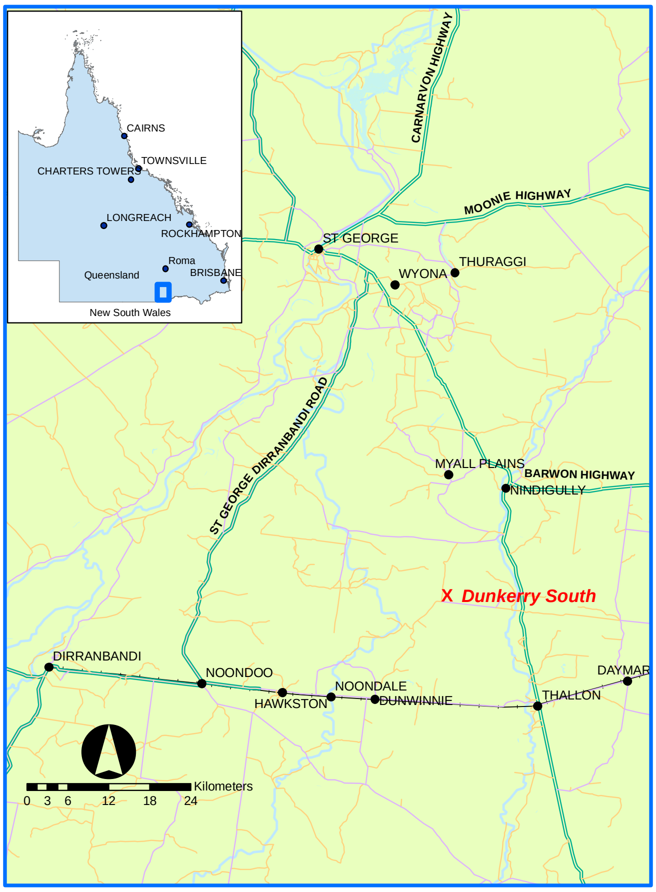

Figure 5.25 Location of the ‘Dunkerry South’ trial, near Nindigully, in south-western Queensland.

The site was set up in 1996 to assess the effect of contrasting "crop-following-crop" and "crop-following-pasture" strategies in a 600 mm sub-tropical rainfall zone (Thomas *et al.* 1998). The site was a grey vertisol (Isbell 1996) that had been under cultivation since 1956.

In 2004, all commodities were sown with a small plot seeder which consisted of 9 rigid spear-point tines followed by solid, centre–ribbed press wheels, at a row spacing of 0.25 m. Sowing depth was 3–8 cm. In the nitrogen fertiliser treatments, urea was applied at sowing in the centre of alternate seed rows. A basal application of 40 kg/ha of fertiliser containing 20.5% P, 9.4% N, 2.5% Zn and 2.2% S was banded with the seed at sowing. All species were sown on 13 May 2004 at the appropriate seeding rate for the district.

Each of the eight main plots within the trial was 40 m long and 36 m wide (16 runs of a 2.25 m wide planter) and replicated 3 times in a randomised block design. The main plots were split into sub-plots with treatments being different '*Crop* x *N application* x *Farming Systems'* combinations. Due to this diversity of treatments, image acquisition efforts were concentrated on areas containing a variety of species and N application rates, those being: 'System 9' (plot 27, 38 and 41) and 'System 11' (plot 29, 39 and 46) areas (refer to Figure 5.26).

5.3.2 System Deployment

Separate image acquisitions were attempted at this site on 12 August 2004 and 13 September 2004.

Deployment on 12 August 2004

The same sensor configuration and stabilising bar as was used in the 'Colonsay' trial (refer to Figure 5.15) was utilised at this site. However, rather than a single tether-line, two tether-lines were used to increase sensor stability and to aid in positioning.

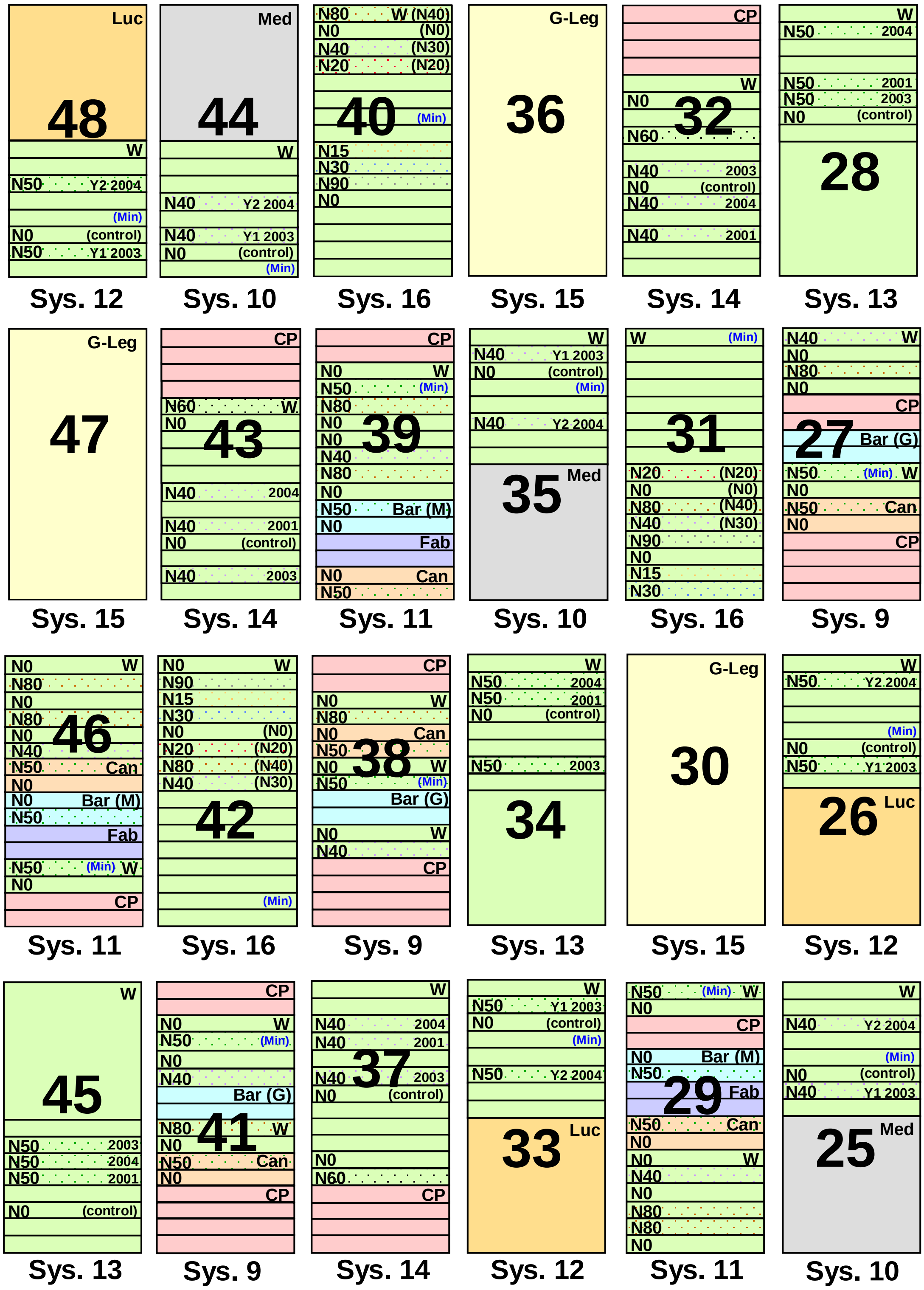

Figure 5.26 Schematic representation of the 'Dunkerry South' farming systems trial showing the treatments and plot layout.

The winds on the day were strong (see Figure 5.27) and the balloon could not be launched higher than 20 m. Had the distance travelled to the trial site not been large (800 km round trip), the acquisition of imagery would have been delayed due to the inclement weather conditions. The breeze made taking images difficult, and eventually resulted in the sensor being whipped around by the wind. Eventually, the digital cameras were dislodged from the balsa box and fell to ground. Repairs could not be carried out to continue the mission. No useful images were captured.

Deployment on 13 September 2004

The second attempt at image acquisition, 13 September 2004 (123 days after sowing), had clear skies and a moderate breeze. The balloon and sensor configuration was the same as used on 12 August and is shown schematically in Figure 5.28. The LCLA remote sensing system ready for deployment is shown in Figure 5.29.

Figure 5.27 The sensor being retrieved at Nindigully (note the breeze blowing the balloon).

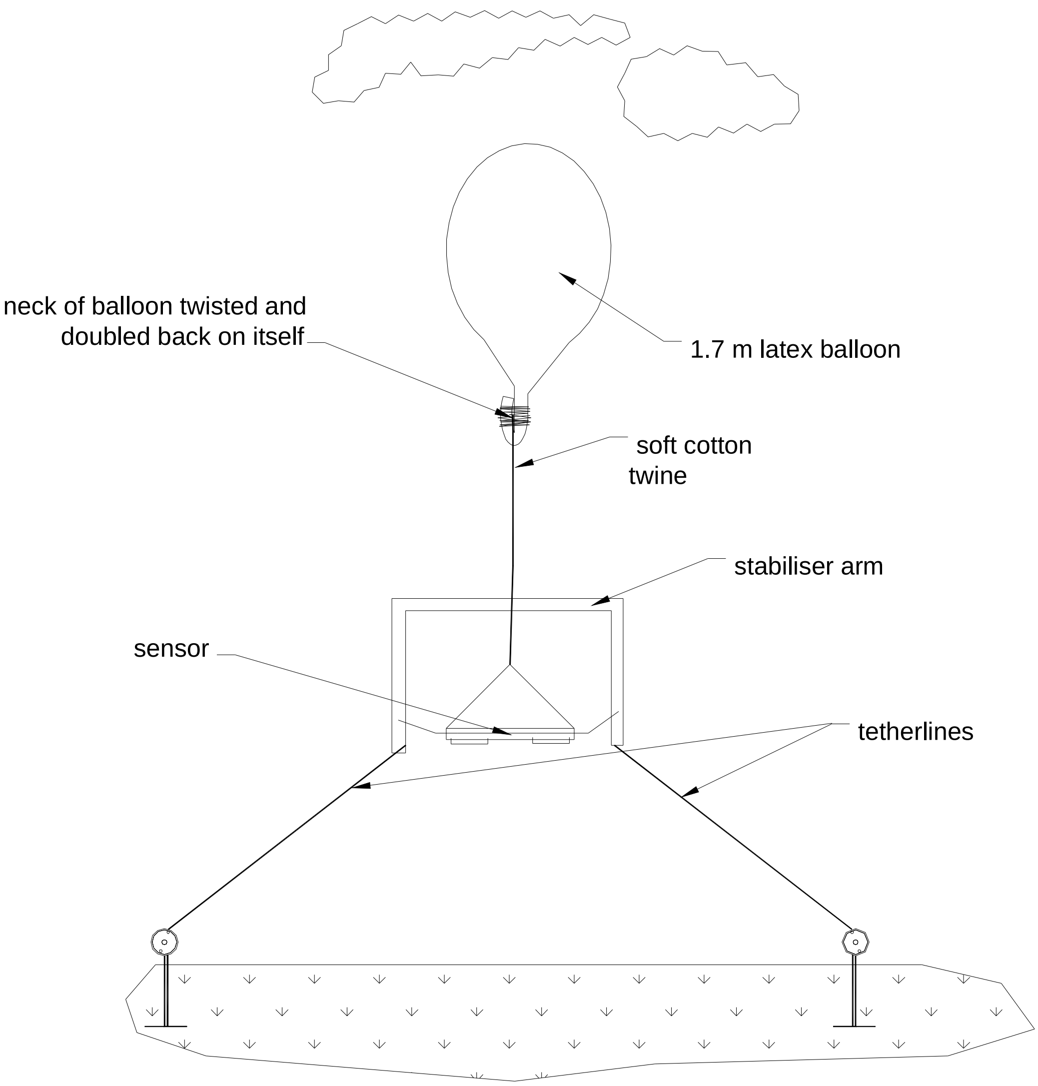

Figure 5.28 A schematic representation of the sensor as deployed, 13 September 2004.

The balloon and sensor were deployed by playing out the tether-lines by releasing the brakes on the Alvey® sidecast fishing reels. As the line was run out, the persons controlling the lines moved further apart giving the sensor increased stability. With two fixed points, the balloon and sensor could now only move in an arc. The sensor, consisting of the two digital cameras and video camera, was positioned above the area of interest by viewing the video footage that was being transmitted from the sensor and by adjusting the tether-lines accordingly. The areas targeted for imaging included the plots containing wheat along with a range of other species (‘System 9’ and ‘System 11’ plots as detailed in section 5.3.1).

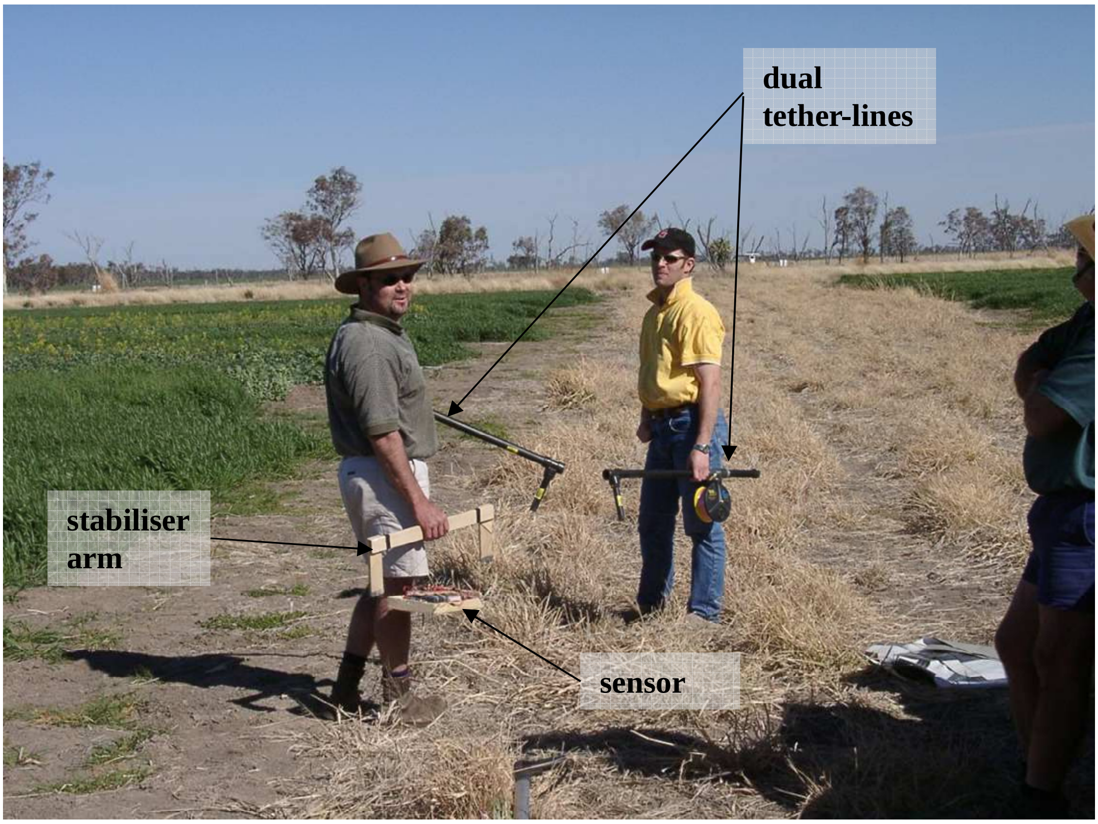

Figure 5.29 The sensor ready to be deployed at Nindigully, with two tether-lines for increased stability.

The first mission undertaken on the day was with the balloon at approximately 150 m (to capture the whole plot, refer to Figure 5.30) and the later mission at approximately 400 m (an attempt to capture the whole trial area, refer to Figure 5.31). The colour camera failed at the start of the second mission resulting in only 83 images captured, while 163 images were captured with the NIR camera on both missions in the hour either side of solar noon. The failure of the colour camera was diagnosed afterwards as a loose connector and was rectified prior to subsequent missions.

Figure 5.30 An image captured on the first mission covering adjacent plots showing a range of species present, as captured by the LCLA remote sensing system.

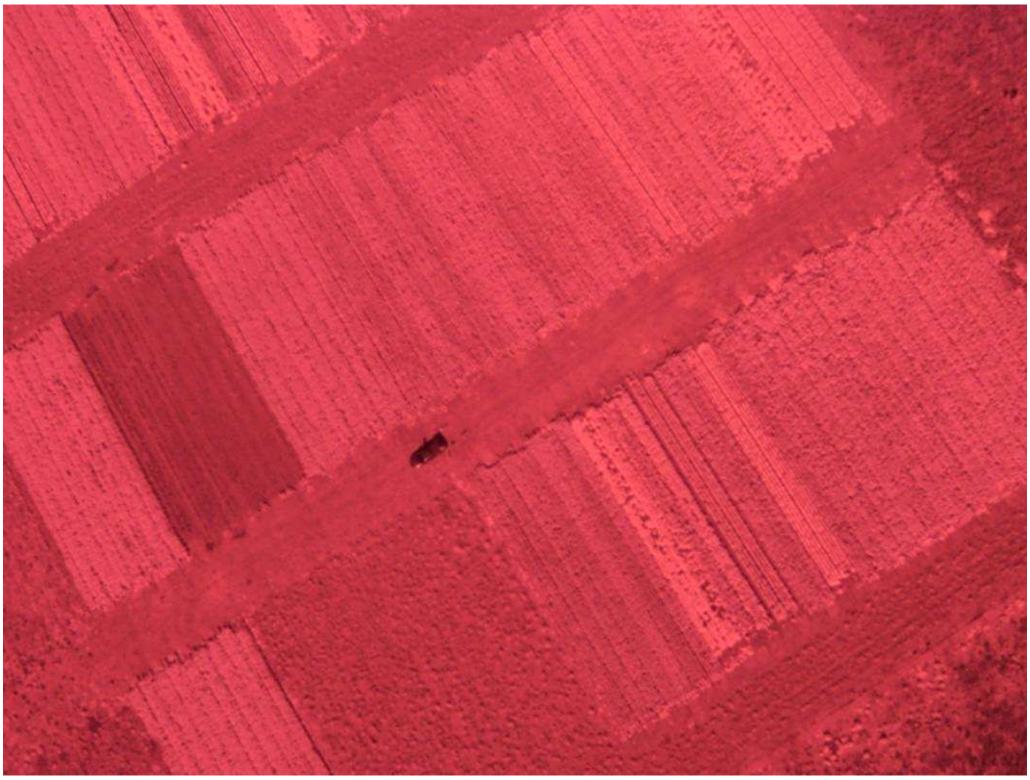

Figure 5.31 The NIR image showing the majority of plots 41-48, as captured by the LCLA remote sensing system.

The images were transferred and viewed on a laptop computer while at the location. All images were later copied into a desktop computer where the most appropriate images were chosen for further processing. The colour image that was chosen for further analysis, with labels added, is shown as Figure 5.32, while the matching NIR image is shown as Figure 5.33. The judgement criteria for image selection were based on plot coverage, species present, orientation, and the clarity of the image.

Using the criteria detailed above, two pairs of images were chosen to be imported into ERDAS Imagine 8.7 (ERDAS 2003) and analysed. The first pair of images covered the majority of plot 38 and contained the following treatments: wheat (0, 40, 50 and 80 kg/ha N applied), canola (0 and 50 kg/ha N applied), barley and chickpeas. The second pair of images covered the majority of plot 41 and contained the same treatments as in plot 38. The analysis conducted on each plot was slightly different and so will be detailed individually (refer to Chapter 5.3.3).

Due to the large range of species at this site, the primary objective of this acquisition was to assess the ability of the sensor to differentiate between these different species. Of the two approaches taken to analyse the data, the first was to use a statistical package to perform the analysis. The second one was to use image analysis software to perform the classifications.

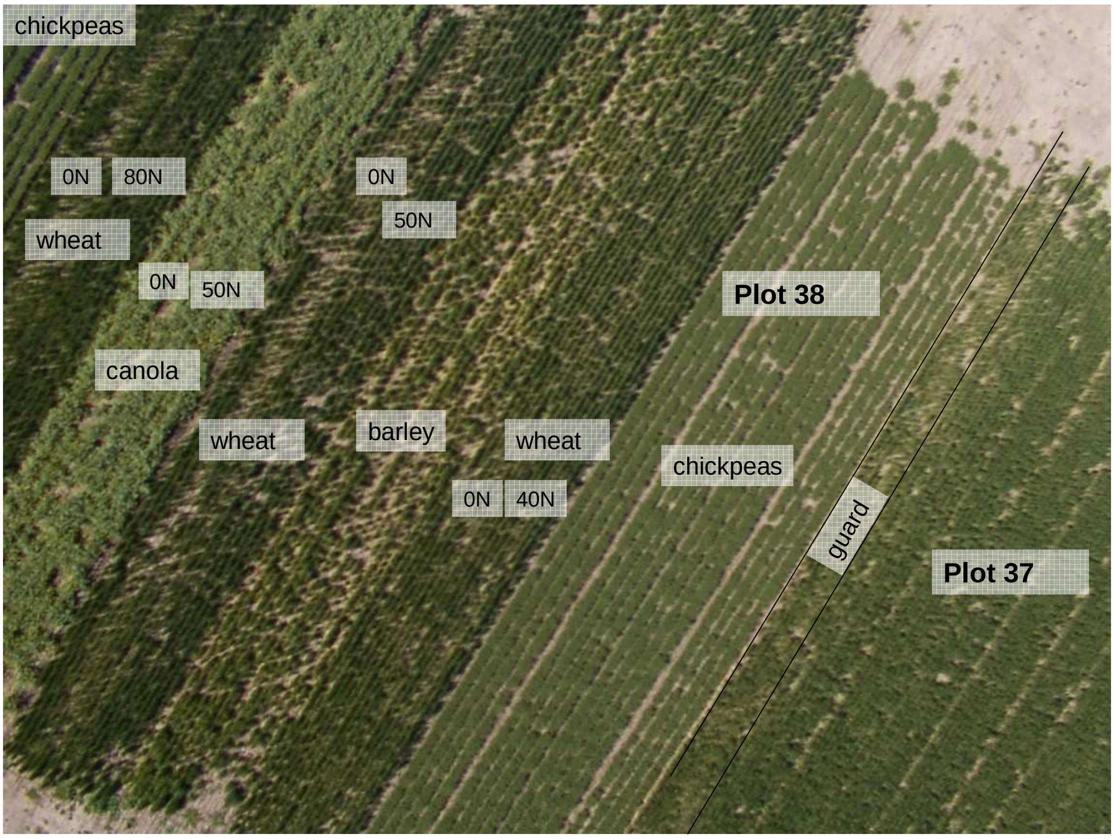

Figure 5.32 The species present in plot 38, as captured by the LCLA RS system.

Figure 5.33 The NIR image that matches with the colour image shown in Figure 5.32.

5.3.3 Pixel-based Image Processing and Analysis

GPS co-ordinates were not recorded for this trial, as the available GPS (the same as used at Colonsay) utilised the AMSA beacons for the differential correction. As the distance to the nearest beacon (Brisbane) was over 400 km, the differential correction was intermittent, and hence, unreliable. As the objective at this trial was to perform crop-type discrimination using spectral data, geo-referencing was not essential as relative location and size still enabled this type of analysis to be conducted.

Plot 38

In analysing the images covering plot 38, two approaches were taken. One approach was to use a statistical package, SPSS Version 12.0.1 (SPSS 2003), to investigate the potential of the LCLA remote sensing system to discriminate between different crop types. The other method was to use the image analysis software ERDAS Imagine 8.7 (ERDAS 2003) to look for relationships between the spectral signatures obtained from the images and the crop attributes. The analysis conducted on images covering plot 38 was the first one undertaken for the 'Nindigully' trial. The colour image was registered to the near infrared image using 10 ground control points resulting in a checkpoint error of 1.7 pixels. With a pixel resolution of 40 mm, this equates to a checkpoint error of less than 70 mm. As the resolution of the imagery is so fine, these GCPs were based on the centre of an area rather than an individual pixel, and may have contributed to this checkpoint error.

Statistical Analysis

Two approaches were taken to statistically analyse the data for this plot:

a) The first procedure was the same as performed to evaluate the 'Colonsay' data (detailed in section 5.2.4), where areas of interest (AOIs) were created around the sub-plot and the data analysed. Within plot 38, there were a number of subplots (see Figure 5.32), those being: 2 x barley; canola (50 N); canola (0 N); 4 x chickpea; 2 x wheat (0 N); wheat (40 N); and wheat (80 N).

b) The second method undertaken was to extract several AOIs within each subplot. SPSS Version 12.0.1 (SPSS 2003) was used to perform discriminant function analysis (DA) on the digital number (DN) values to see if the sensor could accurately discriminate between the species present in the trial (i.e. if the plots that were planted to wheat could be differentiated from the canola, barley and chickpea plots). The DA procedure generates one or more discriminant functions based on linear combinations of the predictor variables that provide the best discrimination between groups. It has been used successfully in spectral discrimination studies (Strachan *et al.* 2002). The entire sample set was used in the DA calculations and was cross-validated.

In method (a) above, AOIs were defined around the perimeter of each sub-plot (see Figure 5.34). This resulted in >40 000 pixels selected for each of the six bands for the sub-plot. Box-plots of the data exported for selected treatments are displayed in Figure 5.35. A large range of DN values (from less than 50 to approaching 250) are evident for each band. The chickpea crop in this trial was shorter than the other species, and as a result, the image was less affected by shadow. As it was also closer to canopy closure, there was less reflectance from the bare soil in the inter-row. This is evident in Figure 5.35 by the tighter range of values across all bands compared with the wheat 40 N graph. With the wheat being a taller crops and less uniform in growth habit, there was more influence from shadows within and between rows resulting in more contrasting reflectance and a greater ranges of values.

By having a large AOI around the whole treatment, the potential to approximate the texture of the crop, its growth habits, establishment and degree of canopy closure is enhanced.

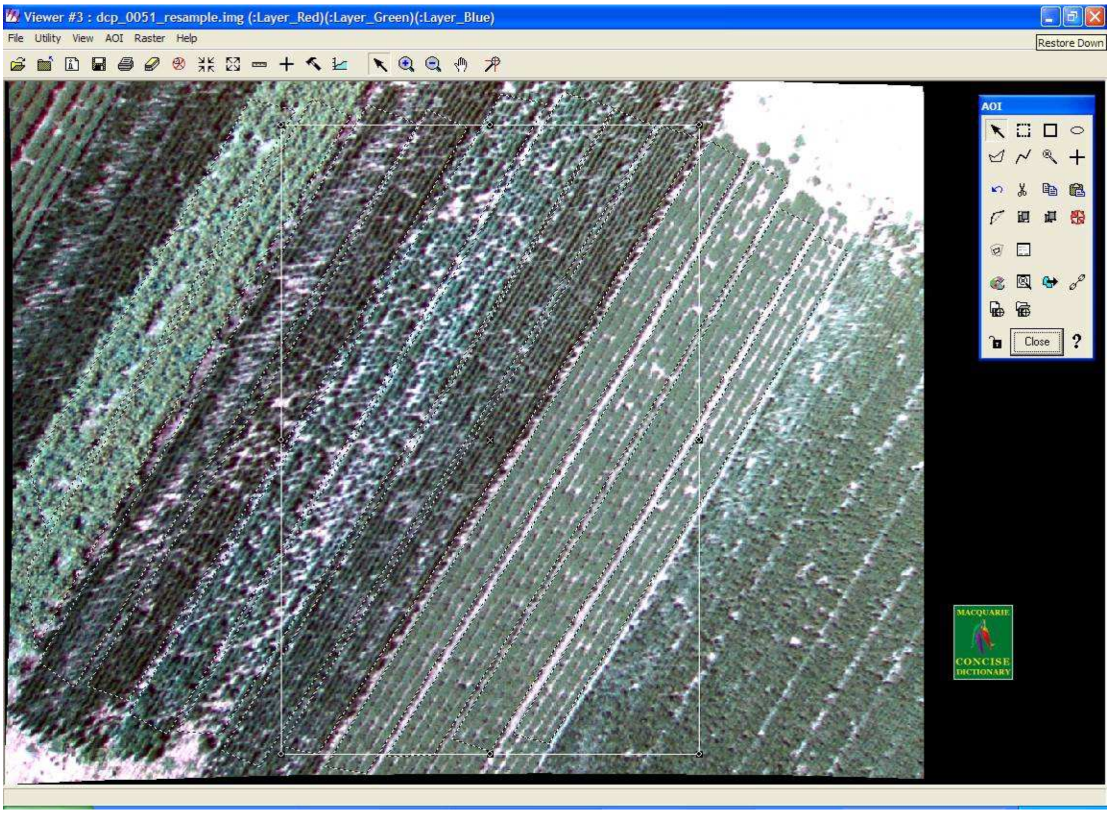

Figure 5.34 Selecting AOIs for each of the subplots within plot 38.

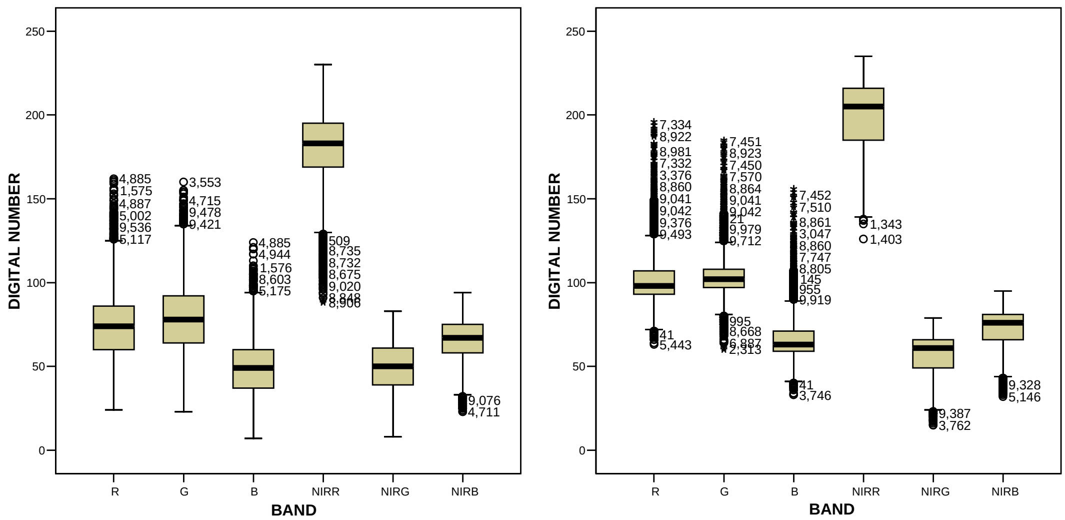

Figure 5.35 Box-plots for wheat 40 N (left) and chickpeas (right) for the 6 bands.

Shown in Figure 5.36 are the average DN values for all bands for each of the treatments within plot 38. As the nutrition levels increased, the crops' health status improved. Healthy plants lead to increased vigour, which means more photosynthesis. The process of photosynthesis absorbs light in the visible portion of the spectrum (particularly the R and B) and reflects light in the NIR. As the red sensor in the CCD is the most sensitive to NIR (indicated by the area under the curve above 700 nm in Figure 3.7), the DN values for NIRR is much higher than for both the other sensors in the CCD (NIRB and NIRG) of the 'NIR' camera.

When a plant is stressed, the spectral characteristics of the leaf change, with the changes happening more or less simultaneously in both the visible and NIR regions (Campbell 2002). The spectral change induced by the stress associated with the varying nutrition levels is particularly evident in the wheat spectra (the blue lines) in Figure 5.36. The reflectance of the crop increases as the nutrition levels decrease.

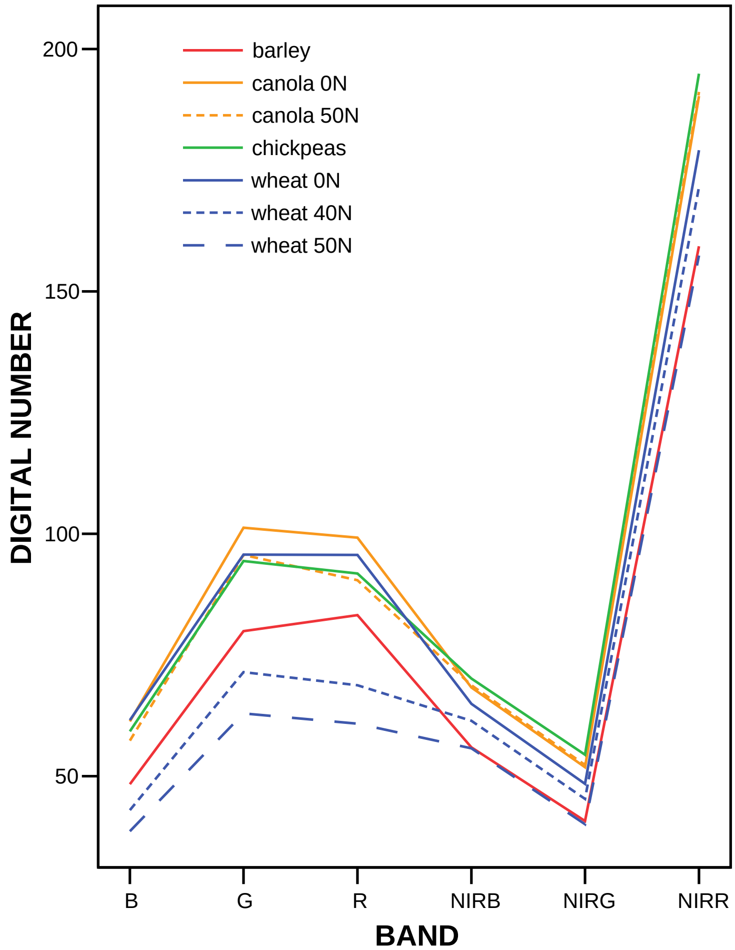

Figure 5.36 Average digital number values for the sub-plots within plot 38 for the various bands.

The potential to perform statistical procedures was limited by the number of samples. When using the 'whole sub-plot AOI method' for the image covering plot 38 (shown in Figure 5.34) there were only 19 plots and not a large enough sample size to investigate statistical associations. In order to increase the sample size, each subplot representing the different species was split into initially five and then 10 equal sized AOIs. The results were analysed using SPSS and will be discussed in section 6.3.1.

Image Classification

Image classification is the process of sorting pixels into a finite number of individual classes, or categories of data, based on their data file values (Leica 2005). That is, the pixels are grouped together with other pixels that have similar brightness across multiple bands of an image (Campbell 2002). These classes have been shown to correspond to regions on the ground that have common biological properties.

To perform an image classification, signatures for target classes had to be identified. The AOIs chosen for each sub-plot (detailed in the above section) were too broad for this purpose as they contained signatures for bare soil, shadows, crop etc. To provide representative pixels for the signatures, pixels were selected by positioning polylines down the middle of uniform rows of the target species. This resulted in approximately 150 pixels selected per species present. These pixels had little influence from shadows, soil reflectance and crop misses that were causing the scatter in the DN values depicted in Figure 5.35. The boxplots of the actual DN values using this method, for the same species as shown in Figure 5.35, are shown in Figure 5.37.

Plotting the DN values for these 'pure' polylines shows that it is difficult to truly obtain consistent values in variable crops. The variability is evident by the range of values in the 'wheat 40 N' spectra. Where the crop was inherently more uniform, as in the chickpeas, this variability is considerably reduced. The pure signatures were exported and the analysis is discussed in section 6.3.2.

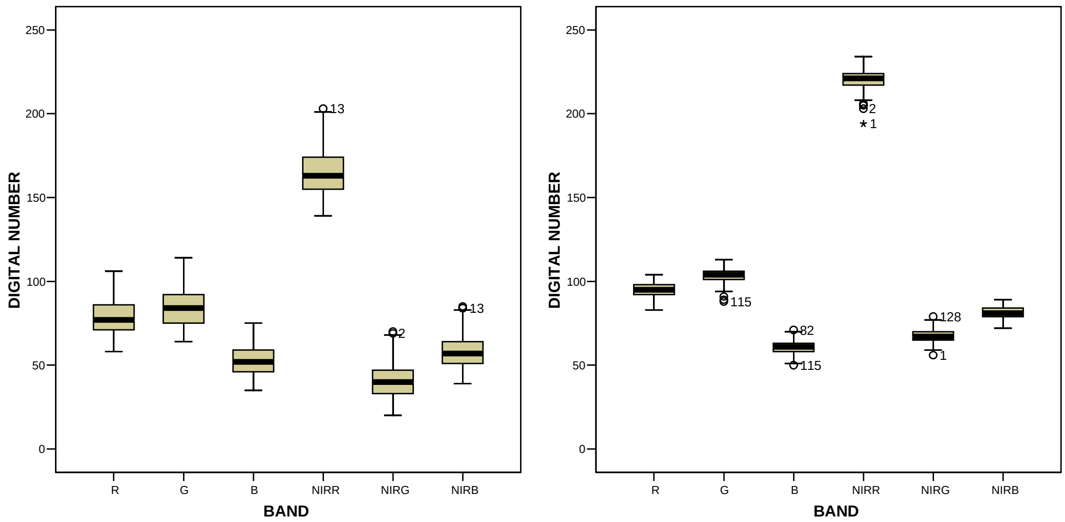

Figure 5.37 Box-plots of the pixel values for the polyline positioned down the centre of the row for each of the six bands for wheat 40 N (left) and chickpeas (right).

Although obtaining pure pixels for a species provides the most accurate data, it does not however take into consideration other parameters such as texture, growth habits, height (and hence likelihood of shadows), how well the crop established (the possibility of missing plants), aspect of the foliage to the sun, position of the sensor and whether canopy closure has been achieved. This could be accounted for by having many classes for the same species, but analysis is not possible using conventional ‘pixel-based’ analysis. Object-orientated image analysis is, however, better able to handle these phenomena and was investigated in section 5.3.4.

Plot 41

The matching colour and NIR image pair covering plot 41 were used to perform this investigation. The colour image is shown in Figure 5.38. Within this image, there were a number of subplots within the main plot as well as other land management features. The image was split into 12 management classes: bare soil, non-photosynthetic vegetation, green weeds, vehicle, shadow, chickpeas, three classes of wheat (0, 40 and 50 N), two classes of canola (0 and 50 N) and barley.

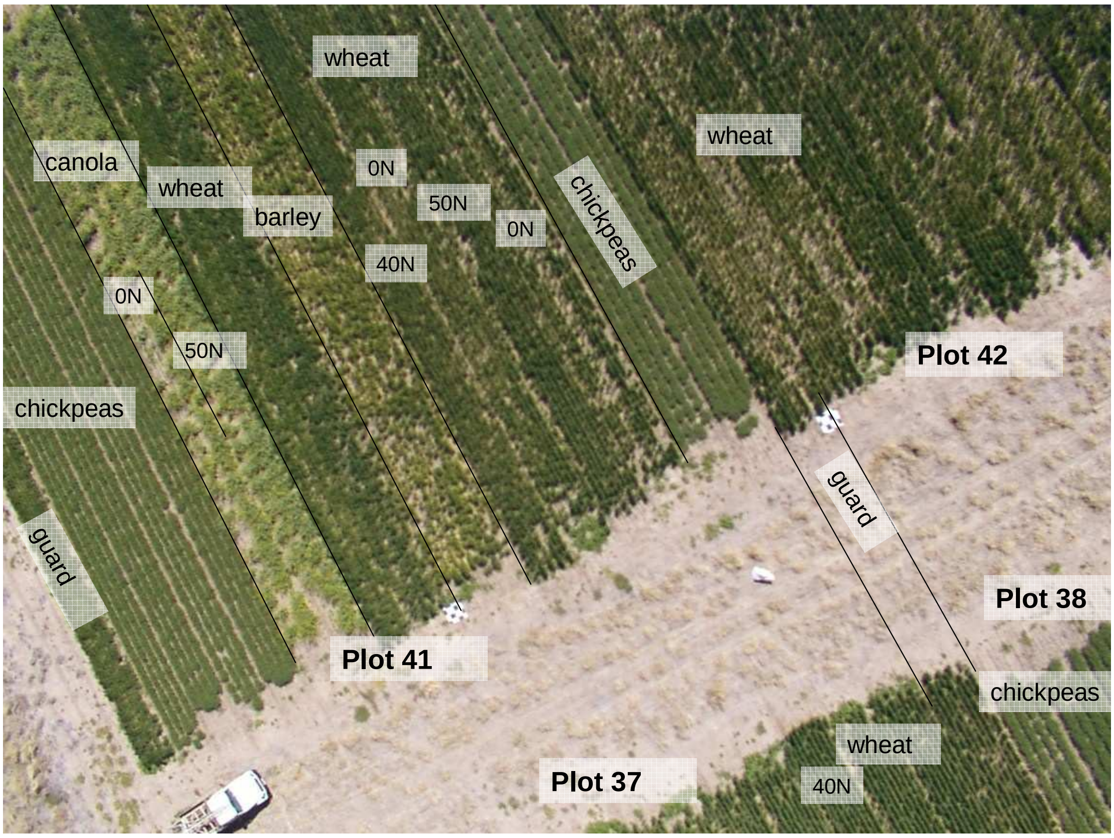

Figure 5.38 Plot 41 and surrounding plots showing different species present.

The infrared image was registered to the colour image utilising the 'layer stack' function of ERDAS Imagine 8.7 (ERDAS 2003). A total of 18 ground control points were used, resulting in a total checkpoint error of 1.2 pixels (see Figure 5.39). With a 45 mm pixel resolution, this equates to an error of less than 60 mm. Once again, the GCPs were based on the centre of an area rather than a discrete pixel, resulting in a slightly larger error than expected. The image was resampled using the nearest neighbour resampling. The resulting image had 6 bands that are detailed in Table 5.1.

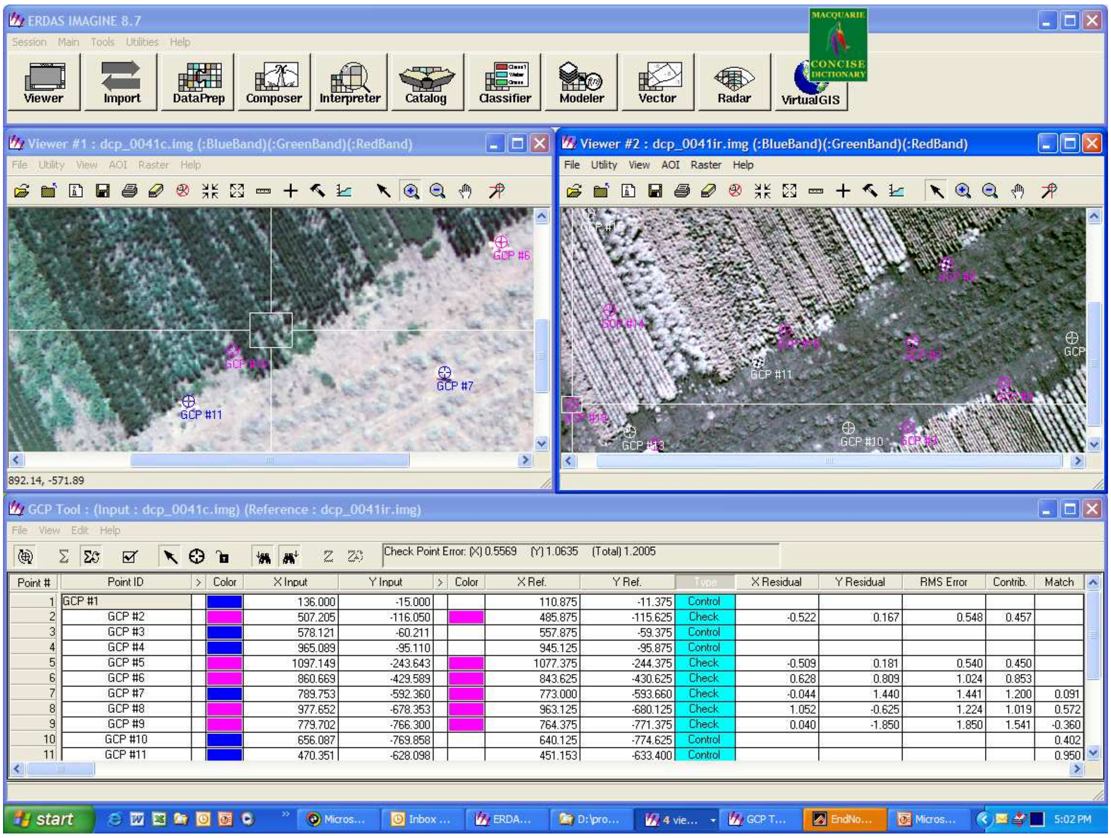

Figure 5.39 The layer stacking procedure of the 2 images in the analysis software.

Table 5.1 The band information for the stacked image.

Camera	Sensor	Band
Colour	Blue	1
	Green	2
	Red	3
Near infrared	Blue	4
	Green	5
	Red	6

Due to the slight misalignment of the colour and IR camera, some areas did not have the colour bands whilst other areas did not have the IR bands (approximately 5% of the image), particularly around the periphery of the image. The image was clipped to exclude these areas from further analysis.

Image Classification

The approach taken with this dataset was to use the image analysis software ERDAS Imagine 8.7 (ERDAS 2003) to perform image classifications. According to Campbell (2002), supervised classification is usually considered appropriate when you want to identify relatively few classes, when training sites can be verified with ground truth data, and when distinct and homogenous regions can be identified to represent each class. All of these criteria were meet in this dataset.

To perform the supervised classification, spectral signatures that were representative of the 12 management classes (detailed above) were selected using the signature editor function of the software. Following the recommendations of Campbell (2002), several individual training areas were selected for each class and these areas were selected from throughout the image. The total number of pixels selected far exceeded the ‘at least 100 pixels for each category’ recommended by Campbell (2002). In some of the classes (car, bare soil and non-photosynthetic material), it was easy to select large homogenous areas (>500 pixels) using the polygon area-of-interest (AOI) tool. Four areas were selected for each of these classes.

Conversely, in the cropping areas, it was more difficult to find homogenous areas from which to select signatures. Due to the growth habit and the wider row spacing (4 rows across the 2.25 m row) for the chickpeas and canola, they tended to fill-in the inter-row space, and made selecting areas possible, albeit smaller in pixel count compared to previously mentioned three classes. Seven areas for each class were selected and the pixel count ranged from 50 to over 400. With the wheat and barley planted on 0.25 m row spacing (9 rows per plot), it was difficult to find consistent areas. For the barley signature, 9 areas were chosen with the pixel count ranging from 59 to 247. It was not possible to use the area function for the wheat signatures. Instead, the polyline function of the AOI tool was used (see Figure 5.40). Across the three wheat classes, 20 polylines were selected with pixel counts ranging from 10–33 for each of the classes with approximately 500 pixels being collected for each class.

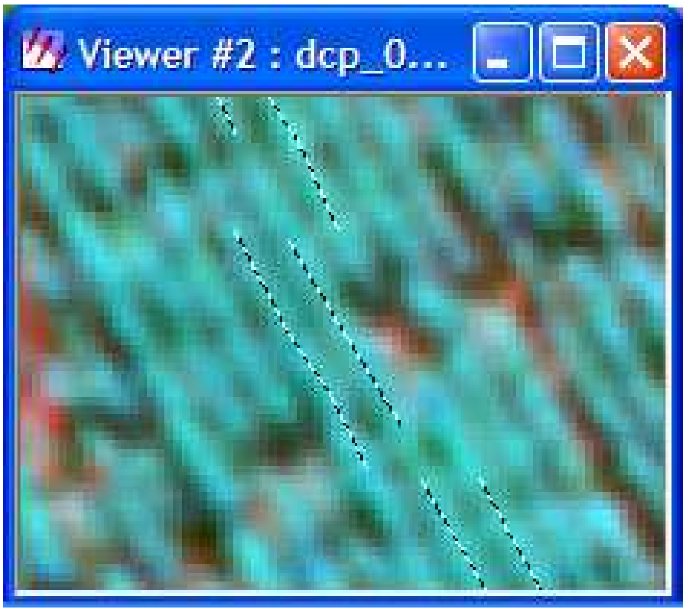

Figure 5.40 A close-up of the polyline area-of-interest for the wheat 50 N plot.

The 12 management classes along with the 'count' of pixels making up each class are shown in Figure 5.41. The number of pixels per class ranged from over 400 pixels for wheat with no N applied to over 4000 pixels for bare soil. The colours used in Figure 5.41 (black for shadow, red for car etc.) will be the same colours used in the results and discussion detailed in section 6.3.2.

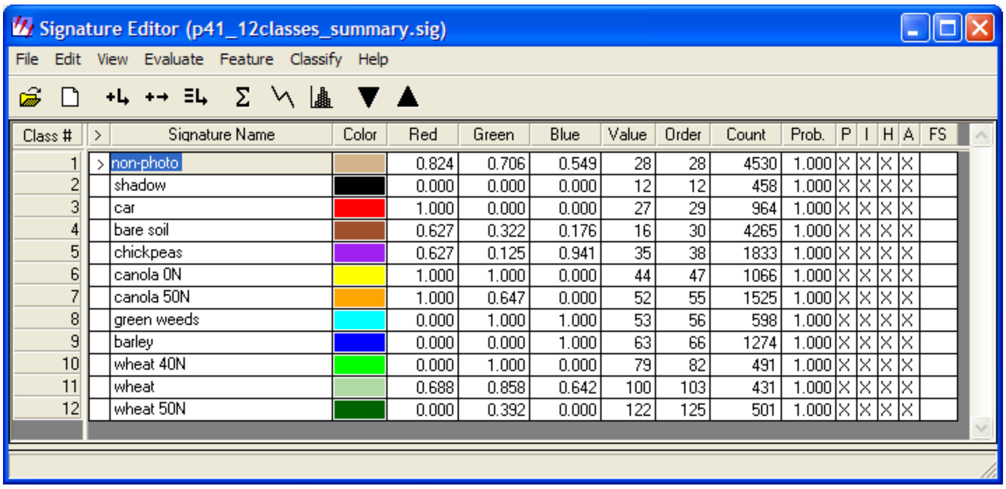
Signature Editor (p41_12classes_summary.sig)

File Edit View Evaluate Feature Classify Help

Class #	>	Signature Name	Color	Red	Green	Blue	Value	Order	Count	Prob.	P	I	H	A	FS
1	>	non-photo		0.824	0.706	0.549	28	28	4530	1.000	X	X	X	X	
2		shadow		0.000	0.000	0.000	12	12	458	1.000	X	X	X	X	
3		car		1.000	0.000	0.000	27	29	964	1.000	X	X	X	X	
4		bare soil		0.627	0.322	0.176	16	30	4265	1.000	X	X	X	X	
5		chickpeas		0.627	0.125	0.941	35	38	1833	1.000	X	X	X	X	
6		canola 0N		1.000	1.000	0.000	44	47	1066	1.000	X	X	X	X	
7		canola 50N		1.000	0.647	0.000	52	55	1525	1.000	X	X	X	X	
8		green weeds		0.000	1.000	1.000	53	56	598	1.000	X	X	X	X	
9		barley		0.000	0.000	1.000	63	66	1274	1.000	X	X	X	X	
10		wheat 40N		0.000	1.000	0.000	79	82	491	1.000	X	X	X	X	
11		wheat		0.688	0.858	0.642	100	103	431	1.000	X	X	X	X	
12		wheat 50N		0.000	0.392	0.000	122	125	501	1.000	X	X	X	X	

Figure 5.41 Signature editor showing the 12 classes.

In addition to the visual examination of the imagery, the data was further explored by examining band histogram and statistics, determining correlation of bands using scatterplots and calculating correlation of pairs of wavelength bands. The results of the analysis are discussed in section 6.3.2.

5.3.4 Object Orientated Image Classification

In section 5.3.3, the image processing and analysis tasks focused on the traditional pixel-based classification technique (i.e. supervised classification). In this current section, the new generation object-oriented approach (Blaschke *et al.* 2000) was tested and the results compared with the pixel-based method. In the object-oriented paradigm, an object can be defined as a grouping of pixels of similar spectral and spatial properties (Navulur 2007). In addition to spectral values, an object has other attributes that can be used in image classification, such as shape, texture, morphology, context, etc. Thus, an object-oriented approach has better potential of achieving higher accuracy.

The first step in the object-oriented approach is *image segmentation*. Image segmentation is a technique that is used to divide a scene or image into regions or objects that have common properties. Two techniques for image segmentation can be separately implemented (Navulur 2007): a) region merging according to some measure of homogeneity and, b) separation of objects by finding edges using gradients of digital numbers between neighbouring pixels. The user can also specify other attribute parameters during the segmentation process.

For this study, the software *Definiens Professional 5* (Definiens 2007) was used for the object-oriented image processing. The segmentation algorithm creates image segments based on the following four criteria: *scale* (to determine the maximum allowed heterogeneity within an object), *colour* (to determine overall contribution of spectral values to define homogeneity), *smoothness* (to optimise image objects for smoother borders) and *compactness* (to optimise image compactness).

After a series of tests, the following segmentation parameters were finally applied to the 6-layer image (Figure 5.42):

- 30 scale, 0.9 colour, 0.5 compactness
- 50 scale, 0.9 colour, 0.5 compactness
- 80 scale, 0.9 colour, 0.5 compactness
- 100 scale, 0.9 colour, 0.5 compactness

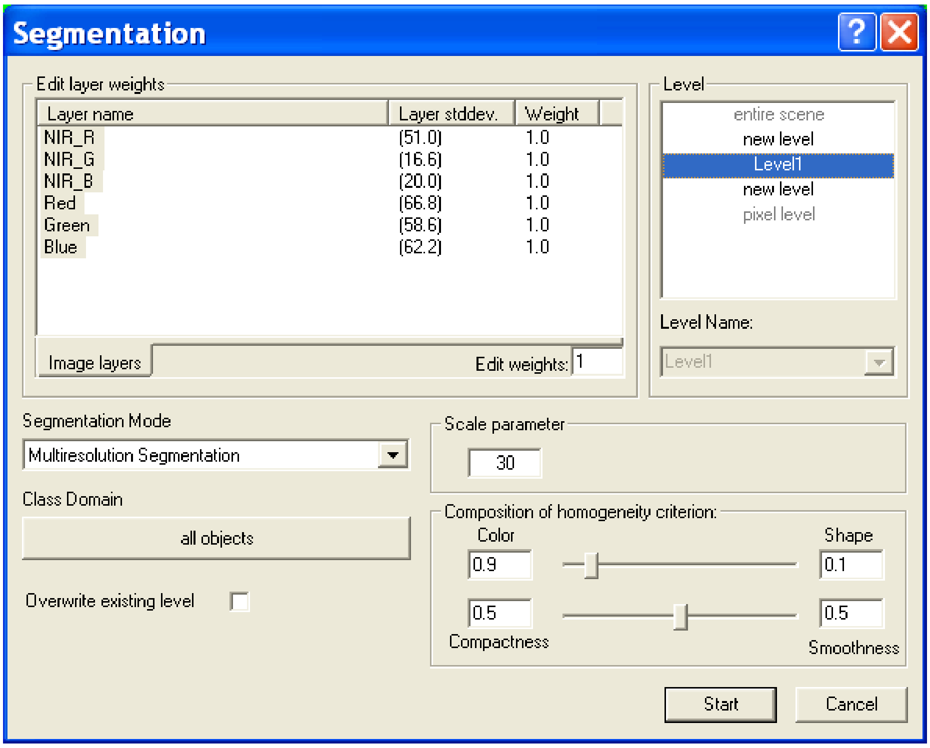

Figure 5.42 Segmentation parameters used in the object-oriented approach (showing the 30 scale as an example)

The importance of colour over shape was set to 0.9 out of 1.0, while an equal (50%) weight was used for compactness and smoothness criteria. The 9-class grouping ("class hierarchy") was used to enable comparison of the results with the pixel-based approach (Figure 5.43). Samples were selected and then pre-assessed based on "colour" (DN value), shape and texture criteria.

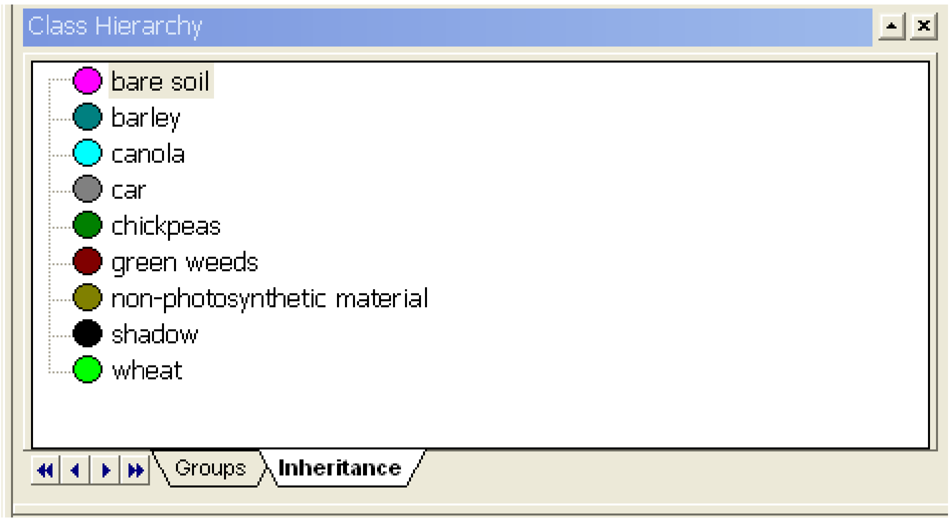

Figure 5.43 Classes adopted in the classification

Finally, the image was classified based only on colour and texture, i.e. shape was excluded due to its low importance in the segmentation scale used. The nearest neighbour technique was utilised. With this approach, it classified image objects in a given feature space based on given samples for the classes concerned (Definiens 2007). The distance in the feature space to the nearest sample object of each class was calculated for each image object. The image object was assigned to the class represented by the closest sample object. Once classified, accuracy assessment was conducted for each output image using the same procedure in the per-pixel based approach.

The results of the analysis were discussed in the next chapter, section 6.3.3.

5.4 Further Refinement

Since the loss of the original 1.0 Megapixel sensor on mission #21 (Table 4.1), the LCLA system was refined further with the new 5.0 Megapixel sensor. The latter was used on a number of imaging missions to investigate crop maturity in wheat and barley (mission #24), crop uniformity and nodes above cracked boll in cotton (missions #25&26), growth rates due to irrigation non-uniformity in lettuce (mission #27&28), and an evaluation of the UAV autopilot system (mission #29). As the primary focus of this research is on cereal grain crops, the crop maturity mission was further investigated along with the autopilot evaluation. The autopilot system has the potential to overcome the constraints of planning the imaging schedule to ensure coverage of the target area—the major constraint to the application of the existing LCLA remote sensing system to broader-scale cereal production.

5.4.1 Crop Maturity Mapping

Study Area

The study area was located at 'Lundavra', a wheat and barley variety trial site in the Goondiwindi district of southern Queensland (150.087º, -28,056º), Australia (see Figure 5.44). The site was established to screen both wheat and barley varieties for adaptation to a potentially tough season, generally caused by lack of rain and heat stress during the early part of the growing season. In 2005, the trial was high yielding due to favourable seasonal conditions.

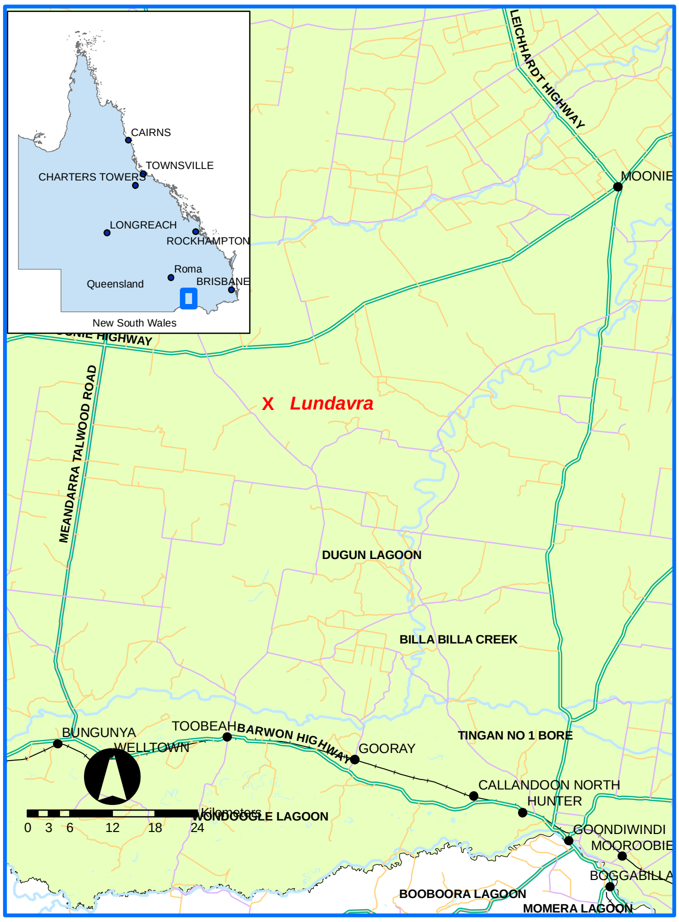

Figure 5.44 The location of the trial site at 'Lundavra' in southern Queensland.

The original intention of this investigation was to compare traditional meter-resolution aerial imagery to that of the updated LCLA remote sensing system. Due to unforseen delays by the commercial imagery provider, the acquired image was captured late in the growing season. In the conventional aerial image of the entire trial site (shown in Figure 5.45), little variability is evident due to the mature growth stage of the crop. Even though the site was imaged with the updated LCLA system, the planned comparison could not be undertaken due to the maturity of the crop. The potential of using the updated LCLA system to predict the stage of crop maturity was however evaluated, and was reported in the following section.

Figure 5.45 Conventional aerial image taken of the wheat (top) and barley (bottom) variety trial site at 'Lundavra', October 2005. The area indicated in the red box is the area analysed.

A schematic representation of the barley trial layout is shown in Figure 5.46. Each plot consisted of four rows of plants, totalling 1.05 m wide and 5.0 m long. There are 192 plots per row and eight rows in total. The extent of the barley trial was 200 long x 50 m wide. The trial was planted on 24 May 2005 and harvested on 26 October 2005. The area analysed is indicated by the red box in both Figure 5.45 and 5.46.

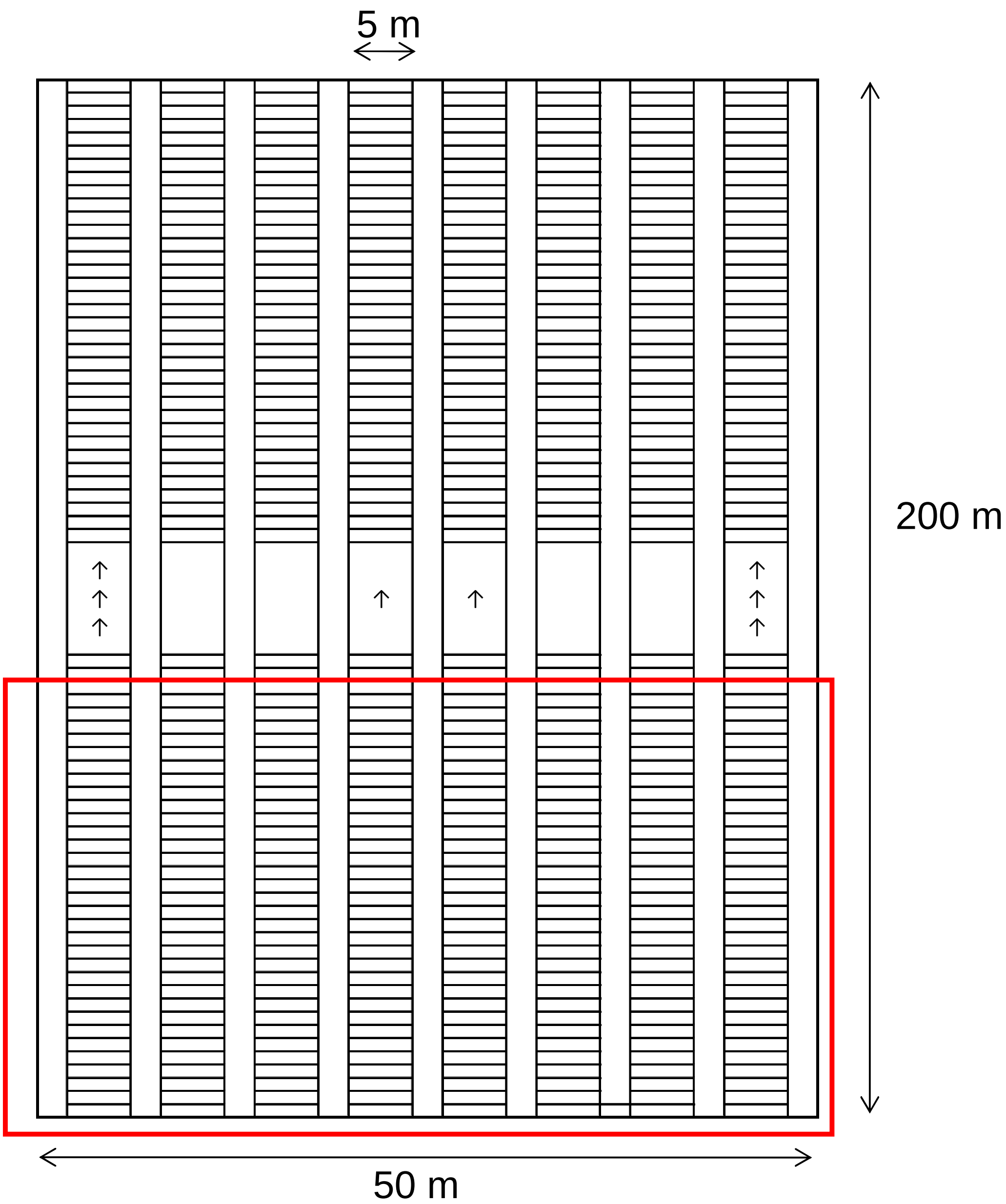

Figure 5.46 Schematic layout of the barley variety trial at ‘Lundavra’ showing the area analysed in the red box.

Deployment

The crop condition at the trial site is shown in Figure 5.47, and was approaching maturity, with noticeable variability evident in the image. The LCLA remote sensing system was deployed on 5 October 2005 (see Figure 5.48). The sky was nearly cloud free. As problems were initially encountered with the fuel filter, the first images were only acquired at 1300 hrs.

The flying height during this mission was 150 m (500 ft) with some images collected at 300 m (1000 ft). At the greater height, viewing the aircraft was difficult and control was nearly lost. The system was brought back to the ground and the cameras checked. Each camera had logged 150 photos, however the radio control receiver aerial was across some of the images. This was rectified and a second mission undertaken, but staying at 300 m (500 ft). Images were only taken when heading in a northerly direction, and acquired over both the barley and wheat trial areas. One of the images captured over the wheat trial area is shown in Figure 5.49. Unfortunately, the aircraft crashed on landing but only sustained repairable damage.

Figure 5.47 Looking into the field towards the wheat trial area (note the advanced stage of the crop).

Figure 5.48 Preparing the ‘Milne’ UAV for deployment at ‘Lundavra’.

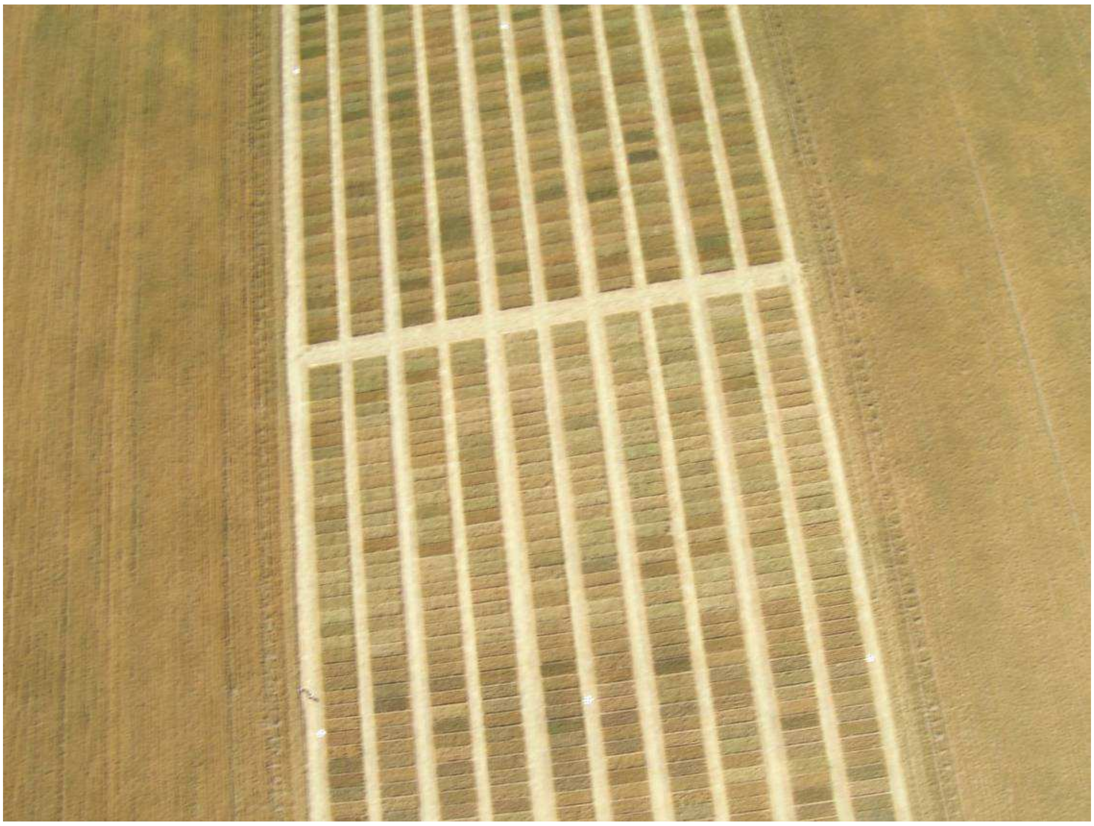

Figure 5.49 Some of the variability evident in the wheat trial area.

Analysis

Although images were acquired from across both the wheat and barley trial areas, particular attention was given to the barley as it was the main focus of this investigation. The most appropriate colour and near-infrared images covering the focus area were selected and imported into ERDAS Imagine 9.1 (Leica 2007) for analysis. The near-infrared image covering the focus area was rectified to the corresponding colour image with a total control point error of 5.17. These two images were then layer stacked with a total control point error of 2.46 pixels. This stacked image was then rectified to the 1.0 m resolution conventional aerial image using a geometric model with 24 ground control points, producing a total control checkpoint error of 2.72 pixels and an output cell size equal to 0.0627 m.

One of the replicates in the barley trial area (see Figure 5.50) was the focus of this investigation, with 79 areas of interest (AOIs) randomly selected from the 176 variety plots displayed in this image. As this was a variety evaluation trial, there were varying physiological characteristics that were selected, to enable the plant to cope with the contrasting environmental conditions present at this site. The contrasting physiological characteristics made this trial an ideal crop maturity study. Maturity assessments were conducted at anthesis (31 August 2005), about four weeks prior to the aerial image acquisition. The range of growth stages varied from Zadok 43 to 59, including 14 different classes signifying the range of crop maturities. Descriptions of these particular stages are given in Table 5.2.

Statistical analysis was undertaken to evaluate the ability of the updated LCLA remote sensing system to predict the growth stage of the crop and was discussed in the next chapter, section 6.4.1.

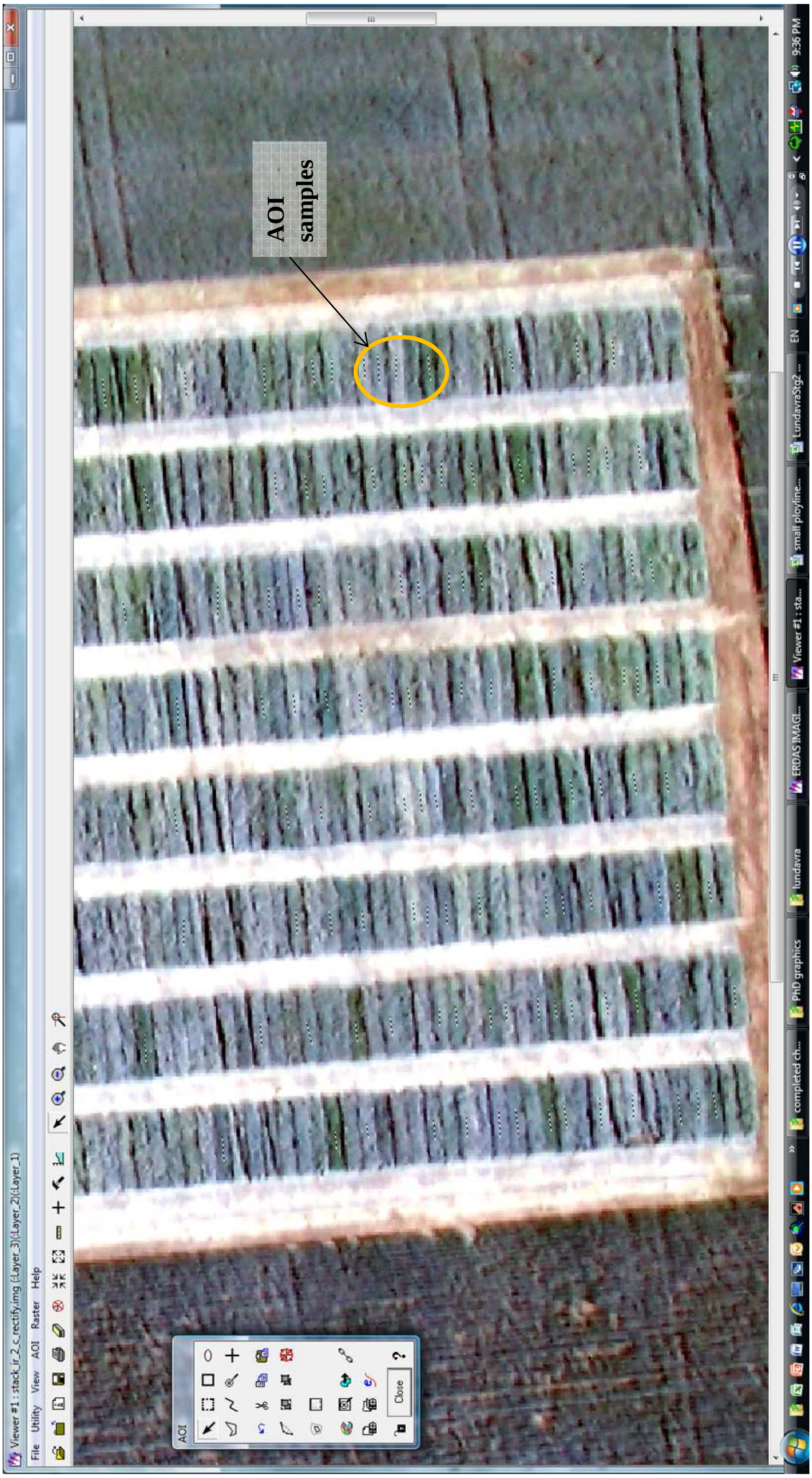

Figure 5.50 Selecting the AOIs from the individual plots in the investigated area covered by the red box in Figure 5.46.

Table 5.2 Explanation of the growth stages describing the barley crop based on Zadok et al. (1974).

Zadok Scale	***Booting***
40	
41	Flag leaf sheath extending
43	Boots just visibly swollen
45	Boots swollen
47	Flag leaf sheath opening
49	First awns visible
	Inflorescence emergence
50	First spikelet of inflorescence just visible
53	¼ of inflorescence emerged
55	½ of inflorescence emerged
57	¾ of inflorescence emerged
59	Emergence of inflorescence completed
	Anthesis

5.4.2 Autopilot Evaluation

The purpose of this mission was to evaluate the fully autonomous image acquisition system. To achieve this objective, the ability of the autopilot to trigger the updated LCLA remote sensing camera system was tested. The accuracy of the autopilot (in an *x y z* direction) was also evaluated. The procedures to perform this testing and evaluation are detailed in the following sections.

Study area

The study area was located at Watts Bridge Memorial Airfield, near Toogoolawah in South East Queensland, (152.460º, -27.098º), Australia (see Figure 5.51). The airfield was originally built in 1942 as part of the Australian World War II defence program. It is now a centre for all forms of recreational aviation in the South East Queensland, and has dedicated areas for use of remotely controlled aircraft. This mission (#29) was undertaken on 5 March 2008.

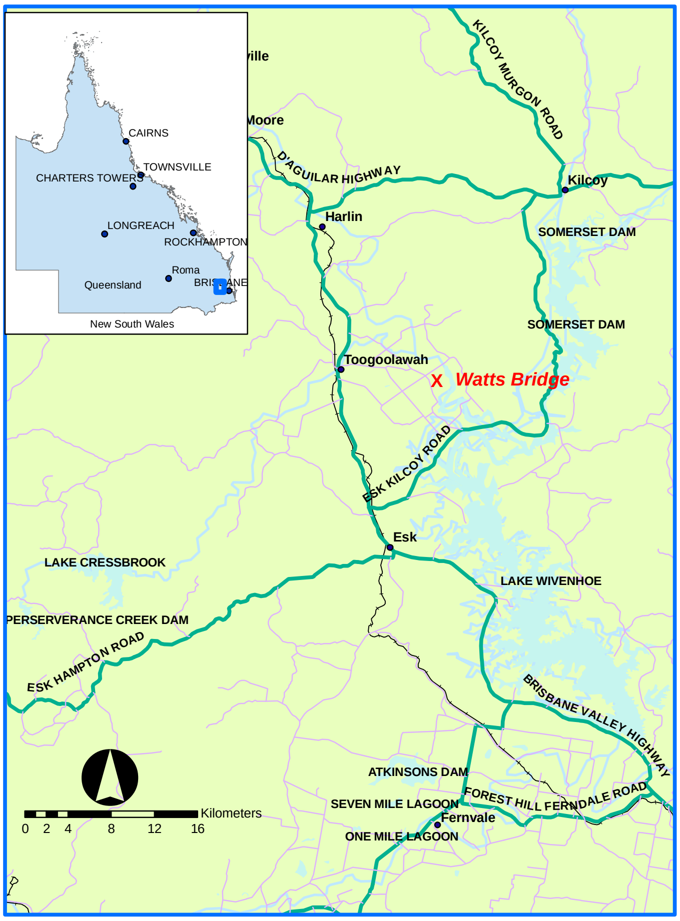

Figure 5.51 Location of the Watts Bridge Memorial Airfield.

Deployment

To undertake this evaluation, a specially modified version of a "*Phoenix Boomerang*" 60 Size Trainer was utilised (details at http://www.modelsports.com.au/). The platform consisted of two 60 size Boomerangs merged together. The platform (shown in Figure 5.52) was powered by an "*OS Engines*" 91FX (16 cc) (details at http://www.osengines.com/) methanol-glow motor.

The baseline avionics on the platform (see Figure 5.53) included the "*MicroPilot* MP2028[g]" autopilot (details at http://www.micropilot.com/) and a "*microhard Systems Inc.* Spectra 910A" 900 MHz spread spectrum modem (details at http://microhardcorp.com) for communications with the ground control station.

Figure 5.52 The QUT UAV ready for take-off.

The updated LCLA sensor system was housed in a streamlined pod attached to the underside of the fuselage directly beneath the wing. The pod was hinged for easy access and download of the cameras (see Figure 5.54). As the sensor had been previously triggered using a spare output channel of the radio control equipment, this was easily adapted to suit the autopilot system. When the UAV was within a certain distance of the designated location (within a 20 m radius to allow for cross-winds, GPS error and misalignment) the autopilot set a spare servo channel to the maximum output for 600 ms. The microprocessor, previously used and discussed in Chapter 4.2.3, detected this change in state of the servo output to trigger both cameras. The microprocessor also gave both cameras a pulse every 10 s to ensure that they did not power down.

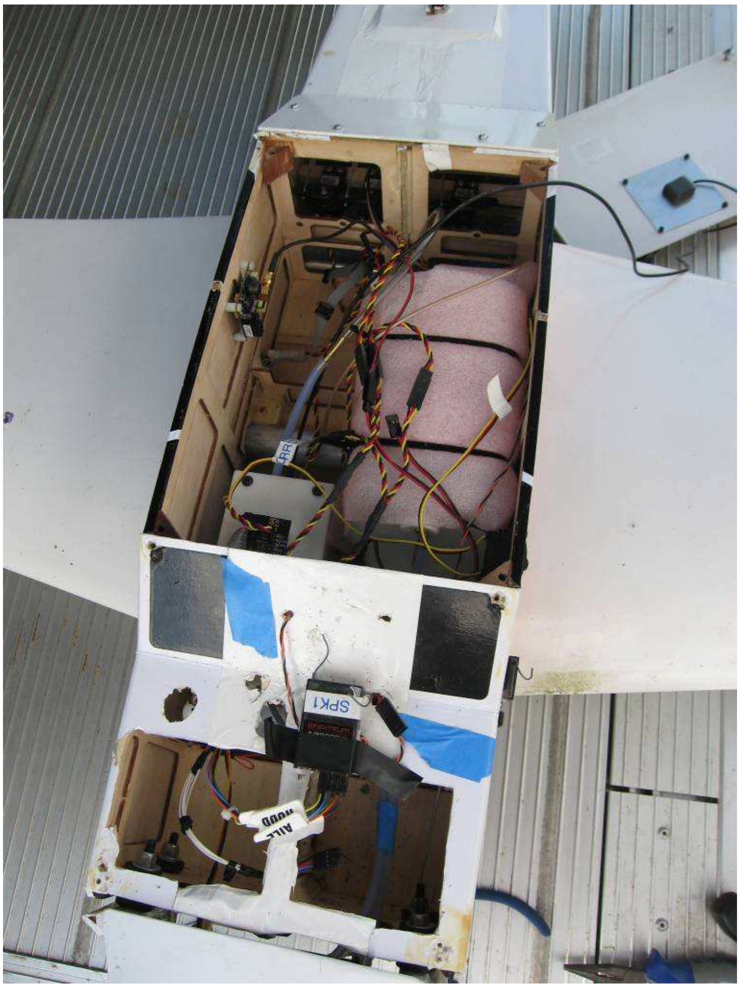

Figure 5.53 The avionics installed in the QUT UAV.

Figure 5.54 The pod opened to remove the SD cards from the LCLA sensors.

The UAV was programmed with a flight plan instructing it to do a number of left circuits over a series of pre-determined waypoints (see the Horizon Flight Schedule software in Figure 5.55). The waypoints are shown as pink dots in this image. One of the dots is green, indicating that this is the next waypoint that the UAV is heading towards. When passing above the origin point (the target of the image acquisition and where the UAV was initialised), the autopilot triggered the cameras.

The takeoff of the UAV was performed manually. Upon reaching a safe altitude (30 m – 100 ft), the UAV was switched into autonomous mode and the autopilot started guiding the aircraft along the set track, with flight height targeted at 120 m above ground level (AGL). When the UAV approached the imaging target (the initialisation point) the UAV was instructed to change altitude to 90 m AGL. The change in altitude was performed so that most of the flight was at a higher (hence perceived safer) altitude and likewise to simulate flying over obstructions and coming down to image acquisition height. Once past the target, the UAV resumed normal flying height. After 15–20 minutes of autonomous flying, the UAV was manually landed and the flight log was downloaded from the autopilot.

The log contained 52 columns of information, recorded at 5 Hz, about the aircraft's state that includes the following attributes: attitude, position, speed, heading, servo values, etc. Four flights were undertaken on the day of testing with images successfully captured on three of these. The second flight had to be aborted and the UAV landed immediately, as conventional aircraft came into the proximity of the UAV. The imagery acquired was analysed to provide flight path accuracies and is reported in the next chapter, section 6.4.2.

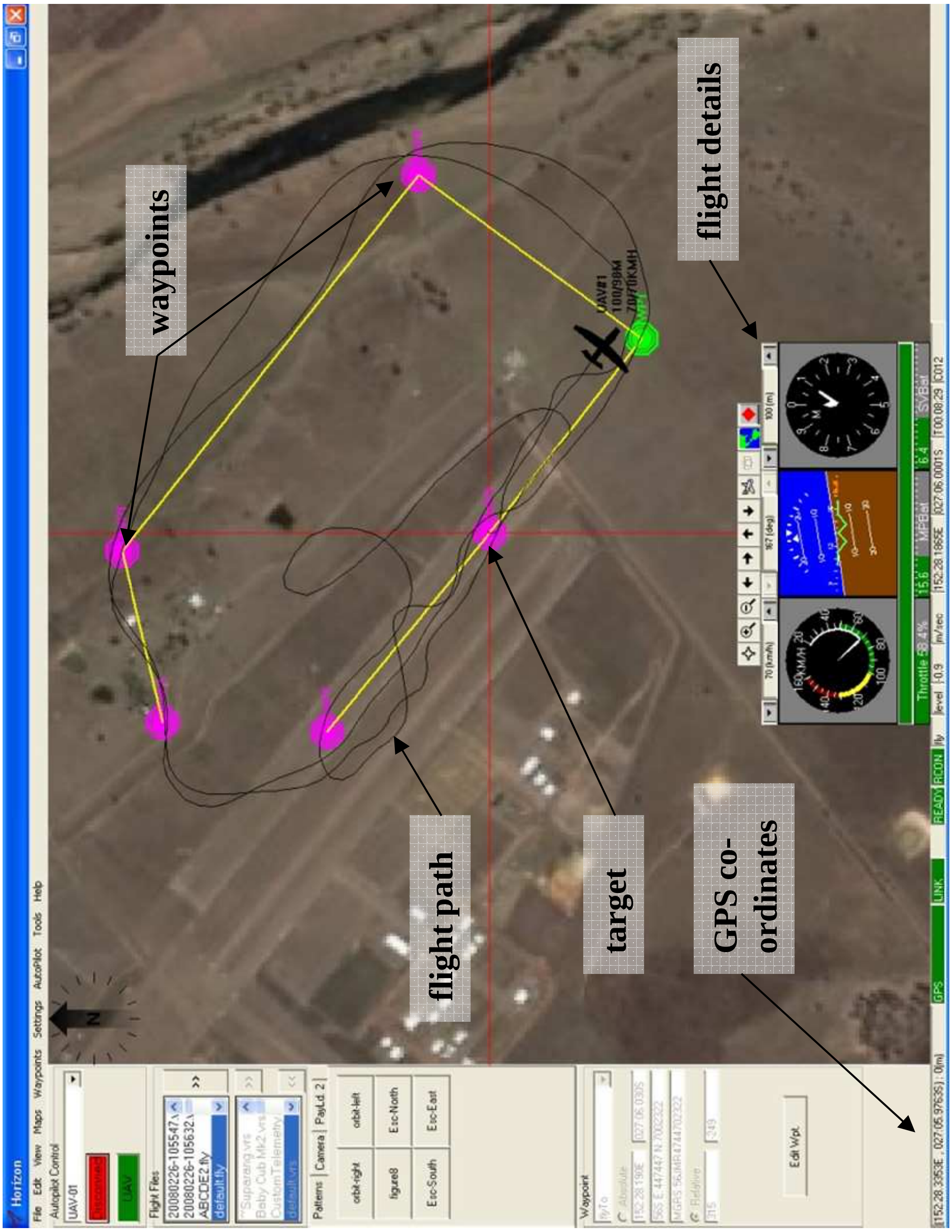

Figure 5.55 The ground control station software showing the path and the flight details of the UAV being monitored in the autopilot flight software (note the waypoints in pink).

5.5 Conclusions

The LCLA remote sensing system, following some initial developmental problems, proved to have the capabilities to successfully acquire images over targets that meet the spectral, spatial and temporal requirements specified in the research objectives of this study. The LCLA system provided imagery datasets needed to investigate spectral relationships with cereal crop parameters (including yield, protein, crop types and maturity). The 2-camera system was successfully deployed on a number of platforms (including helium balloons, unmanned aerial vehicles and ground based platforms), and in addition to targeting cereal crops, was also used in other agricultural and plant based studies.

Chapter 6 will quantify how well the LCLA remote sensing system has achieved its objectives, as well as how it compares to other studies and technologies.

Chapter 6

Performance of the LCLA system for Crop Mapping

6.1 Introduction

The previous chapter detailed the methods undertaken (see Figure 5.1) to map the various crop attributes of interest. This included the pre-processing and preliminary analysis of the data to eliminate obvious errors, to refine analytical techniques, and to extract data and information that were analysed with statistical and image analysis software. The results are presented and discussed in this present chapter.

A detailed analysis of the ability of the low-cost low-altitude (LCLA) remote sensing system to successfully map grain yield, protein and maturity, and to discriminate between different crop types, was presented in this chapter. Comparisons were made with other studies that have endeavoured to map these parameters using remote sensing techniques.

6.2 Grain Yield and Protein Mapping

This section examines the relationship between both grain yield and protein and the information recorded by the LCLA remote sensing system. This investigation utilised the ‘Colonsay’ dataset captured by the system in 2003 (detailed in Chapter 5.2).

6.2.1 The Yield-Protein Relationship

Studies have shown that there is a negative association between yield and protein for fields with uniform nitrogen treatments (Algerbo & Thylén 1998; Reyns *et al.* 2001; Stewart *et al.* 2002) and that this negative relationship (R^2=0.69) exists on a micro-scale (<100 m) within fields (Norng *et al.* 2005). This negative correlation is connected with nitrogen fertilisation near or above optimum, with positive correlations possible with below optimum rates (Delin 2004). The correlation for the yield and protein relationship for this trial is shown in Figure 6.1.

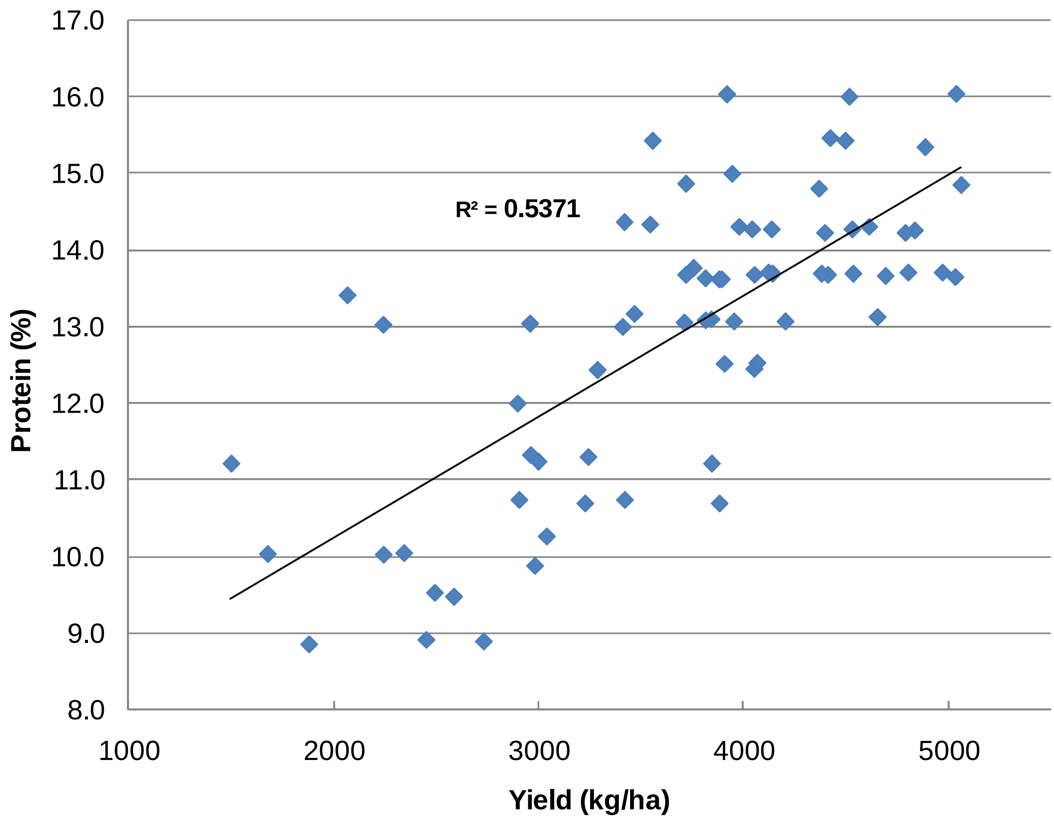

Figure 6.1 The relationship between yield and protein for the 'Colonsay' dataset.

6.2.2 Analysis of Variance

An analysis of variance was performed on the data to check for statistical differences (at the 0.05 level) between both yield and protein and the amount of N fertiliser applied. As can be seen from Table 6.1, all the results were significant except at the higher application rates (80–120 kg/ha) for both yield and protein. This plateau in protein at the higher N rates indicate that these plots were not limited by N, but some other variable such as moisture or other nutritional factors.

Table 6.1 The analysis of variance (ANOVA) conducted to determine statistical differences between the classes.

N applied	Mean ± standard error	
	Protein	Yield
(kg/ha)	(%)	(kg/ha)
0	9.92 ± 0.24 [(a)]	2237 ± 72 [(a)]
40	11.69 ± 0.20 [(b)]	3182 ± 75 [(b)]
80	13.77 ± 0.18 [(c)]	3989 ± 70 [(c)]
120	13.76 ± 0.27 [(c)]	4162 ± 130 [(c)]

[(a,b,c)]Significance at the 0.05 level

6.2.3 Correlation Analysis

Correlation analysis was used to quantify the associations between the information collected with the LCLA remote sensing system and the at-harvest parameters (yield and protein). A preliminary evaluation of the data was undertaken using scatterplots (see Figure 6.2) to display the relationships between the six camera bands and the yield / protein. This figure shows that there is a relationship between the colour bands and both yield and protein. The best relationship exists with the near infrared (NIR) bands with an excellent relationship evident with yield, while a good relationship with protein was found.

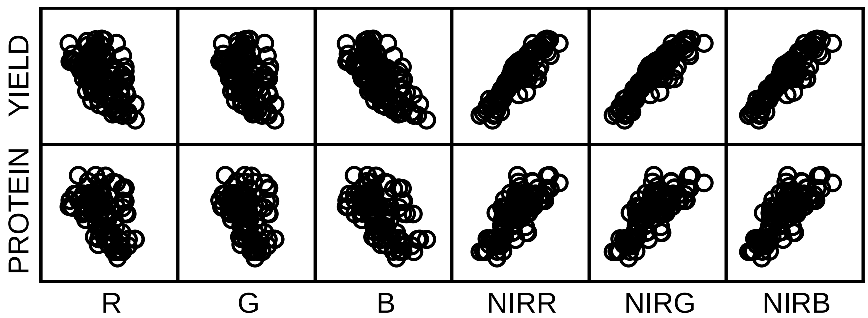

Figure 6.2 Scatterplot of the 6 bands* and yield / protein.

*colour camera (R-red sensor, G-green, B-blue) NIR camera (NIRR-red sensor, NIRG-green, NIRB-blue)

Vegetation indices theoretically provide values that are more highly correlated to plant parameters than the raw reflectance measurements (Wanjura & Hatfield 1986). The indices that are mostly used in the literature and which can be applied to the visible (blue-green-red) and near infrared portions of the spectrum were detailed previously in Table 2.2. These were analysed and the four indices found to have the best associations are highlighted below. Scatterplots were once again used as a preliminary evaluation method and are shown in Figure 6.3. The use of indices improved the associations evident with the raw bands displayed in Figure 6.2. The bands used in these indices primarily incorporated the red and the near infrared bands with one index using the green.

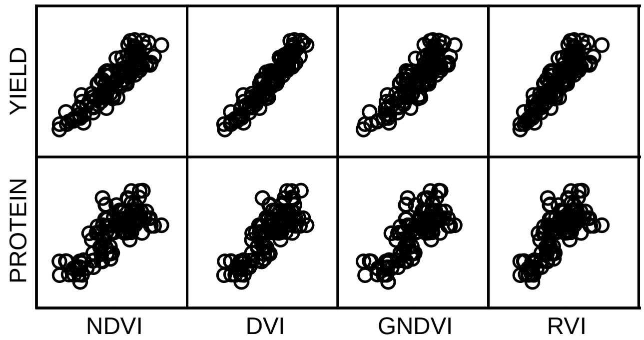

Figure 6.3 Scatterplot of the derived indices and yield / protein.

A tabulated form of results displayed in Figures 6.3 and 6.4 are given in Table 6.2. A good correlation was found between the near infrared and yield. The consistency between the near infrared bands was due to the similar nature of information recorded by the sensor, with correlations ranging from R^2=0.835 for NIRB to R^2=0.807 for NIRR.

Table 6.2 Correlations between yield / protein and the 6 bands and 5 indices*.

Yield	R	G	B	NIRR	NIRG	NIRB	RVI	NDVI	DVI	GNDVI	PSRI
Pearsons	0.523	0.403	0.664	0.898	0.911	0.914	0.886	0.894	0.950	0.871	0.923
R^2	0.274	0.162	0.441	0.807	0.831	0.835	0.785	0.799	0.902	0.759	0.853

Protein	R	G	B	NIRR	NIRG	NIRB	RVI	NDVI	DVI	GNDVI	PSRI
Pearsons	0.453	0.357	0.544	0.764	0.776	0.787	0.750	0.771	0.813	0.760	0.783
R^2	0.205	0.128	0.296	0.584	0.601	0.620	0.563	0.595	0.660	0.578	0.613

* notation for above table (R-red, G-green, B-blue, NIRR-near infrared red, NIRG-near infrared green, NIRB-near infrared blue, RVI-red ration vegetation index, NDVI-normalised difference vegetation index, DVI-difference vegetation index, GNDVI-green normalised difference vegetation index, PSRI-plant senescence reflectance index.)

This study was in agreement with other investigators who found that the correlations between yield and imagery are improved by the use of indices based on the red and NIR bands (Liu *et al.* 2006; Yang *et al.* 2000). The reported findings in other studies, of the yield-image relationship, include the following: the best correlation (GNDVI) in sorghum of r=0.720, and in corn (RVI) of r=0.872 (Yang *et al.* 2001); correlations (GNDVI) in sorghum ranging from r=0.735 to 0.906 for various fields (Yang & Everitt 2002); and the best reported correlation that could be found in the literature r=0.930 with NDVI and yield in corn (Gopalapillai & Tian 1999).

The single band correlations for yield were improved by combining the red with the NIR (DVI index), resulting in a R^2=0.902. This improvement in the relationship, when progressing from the NIR band to the DVI index, is shown in Figure 6.4. The higher the N applied rate, the greater the yield. The magnitude of the correlation between grain yield and single date remotely sensed imagery of this study exceeds all other studies.

In Figure 6.4, in addition to displaying the yield and image values for each of the 120 plots, the amount of N applied is also displayed. The four different rates are displayed as different symbols, and give a good visual representation of the grouping of the data. The plots with 0 unit of N applied were suffering from nutrient deficiency and resulted in a low crop growth / vigour and with reduced biomass. This low fertiliser rate equates to a lower protein and yield, and a corresponding low DVI values. This class is represented by the + sign in the graph and occurs in the bottom left-hand corner of both graphs. The other three classes (with 40, 80 and 120 units of N applied) do not fall into similarly tight clusters. However, grouping is still evident.

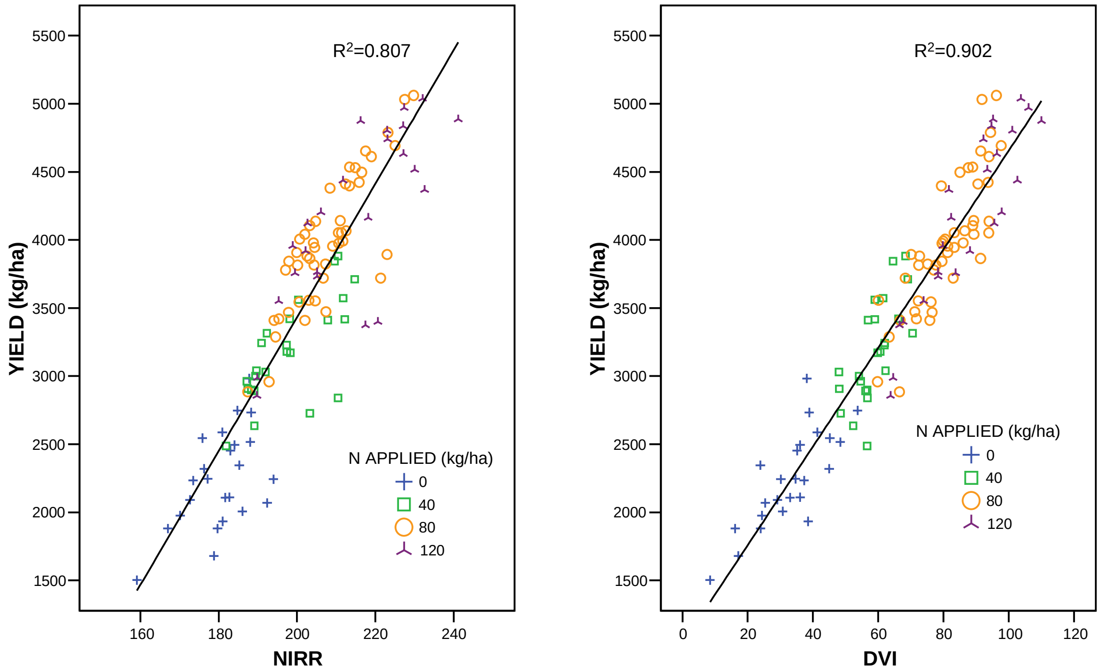

Figure 6.4 The relationship between yield and digital number for the NIRR band (left) and DVI (right) for the various N application rates.

The correlation between image and protein (displayed in the scatterplots Figures 6.2 & 6.3 and tabulated in Table 6.2) is not a strong as with yield. This study is one of a few that has endeavoured to find a relationship between single-date remotely sensed imagery and grain protein. Other studies have:

a) Used a series of Landsat images targeting tillering, booting, anthesis and grain-filling stages to look for single date relationships with protein in wheat (Zhao *et al.* 2005). A total of 48 plots within one Landsat scene was used to derive a correlation, with the best (R^2=0.455) found between protein and RGNDI (calculated at anthesis). Rather than having the complexity of an index, it was also found that a single Landsat band (band 5) had a better relationship (R^2=0.495) than the index when captured at the same time. The relationship reduced to an R^2=0.365 at grain filling.

b) Found grain protein correlations of r=0.82 for barley with Landsat band 4, and r=0.80 with the same Landsat band and wheat (Basnet *et al.* 2003).

Other more complicated studies incorporating modelling, multiple acquisition dates and/or complicated sensors have produced comparable results:

a) Hand-held spectrometer, modelling of temperature during grain filling and taking account of plant date were used to predict the ‘at-harvest’ grain protein for a specific cultivar of barley with a correlation of R^2=0.78 (Pettersson & Eckersten 2007). The complexity of this work precluded it from being used over a whole field.
b) Numerous proximally-sensed (CropScan MSR87) multi-spectral datasets were collected throughout the growing season and used in a partial least squares regression (PLS) to produce regression coefficients of r=0.754 for wheat, and r=0.457 for barley (Hansen *et al.* 2002).
c) Strong relationship between leaf N status and grain protein content (R^2= 0.829 to 0.914 depending on variety) were found, and this relationship indicated that canopy spectra could be used to predict grain protein content. (Xue *et al.* 2007)
d) Robust correlations between plant pigment ratio (PPR), leaf chlorophyll concentration and leaf N concentration suggested that PPR was a promising indicator for wheat grain protein for different genotypes. To determine the correlation reported (R^2=0.848, n=14), an agronomic model was combined with the hyperspectral model (based on hyperspectral radiometer (ASD) data collected 7 times during the growing season) (Wang *et al.* 2004).
e) Relationship between protein and remotely sensed data, albeit hyperspectral proximally-sensed (ASD), had a strong correlation (R^2=0.86) in wheat (Apan *et al.* 2006).
f) Correlation between grain protein content and a structure insensitive pigment index (SIPI)—a combination of Landsat bands 1, 3 and 4) of r=0.53 was reported for wheat, with the correlation improved to r=0.75 by incorporating the SIPI and Envisat synthetic aperture radar image (Liu *et al.* 2006).

For this study using the LCLA remote sensing system, the grain protein was correlated with all the near infrared bands (refer Table 6.2), with correlations ranging from R^2=0.620 for NIRB to R^2=0.584 for NIRR. The single band correlations for protein were improved by combining the red with the NIRR in the form of the DVI index. This improvement in the relationship, when progressing from the NIR band to the DVI index, is shown in Figure 6.5. The DVI was moderately correlated with grain protein (R^2=0.660).

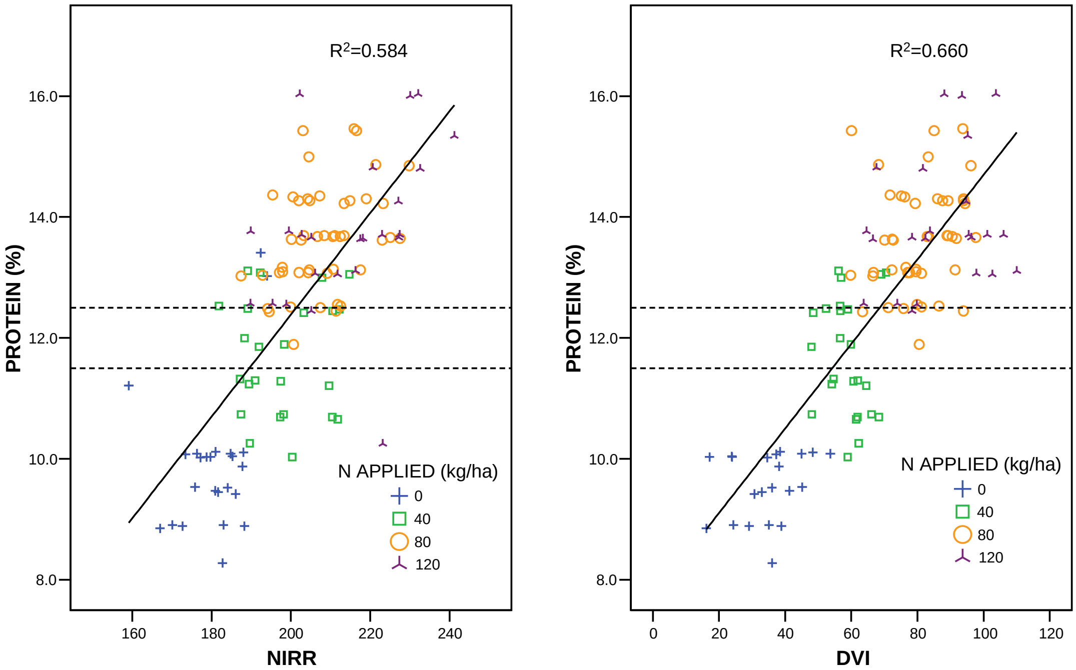

Figure 6.5 The relationship between grain protein and digital number for the NIRR band (left) and from DVI (right) for the various N application rates.

As with the yield-image relationship, the amount of fertiliser applied to each treatment is also indicated in Figure 6.5, allowing the figure to be better interpreted. It is evident that higher fertiliser application rates consequently produced higher grain protein levels. Conversely, lower fertiliser application rates produced lower protein levels. When combining this protein relationship with the yield relationships (Figure 6.4) an added understanding can be derived. Work on cereal wheat (Kelly *et al.* 2004; Strong & Holford 1997) in Northern Australia indicated that there is a high likelihood that a yield response would occur to added N, when grain protein is <11.5 %. Conversely, there is a low likelihood that a yield response would occur to added N when grain protein is >12.5%. Looking at this relationship in another way: if the final grain protein is <11.5%, then the crop has been limited by nutrition. However, if the final grain protein is >12.5%, then the crop has been limited by moisture. Between 11.5–12.5%, the available moisture has matched the amount of nutrition.

These protein thresholds have been shown in Figure 6.5. This identifies the areas in the trial where the yield had been limited by rainfall and stored moisture (that is >12.5% protein), and those areas where nutrition had been limiting (where protein <11.5%). It is not surprising that the areas limited by nutrition were the areas where the fertiliser application rates were low, with all of the 0 N applied and approximately half of the 40 N applied rates falling below this 11.5% protein threshold. In the nutrient-rich areas (80 N applied and above), the yield potential had been limited by water.

The limitations, be they water or nutrition, are expressed in the plant as crop stress. When the plant is stressed, the spectral characteristics of the leaf change. These changes occur more or less simultaneously in both the visible and near infrared regions, but the changes in the near infrared are often more noticeable (Campbell 2002). Reflectance in the near infrared region is apparently controlled by the nature of the complex cavities within the leaf and internal reflections of infrared radiation within these cavities. Thus, changes in infrared reflectance can reveal changes in vegetative vigour with vigour being a good indicator of plant health.

The LCLA remote sensing system was able to differentiate these subtle differences to provide the best correlations reported in the literature with relation to yield, as well as the best reported for a single-date low-cost method with protein. This system shows great potential for a low-cost, portable and easy-to-use system.

6.2.4 Discriminant Function Analysis

A discussion on discriminant analysis (DA) was included in the previous chapter, section 5.2.4. The *Discriminant Function Analysis* feature of SPSS Version 12.0.1 (SPSS 2003) was used to predict the amount of fertiliser applied to the crop using the raw digital camera values. Outputs from the package (for this study) are given in Appendix 1, with selected outputs following to aid the discussion.

In the ANOVA table (Table 6.3), the Wilks' Lambda indicated that the NIRB was the most important band to the discriminant function, closely followed by the other NIR bands. This is in agreement with the work of Price *et al.*(2002) who found that NIR is always selected in DA as best discriminating variable. The colour bands are of lesser importance, with GREEN being the least important. The F test indicates that the Wilks' lambda is significant for all variables.

Table 6.3 Tests of equality of group means.

	Wilks' Lambda	F	df1	df2	Sig.
RED	.588	26.892	3	115	.000
GREEN	.677	18.311	3	115	.000
BLUE	.481	41.403	3	115	.000
NIRR	.435	49.706	3	115	.000
NIRG	.418	53.387	3	115	.000
NIRB	.393	59.303	3	115	.000

The covariance matrix (Table 6.4) indicates that there is a strong correlation within both the three NIR and three Colour bands, but not between the two groups of three.

In the summary of canonical discriminant functions (Table 6.5), it shows that 95.2% of the variance is attributed to function 1, with an additional 3.9% to function 2 with both functions being highly significant.

Table 6.4 Pooled within-group matrices.

		RED	GREEN	BLUE	NIRR	NIRG	NIRB
Covariance	RED	107.478	97.176	79.804	55.675	24.968	26.310
	GREEN	97.176	89.931	71.856	60.448	27.705	29.160
	BLUE	79.804	71.856	64.662	29.638	12.761	13.699
	NIRR	55.675	60.448	29.638	112.508	54.825	56.544
	NIRG	24.968	27.705	12.761	54.825	27.057	27.753
	NIRB	26.310	29.160	13.699	56.544	27.753	28.682
Correlation	RED	1.000	.988	.957	.506	.463	.474
	GREEN	.988	1.000	.942	.601	.562	.574
	BLUE	.957	.942	1.000	.347	.305	.318
	NIRR	.506	.601	.347	1.000	.994	.995
	NIRG	.463	.562	.305	.994	1.000	.996
	NIRB	.474	.574	.318	.995	.996	1.000

Table 6.5 Summary of canonical discriminant functions (Eigenvalues (top) and Wilks' lambda (bottom)).

Function	Eigenvalue	% of Variance	Cumulative %	Canonical Correlation
1	7.342[a]	95.2	95.2	.938
2	.298[a]	3.9	99.0	.479
3	.073[a]	1.0	100.0	.261

a. First 3 canonical discriminant functions were used in the analysis.

Test of Function(s)	Wilks' Lambda	Chi-square	df	Sig.
1 through 3	.086	277.170	18	.000
2 through 3	.718	37.464	10	.000
3	.932	7.995	4	.092

In the structure matrix (Table 6.6), the pooled within-group correlations between independent variables and the discriminant functions are listed. The first function is positively influenced by the NIR bands, and negatively by the colour bands. The third function is contributed to by all bands but more so by the colour bands. The asterisks mark the correlations with the higher value for each variable.

Table 6.6 The structure matrix.

	Function		
	1	2	3
NIRB	.457*	.002	.393
NIRG	.434*	.033	.348
NIRR	.419*	-.057	.357
GREEN	-.248	.011	.581*
RED	-.304	-.018	.563*
BLUE	-.380	.116	.445*

Pooled within-groups correlations between discriminating variables and standardized canonical discriminant functions
Variables ordered by absolute size of correlation within function.

*. Largest absolute correlation between each variable and any discriminant function

Canonical plots are created by having the first two discriminant functions as the axes for the plot. The farther apart one point is from another on the plot, the more the dimension represented by that axis differentiates those two groups. The 0 class is quite removed from the 40 class with very little overlap indicating good separation between the classes. The higher applied rates (80 & 120) are well separated from both the lower rates (0 & 40); however there is overlap within the grouping (see Figure 6.6).

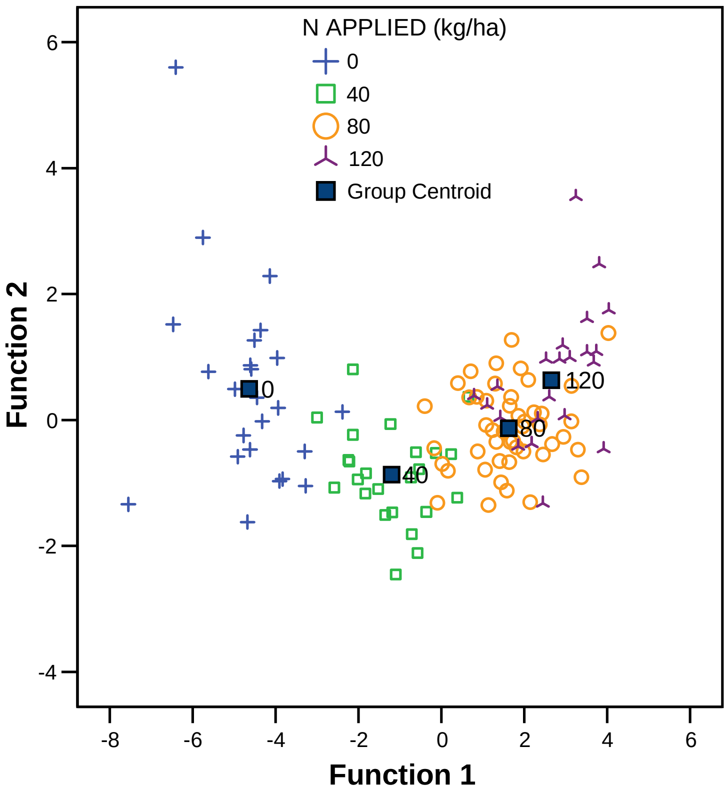

Figure 6.6 The canonical plot for the various N application rates.

The classification results (Table 6.7) provide an indication of the success rate for prediction of membership of the classes. Of the original grouped cases, 90 of the 119 plots (75.6%) were correctly classified. However, in the nutrient deficient plots where plant available N had run down (the 0 and 40 unit treatments), the sensors were able to predict these areas with 92% accuracy. It was more difficult to predict the 80 kg treatments (68% accuracy) and the 120 kg treatments (58% accuracy). The 80 kg treatments were sufficient to sustain the crop (no build-up or run down of plant available N) and the 120 kg treatments had excess nutrients to requirements (N building up). This indicates that the sensor is better at detecting “symptoms” where nutrients are limited rather than where they are in excess.

Table 6.7 Predictive accuracy of fertiliser treatment classification using discriminant analysis.

			Predicted Group Membership				
		N APPLIED	0	40	80	120	Total
Original	Count	0	22	2	0	0	24
		40	1	22	1	0	24
		80	0	5	32	10	47
		120	0	0	10	14	24
	%	0	91.7	8.3	.0	.0	100.0
		40	4.2	91.7	4.2	.0	100.0
		80	.0	10.6	68.1	21.3	100.0
		120	.0	.0	41.7	58.3	100.0

a. 75.6% of original grouped cases correctly classified.

This study agrees with other studies (Filella *et al.* 1995) that spectral indices based on 430, 550 and 680 nm allowed a clear separation within the N-deficient treatments (0 & 50 kg N / ha) and between those and the well-fertilised treatments (100, 150 & 200 kg N / ha). This same work (Filella *et al.* 1995) also stated that differentiating within the high treatments was difficult, as was the case in this present study.

Regarding the accuracy of the predictions, this study attained comparable accuracy with the work of Strachan *et al.* (2002) who used canonical discriminant analysis to accurately classify different levels of crop nutrition using reflectance data. The overall success rate of the classification varied from 70–93 %, depending on timing during the season. This study, however used only three N application rates covering a much broader range (17, 99 & 155 N) and used a ground based hyperspectral sensor to capture the spectral data. This system was much more complicated and expensive compared to the LCLA remote sensing system reported in this study, to achieve a comparable classification accuracy.

6.2.5 Partial Least Squares Regression

To assess the predictive power of the relationship between grain yield / protein and imagery values, a Partial Least Squares (PLS) Regression using Unscrambler 9.1 (CAMO 2004) software was implemented. PLS performs particularly well when the various X-variables have high correlation (which is often the case for multispectral data). Information in the original X-data is projected onto a small number of underlying (“latent”) variables called PLS components.

Aside from the raw imagery data, the set of derived vegetation indices was also calculated and analysed using the full the cross-validation (leave-one-out) technique. The root mean squared error of prediction (RMSEP) was calculated, which gave the measurement of the average difference between predicted and measured response values.

Predicted versus measured values for both the raw camera bands and the derived indices were plotted for both yield (Figures 6.7 & 6.8) and for protein (Figures 6.9 & 6.10). These results are summarised in Table 6.8.

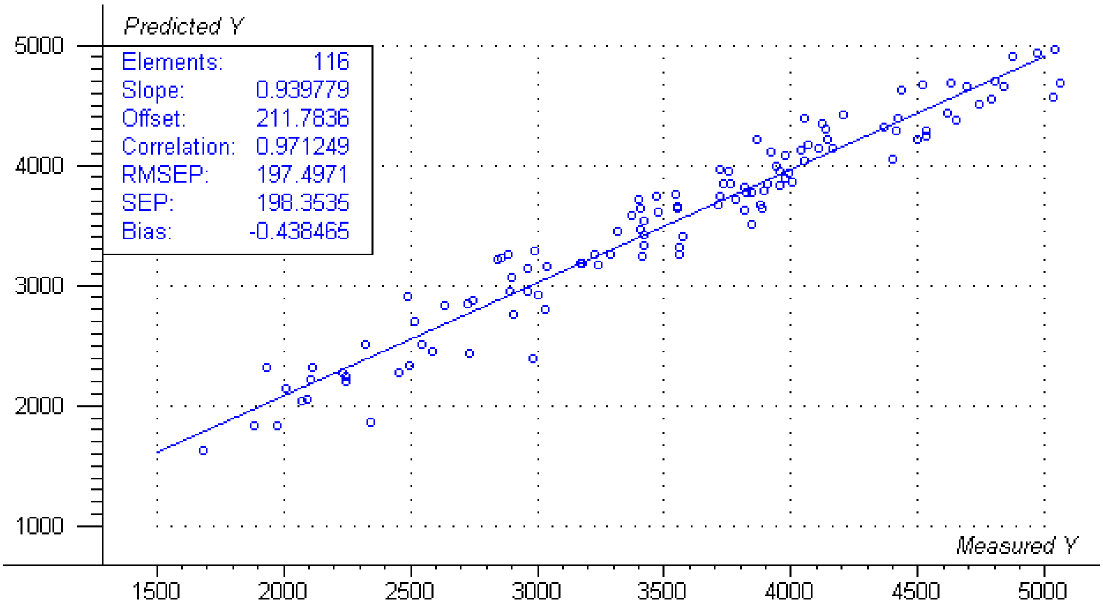

Figure 6.7 Plot of predicted grain yield values vs. measured grain yield values from the PLS regression model involving raw imagery values.

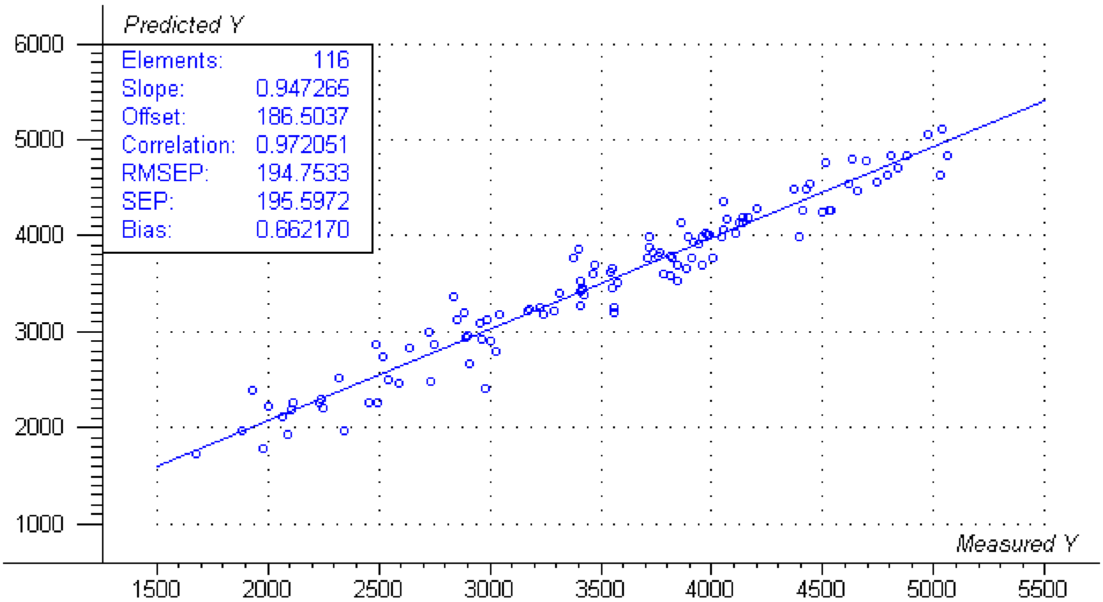

Figure 6.8 Plot of predicted grain yield values vs. measured grain yield values from the PLS regression model involving vegetation index values.

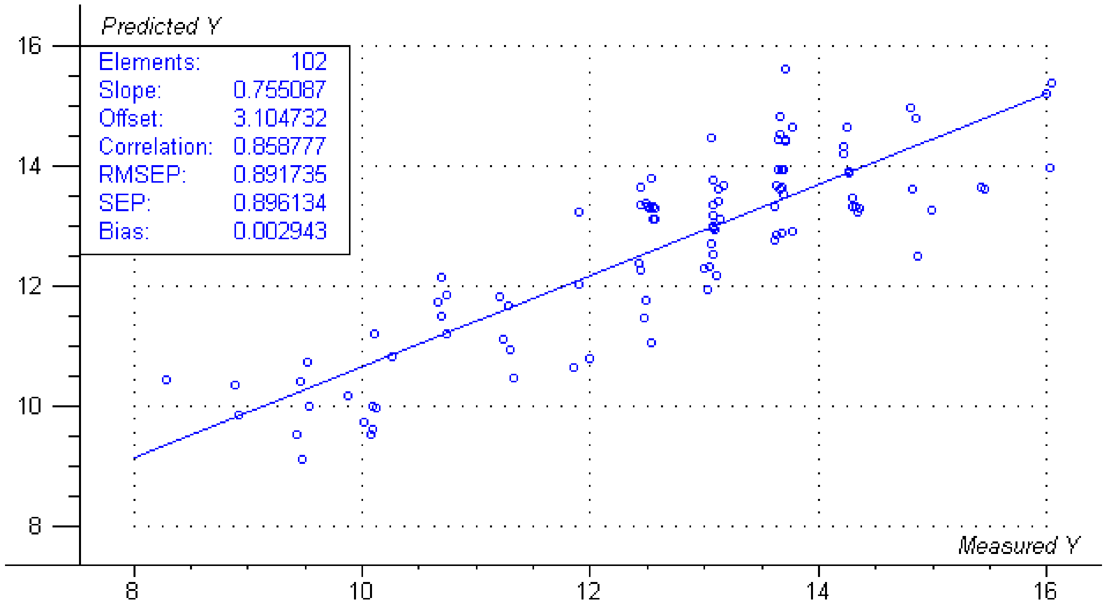

Figure 6.9 Plot of predicted grain protein values vs. measured grain protein values from the PLS regression model involving raw imagery values.

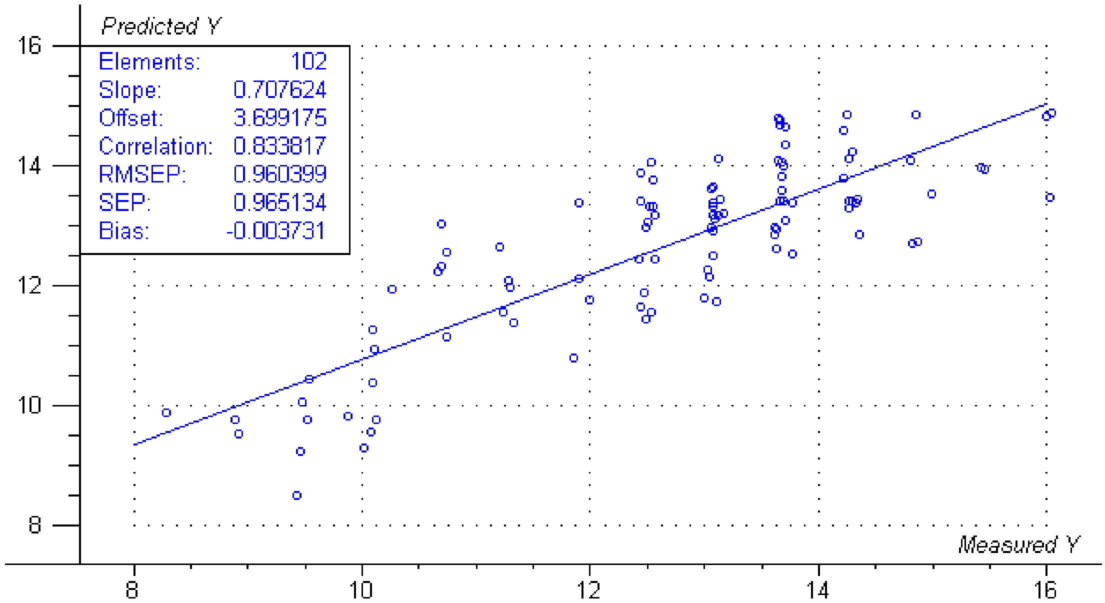

Figure 6.10 Plot of predicted grain protein values vs. measured grain protein values from the PLS regression model involving vegetation index values.

The PLS regression results showed that it is possible to predict grain yield using digital camera imagery obtained from a balloon platform. Correlations between predicted and measured values for the calibrated and validated samples were very high (r=0.97 for all models) (Table 6.8). For both raw imagery and vegetation indices, the root mean squared error of prediction (RMSEP) values were relatively low, equivalent to prediction accuracy of 94.1% and 94.2%, respectively. The optimal number of PLS factors (components) was minimal (i.e. one for the raw imagery and two for the vegetation indices), but was able to explain the Y-variance sufficiently (i.e. over 94%). This is desirable as it is good to have simple models, where the total explained variance close to 100% with as few components as possible.

Table 6.8 PLS regression results of imagery values and yield and protein

Data	Optimal no. of PLS factors	Calibration		Cross-Validation (leave-one-out)			
		R*	RMSEC **	R*	RMSEP ***	Prediction Accuracy (%)	% of Y Variance Explained
YIELD (n=117)							
1. Raw values	1	0.97	193.0	0.97	197.5	94.1	94.4
2. Indices	2	0.97	189.1	0.97	194.7	94.2	94.6
PROTEIN (n=102)							
1. Raw values	4	0.88	0.83	0.86	0.89	88.5	74.2
2. Indices	3	0.85	0.92	0.83	0.96	87.6	70.1

*R – Correlation is between predicted and measured values
** RMSEC – root mean square error of calibration
*** RMSEP – root mean square error of prediction

For the grain protein, the correlations between predicted and measured values for the calibrated and validated samples were also high (i.e. from r=0.83 to r=0.88), although they are lower than the grain yield values (Table 6.5). Consequently, the prediction accuracies for the grain protein were lower than the grain yield, i.e. 87.6% to 88.5% for the validated model. The regression models needed three to four PLS components to explain 70.1% to 74.2% of the variation in grain protein. Compared with grain yield, these values indicate that imagery has less predictive power for grain protein.

Based on the regression coefficient plot of grain yield (Figure 6.11), the NIR bands (consisting of the NIR values for the blue (NIR-B), green (NIR-G), and red sensor (NIR-R)) attained relatively higher coefficient values compared to the visible bands (consisting of blue (DC-CB) green (DC-CG) and red (DC-CR)), indicating their relatively higher significance in the grain yield prediction. This agrees with the previous findings in the correlation analysis that the response seen in the NIR region has a strong relationship with yield (Staggenborg & Taylor 2000; Yang *et al.* 2000). For the vegetation indices (Figure 6.12), the difference vegetation index (DC_DVI) produced the highest regression coefficient, indicating that this is the most significant predictor variable among the vegetation indices used and is in agreement with the correlation study detailed in section 6.2.3.

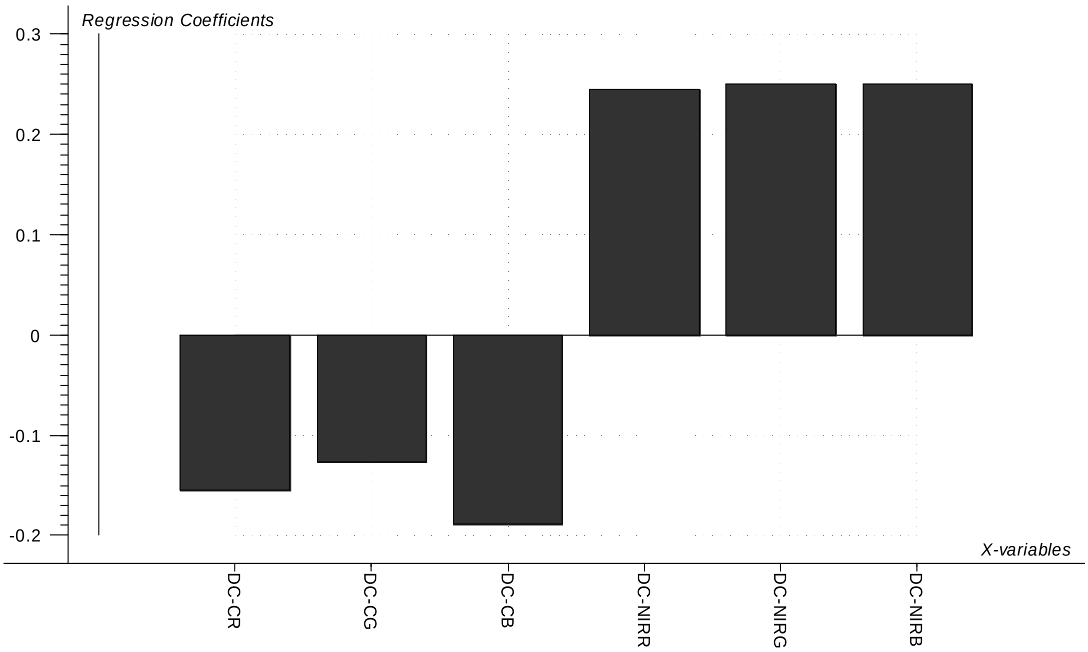

Figure 6.11 Regression coefficients for the cross-calibrated prediction model involving grain yield and raw imagery values.

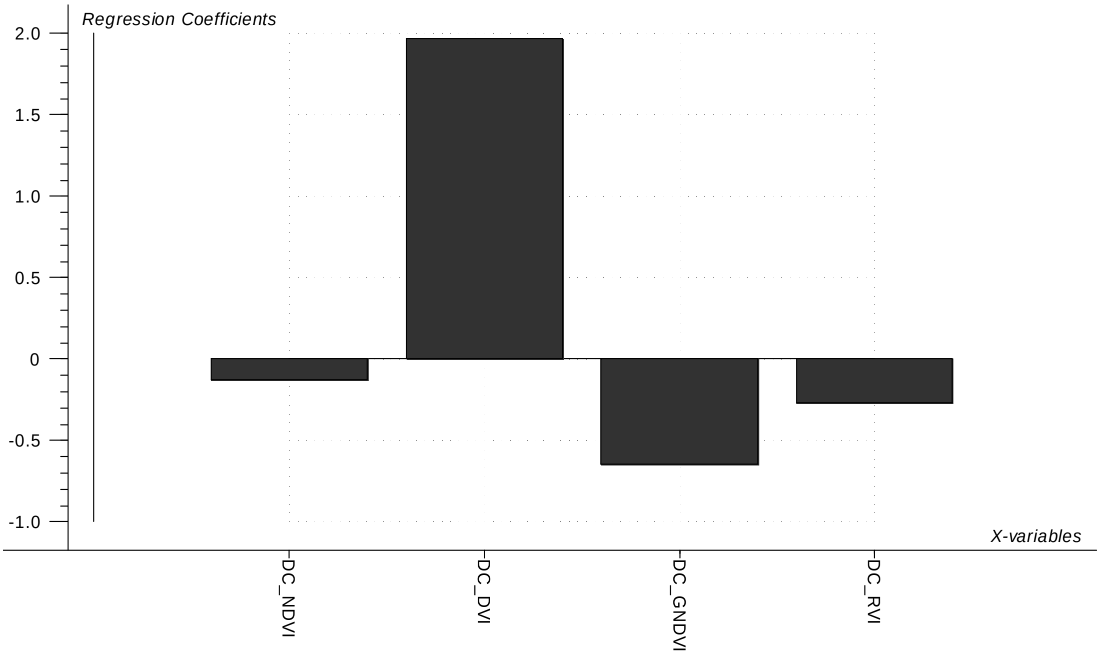

Figure 6.12 Regression coefficients for the cross-calibrated prediction model involving grain yield and vegetation index values.

Notation (DC_NDVI-normalised difference vegetation index, DC_DVI-difference vegetation index, DC_GNDVI-green normalised difference vegetation index, DC_RVI-red ratio vegetation index)

With regards to grain protein, the regression coefficient plots (Figure 6.13) indicated that the near infrared band (NIRB) and the visible wavelength green band (G) were the most significant predictor variables among the raw imagery. These results further reinforce the importance of the NIR bands in grain protein prediction. These findings agree with the results of Basnet *et al.* (2003) that listed the tasselled cap greenness index (a transformation involving the NIR and VIS bands) as among those with the highest statistical association with grain protein content. The RVI and DVI were the best performing vegetation indices (Figure 6.14). The simple ratio image RVI and the difference image DVI performed better than the normalised ratios. This agrees with a study (Wright *et al.* 2003) of spectral data and grain protein content which found that the simple ratio of NIR and red bands achieved the highest correlation coefficient (r=0.59) and is in agreement with the correlation analysis reported in section 6.2.3.

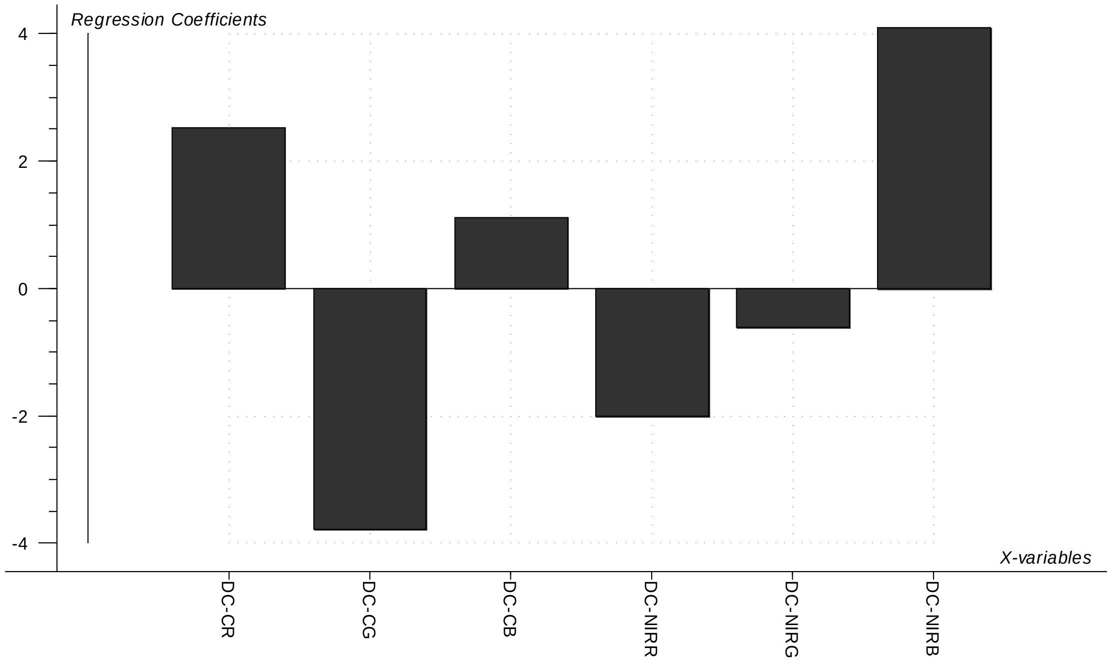

Figure 6.13 Regression coefficients for the cross-calibrated prediction model involving grain protein and raw imagery values.

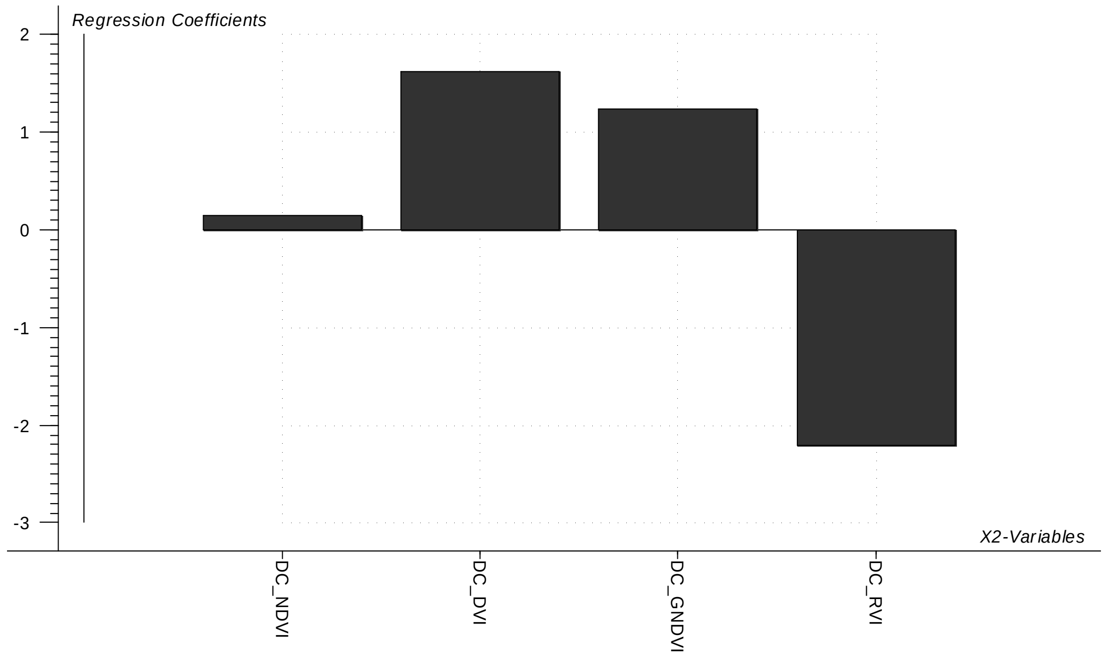

Figure 6.14 Regression coefficients for the cross-calibrated prediction model involving grain protein and vegetation index values.

6.3 Crop Type Discrimination and Mapping

As the focus of the 'Nindigully' study was on crop type discrimination and mapping, two approaches were undertaken to achieve this objective. In addition to using a statistical package to discriminate between different classes (as was done in the 'Colonsay' study detailed in section 6.2.4), image analysis software was used to classify various crop types present in the images.

6.3.1 Discriminant Function Analysis

Each of the subplots for the different species present in plot 38 were split into initially 5 and then 10 equal sized areas. The average digital number (DN) values were recorded and analysed using SPSS 12.0.1 (SPSS 2003). Discriminant function analysis (DA) was used to determine which variables discriminate between the naturally occurring groups. Selected outputs from the package have been included below.

Total Sample Size N = 50

A preliminary analysis was carried out where the number of samples for each different fertiliser regime was 5 (n=50).

In the ANOVA table (Table 6.9), the Wilks' Lambda indicated that the NIRR was the most important to the discriminant function, closely followed by the other NIR bands, with the least important being BLUE. The F test indicates that the Wilks' lambda is significant for all variables.

Table 6.9 Tests of equality of group means

	Wilks' Lambda	F	df1	df2	Sig.
BLUE	.447	8.850	6	43	.000
GREEN	.304	16.425	6	43	.000
RED	.341	13.879	6	43	.000
NIRB	.196	29.310	6	43	.000
NIRG	.161	37.415	6	43	.000
NIRR	.140	44.039	6	43	.000

The covariance matrix (Table 6.10) indicates a strong correlation within both the three NIR and three Colour band, but not between the two groups of three.

Table 6.10 Pooled within-group matrices

		BLUE	GREEN	RED	NIRB	NIRG	NIRR
Covariance	BLUE	54.343	60.781	65.052	14.239	12.990	29.982
	GREEN	60.781	69.815	74.157	17.317	15.795	37.025
	RED	65.052	74.157	80.916	15.553	14.707	34.228
	NIRB	14.239	17.317	15.553	9.508	7.988	19.217
	NIRG	12.990	15.795	14.707	7.988	6.977	16.836
	NIRR	29.982	37.025	34.228	19.217	16.836	41.055
Correlation	BLUE	1.000	.987	.981	.626	.667	.635
	GREEN	.987	1.000	.987	.672	.716	.692
	RED	.981	.987	1.000	.561	.619	.594
	NIRB	.626	.672	.561	1.000	.981	.973
	NIRG	.667	.716	.619	.981	1.000	.995
	NIRR	.635	.692	.594	.973	.995	1.000

In the summary of canonical discriminant functions (Table 6.11), it shows that 55.3% of the variance is attributed to function 1 with an additional 29.0% to function 2, with both functions being highly significant. However, the third function, which adds an additional 13.1%, is not significant.

Table 6.11 Summary of canonical discriminant functions (Eigenvalues (top) and Wilks' lambda (bottom)).

Function	Eigenvalue	% of Variance	Cumulative %	Canonical Correlation
1	13.825[a]	55.3	55.3	.966
2	7.256[a]	29.0	84.4	.937
3	3.272[a]	13.1	97.5	.875
4	.553[a]	2.2	99.7	.597
5	.055[a]	.2	99.9	.229
6	.029[a]	.1	100.0	.167

a. First 6 canonical discriminant functions were used in the analysis.

Test of Function(s)	Wilks' Lambda	Chi-square	df	Sig.
1 through 3	.086	277.170	18	.000
2 through 3	.718	37.464	10	.000
3	.932	7.995	4	.092

In the structure matrix (Table 6.12), the pooled within-group correlations between independent variables and the discriminant functions are listed. The first function has a positive contribution by the NIR bands and a negatively one by the colour bands. The third function is influenced by all bands but more so by the colour bands. The asterisks mark the correlations with the higher value for each variable.

Table 6.12 The structure matrix.

	Function					
	1	2	3	4	5	6
NIRR	.619*	-.062	.489	.221	.571	-.011
NIRB	.504	-.074	.378	.261	.723*	-.077
BLUE	.215	.167	.332	-.056	.647*	.628
GREEN	.311	.267	.354	-.063	.636*	.547
NIRG	.559	-.083	.500	.172	.634*	-.008
RED	.218	.320	.393	-.092	.550	.621*

Pooled within-groups correlations between discriminating variables and standardized canonical discriminant functions
Variables ordered by absolute size of correlation within function.

*. Largest absolute correlation between each variable and any discriminant function

Each of the species represented show good separation with chickpea (4) being the most coherent group. There is however, overlap within species groups (canola (2 & 3) and wheat (5–7)) due to the various spectral responses attributed to the varying amounts of applied fertiliser (see Figure 6.15).

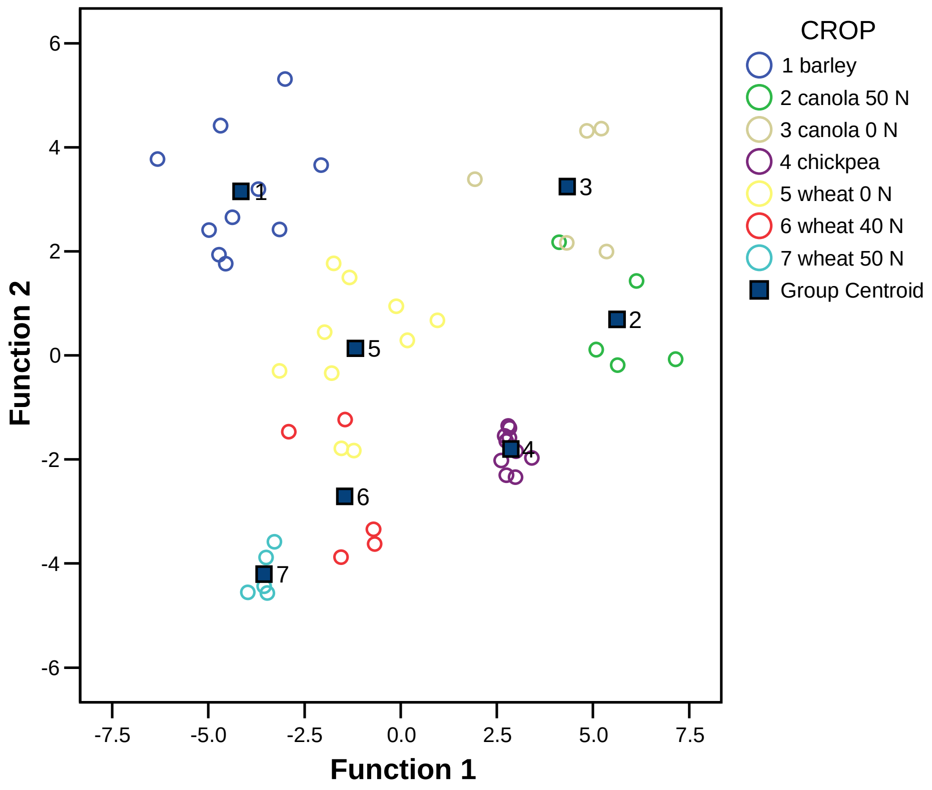

Figure 6.15 The canonical plot for the various species and fertiliser rates.

The classification results (Table 6.13) provide an indication of the success rate for prediction of membership of the classes. Of the original 50 grouped cases 96.0% were correctly classified with only 2 wheat cases being misclassified into a differing fertiliser treatment. In the cross-validated analysis, 78.0% of the cases were correctly classified. Once again, there were problems differentiating fertiliser treatments. But within species, the agreement was high, with only one barley and one canola case classified as the wrong species.

Table 6.13 Classification results for the n=50 case study.

Classification Results[b,c]

		CROP	Predicted Group Membership 1	2	3	4	5	6	7	Total
Original	Count	1	10	0	0	0	0	0	0	10
		2	0	5	0	0	0	0	0	5
		3	0	0	5	0	0	0	0	5
		4	0	0	0	10	0	0	0	10
		5	0	0	0	0	8	2	0	10
		6	0	0	0	0	0	5	0	5
		7	0	0	0	0	0	0	5	5
	%	1	100.0	.0	.0	.0	.0	.0	.0	100.0
		2	.0	100.0	.0	.0	.0	.0	.0	100.0
		3	.0	.0	100.0	.0	.0	.0	.0	100.0
		4	.0	.0	.0	100.0	.0	.0	.0	100.0
		5	.0	.0	.0	.0	80.0	20.0	.0	100.0
		6	.0	.0	.0	.0	.0	100.0	.0	100.0
		7	.0	.0	.0	.0	.0	.0	100.0	100.0
Cross-validated[a]	Count	1	9	0	0	0	1	0	0	10
		2	0	5	0	0	0	0	0	5
		3	0	1	3	0	1	0	0	5
		4	0	0	0	10	0	0	0	10
		5	0	0	0	0	6	4	0	10
		6	0	0	0	0	2	3	0	5
		7	0	0	0	0	0	2	3	5
	%	1	90.0	.0	.0	.0	10.0	.0	.0	100.0
		2	.0	100.0	.0	.0	.0	.0	.0	100.0
		3	.0	20.0	60.0	.0	20.0	.0	.0	100.0
		4	.0	.0	.0	100.0	.0	.0	.0	100.0
		5	.0	.0	.0	.0	60.0	40.0	.0	100.0
		6	.0	.0	.0	.0	40.0	60.0	.0	100.0
		7	.0	.0	.0	.0	.0	40.0	60.0	100.0

a. Cross validation is done only for those cases in the analysis. In cross validation, each case is classified by the functions derived from all cases other than that case.

b. 96.0% of original grouped cases correctly classified.

c. 78.0% of cross-validated grouped cases correctly classified.

Total Sample Size N = 80

In an attempt to improve the classification accuracy, the number of samples per class was increased to 10 (resulting in n = 80). The accuracy of the canonical discriminant function was improved.

In the ANOVA table (Table 6.14), the Wilks' Lambda indicated that the NIRR was the most important to the discriminant function, closely followed by the other NIR bands, with the least important being BLUE. Wilks' lambda is significant by the F test for all variables.

Table 6.14 Tests of equality of group means

	Wilks' Lambda	F	df1	df2	Sig.
BLUE	.416	17.104	6	73	.000
GREEN	.257	35.089	6	73	.000
RED	.290	29.796	6	73	.000
NIRB	.269	33.096	6	73	.000
NIRG	.224	42.106	6	73	.000
NIRR	.200	48.778	6	73	.000

The covariance matrix (Table 6.15) indicates a strong correlation within both the three NIR and three Colour band, but not between the two groups of three.

Table 6.15 Pooled within-group matrices

		BLUE	GREEN	RED	NIRB	NIRG	NIRR
Covariance	BLUE	46.986	50.756	55.328	11.354	10.182	23.402
	GREEN	50.756	57.762	61.739	15.100	13.502	32.045
	RED	55.328	61.739	69.222	11.474	10.873	25.349
	NIRB	11.354	15.100	11.474	12.736	10.578	26.009
	NIRG	10.182	13.502	10.873	10.578	9.073	22.369
	NIRR	23.402	32.045	25.349	26.009	22.369	55.708
Correlation	BLUE	1.000	.974	.970	.464	.493	.457
	GREEN	.974	1.000	.976	.557	.590	.565
	RED	.970	.976	1.000	.386	.434	.408
	NIRB	.464	.557	.386	1.000	.984	.976
	NIRG	.493	.590	.434	.984	1.000	.995
	NIRR	.457	.565	.408	.976	.995	1.000

In the summary of canonical discriminant functions (Table 6.16), it shows that 56.7% of the variance is attributed to function 1, an additional 30.6% to function 2 and 9.9% to function 3. The first four functions are significant.

Table 6.16 Summary of canonical discriminant functions (Eigenvalues top and Wilks lambda bottom).

Function	Eigenvalue	% of Variance	Cumulative %	Canonical Correlation
1	11.583[a]	56.7	56.7	.959
2	6.252[a]	30.6	87.4	.928
3	2.020[a]	9.9	97.3	.818
4	.505[a]	2.5	99.7	.579
5	.034[a]	.2	99.9	.182
6	.019[a]	.1	100.0	.138

a. First 6 canonical discriminant functions were used in the analysis.

Test of Function(s)	Wilks' Lambda	Chi-square	df	Sig.
1 through 6	.002	440.837	36	.000
2 through 6	.029	257.241	25	.000
3 through 6	.209	113.602	16	.000
4 through 6	.630	33.480	9	.000
5 through 6	.948	3.840	4	.428
6	.981	1.395	1	.238

In the structure matrix (Table 6.17), all bands have a negative influence on the first function with the largest absolute correlations between the NIR bands and function 3 and the colour bands and function 5. The asterisks mark the correlations with the higher value for each variable.

Table 6.17 The structure matrix.

	Function					
	1	2	3	4	5	6
NIRG	-.485	-.067	.572*	.281	.494	-.333
NIRR	-.534	-.057	.554*	.336	.430	-.327
BLUE	-.256	.243	.357	-.032	.714*	.488
GREEN	-.392	.358	.374	-.008	.671*	.358
RED	-.280	.443	.384	-.055	.580*	.489
NIRB	-.437	-.074	.448	.343	.577*	-.391

Pooled within-groups correlations between discriminating variables and standardized canonical discriminant functions
Variables ordered by absolute size of correlation within function.

*. Largest absolute correlation between each variable and any discriminant function

In the canonical plots, each of the species represented show good separation, with chickpea (4) being the most coherent group once again. As was the case with the n=50 analysis, there was overlap within species groups (canola (2 & 3) and wheat (5–7)) due to the various spectral responses attributed to the varying amounts of applied fertiliser (see Figure 6.16).

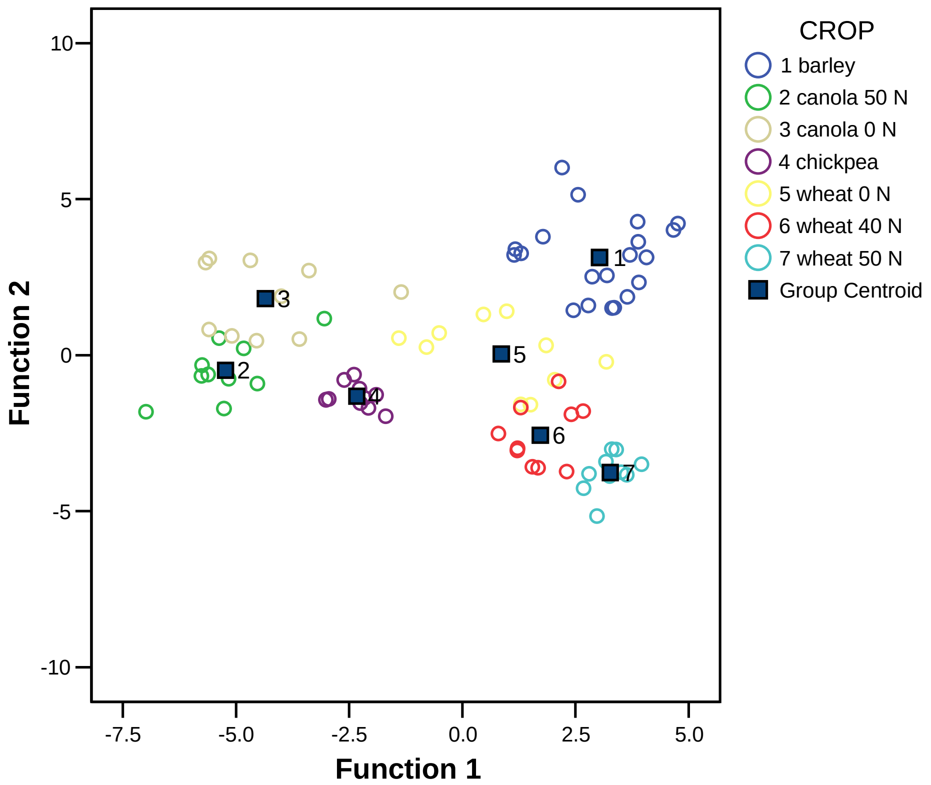

Figure 6.16 The canonical plot for the various species and fertiliser rates.

The classification results (Table 6.18) provide an indication of the success rate for predictions of membership of the classes. Of the original 80 grouped cases, 96.3% were correctly classified.

In the cross-validated assessment, there were some misclassifications within species due to the differing fertiliser treatment levels. However, there were only three (of 80) cases where species were wrongly classified with one barley classified as low-nutrition wheat, one low-nutrition canola classified as chickpeas, and one low-nutrition wheat classified as chickpeas. The greater sample number better represented the variability evident in the subplots, enabling a more accurate classification indicated by the higher cross-validated classification accuracy.

Other studies have used DA to differentiate between weeds and carrot plants using 22 bands on a ground-based device for an overall classification accuracy of 72% (Piron *et al.* 2008). Sugarcane varieties could be discriminated using hyperspectral satellite (EO-1 Hyperion) data. A classification accuracy of 87.5% was reported from a single date acquisition (Galvao *et al.* 2005). Once again, the results from the LCLA remote sensing system study are equal to or better than other reported studies. The system, however, is far less expensive and complicated and achieved comparable or better results.

Table 6.18 Classification results for the n=80 case study.

Classification Results[b,c]

			Predicted Group Membership							
		CROP	1	2	3	4	5	6	7	Total
Original	Count	1	20	0	0	0	0	0	0	20
		2	0	10	0	0	0	0	0	10
		3	0	0	9	0	1	0	0	10
		4	0	0	0	10	0	0	0	10
		5	0	0	0	0	8	2	0	10
		6	0	0	0	0	0	10	0	10
		7	0	0	0	0	0	0	10	10
	%	1	100.0	.0	.0	.0	.0	.0	.0	100.0
		2	.0	100.0	.0	.0	.0	.0	.0	100.0
		3	.0	.0	90.0	.0	10.0	.0	.0	100.0
		4	.0	.0	.0	100.0	.0	.0	.0	100.0
		5	.0	.0	.0	.0	80.0	20.0	.0	100.0
		6	.0	.0	.0	.0	.0	100.0	.0	100.0
		7	.0	.0	.0	.0	.0	.0	100.0	100.0
Cross-validated[a]	Count	1	19	0	0	0	1	0	0	20
		2	0	10	0	0	0	0	0	10
		3	0	1	8	0	1	0	0	10
		4	0	0	0	10	0	0	0	10
		5	0	0	0	1	5	4	0	10
		6	0	0	0	0	1	9	0	10
		7	0	0	0	0	0	2	8	10
	%	1	95.0	.0	.0	.0	5.0	.0	.0	100.0
		2	.0	100.0	.0	.0	.0	.0	.0	100.0
		3	.0	10.0	80.0	.0	10.0	.0	.0	100.0
		4	.0	.0	.0	100.0	.0	.0	.0	100.0
		5	.0	.0	.0	10.0	50.0	40.0	.0	100.0
		6	.0	.0	.0	.0	10.0	90.0	.0	100.0
		7	.0	.0	.0	.0	.0	20.0	80.0	100.0

a. Cross validation is done only for those cases in the analysis. In cross validation, each case is classified by the functions derived from all cases other than that case.

b. 96.3% of original grouped cases correctly classified.

c. 86.3% of cross-validated grouped cases correctly classified.

6.3.2 Pixel-Based Image Classification

The production of thematic maps using image classification is one of the most common applications of remote sensing (Foody 2002). In classification, individual pixels are grouped together with other pixels that correspond to regions that have common properties (Campbell 2002). There are two alternative approaches to image classification: *supervised* and *unsupervised*. Supervised classification is recommended when there are a few areas of known identity to classify the remainder of the image. For this study, supervised classification was conducted due to the desire to identify relatively few classes, with training sites that could be verified with ground truth data and where distinct homogeneous regions that represent each class could be identified (Campbell 2002).

Plot 41

As provided by the software package ERDAS IMAGINE 8.7 (ERDAS 2003), various signature separability assessment tools (e.g. histograms, ellipses, descriptive statistics, error matrix and divergence measures etc.) were utilised.

Modality and variation evaluation using histograms

The histogram function was used to check the individual training areas, with selected histogram examples shown in Figure 6.17 (chickpea) and Figure 6.18 (wheat 50 N). The band assignments in these figures are bands 1–3 (B, G, R) and 4–6 (NIRB, NIRG, NIRR). The histograms were checked to ensure they were homogenous and normally distributed, as a bimodal distribution is indicative of more than one spectral class being captured. It is important that the training signatures approximate normal distribution to satisfy the assumption of the parametric decision rules used to assign pixels from the image to an output class (ERDAS 1999).

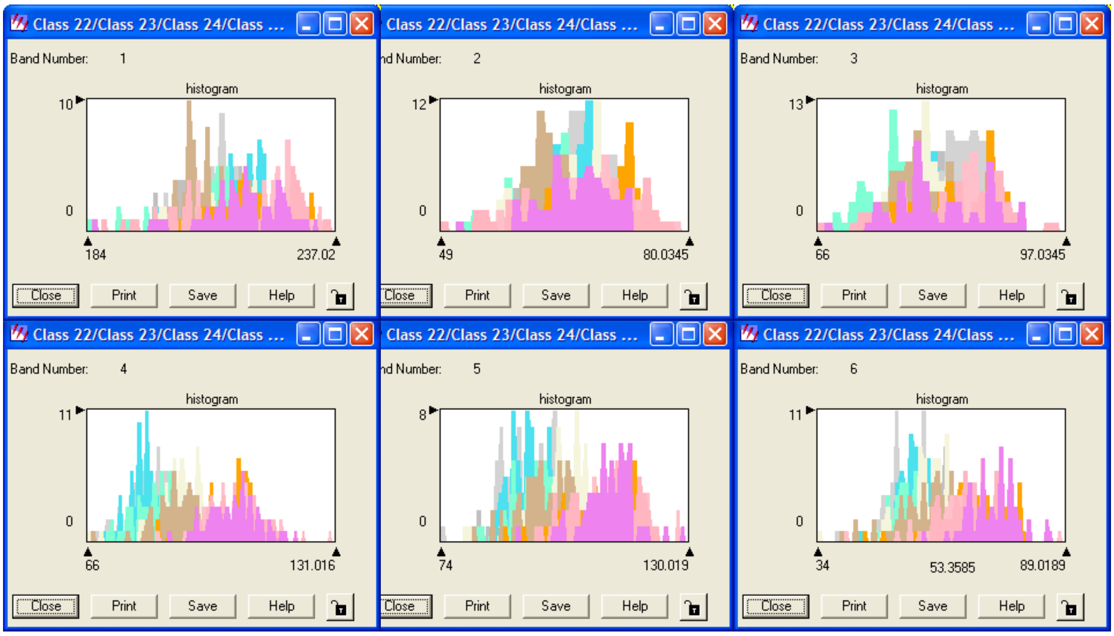

Figure 6.17 The band histogram information for the training sets for the chickpea signature

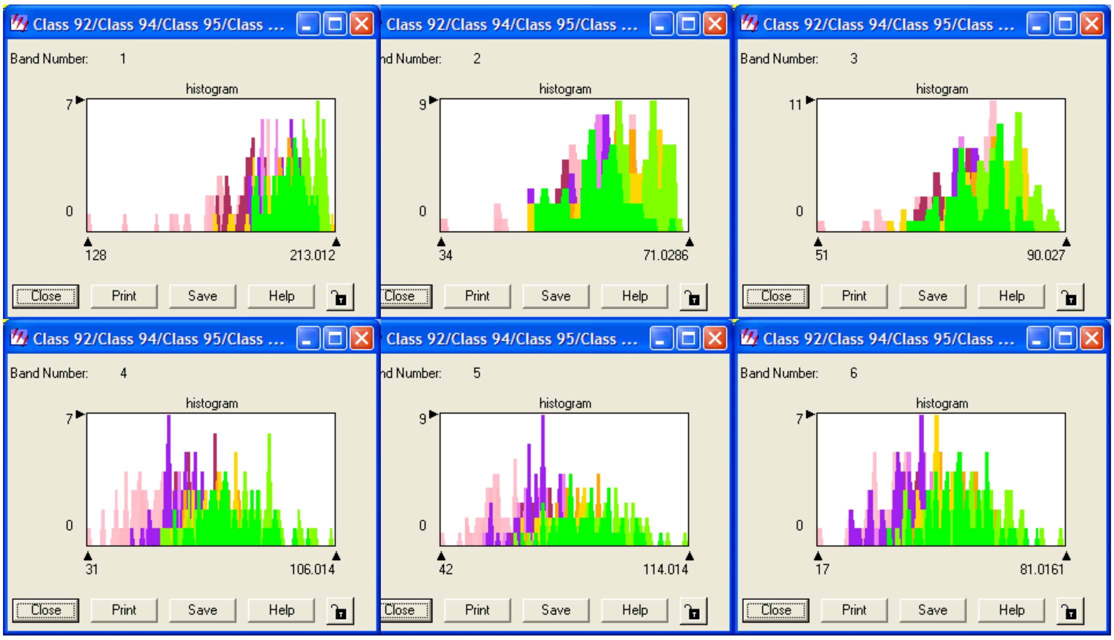

Figure 6.18 The band histogram information for the training sets for the wheat 50N signature

The individual training areas were merged to provide a signature for each of the 12 classes. The colours used to represent each of the '12 signature' classes are shown in Figure 6.19. These same colours are used throughout the 12-class study.

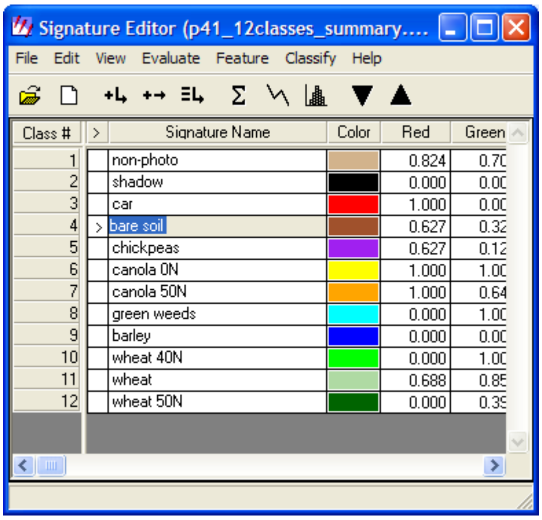

Figure 6.19 The key to the colours used in the histograms and the classification.

The histograms for some of the non-cropped classes are shown in Figure 6.20, while the signatures for the cropped areas are shown in Figure 6.21.

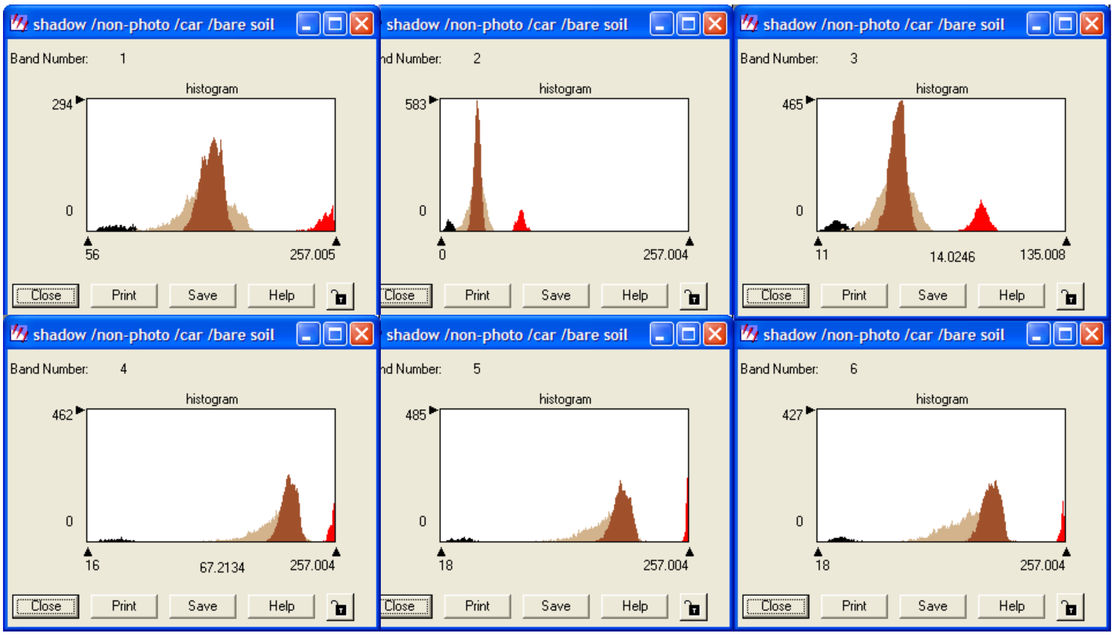

Figure 6.20 The histograms for the merged signatures of the non-cropped areas

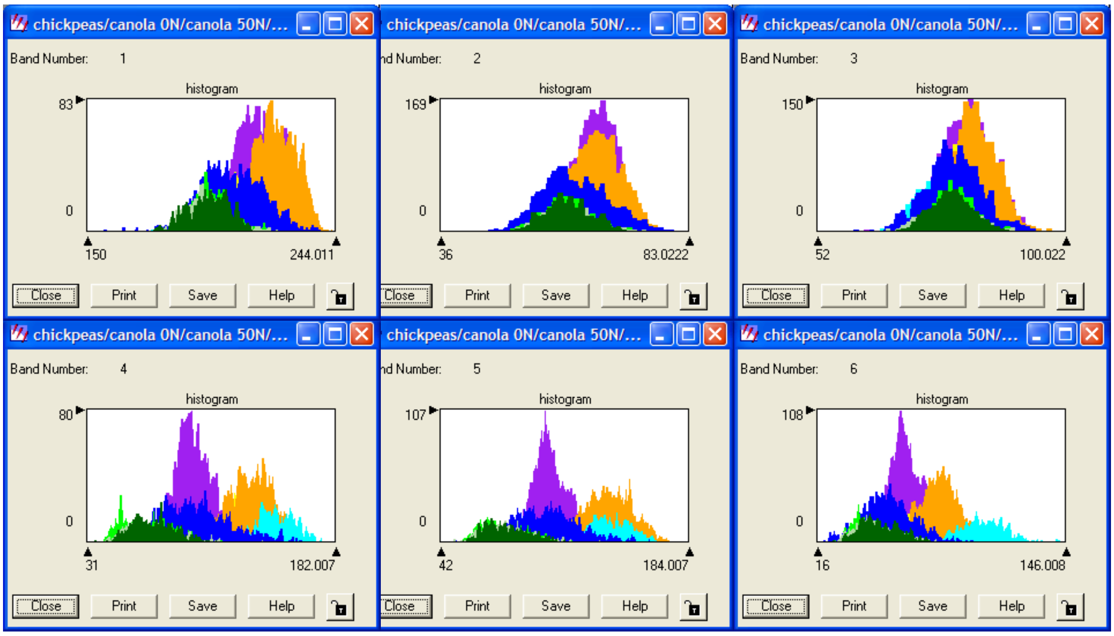

Figure 6.21 The histograms for the merged signatures of the cropped areas

The signatures all show a good distribution with none having a bimodal pattern that is a sign of a non-homogenous signature or two nonrelated signatures being merged. The colour bands do not provide much capacity to discriminate between the signatures, particularly within the vegetation grouping. Fortunately, the NIR does and this concurs with the results found during the DA analysis.

Separability and Band Correlations Based on Feature Space

The feature space plot is also know as a 2D histogram. The frequency of occurrence in the image of a pair of values is indicated by the colour. That is, pairs of values that occur least frequently are in magenta, while those that occur most frequently are in yellow to red. The centre of the ellipse is the main value of the signature for the two bands displayed and the size of the ellipse (outer boundary) represents two standard deviations from the mean. Signature ellipses that have relatively narrow boundaries, do not overlap, and cover different regions of the feature space are ideal. The most discrimination was accomplished using the combination of bands 1 and 4 and their feature space plots are shown as Figure 6.22.

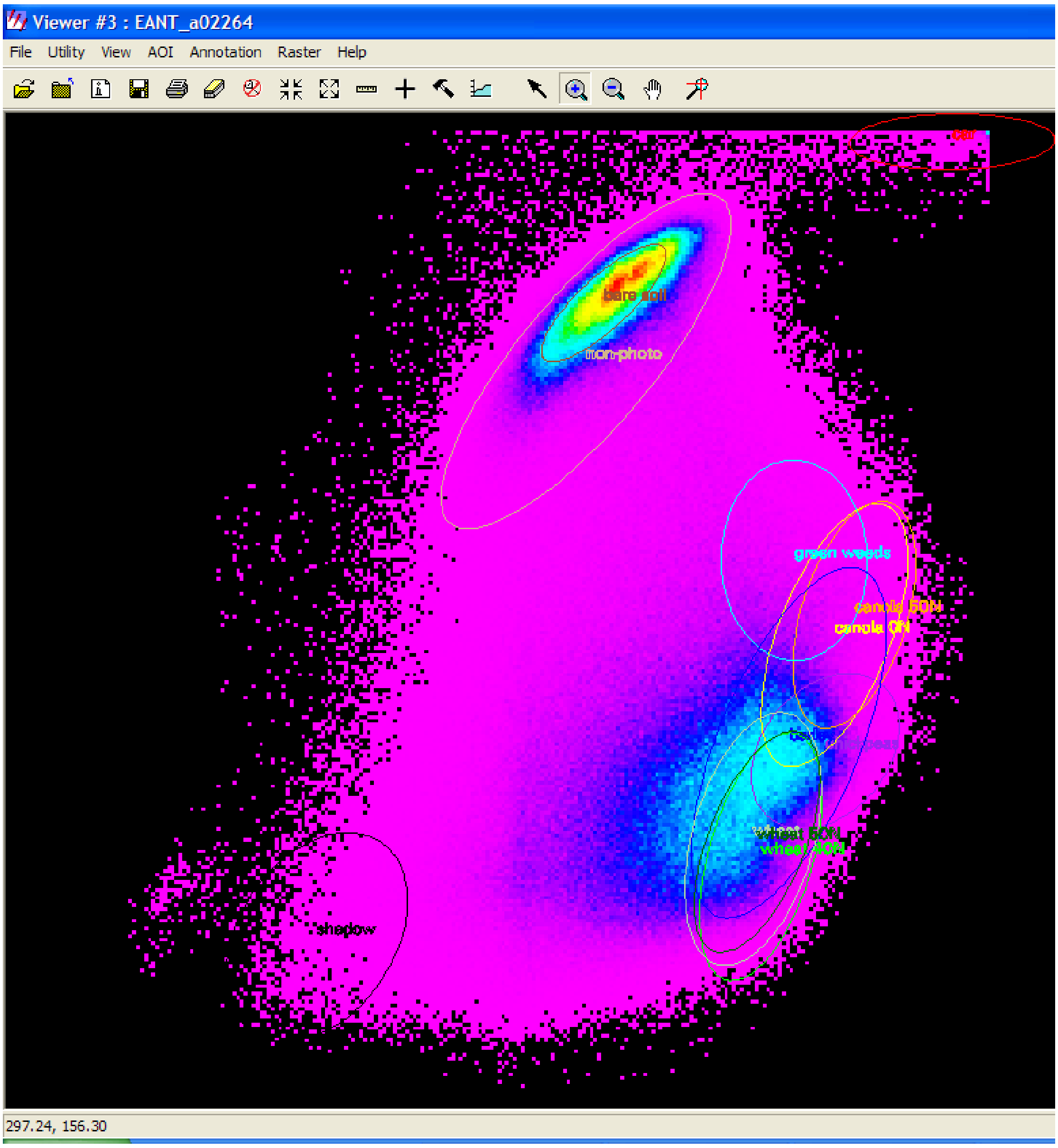

Figure 6.22 The feature space plot for the 12 classes.

The car information class is displayed in the top right-hand corner of plot with the shadow being in the bottom left. The bare soil class is fully contained within the non-photosynthetic class and there is considerable overlap within the 3 wheat classes and the 2 canola classes, with all of the Gramineae being centred around the middle of the right hand edge of the scatterplot. This re-emphasises the difficulty of detecting slight nutritional differences within the same species.

Quantitative Separability/Confusion Determined by Contingency Matrix

The purpose of the contingency matrix (see Table 6.19) is to classify the training site pixels and assess how many are assigned to the correct class. Ideally, the output class for the pixels will be the same as the input training class, but this is not the case in this dataset. As can be seen from the matrix, there is definite confusion between the different fertiliser treatments for both canola and wheat. The chickpeas were often confused with wheat and barley, and barley being confused with all of the other cereal crops. The wheat signatures show the most confusion with values ranging from 45% for wheat with no N applied to 63% for wheat with 50N applied. The confusion matrix indicates that there is merit in combining some classes, especially the fertiliser treatment classes.

Table 6.19 Contingency matrix for the 12 classes.

Reference Data

Classified Data	shadow	non-photo	car	bare soil	chickpeas	canola 0N	canola 50N	green weed	barley	wheat 40N	wheat	wheat 50N
shadow	461	13	0	0	0	0	0	0	0	0	0	0
non-photo	1	3980	2	181	0	0	0	0	0	0	0	0
car	0	0	962	0	0	0	0	0	0	0	0	0
bare soil	0	546	0	4084	0	0	0	0	0	0	0	0
chickpeas	0	0	0	0	1593	19	17	1	69	46	18	16
canola 0N	0	0	0	0	19	675	422	18	99	1	0	0
canola 50N	0	0	0	0	34	296	1022	20	34	0	0	0
green weed	0	0	0	0	3	11	27	559	10	1	1	0
barley	0	0	0	0	55	66	37	2	919	6	22	9
wheat 40N	0	0	0	0	25	0	0	0	36	244	76	74
wheat	0	0	0	0	44	0	0	0	93	82	192	85
wheat 50N	0	0	0	0	59	0	0	0	14	111	122	317
Column Total	462	4539	964	4265	1832	1067	1525	600	1274	491	431	501

Reference Data

Classified Data	shadow	non-photo	car	bare soil	chickpeas	canola 0N	canola 50N	green weed	barley	wheat 40N	wheat	wheat 50N
shadow	99.8	0.3	0.0	0.0	0.0	0.0	0.0	0.0	0.0	0.0	0.0	0.0
non-photo	0.2	87.7	0.2	4.2	0.0	0.0	0.0	0.0	0.0	0.0	0.0	0.0
car	0.0	0.0	99.8	0.0	0.0	0.0	0.0	0.0	0.0	0.0	0.0	0.0
bare soil	0.0	12.0	0.0	95.8	0.0	0.0	0.0	0.0	0.0	0.0	0.0	0.0
chickpeas	0.0	0.0	0.0	0.0	87.0	1.8	1.1	0.2	5.4	9.4	4.2	3.2
canola 0N	0.0	0.0	0.0	0.0	1.0	63.3	27.7	3.0	7.8	0.2	0.0	0.0
canola 50N	0.0	0.0	0.0	0.0	1.9	27.7	67.0	3.3	2.7	0.0	0.0	0.0
green weed	0.0	0.0	0.0	0.0	0.2	1.0	1.8	93.2	0.8	0.2	0.2	0.0
barley	0.0	0.0	0.0	0.0	3.0	6.2	2.4	0.3	72.1	1.2	5.1	1.8
wheat 40N	0.0	0.0	0.0	0.0	1.4	0.0	0.0	0.0	2.8	49.7	17.6	14.8
wheat	0.0	0.0	0.0	0.0	2.4	0.0	0.0	0.0	7.3	16.7	44.6	17.0
wheat 50N	0.0	0.0	0.0	0.0	3.2	0.0	0.0	0.0	1.1	22.6	28.3	63.3
Column Total	462	4539	964	4265	1832	1067	1525	600	1274	491	431	501

Quantitative Separability and Band Selection Using Transformed Divergence

Transformed divergence evaluates the separability between each pair of signatures for a given number of image bands (see Table 6.20). The best average or minimum transformed divergence was used to determine how many and which bands to use in the classification. Values greater than 1900 have good separability, while values less than 1700 have poor separability (ERDAS 1999). In the report, rather than giving all possible band combinations, the information is only given for the bands that produced the best average separability and the best minimum separability, i.e. bands 1 and 4 in the 'taken 2 at a time' case and bands 1, 4 and 6 in the 'taken 3 at a time'. These separability results indicate that bands 1 and 4 would provide good discrimination.

As can be seen from Table 6.20, there is good separability between most of the signatures except for the different fertiliser treatments for the same species (8 & 9 for canola and between 10, 11 and 12 for wheat) which has a very poor separability. The separability is improved slightly by taking 3 bands at a time. This is consistent with the contingency matrix in which these classes showed some confusion.

Completeness of Signature Set Using Image Alarm

The alarm mask function (Figure 6.23) was utilised to perform a quick "pre-classification" check of the image data. This function colours all pixels in the image that are estimated to belong to a particular class (using the colours from Figure 6.19). The areas coloured white indicate signature overlap and confusion between the classes. There is very little green (wheat) and yellow / orange (canola) colour evident, emphasising the confusion caused by the various fertiliser levels. There is little confusion with the non-cropped areas (car, bare soil, non-photosynthetic and shadow).

Table 6.20 Transformed divergence for the 12 classes.

Separability CellArray

Distance Measure: Transformed Divergence
Using Layers: 1 2 3 4 5 6
Taken 2 at a time
Best Average Separability: 1899.99
Combination: 1 4

Signature Name		1	2	3	4	5	6	7	8	9	10	11	12
non-photo	1	0	2000	2000	1999.96	2000	2000	2000	2000	2000	2000	2000	2000
shadow	2	2000	0	2000	2000	2000	2000	2000	2000	2000	2000	2000	2000
car	3	2000	2000	0	2000	2000	2000	2000	2000	2000	2000	2000	2000
bare soil	4	1999.96	2000	2000	0	2000	2000	2000	2000	2000	2000	2000	2000
chickpeas	5	2000	2000	2000	2000	0	1999.82	1999.99	2000	1649.51	1999.94	1999.57	1999.79
canola 0N	6	2000	2000	2000	2000	1999.82	0	848.96	1989.73	1999.43	2000	2000	2000
canola 50N	7	2000	2000	2000	2000	1999.99	848.96	0	1990.59	1999.96	2000	2000	2000
green weeds	8	2000	2000	2000	2000	2000	1989.73	1990.59	0	2000	2000	2000	2000
barley	9	2000	2000	2000	2000	1649.51	1999.43	1999.96	2000	0	1998.71	1994.15	1998.02
wheat 40N	10	2000	2000	2000	2000	1999.94	2000	2000	2000	1998.71	0	422.591	371.996
wheat	11	2000	2000	2000	2000	1999.57	2000	2000	2000	1994.15	422.591	0	136.904
wheat 50N	12	2000	2000	2000	2000	1999.79	2000	2000	2000	1998.02	371.996	136.904	0

Close

Separability CellArray

Distance Measure: Transformed Divergence
Using Layers: 1 2 3 4 5 6
Taken 3 at a time
Best Average Separability: 1911.71
Combination: 1 4 6

Signature Name		1	2	3	4	5	6	7	8	9	10	11	12
non-photo	1	0	2000	2000	2000	2000	2000	2000	2000	2000	2000	2000	2000
shadow	2	2000	0	2000	2000	2000	2000	2000	2000	2000	2000	2000	2000
car	3	2000	2000	0	2000	2000	2000	2000	2000	2000	2000	2000	2000
bare soil	4	2000	2000	2000	0	2000	2000	2000	2000	2000	2000	2000	2000
chickpeas	5	2000	2000	2000	2000	0	1999.84	1999.99	2000	1910.13	2000	1999.95	1999.98
canola 0N	6	2000	2000	2000	2000	1999.84	0	966.999	1984.16	1999.86	2000	2000	2000
canola 50N	7	2000	2000	2000	2000	1999.99	966.999	0	1982.66	2000	2000	2000	2000
green weeds	8	2000	2000	2000	2000	2000	1984.16	1982.66	0	2000	2000	2000	2000
barley	9	2000	2000	2000	2000	1910.13	1999.86	2000	2000	0	1999.2	1994.24	1998.52
wheat 40N	10	2000	2000	2000	2000	2000	2000	2000	2000	1999.2	0	483.607	523.218
wheat	11	2000	2000	2000	2000	1999.95	2000	2000	2000	1994.24	483.607	0	330.56
wheat 50N	12	2000	2000	2000	2000	1999.98	2000	2000	2000	1998.52	523.218	330.56	0

Close

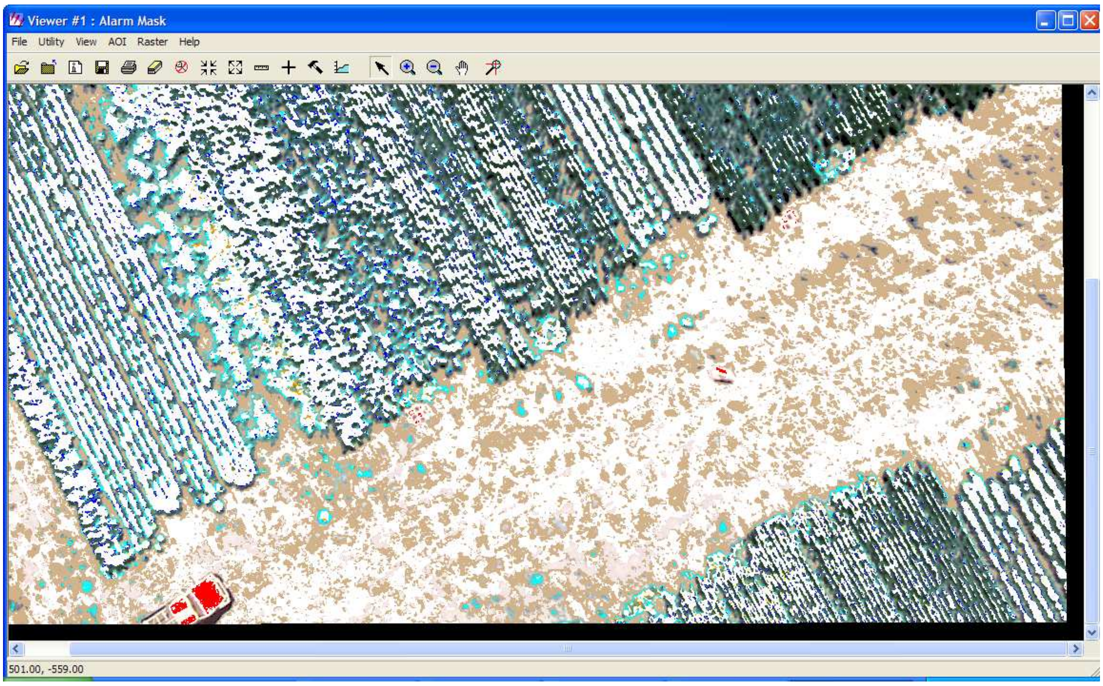

Figure 6.23 The alarm mask function of ERDAS Imagine

Supervised Classification

Once a reliable set of signatures had been created and evaluated, the next step was to perform a classification of the data by using the samples of known identity to classify pixels of unknown identity. ERDAS Imagine 8.7 (ERDAS 2003) has the capacity to classify the data both parametrically with statistical representation, and non-parametrically as objects in feature space. By initially choosing the parallelepiped non-parametric decision rule, the pixels were checked for class membership. If the test resulted in one unique class, then the pixel was assigned to that class. However, if the test resulted in zero class membership, or membership in multiple classes, the pixel was then classified by parametric rules (ERDAS 1999).

In this dataset as well as in nature, the classified classes exhibit natural variation in their spectral patterns and this is further exacerbated by topographic shadowing, system noise and the effects of mixed pixels. It was noted by Campbell (2002, p.342) that "*remote sensed images seldom record spectrally pure class; more typically, they display a range of brightnesses in each band*". It is for this reason that the maximum likelihood (ML) decision rule was chosen for its superior ability to handle this situation. ML classification not only considers the mean / average values in assigning a classification, but also the variability in brightness in each class. This is particularly useful when the distribution of spectral values from separate categories overlaps.

The image was classified using the 12 predetermined classes and the classification is shown in Figure 6.24.

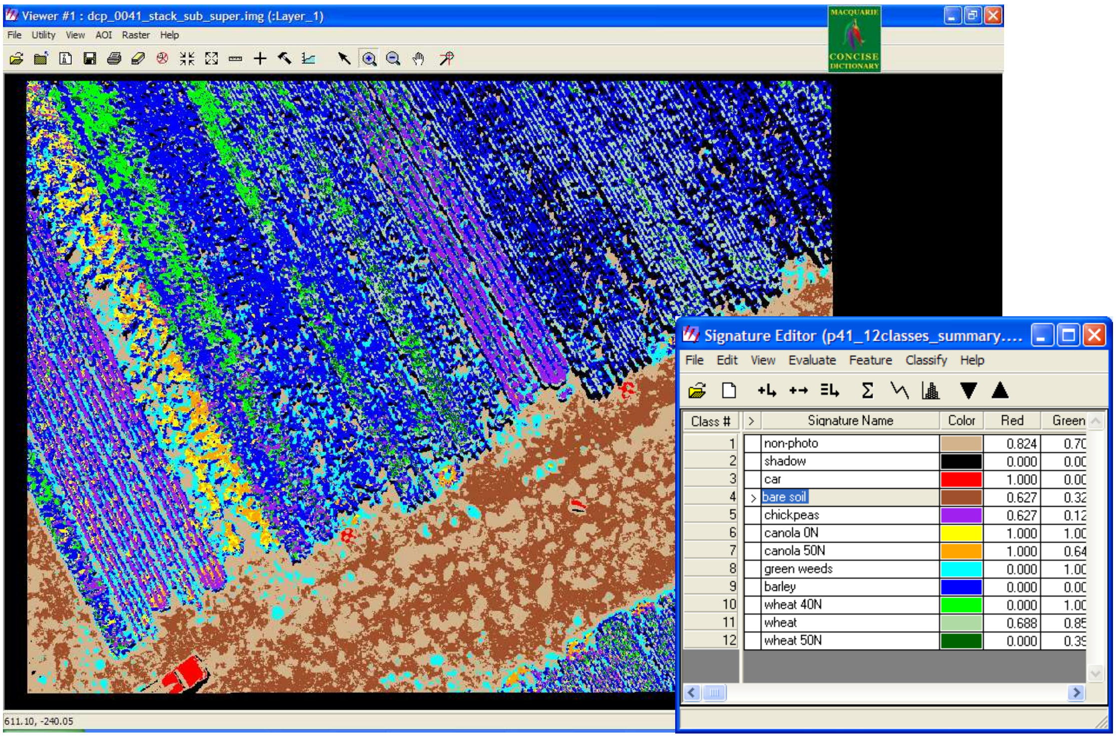

Figure 6.24 The classified image using the 12 classes.

The accuracy of the classified image is determined by the 'accuracy assessment' tool in the software. Accuracy assessment is the process of comparing the classification to ground-truthed data that is assumed to be true in order to determine the accuracy of the classification process. It is not practical to test every pixel of the classified image. The approach taken with this analysis was to have ERDAS Imagine 8.7 (ERDAS 2003) randomly select the pixels that were used in the accuracy assessment.

Accuracy Assessment of the '12 class' Classification

The procedures undertaken to perform a supervised classification using the signature information for the 12 classes was discussed in section 5.3.3. The accuracy assessment was performed with 180 random points equalised within the 12 classes (15 points/class) to ensure the smaller classes were not under-sampled. Several of the randomly generated points coincided with areas where some of the data layer information was missing, resulting in 171 points being used in the analysis. A screen grab showing the random points and the set up for the accuracy assessment is shown in Figure 6.25.

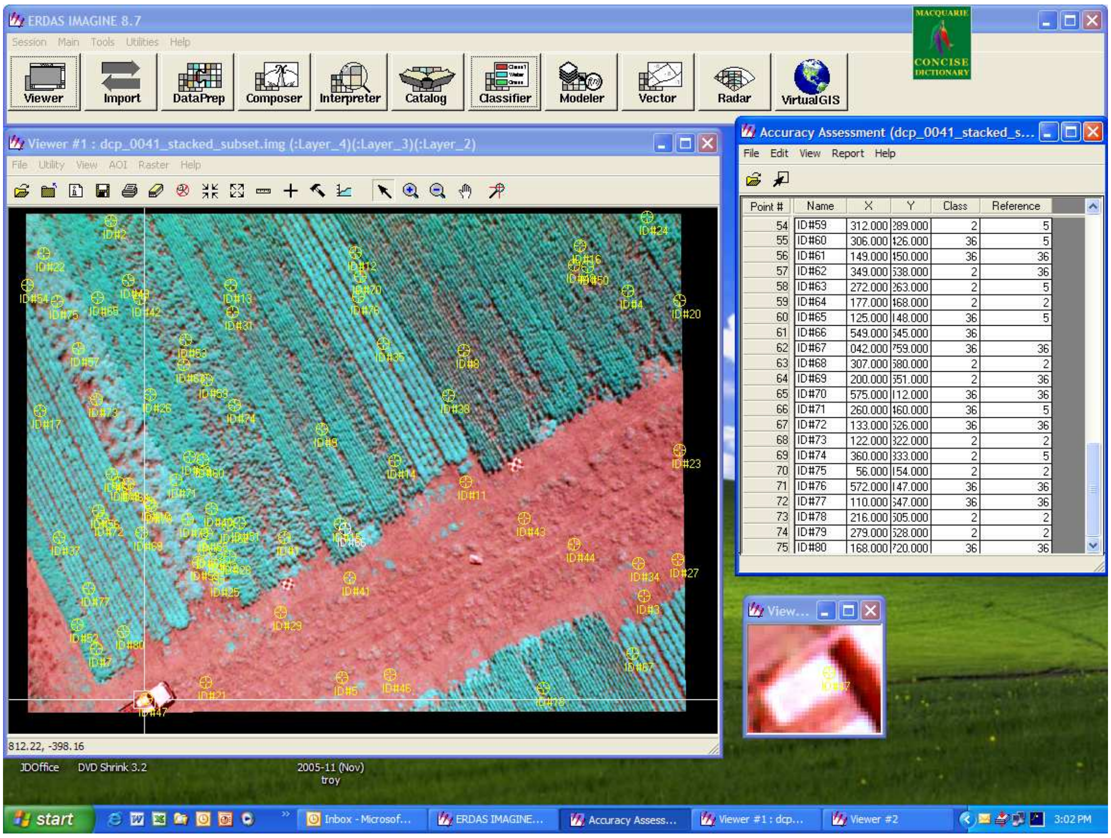

Figure 6.25. Performing an accuracy assessment on the image

The error matrix (Table 6.21) is similar to the contingency matrix (Table 6.19) and is the most common way to represent the classification accuracy of remotely sensed data (Congalton 1991). The matrix provides a cross-comparison of pixels taken from the classified image with corresponding ground reference data, with one dimension of the matrix being the reference data and the other being the classified pixels.

As with the contingency matrix for the 12 classes (Table 6.19), the error matrix (Table 6.21) confirms that confusion exists between the classes. This is particularly evident when trying to distinguish between the various fertiliser levels, with chickpeas being misclassified as wheat and with barley pixels being confused with wheat and canola.

Table 6.21 The error matrix for the 12-class accuracy assessment.

ERROR MATRIX

Classified Data	Unclass	shadow	bare soil	car	non-photo	chickpeas	canola 0N	canola 50N	green weec	barley	wheat 40N	wheat	wheat 50N	Row Total
				Reference Data										
Unclass	0	0	0	0	0	0	0	0	0	0	0	0	0	0
shadow	0	4	1	0	0	0	0	0	0	0	0	1	0	6
bare soil	0	0	14	0	1	0	0	0	0	0	0	0	0	15
car	0	0	0	15	0	0	0	0	0	0	0	0	0	15
non-photo	0	0	7	0	6	0	0	0	2	0	0	0	0	15
chickpeas	0	0	0	0	0	11	0	0	0	0	0	3	1	15
canola 0N	0	0	0	0	0	5	1	7	0	1	0	1	0	15
canola 50N	0	0	0	0	0	0	5	5	2	1	0	2	0	15
green weeds	0	0	0	0	2	2	1	1	2	2	2	3	0	15
barley	0	1	0	0	0	0	1	1	0	3	3	6	0	15
wheat 40N	0	0	0	0	0	1	0	0	0	0	2	11	1	15
wheat	0	0	0	0	0	2	0	0	0	0	0	13	0	15
wheat 50N	0	0	0	0	0	3	0	0	0	0	2	7	3	15
Column Total	0	5	22	15	9	24	8	14	6	7	9	47	5	171

----- End of Error Matrix -----

The simplest descriptive statistic is the overall classification accuracy, which is calculated by dividing the number correctly classified by the total number of pixels in the error matrix. The overall classification accuracy (see Table 6.22) using the 12 classes was 46.2%. This however, does not give any indication of the accuracy in each of the classes/categories. This is accomplished by reviewing the errors of inclusion (commission errors) and errors of exclusion (omission errors) present in the classification (Congalton 1991).

The error of omission ("producer's accuracy") is determined by the total number of reference pixels that were not assigned to the correct class, or "omitted". This accuracy measure indicates the probability of a reference pixel being correctly classified. Corollary, if the total number of correctly assigned pixels in a category is divided by the total number of pixels that were classified in that category, then the result is a measure of the error of commission, i.e. pixels that were included in a class that should not have been there. This "user's accuracy" is a measure of reliability and is indicative of the probability that a pixel classified on the map/image actually represents that category on the ground (Story & Congalton 1986).

Table 6.22 The accuracy totals for the 12 class classification.

ACCURACY TOTALS

Class Name	Reference Totals	Classified Totals	Number Correct	Producers Accuracy	Users Accuracy
Unclassified	0	0	0	---	---
shadow	5	6	4	80.0%	66.7%
bare soil	22	15	14	63.6%	93.3%
car	15	15	15	100.0%	100.0%
non-photo	9	15	6	66.7%	40.0%
chickpeas	24	15	11	45.8%	73.3%
canola 0N	8	15	1	12.5%	6.7%
canola 50N	14	15	5	35.7%	33.3%
green weeds	6	15	2	33.3%	13.3%
barley	7	15	3	42.9%	20.0%
wheat 40N	9	15	2	22.2%	13.3%
wheat	47	15	13	27.7%	86.7%
wheat 50N	5	15	3	60.0%	20.0%
Totals	171	171	79		

Overall Classification Accuracy = 46.20%

----- End of Accuracy Totals -----

Another method of determining accuracy assessment is the kappa coefficient (Cohen 1960). Kappa values can range for +1 to -1, however, positive values are expected as there should be a positive correlation between the remotely sensed classification and the reference data. Landis & Koch (1977) suggested some possible ranges for kappa values: > 0.80 (i.e. 80%) represents strong agreement, 0.40–0.80 (i.e. 40–80%) represents moderate agreement and < 0.40 (i.e. 40%) represents poor agreement.

With kappa analysis, it is possible to test whether a classified map generated using remotely sensed data is significantly better than a map generated by randomly assigning labels to areas. It is also possible to compare matrices to see whether they are statistically significantly different, based on the overall accuracy, to conclude which algorithm or method is better. This indicates that the current classification achieved an accuracy that is 41% better than would be expected from chance assignment of pixels to categories. Also evident in Table 6.23 is that skill in classifying some of the classes (especially canola 0N, wheat 40N and green weeds) is only slightly better than a random classification. This result re-emphasises the fact that there is considerable overlap in some of the signatures and the classification could be improved by removing the different nutrition classes for the same species.

Table 6.23 Kappa statistics for the 12 class classification

KAPPA (K^) STATISTICS

Overall Kappa Statistics = 0.4112

Conditional Kappa for each Category.

Class Name	Kappa
Unclassified	0
shadow	0.6566
bare soil	0.9235
car	1
non-photo	0.3667
chickpeas	0.6898
canola 0N	0.0209
canola 50N	0.2739
green weeds	0.1018
barley	0.1659
wheat 40N	0.0852
wheat	0.8161
wheat 50N	0.1759

----- End of Kappa Statistics -----

Accuracy Assessment of the ‘9 Class’ Classification

In reviewing the accuracy assessment report and with the knowledge from the discriminant function analysis, determining crop type with varying levels of nutrition is difficult. In an attempt to further improve the classification accuracy, the various nutrition levels were dropped for both wheat and canola. Rather than having various signatures for the varying nutrition levels, these signatures were amalgamated to provide one signature per species, with the new class being signified as WHEAT (for the three combined nutrition levels) and CANOLA (for the two combined nutrition levels). This resulted in 9 classes (see Figure 6.26 for the colour assignments) with 90 random equalised points chosen on which to perform the assessment.

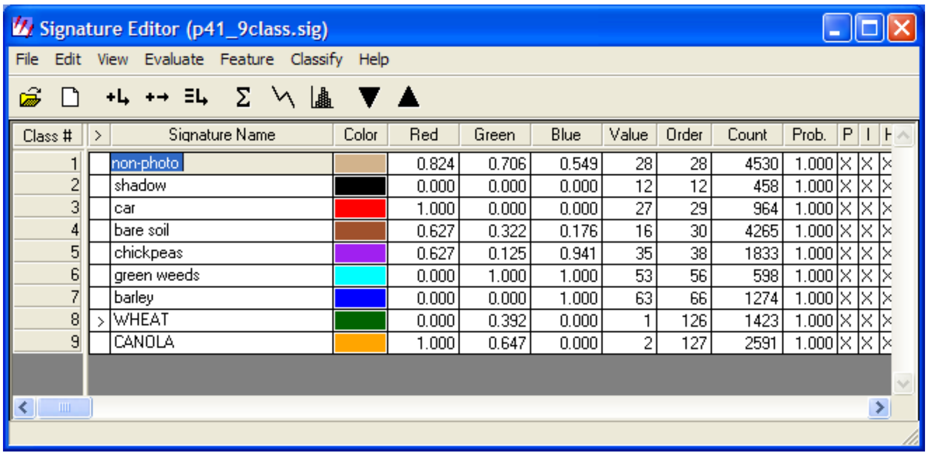

Class #	>	Signature Name	Color	Red	Green	Blue	Value	Order	Count	Prob.	P	I	H
1		non-photo		0.824	0.706	0.549	28	28	4530	1.000	X	X	X
2		shadow		0.000	0.000	0.000	12	12	458	1.000	X	X	X
3		car		1.000	0.000	0.000	27	29	964	1.000	X	X	X
4		bare soil		0.627	0.322	0.176	16	30	4265	1.000	X	X	X
5		chickpeas		0.627	0.125	0.941	35	38	1833	1.000	X	X	X
6		green weeds		0.000	1.000	1.000	53	56	598	1.000	X	X	X
7		barley		0.000	0.000	1.000	63	66	1274	1.000	X	X	X
8	>	WHEAT		0.000	0.392	0.000	1	126	1423	1.000	X	X	X
9		CANOLA		1.000	0.647	0.000	2	127	2591	1.000	X	X	X

Figure 6.26 The colours chosen and the pixel count for the 9 classes.

As can be seen from the contingency matrix (Table 6.24), merging classes to remove the different fertiliser levels has reduced the confusion amongst some of the classes. In the 12-class case, the wheat confusion ranged from 45–63% and this has now been increased to 85%. Similar improvements were made with canola. As with the 12-class case, confusion still exists between the other cereal crops and between the non-photosynthetic materials.

Table 6.24 The contingency matrix for the 9 classes.

Reference Data

Classified Data ----------	shadow ----------	non-photo ----------	car ----------	bare soil ----------	chickpeas ----------	green weec ----------	barley ----------	wheat ----------	canola ----------	Row Total ----------
shadow	461	13	0	0	0	0	0	0	0	474
non-photo	1	4105	2	487	0	0	0	0	0	4595
car	0	0	962	0	0	0	0	0	0	962
bare soil	0	421	0	3778	0	0	0	0	0	4199
chickpeas	0	0	0	0	1523	1	60	123	36	1743
green weed	0	0	0	0	2	544	17	2	63	628
barley	0	0	0	0	130	10	991	84	236	1451
WHEAT	0	0	0	0	103	0	104	1213	0	1420
CANOLA	0	0	0	0	74	45	102	3	2257	2481
Column Total	462	4539	964	4265	1832	600	1274	1425	2592	17953

Reference Data

Classified Data ----------	shadow ----------	non-photo ----------	car ----------	bare soil ----------	chickpeas ----------	green weec ----------	barley ----------	wheat ----------	canola ----------	Row Total ----------
shadow	99.8	0.3	0.0	0.0	0.0	0.0	0.0	0.0	0.0	474
non-photo	0.2	90.4	0.2	11.4	0.0	0.0	0.0	0.0	0.0	4595
car	0.0	0.0	99.8	0.0	0.0	0.0	0.0	0.0	0.0	962
bare soil	0.0	9.3	0.0	88.6	0.0	0.0	0.0	0.0	0.0	4199
chickpeas	0.0	0.0	0.0	0.0	83.1	0.2	4.7	8.6	1.4	1743
green weed	0.0	0.0	0.0	0.0	0.1	90.7	1.3	0.1	2.4	628
barley	0.0	0.0	0.0	0.0	7.1	1.7	77.8	5.9	9.1	1451
WHEAT	0.0	0.0	0.0	0.0	5.6	0.0	8.2	85.1	0.0	1420
CANOLA	0.0	0.0	0.0	0.0	4.0	7.5	8.0	0.2	87.1	2481
Column Total	462	4539	964	4265	1832	600	1274	1425	2592	17953

The signature overlap that caused the confusion in the above table is also evident in the histograms (see Figure 6.27) and in the feature space plots (see Figure 6.28). The classified image is shown as Figure 6.29.

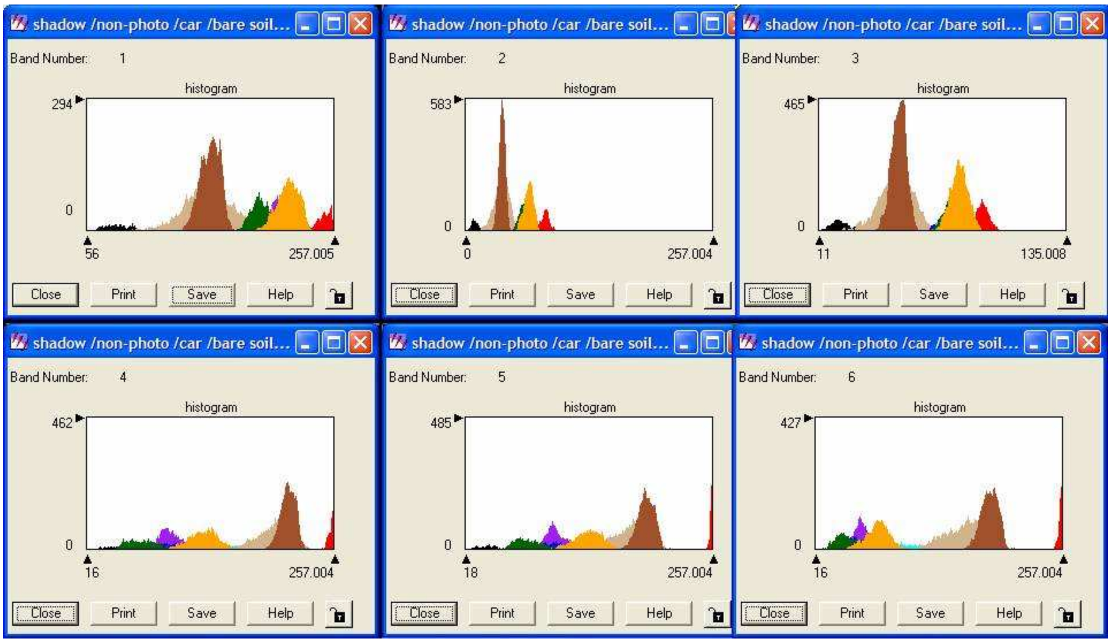

Figure 6.27 Histograms for the 9 classes

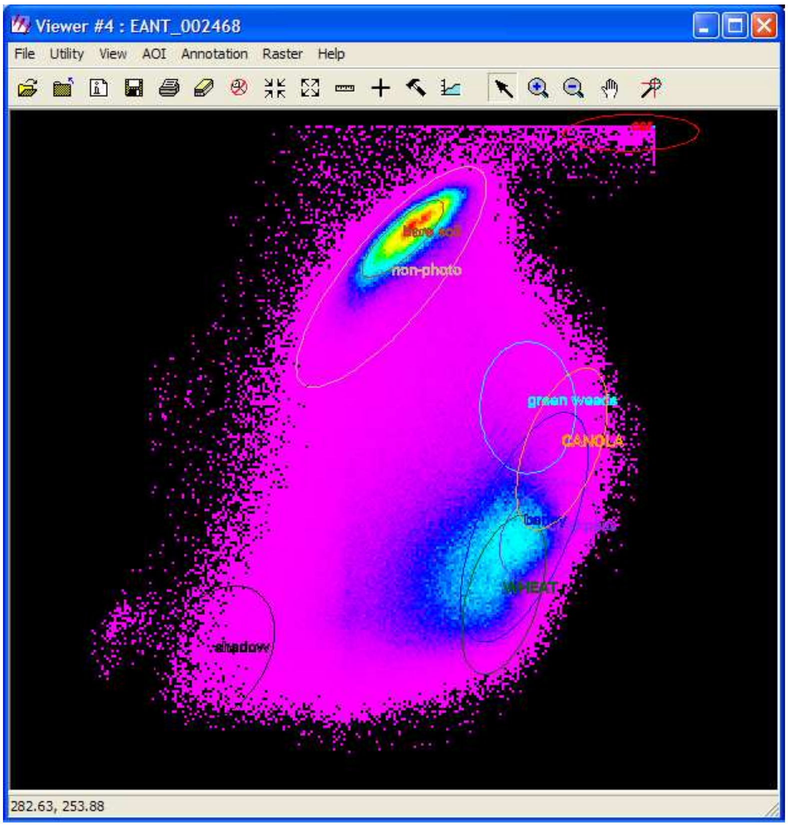

Figure 6.28 Feature space plot for the 9 classes

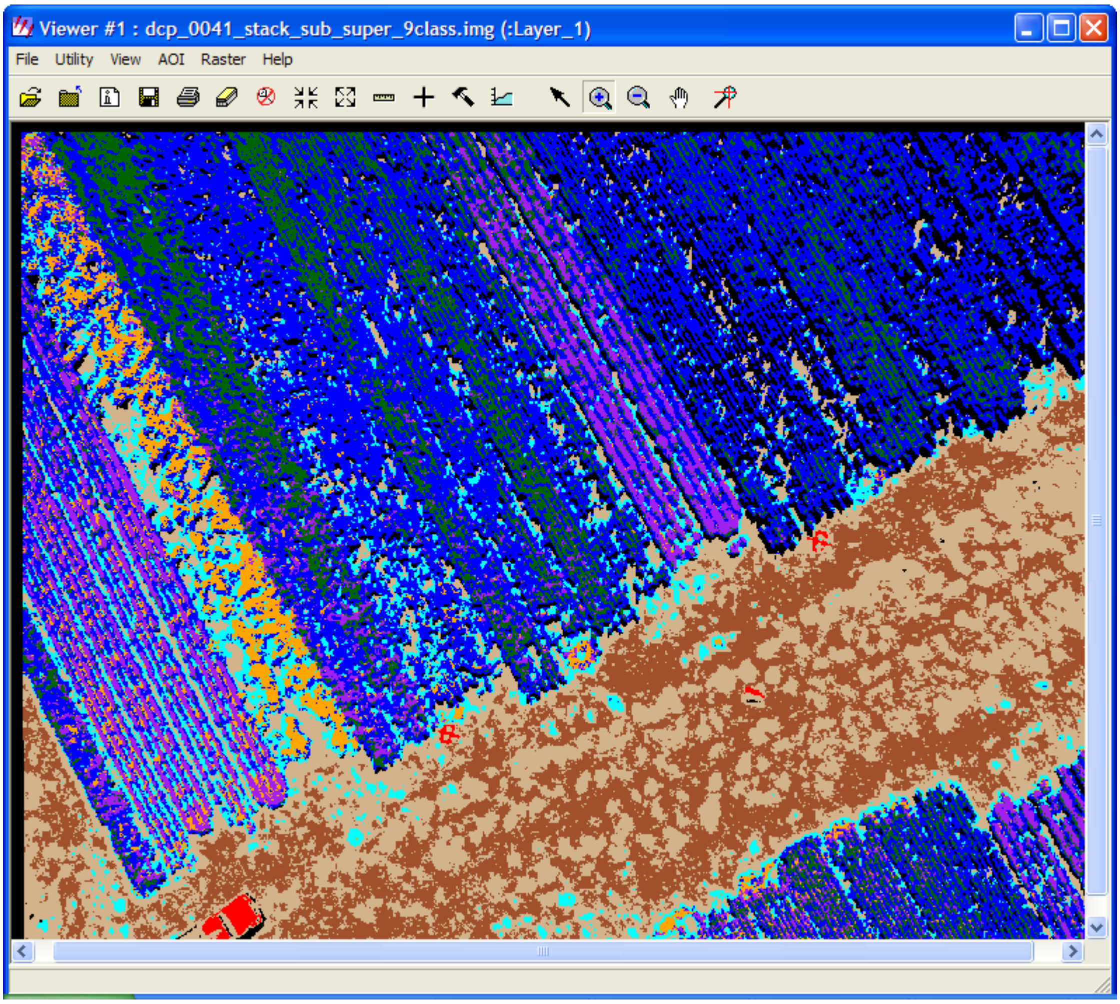

Figure 6.29 The classification using 9 classes.

The overall classification accuracy (see Table 6.25) increased to 66% by reducing the number of classes. The kappa statistic improved to 61% better than would be expected from chance assignment of pixels to categories. There is still some merit in further refining the signatures evident by the overlap in the histograms and feature space plots. This will be progressed in the next iteration.

Table 6.25 The accuracy totals including kappa statistics for the 9 class classification.

ACCURACY TOTALS

Class Name	Reference Totals	Classified Totals	Number Correct	Producers Accuracy	Users Accuracy
Unclassified	0	0	0	---	---
WHEAT	36	20	19	52.78%	95.00%
CANOLA	19	20	14	73.68%	70.00%
shadow	6	7	6	100.00%	85.71%
bare soil	22	20	16	72.73%	80.00%
car	21	20	20	95.24%	100.00%
non-photo	19	20	13	68.42%	65.00%
chickpeas	31	20	16	51.61%	80.00%
green weeds	3	20	1	33.33%	5.00%
barley	10	20	5	50.00%	25.00%
Totals	167	167	110		

Overall Classification Accuracy = 65.87%

----- End of Accuracy Totals -----

KAPPA (K^) STATISTICS

Overall Kappa Statistics = 0.6135

Conditional Kappa for each Category.

Class Name	Kappa
Unclassified	0
WHEAT	0.9363
CANOLA	0.6615
shadow	0.8518
bare soil	0.7697
non-photo	0.6051
chickpeas	0.7544
green weeds	0.0326
barley	0.2022

----- End of Kappa Statistics -----

Accuracy Assessment of the '6 Class' Classification

On reviewing the contingency matrix, histograms and feature space plots, there were several signatures that were very similar and / or overlapped. To improve the classification, wheat, barley and green weeds were merged to form a 'gramineae' class and the non-photosynthetic and bare soil classes were merged to form a 'fallow' class. The classes showing the assigned colours are shown in Figure 6.30 and the contingency matrix in Table 6.26. The histograms (Figure 6.31) are showing much better separation between the classes. The output classified image is shown as Figure 6.32.

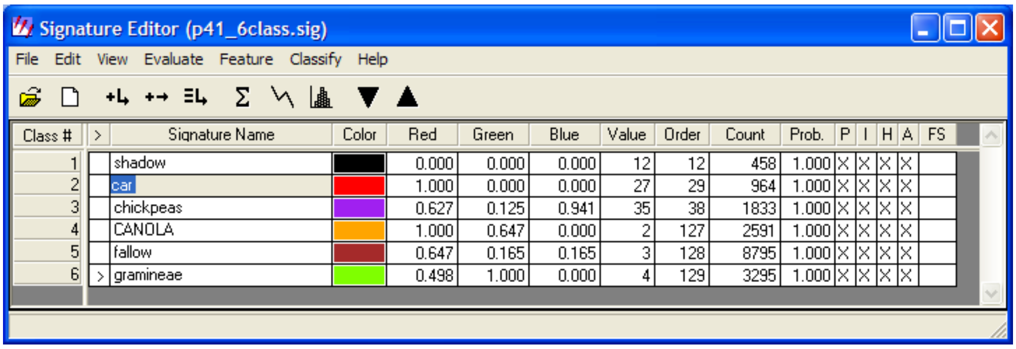

Figure 6.30 The 6-class signatures.

Table 6.26 The contingency matrix for the 6 classes

Reference Data

Classified Data	shadow	car	chickpeas	CANOLA	fallow	gramineae	Row Total
shadow	462	0	0	0	20	0	482
car	0	960	0	0	0	0	960
chickpeas	0	0	1531	47	0	231	1809
CANOLA	0	0	60	2293	0	176	2529
fallow	0	4	0	0	8784	0	8788
gramineae	0	0	241	252	0	2888	3381
Column Total	462	964	1832	2592	8804	3295	17949

Reference Data

Classified Data	shadow	car	chickpeas	CANOLA	fallow	gramineae	Row Total
shadow	100	0	0	0	0.23	0	482
car	0	99.59	0	0	0	0	960
chickpeas	0	0	83.57	1.81	0	7.01	1809
CANOLA	0	0	3.28	88.46	0	5.34	2529
fallow	0	0.41	0	0	99.77	0	8788
gramineae	0	0	13.16	9.72	0	87.65	3381
Column Total	462	964	1832	2592	8804	3295	17949

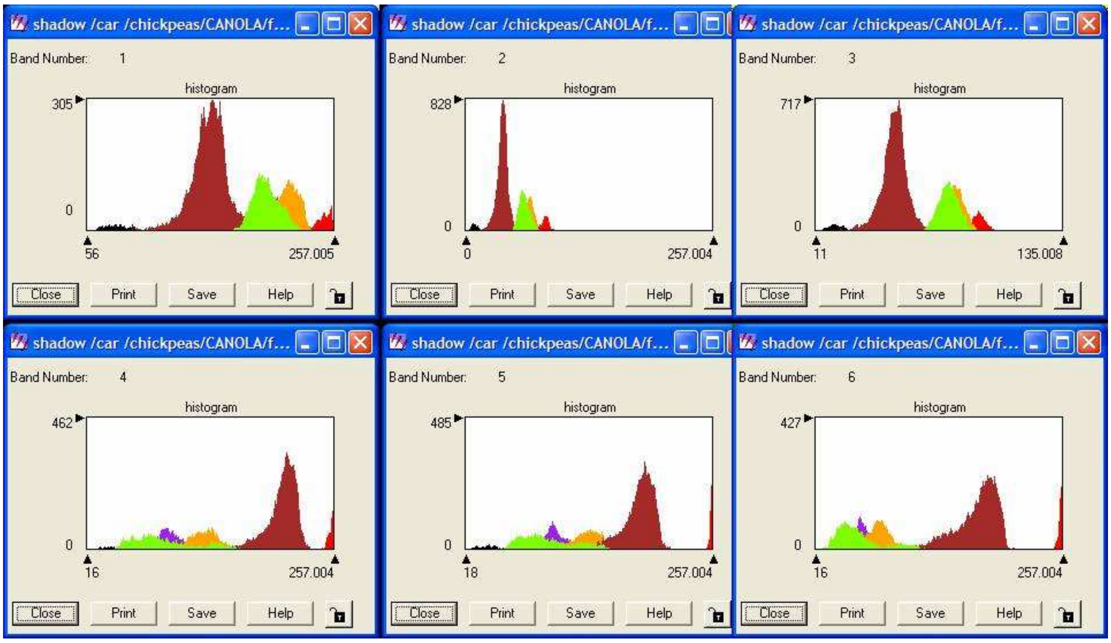

Figure 6.31 The histograms for the 6 classes.

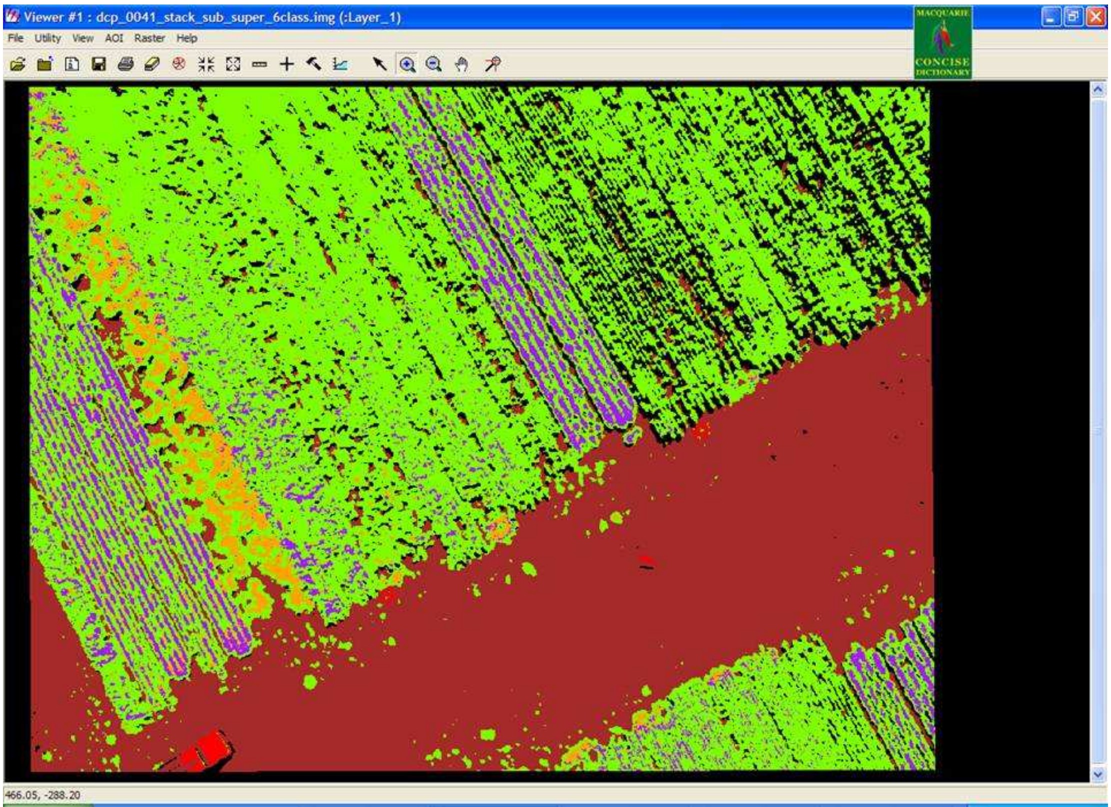

Figure 6.32 The area when classified using 6 classes.

The increased separation in the histograms is quantified in Table 6.27 where the overall classification accuracy has improved to 82%, with the kappa value increased to 78%.

Table 6.27 The accuracy totals including kappa statistics for the 6 class classification.

ACCURACY TOTALS

Class Name	Reference Totals	Classified Totals	Number Correct	Producers Accuracy	Users Accuracy
Unclassified	1	0	0	---	---
CANOLA	15	20	14	93.33%	70.00%
fallow	21	20	19	90.48%	95.00%
gramineae	21	20	13	61.90%	65.00%
shadow	4	6	4	100.00%	66.67%
car	20	20	20	100.00%	100.00%
chickpeas	24	20	17	70.83%	85.00%
Totals	106	106	87		

Overall Classification Accuracy = 82.08%

----- End of Accuracy Totals -----

KAPPA (K^) STATISTICS

Overall Kappa Statistics = 0.7809

Conditional Kappa for each Category.

Class Name	Kappa
Unclassified	0
CANOLA	0.6505
fallow	0.9376
gramineae	0.5635
shadow	0.6536
car	1
chickpeas	0.8061

----- End of Kappa Statistics -----

In one final iteration, the number of class was further reduced to 4 classes (photosynthetic material, fallow, car and shadow) with the corresponding colours being green, maroon, red and black, respectively.

Accuracy Assessment of the '4 Class' Classification

With only 4 classes, the contingency matrix (Table 6.28) shows a very high level of agreement within the classes and there is extremely good separability in the histogram plots (Figure 6.33). The classified image (Figure 6.34) accurately maps the cropped (photosynthetic) area from the fallow and other two classes. This is represented in the accuracy table (Table 6.29) where the overall classification accuracy is 97%, with a 96% kappa coefficient.

Table 6.28 The contingency matrix for the 4 classes.

ERROR MATRIX

Reference Data

Classified Data	shadow	car	fallow	photosynth
shadow	462	0	20	0
car	0	960	0	0
fallow	0	4	8784	0
photosynth	0	0	0	7713
Column Total	462	964	8804	7713

----- End of Error Matrix -----

RROR MATRIX

Reference Data

Classified Data	shadow	car	fallow	photosynth
shadow	100.0	0.0	0.2	0.0
car	0.0	99.6	0.0	0.0
fallow	0.0	0.4	99.8	0.0
photosynth	0.0	0.0	0.0	100.0
Column Total	462	964	8804	7713

----- End of Error Matrix -----

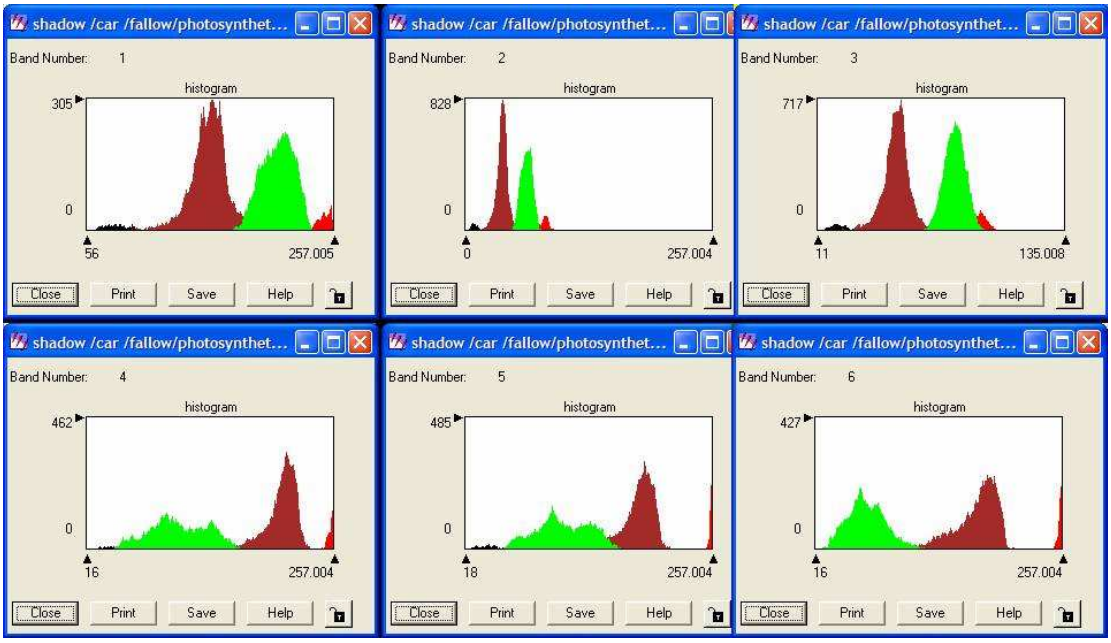

Figure 6.33 The histograms for the 4 classes.

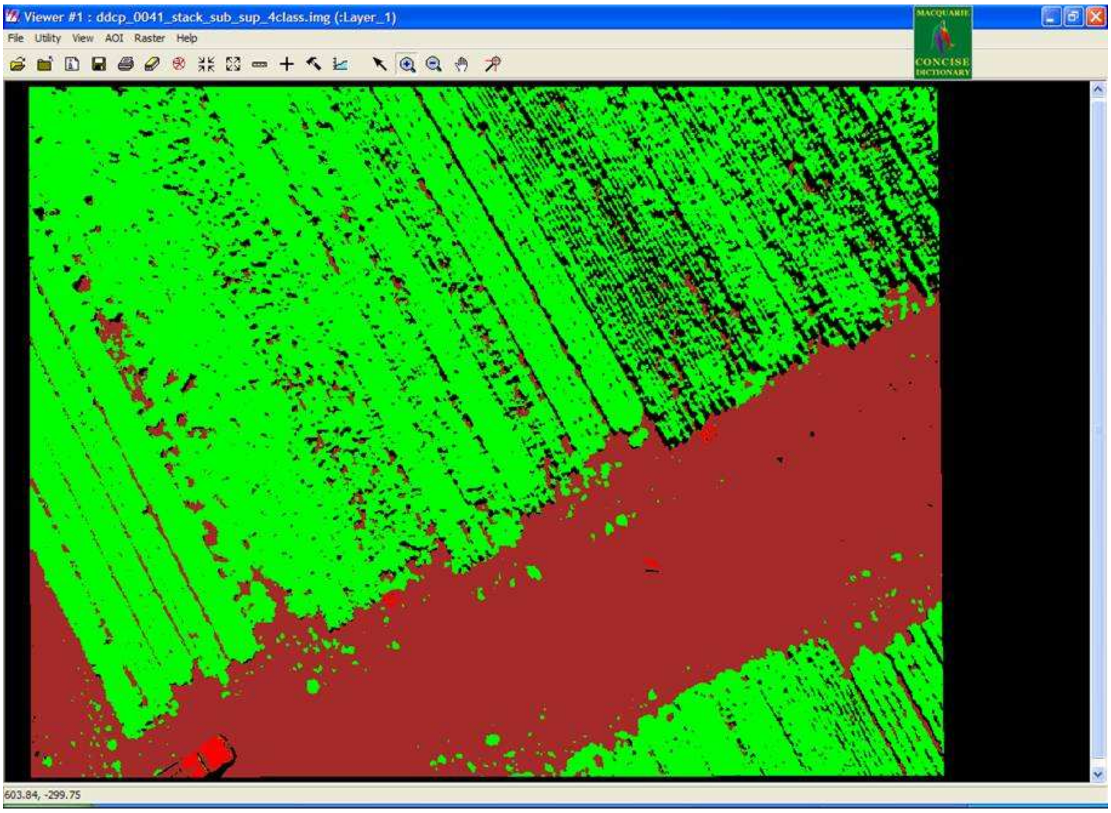

Figure 6.34 The area when classified using 4 classes.

Table 6.29 The accuracy totals including kappa statistics for the 4-class classification.

ACCURACY TOTALS

Class Name	Referenc Totals	Classified Totals	Number Correct	Producers Accuracy	Users Accuracy
----------	----------	----------	-------	---------	-----
Unclassified	0	0	0	---	---
photosynthetic	21	20	20	95.24%	100.00%
fallow	21	20	20	95.24%	100.00%
shadow	8	10	8	100.00%	80.00%
car	20	20	20	100.00%	100.00%
Totals	70	70	68		

Overall Classification Accuracy = 97.14%

----- End of Accuracy Totals -----

KAPPA (K^) STATISTICS

Overall Kappa Statistics = 0.9609

Conditional Kappa for each Category.

Clas	Kappa
-----	-----
Unclassified	0
photosynthetic r	1
fallow	1
shadow	0.7742
car	1

----- End of Kappa Statistics -----

This assessment has taken the refining of the signatures to the extreme, but it does prove that the LCLA remote sensing system can provide very useful discrimination of crops and the level of accuracy that may be expected depending on the level of classification (family, genus, species and variety). If the purpose is to differentiate green plant material from all other features, then this system can provide a near perfect discrimination. If the task is to distinguish different fertiliser regimes (which arguably is similar to detecting different varieties within species), then the accuracy is 41% better than chance. Detecting between species, and then genus, is somewhere in-between these upper and lower limits.

6.3.3 Object-Oriented Image Classification

The image segmentation process at different “scales” produced objects of various attributes (Figure 6.35). As expected, increasing the scale parameter produced fewer objects, but each was relatively larger in average area. Visual interpretation of the results showed the detailed or “more pure” aggregation of objects in the 30-scale parameter. Conversely, the 100-scale parameter image produced more generalised groupings.

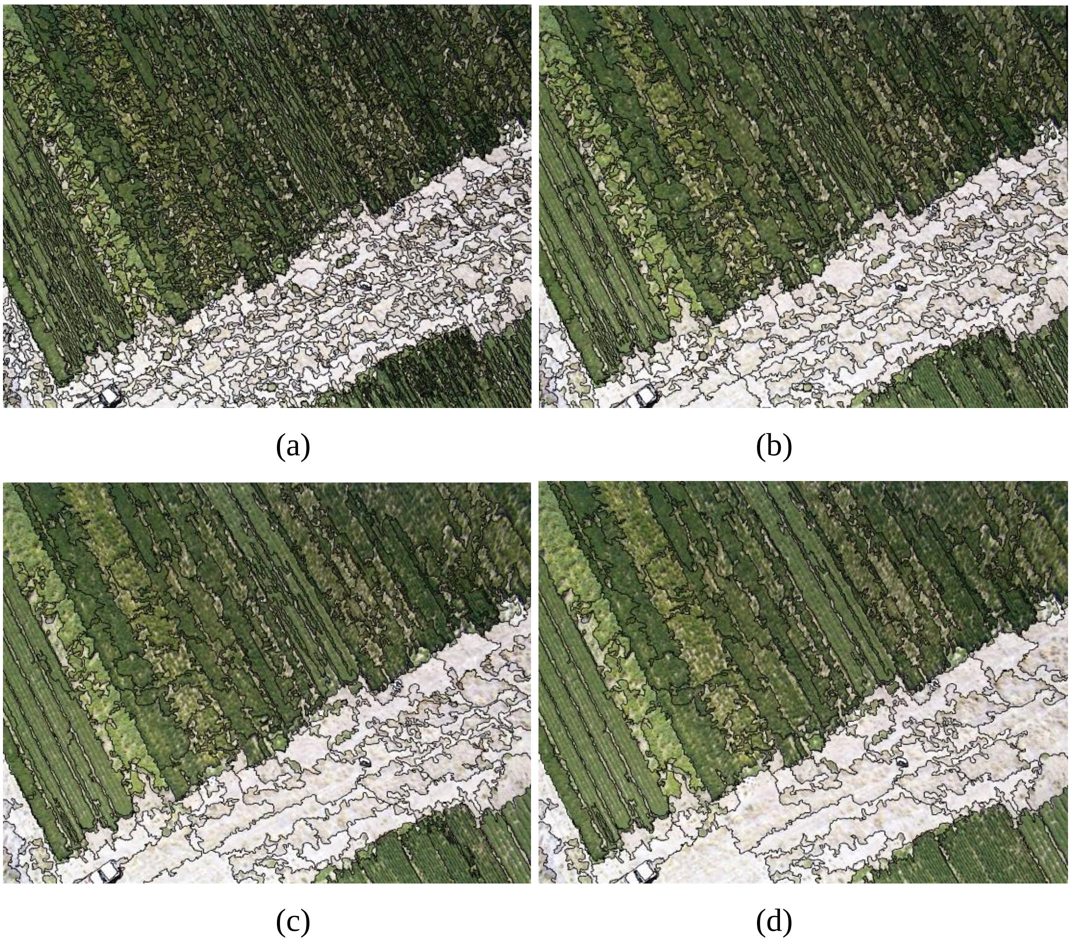

Figure 6.35 Objects created after image segmentation at various scales: (a) 30 scale, (b) 50 scale, (c) 80 scale, and (d) 100 scale.

With the focus on colour (spectral values) and texture, 49 object attributes (e.g. mean of red band, standard deviation of NIR_R, grey level co-occurrence matrix (GLCM) values, etc.) were included in the assessment. The use of “feature space optimisation” procedure, available in the software, has flagged the best five features for each scale parameter (Table 6.30). While the results show differences in the features selected as optimum, the general trend is clear: the use of both spectral values and texture (rather than separate) is important in optimising class separation.

The results also showed the effect of scale in the value of the separation distance (i.e. the ability of the attributes or features to separate classes based on the five best features). The smallest scale parameter (30 scale) produced the lowest separation distance value (0.52), while the 80-scale parameter gained the highest value (0.86). This indicates the non-linear relationship between scale parameter and separability measure, although an optimum scale can be determined.

Table 6.30 Results of image segmentation and feature optimisation

Scale for Segmentation	No. of Objects	Best Separation Distance	Best 5 Features for Separation
30 scale	2011	0.52	GLCM Homogeneity NIR_R (0°), GLCM Homogeneity Blue (0°), Max diff, Mean NIR_R, STD Green
50 scale	659	0.69	Mean NIR_R, GLCM Homogeneity Blue (135°), GLCM Homogeneity (0°), Max diff, STD NIR_R
80 scale	220	0.86	GLCM Homogeneity NIR_R (90°), GLCM Homogeneity NIR_G (135°), Max diff, Mean NIR_R, Mean NIR_G
100 scale	146	0.61	Mean Red, GLCM Homogeneity NIR_R (90°), STD Red, Mean NIR_R

GLCM = grey level co-occurrence matrix (a measure of texture)
Max diff – maximum difference of spectral values
STD = standard deviation
0°, 90°, 135° = direction used in GLCM calculation

The outputs of image classification using the object-oriented approach are shown in Figures 6.36 to 6.39). From visual inspection alone, it is evident that the 80-scale parameter produced the highest classification accuracy. From the resulting image, the main strips of various crop types were adequately classified (Figure 6.38). The following major errors were identified from the 80-scale parameter image:

- a few patches of canola were misclassified as barley, green weeds or non-photosynthetic material
- a few patches of barley were misclassified as wheat or canola
- some patches of wheat, particularly those located near the edge of strips, were misclassified as canola

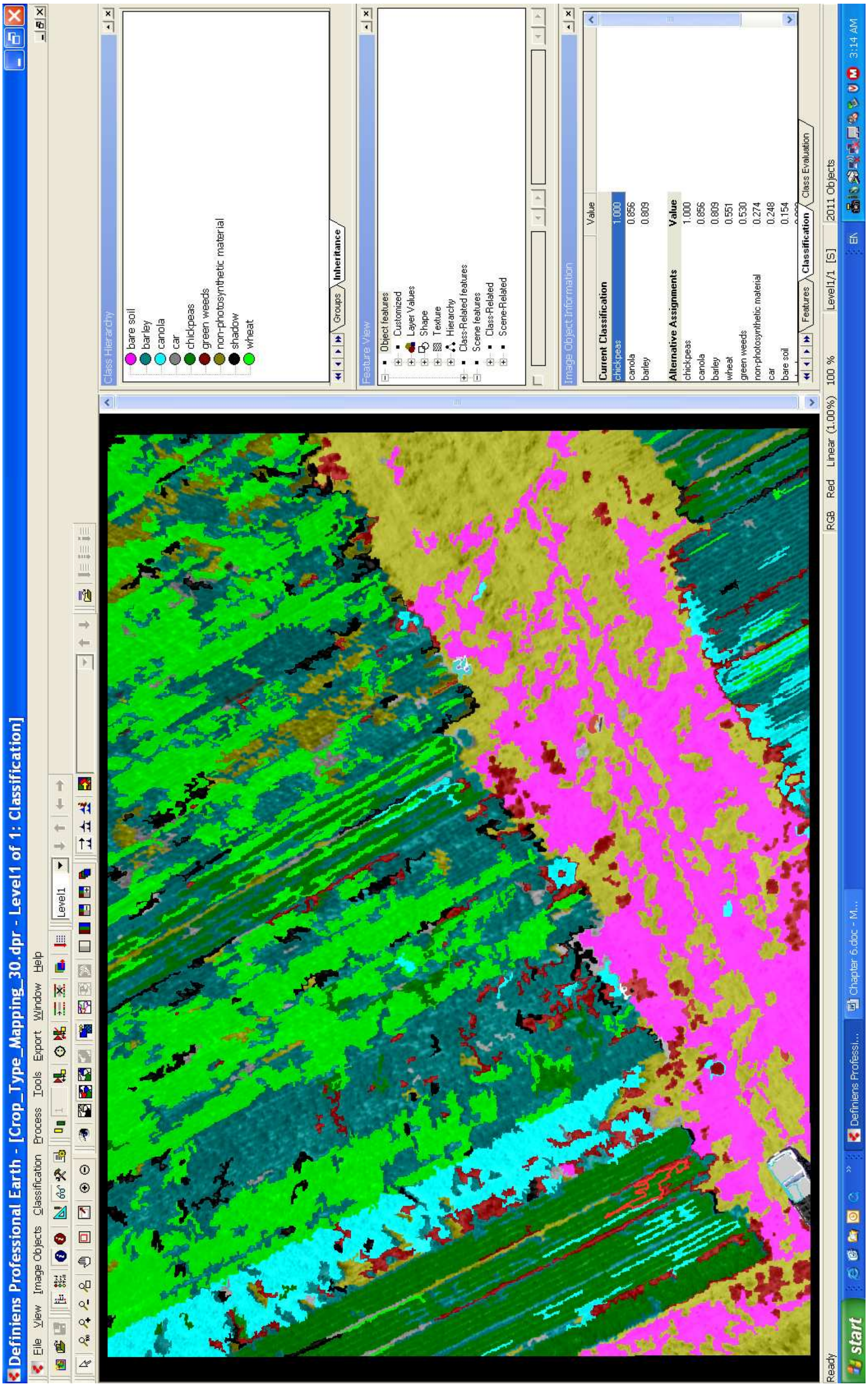

Figure 6.36 Classified image from the 30-scale image segmentation

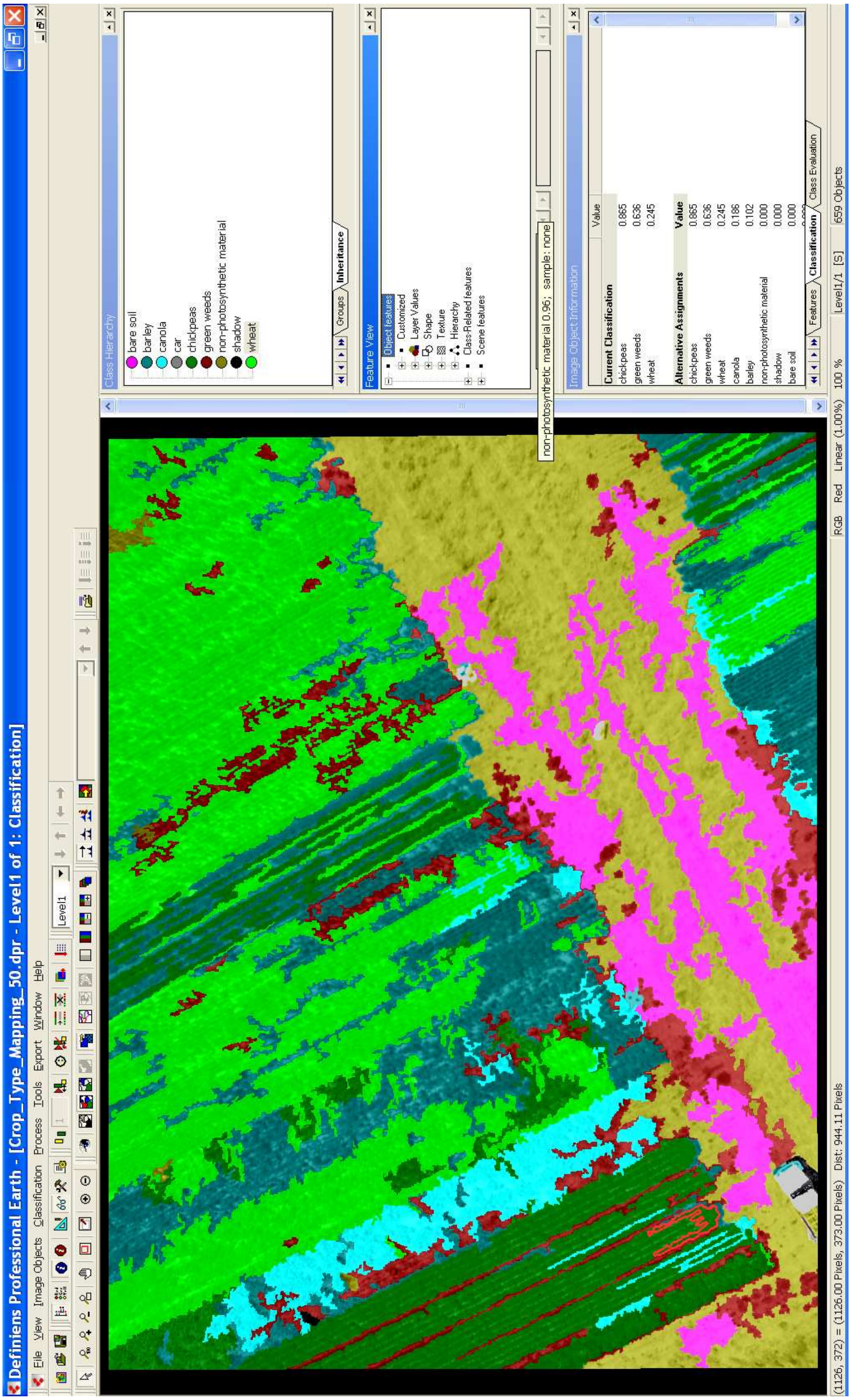

Figure 6.37 Classified image from the 50-scale image segmentation

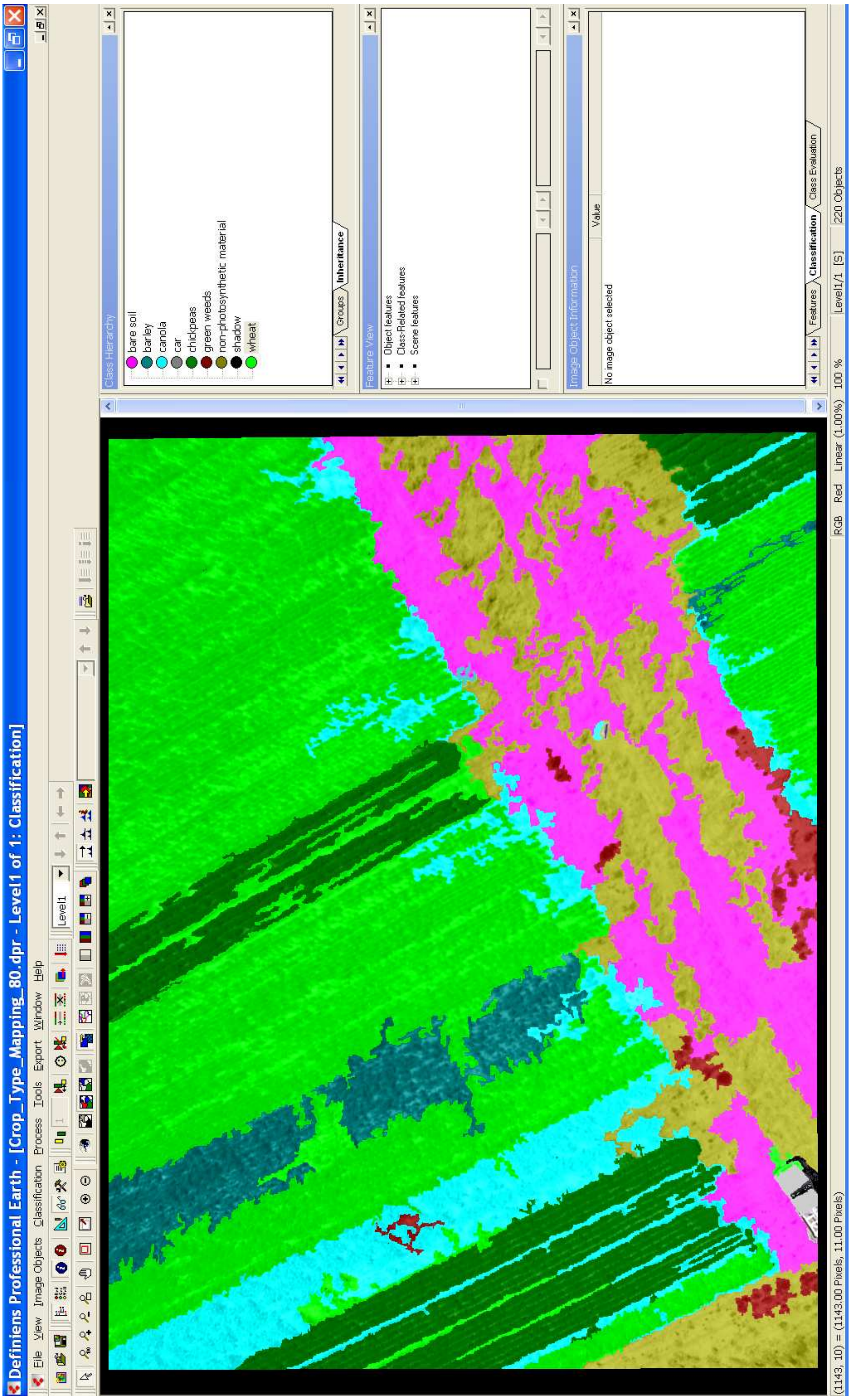

Figure 6.38 Classified image from the 80-scale image segmentation

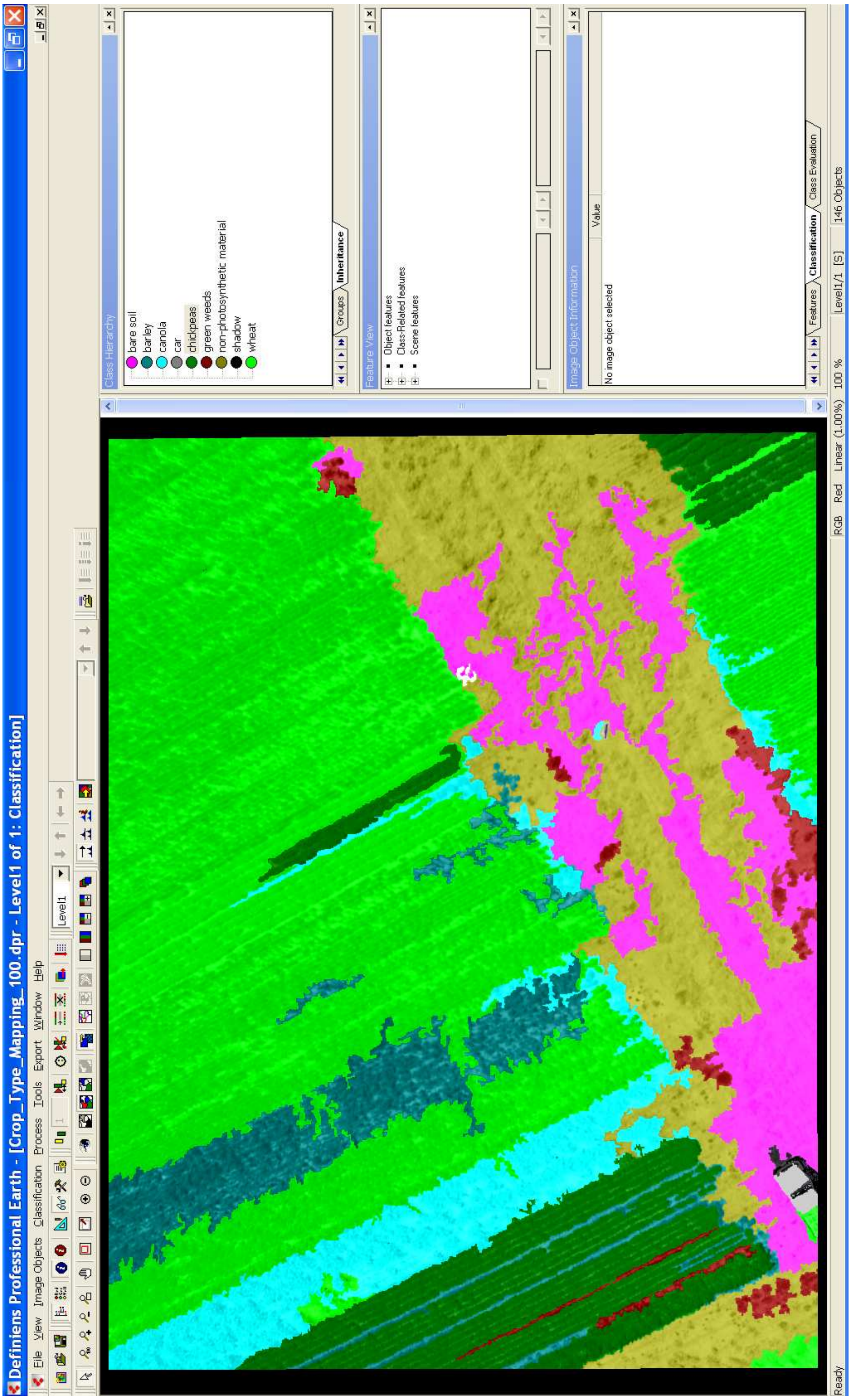

Figure 6.39 Classified image from the 100-scale image segmentation

The accuracy assessment for the object-orientated approach used the same ground-truthing dataset as in the pixel-based analysis. The same analysis methods (% overall accuracy and kappa index) were utilised allowing a directly comparison to be made between the two methods.

The results of accuracy assessment indicated that the 80-scale parameter image produced the highest accuracy (overall accuracy = 81% and kappa index = 0.76) (Table 6.31). This is higher than the result achieved by the pixel-based approach (overall accuracy = 66% and kappa index = 0.61) for the 9-class aggregation (refer to section 6.3.2). This higher accuracy achieved for the object-oriented approach was due to texture-related information (e.g. GLCM) incorporated in the classification decision rule (see Table 6.30). This result agrees with previous studies on the importance of image-based texture in vegetation mapping from high spatial resolution digital imagery (Chubey *et al*. 2006; St-Onge & Cavayas 1997).

Table 6.31. Accuracy of images classified from the object-oriented approach

Scale for Segmentation	**% Overall Accuracy**	**Kappa Index of Agreement**
30 scale	47	0.42
50 scale	67	0.63
80 scale	81	0.76
100 scale	61	0.56

However, it must be noted that not all segmentation parameters achieved better results than the pixel-based method. For instance, the results that deployed 30-scale and 100-scale parameters have produced a lower accuracy (47 % and 61 %, respectively). "Extreme" values for scale parameters did not produce better accuracy, and thus the optimum parameter should be determined through iterative runs. It is apparent that the "best separation distance" (BSD) values generated by the feature space optimisation procedure can be a good guide to consider. The BSD results are consistent with the results of classification accuracy assessment.

6.4 Further Refinements

To further refine the LCLA remote sensing system, acquisitions were made to test the capacity of the system to detect crop maturity at Lundavra in 2005 and to quantify the capacity of an autopilot to control the flight path of a UAV and to initiate image acquisition. The details of these two evaluations were described in Chapter 5.4 and the results will be discussed in this section.

6.4.1 Crop Maturity Mapping

The 79 area-of-interests (AOIs) that were randomly selected from within one replicate of the variety trial were detailed in Chapter 5. These 79 samples corresponded to 14 differing Zadok scale classes, with the histogram of the spread of classes being shown in Figure 6.40. The description of the growth stage associated with the Zadok scale classes is detailed in Table 5.2.

The statistical package SPSS version 12.0 was utilised to perform the DA and was conducted using a stepwise method of entering a variable based on the Wilks' lambda using the observed group sizes to determine the probabilities of group membership.

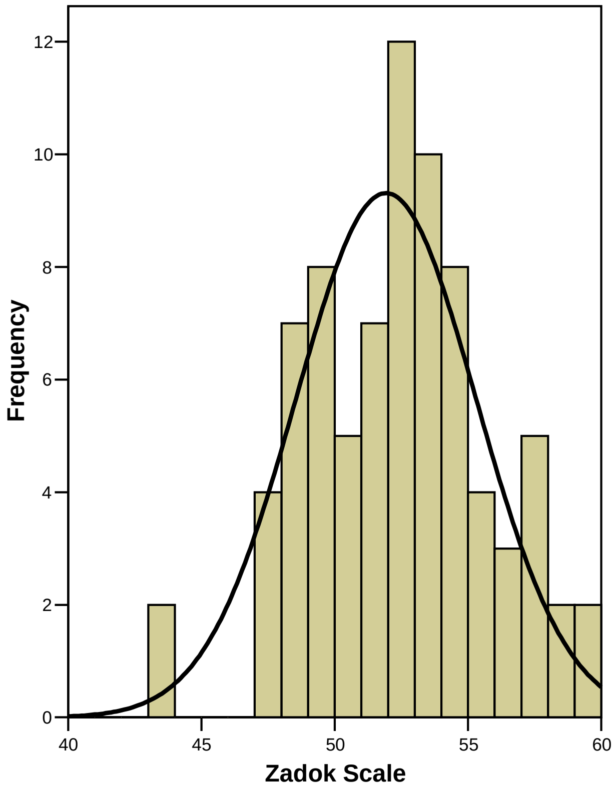

Figure 6.40 The frequency and distribution for the 14 different growth stages.

In the ANOVA table (Table 6.32), the Wilks' Lambda indicated that the colour bands were the most important to the discriminant function, with very little difference between the three. The Wilks' lambda is significant by the F test for all colour bands, but not the NIR.

Table 6.32 Tests of equality of group means

Tests of Equality of Group Means

	Wilks' Lambda	F	df1	df2	Sig.
RED	.526	4.511	13	65	.000
GREEN	.534	4.355	13	65	.000
BLUE	.525	4.530	13	65	.000
NIR	.831	1.017	13	65	.446

The covariance matrix (Table 6.33) indicates a good correlation within the three colour band, but no correlation with the NIR.

Table 6.33 Pooled within-group matrices

Pooled Within-Groups Matrices[a]

		RED	GREEN	BLUE	NIR
Covariance	RED	102.511	76.896	96.894	-2.721
	GREEN	76.896	79.998	91.403	13.383
	BLUE	96.894	91.403	121.002	9.447
	NIR	-2.721	13.383	9.447	25.651
Correlation	RED	1.000	.849	.870	-.053
	GREEN	.849	1.000	.929	.295
	BLUE	.870	.929	1.000	.170
	NIR	-.053	.295	.170	1.000

a. The covariance matrix has 65 degrees of freedom.

In the summary of canonical discriminant functions (Table 6.34), the first function accounts for 100% of the variance and the function is significant.

Table 6.34 Summary of canonical discriminant functions (Eigenvalues top and Wilks' lambda bottom).

Eigenvalues

Function	Eigenvalue	% of Variance	Cumulative %	Canonical Correlation
1	.906[a]	100.0	100.0	.689

a. First 1 canonical discriminant functions were used in the analysis.

Wilks' Lambda

Test of Function(s)	Wilks' Lambda	Chi-square	df	Sig.
1	.525	45.475	13	.000

The structure matrix (Table 6.35) indicates that only the blue band is used in the analysis.

Table 6.35 The structure matrix.

Structure Matrix

	Function
	1
BLUE	1.000
GREEN[a]	.929
RED[a]	.870
NIR[a]	.170

Pooled within-groups correlations between discriminating variables and standardized canonical discriminant functions
Variables ordered by absolute size of correlation within function.

a. This variable not used in the analysis.

The classification results (Table 6.36) indicated that the predictive power is weak, as only 23% of the original grouped classes were correctly classified and only 14% of the cross-validated cases correct. This lack of power was resultant from the large number of original classes. As the classes represent individual growth stages of the crop (Zadoks *et al.* 1974), a difference of one in the Zadok scale can mean as little as an extra leaf unfolded or an extra tiller on the plant.

Due to the large number of classes and the minor difference between each class, classifying into 14 classes was going to be problematic, resulting in the low accuracy of classification.

Table 6.36 The classification results for the 14 Zadoks class study.

Classification Results[b,c]

		ZADOK	Predicted Group Membership 43.0	47.0	48.0	49.0	50.0	51.0	52.0	53.0	54.0	55.0	56.0	57.0	58.0	59.0	Total
Original	Count	43.0	0	1	1	0	0	0	0	0	0	0	0	0	0	0	2
		47.0	0	3	1	0	0	0	0	0	0	0	0	0	0	0	4
		48.0	0	2	1	0	0	0	1	2	0	0	0	1	0	0	7
		49.0	0	0	0	0	0	0	7	1	0	0	0	0	0	0	8
		50.0	0	0	0	0	0	0	4	1	0	0	0	0	0	0	5
		51.0	0	0	2	0	0	0	2	3	0	0	0	0	0	0	7
		52.0	0	0	1	0	0	0	9	1	1	0	0	0	0	0	12
		53.0	0	0	1	0	0	0	7	2	0	0	0	0	0	0	10
		54.0	0	0	1	0	0	0	4	1	0	0	0	1	0	1	8
		55.0	0	0	0	0	0	0	1	1	1	0	0	1	0	0	4
		56.0	0	0	0	0	0	0	1	0	0	0	0	2	0	0	3
		57.0	0	0	0	0	0	0	2	0	1	0	0	2	0	0	5
		58.0	0	0	0	0	0	0	1	1	0	0	0	0	0	0	2
		59.0	0	0	0	0	0	0	1	0	0	0	0	0	0	1	2
	%	43.0	.0	50.0	50.0	.0	.0	.0	.0	.0	.0	.0	.0	.0	.0	.0	100.0
		47.0	.0	75.0	25.0	.0	.0	.0	.0	.0	.0	.0	.0	.0	.0	.0	100.0
		48.0	.0	28.6	14.3	.0	.0	.0	14.3	28.6	.0	.0	.0	14.3	.0	.0	100.0
		49.0	.0	.0	.0	.0	.0	.0	87.5	12.5	.0	.0	.0	.0	.0	.0	100.0
		50.0	.0	.0	.0	.0	.0	.0	80.0	20.0	.0	.0	.0	.0	.0	.0	100.0
		51.0	.0	.0	28.6	.0	.0	.0	28.6	42.9	.0	.0	.0	.0	.0	.0	100.0
		52.0	.0	.0	8.3	.0	.0	.0	75.0	8.3	8.3	.0	.0	.0	.0	.0	100.0
		53.0	.0	.0	10.0	.0	.0	.0	70.0	20.0	.0	.0	.0	.0	.0	.0	100.0
		54.0	.0	.0	12.5	.0	.0	.0	50.0	12.5	.0	.0	.0	12.5	.0	12.5	100.0
		55.0	.0	.0	.0	.0	.0	.0	25.0	25.0	25.0	.0	.0	25.0	.0	.0	100.0
		56.0	.0	.0	.0	.0	.0	.0	33.3	.0	.0	.0	.0	66.7	.0	.0	100.0
		57.0	.0	.0	.0	.0	.0	.0	40.0	.0	20.0	.0	.0	40.0	.0	.0	100.0
		58.0	.0	.0	.0	.0	.0	.0	50.0	50.0	.0	.0	.0	.0	.0	.0	100.0
		59.0	.0	.0	.0	.0	.0	.0	50.0	.0	.0	.0	.0	.0	.0	50.0	100.0

(continued over)

Table 6.36 (continued) The classification results for the 14 Zadoks class study..

Classification Results[b,c]

		ZADOK	Predicted Group Membership 43.0	47.0	48.0	49.0	50.0	51.0	52.0	53.0	54.0	55.0	56.0	57.0	58.0	59.0	Total
Cross-validated[a]	Count	43.0	0	1	1	0	0	0	0	0	0	0	0	0	0	0	2
		47.0	0	3	1	0	0	0	0	0	0	0	0	0	0	0	4
		48.0	0	3	0	0	0	0	1	2	0	0	0	1	0	0	7
		49.0	0	0	0	0	0	0	7	1	0	0	0	0	0	0	8
		50.0	0	0	0	0	0	0	4	1	0	0	0	0	0	0	5
		51.0	0	0	2	0	0	0	2	3	0	0	0	0	0	0	7
		52.0	0	0	0	0	0	0	6	4	2	0	0	0	0	0	12
		53.0	0	0	1	0	0	0	7	2	0	0	0	0	0	0	10
		54.0	0	0	1	0	0	0	4	1	0	0	0	1	0	1	8
		55.0	0	0	0	0	0	0	1	1	1	0	0	1	0	0	4
		56.0	0	0	0	0	0	0	1	0	1	0	0	1	0	0	3
		57.0	0	0	0	0	0	0	2	0	3	0	0	0	0	0	5
		58.0	0	0	0	0	0	0	1	1	0	0	0	0	0	0	2
		59.0	0	0	0	0	0	0	1	0	0	0	0	1	0	0	2
	%	43.0	.0	50.0	50.0	.0	.0	.0	.0	.0	.0	.0	.0	.0	.0	.0	100.0
		47.0	.0	75.0	25.0	.0	.0	.0	.0	.0	.0	.0	.0	.0	.0	.0	100.0
		48.0	.0	42.9	.0	.0	.0	.0	14.3	28.6	.0	.0	.0	14.3	.0	.0	100.0
		49.0	.0	.0	.0	.0	.0	.0	87.5	12.5	.0	.0	.0	.0	.0	.0	100.0
		50.0	.0	.0	.0	.0	.0	.0	80.0	20.0	.0	.0	.0	.0	.0	.0	100.0
		51.0	.0	.0	28.6	.0	.0	.0	28.6	42.9	.0	.0	.0	.0	.0	.0	100.0
		52.0	.0	.0	.0	.0	.0	.0	50.0	33.3	16.7	.0	.0	.0	.0	.0	100.0
		53.0	.0	.0	10.0	.0	.0	.0	70.0	20.0	.0	.0	.0	.0	.0	.0	100.0
		54.0	.0	.0	12.5	.0	.0	.0	50.0	12.5	.0	.0	.0	12.5	.0	12.5	100.0
		55.0	.0	.0	.0	.0	.0	.0	25.0	25.0	25.0	.0	.0	25.0	.0	.0	100.0
		56.0	.0	.0	.0	.0	.0	.0	33.3	.0	33.3	.0	.0	33.3	.0	.0	100.0
		57.0	.0	.0	.0	.0	.0	.0	40.0	.0	60.0	.0	.0	.0	.0	.0	100.0
		58.0	.0	.0	.0	.0	.0	.0	50.0	50.0	.0	.0	.0	.0	.0	.0	100.0
		59.0	.0	.0	.0	.0	.0	.0	50.0	.0	.0	.0	.0	50.0	.0	.0	100.0

a. Cross validation is done only for those cases in the analysis. In cross validation, each case is classified by the functions derived from all cases other than that case.

b. 22.8% of original grouped cases correctly classified.

c. 13.9% of cross-validated grouped cases correctly classified.

As an alternative approach, classes were grouped according to the secondary growth stages of the crop (according to Zadoks *et al.* (1974)). The new classes ('Grouped Zadok') are detailed in Table 6.37 and the frequencies of distribution within these new classes are shown in Figure 6.41.

Table 6.37 The Zadoks range for the grouped secondary growth stages.

Grouped Zadoks	Zadok range	Crop growth stage
1	40-45	Early booting
2	46-49	Late booting
3	50-52	First spikelets visible to <¼ of inflorescence emerged
4	53-54	¼ to <½ of inflorescence emerged
5	55-56	½ to <¾ of inflorescence emerged
6	57-59	¾ of inflorescence emerged to emergence completed

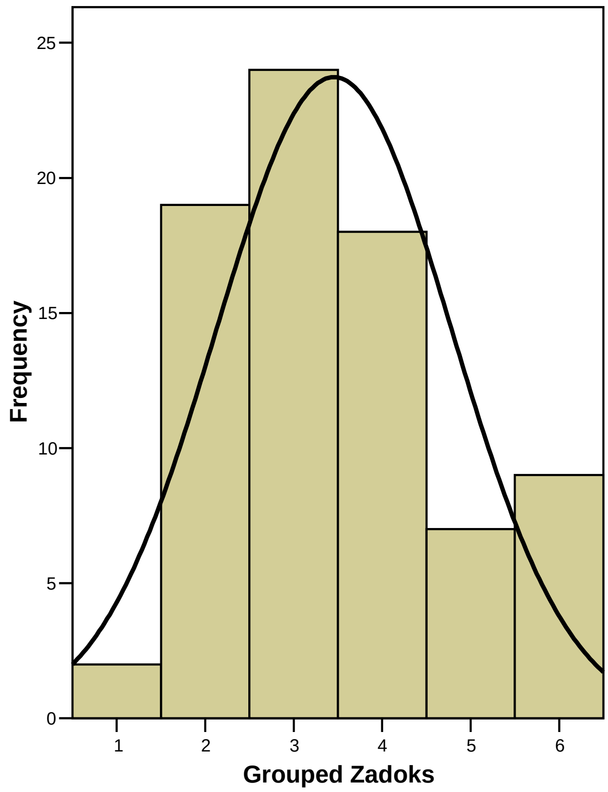

Figure 6.41 The frequency and distribution for the 6 grouped secondary growth stages.

Using the same parameters as the previous case, this classification (see Table 6.38) resulted in an accuracy of 38% of original grouped cases correctly classified, with 34% of cross-validated grouped cases correctly classified. This was an improvement on the previous classification, but the difference between the growth stages of these ‘secondary’ classes was still fine. To further refine the classification, slight variations of the principal plant growth stages (as described by Zadok (1974)), were used to potentially provide a more accurate classification. Details of the principal growth stages are shown in Table 6.39 with a histogram showing the class numbers shown as Figure 6.42.

Table 6.38 The classification accuracy for the grouped secondary growth stages.

Classification Results[b,c]

		Growth Stage	Predicted Group Membership						Total
			1	2	3	4	5	6	
Original	Count	1 Z40-45	1	1	0	0	0	0	2
		2 Z46-49	1	8	9	0	0	1	19
		3 Z50-52	0	3	20	0	0	1	24
		4 Z53-54	0	3	14	0	0	1	18
		5 Z55-56	0	0	6	0	0	1	7
		6 Z57-59	0	0	8	0	0	1	9
	%	1 Z40-45	50.0	50.0	.0	.0	.0	.0	100.0
		2 Z46-49	5.3	42.1	47.4	.0	.0	5.3	100.0
		3 Z50-52	.0	12.5	83.3	.0	.0	4.2	100.0
		4 Z53-54	.0	16.7	77.8	.0	.0	5.6	100.0
		5 Z55-56	.0	.0	85.7	.0	.0	14.3	100.0
		6 Z57-59	.0	.0	88.9	.0	.0	11.1	100.0
Cross-validated[a]	Count	1 Z40-45	0	2	0	0	0	0	2
		2 Z46-49	1	8	8	1	0	1	19
		3 Z50-52	0	4	18	1	0	1	24
		4 Z53-54	0	3	14	0	0	1	18
		5 Z55-56	0	0	6	0	0	1	7
		6 Z57-59	0	0	8	0	0	1	9
	%	1 Z40-45	.0	100.0	.0	.0	.0	.0	100.0
		2 Z46-49	5.3	42.1	42.1	5.3	.0	5.3	100.0
		3 Z50-52	.0	16.7	75.0	4.2	.0	4.2	100.0
		4 Z53-54	.0	16.7	77.8	.0	.0	5.6	100.0
		5 Z55-56	.0	.0	85.7	.0	.0	14.3	100.0
		6 Z57-59	.0	.0	88.9	.0	.0	11.1	100.0

a. Cross validation is done only for those cases in the analysis. In cross validation, each case is classified by the functions derived from all cases other than that case.

b. 38.0% of original grouped cases correctly classified.

c. 34.2% of cross-validated grouped cases correctly classified.

Table 6.39 The Zadoks range of the 3 principal growth stage classes.

Scale	Zadok scale	Crop growth stage
1	40-49	Booting
2	50-54	Early inflorescence emergence
3	55-59	Late inflorescence emergence

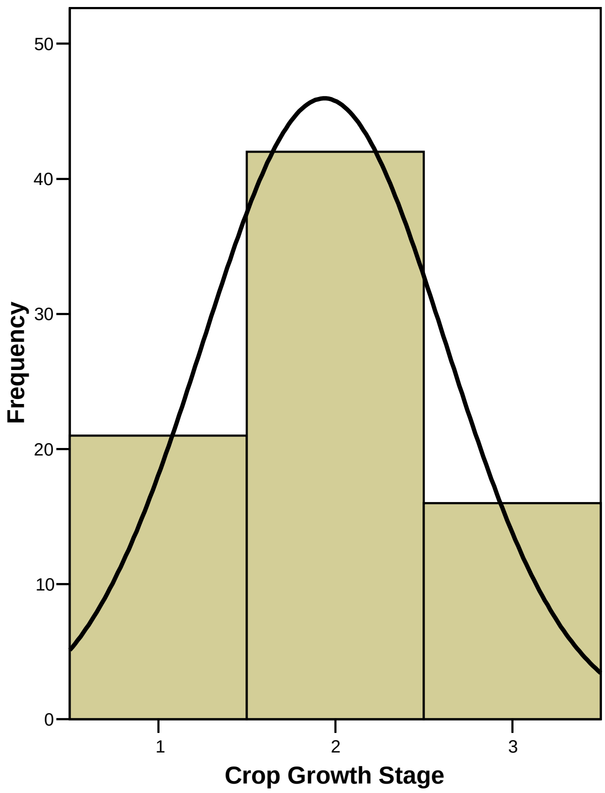

Figure 6.42 The frequency and distribution for the 3 principal growth stage classes.

The classification results for the 3 principal growth stages are shown in Table 6.40. The results are more encouraging with 65% of the original cases classified correctly and 63% of the cross-validated classified correctly. In the booting class (Z40–49) approximately 50% were correctly classified with 50 being classified into both of the emergence classes. The early inflorescence emergence class (Z40–54) has more than 90% correctly classified. In the late inflorescence emergence class, over 90% of the cases were misclassified as early emergence.

Table 6.40 The classification results for the 3 principal growth stages.

Classification Results[b,c]

		Growth Stage	Predicted Group Membership 1	2	3	Total
Original	Count	1 Z40-49	10	10	1	21
		2 Z50-54	2	39	1	42
		3 Z55-59	0	14	2	16
	%	1 Z40-49	47.6	47.6	4.8	100.0
		2 Z50-54	4.8	92.9	2.4	100.0
		3 Z55-59	.0	87.5	12.5	100.0
Cross-validated[a]	Count	1 Z40-49	10	10	1	21
		2 Z50-54	2	39	1	42
		3 Z55-59	0	15	1	16
	%	1 Z40-49	47.6	47.6	4.8	100.0
		2 Z50-54	4.8	92.9	2.4	100.0
		3 Z55-59	.0	93.8	6.3	100.0

a. Cross validation is done only for those cases in the analysis. In cross validation, each case is classified by the functions derived from all cases other than that case.

b. 64.6% of original grouped cases correctly classified.

c. 63.3% of cross-validated grouped cases correctly classified.

To further refine the classification, two classes were attempted based on the primary growth stages: booting (Z40–49) and emergence (Z50–59). The classification results for these classes are shown in Table 6.41.

Table 6.41 The classification results for the primary growth stages.

Classification Results[b,c]

		Primary growth stage	Predicted Group Membership 1	2	Total
Original	Count	1 Z40-49	10	11	21
		2 Z50-59	2	56	58
	%	1 Z40-49	47.6	52.4	100.0
		2 Z50-59	3.4	96.6	100.0
Cross-validated[a]	Count	1 Z40-49	10	11	21
		2 Z50-59	2	56	58
	%	1 Z40-49	47.6	52.4	100.0
		2 Z50-59	3.4	96.6	100.0

a. Cross validation is done only for those cases in the analysis. In cross validation, each case is classified by the functions derived from all cases other than that case.

b. 83.5% of original grouped cases correctly classified.

c. 83.5% of cross-validated grouped cases correctly classified.

The classification results for the classes based on the primary growth stages of the crop is quite acceptable, especially considering that the image was taken over a month after the growth stages were recorded. The varieties of the trial that were not as advanced when the growth stages were recorded have continued to remain behind the more advanced varieties, with this being indicated by the cases correctly classified. Greater differentiation may have been possible had the duration between the growth stages assessment and the image acquisition been minimised.

6.4.2 Autopilot Evaluation

A flight path of the three successful missions is shown in Figure 6.43. Two circuits were completed on both flights one and three, with three circuits being made on flight four. Each dot in the circuit represents the latitude and longitude of the path taken by the UAV that was recorded in the flight log, which was updated with GPS co-ordinates once per second. The activity around the target area and the reduced distance between consecutive dots in this area indicates that this was the takeoff and landing zone. The flight path is superimposed over a Spot 5 satellite image showing the infrastructure of the Watts Bridge Memorial Airfield and other natural features in the close proximity. Also displayed are the waypoints used in determining the flight path and the location of the target, over which the images were captured.

An example of two of the images captured on flight four are shown in Figures 6.44 and 6.45. These images were taken on the last circuits made by the UAV on the day. Even though the images were acquired a little over three minutes apart, there is good consistency in the coverage and positioning of the target within both images. Ideally, if the autopilot was doing a perfect job guiding the UAV, the target should be in the centre of the image. As can be seen from Figures 6.44 and 6.45, this was not quite the case.

The target and waypoints were arranged so that the UAV should in theory fly directly down the centre of the mowed grass runway that ran NE–SW in Figure 6.43. This should have resulted in the runway being positioned vertically in the centre of each image acquired. This was not the case. The misalignment was possibly due to a combination of cross-wind, GPS / autopilot error, the UAV not being level when the image was acquired, and / or inaccuracies in positioning the LCLA sensors in the hinged pod. These difficulties were not part of this research as they had no direct relevance to crop assessment, and were beyond the scope of this work.

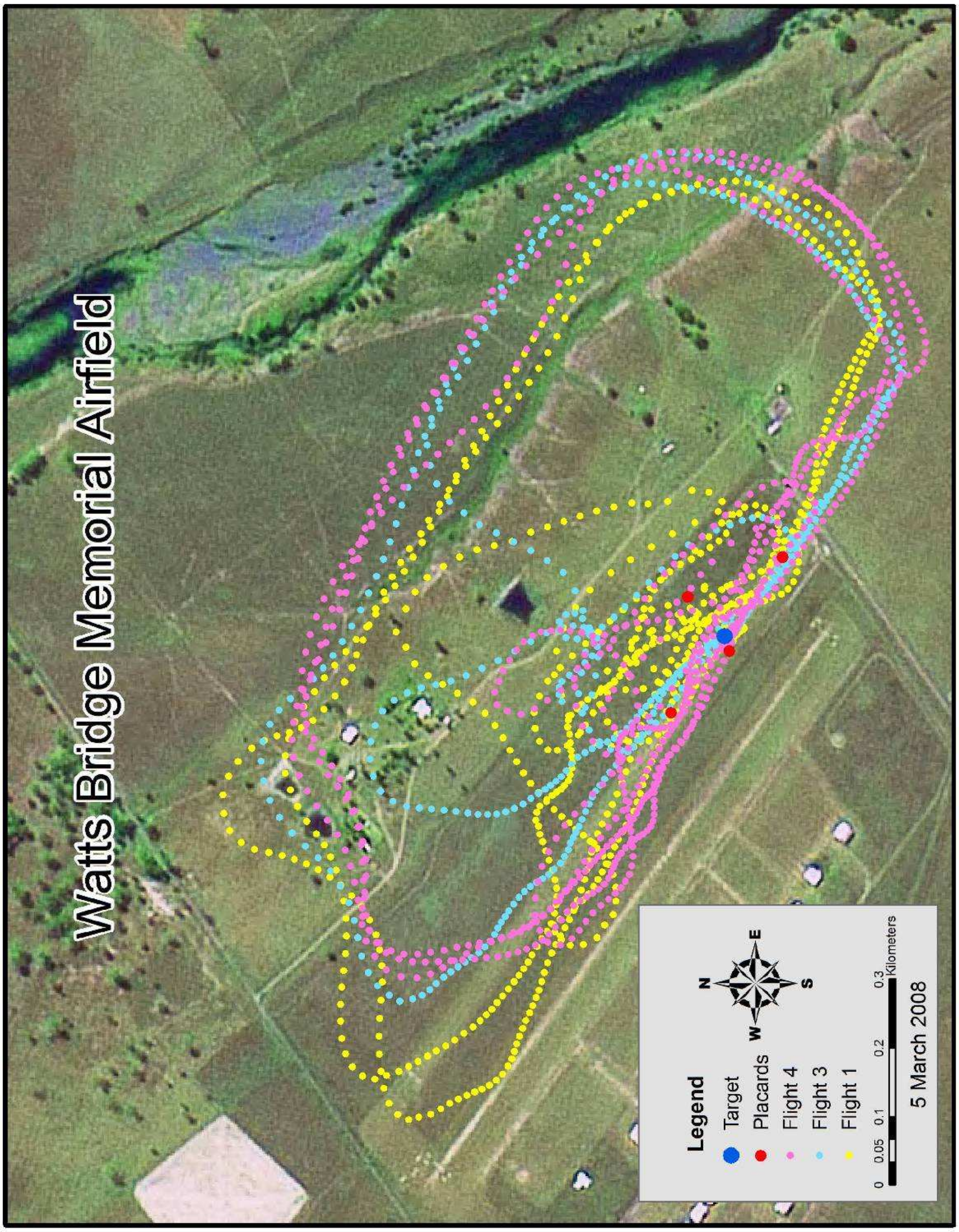

Figure 6.43 The flight paths and target positioning, Watts Bridge on 5 March 2008.

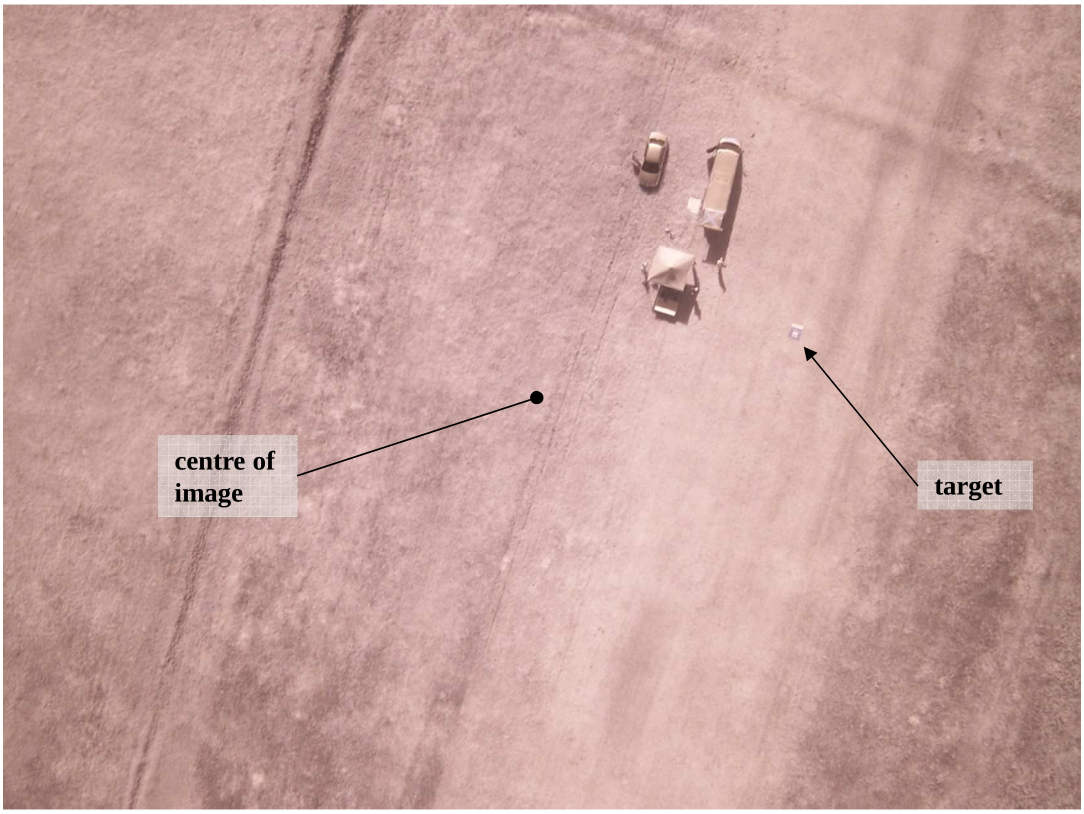

Figure 6.44 Image 100_4814 taken at 3:27:44 pm.

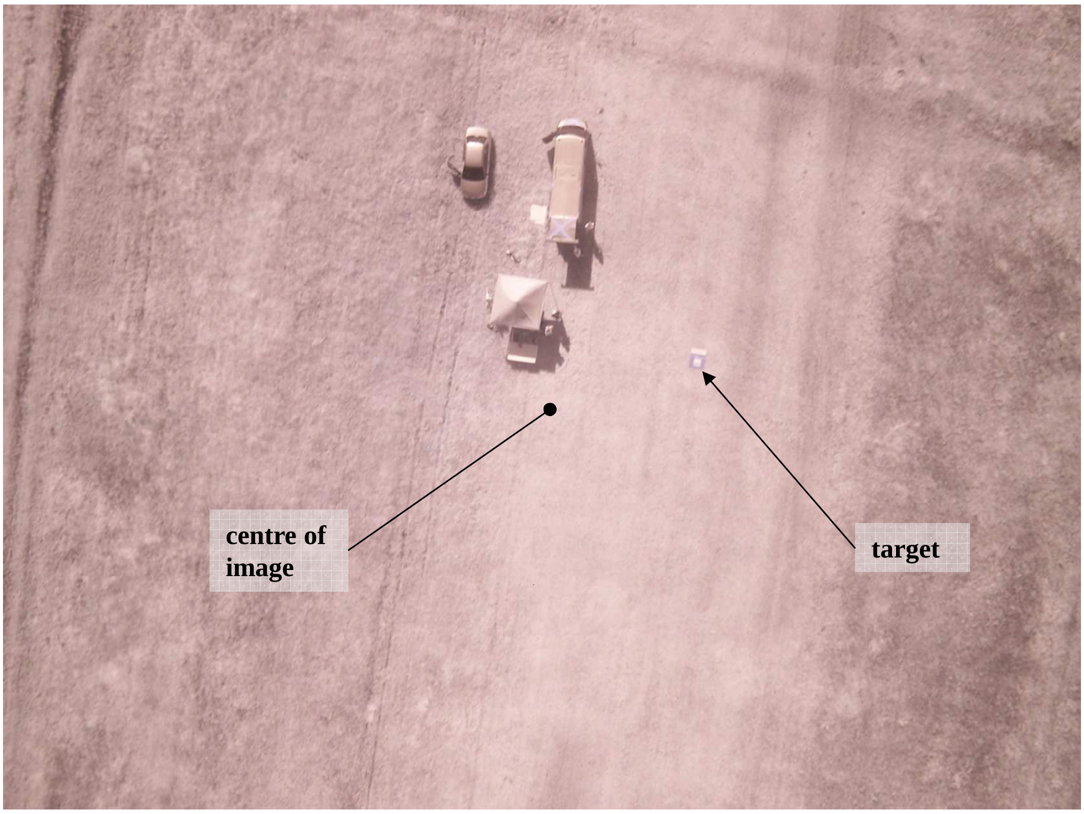

Figure 6.45 Image 100_4815 taken just over 3min after image 100_4814 (shown in Figure 6.44).

Analysis

Details of the various images captured during the flights undertaken are shown in Table 6.42. The inaccuracies in the image acquisition were quantified and detailed in this table. The scale of the images were determined using GPS co-ordinates of known features and the distanced measured from the images. The direction of flight of the UAV was from the top of the image to the bottom. In the image offset column in Table 6.42, the X distance is the cross-track distance with a positive value indicating that it is to the left and negative to the right of the centre of the image. The offset in the direction of flight (undershoot or overshoot) is indicated by the Y column with a positive value indicating that the image was captured before the centre of the image with a negative value indicating after capture. The absolute is the direct distance from the centre of the image to the centre of the target.

Table 6.42 Details of the errors for the images acquired over the target.

	Image #	Time	Altitude (m)	Heading (degrees)	Image Offset X (m)	Image Offset Y (m)	Image Offset absolute	Image Extent X (m)	Image Extent Y (m)	Area (ha)
Flight 1										
	100_4801	1:32:06	157	150	50.4	8.3	51.1	140.4	104.0	1.46
	100_4803	1:35:26			83.7	17.8	85.6	133.4	98.8	1.32
	100_4805	1:38:32			59.6	10.2	60.5	137.4	101.8	1.40
Flight 2										
	100_4806	2:36:10								
Flight 3										
	100_4809	2:57:24	112	146	17.2	-1.9	17.3	103.0	76.3	0.79
	100_4810	3:00:42	104	132	19.1	0.3	19.1	92.2	68.3	0.63
Flight 4										
	100_4812	3:21:48	117	113	39.5	6	40.0	108.7	80.5	0.88
	100_4813	3:24:46			38.2	26.6	46.5	92.0	68.2	0.63
	100_4814	3:27:44	98	114	-19.3	14.1	23.9	100.4	74.4	0.75
	100_4815	3:30:50	72	125	-9.6	4.9	10.8	73.9	54.7	0.40

Capturing the target in the image was achieved on every flight. However, capturing the target in the middle of the image was not as repeatable with the error ranging from just under 15% of the image width (the final image on flight four) to just over 60% of the image width (the second image of flight two).

The capacity to accurately acquire images over pre-determined points is essential to ensure coverage and to expedite mosaicing of the images. It will also expand the application of these technologies into the broader-scale applications, such as imaging in broadacre cereal cropping or imaging along transects (such a river systems etc.).

Also detailed in Table 6.42 are the differing altitudes that were programmed for each of the flight. The first flight was undertaken at 150 m above ground level, with the third at 110 m. The final flight was slightly different. The first image was acquired at the set altitude of 120 m. The three circuits that followed were flown at this same height (120m); however the images were acquired at lower altitudes (100 m for images two and three and 75 m for the final image). These image acquisition heights were changed in-flight with the intention of observing the response of the UAV to changes of the flight schedule. An altitude plot of flight 4 is shown in Figure 6.46.

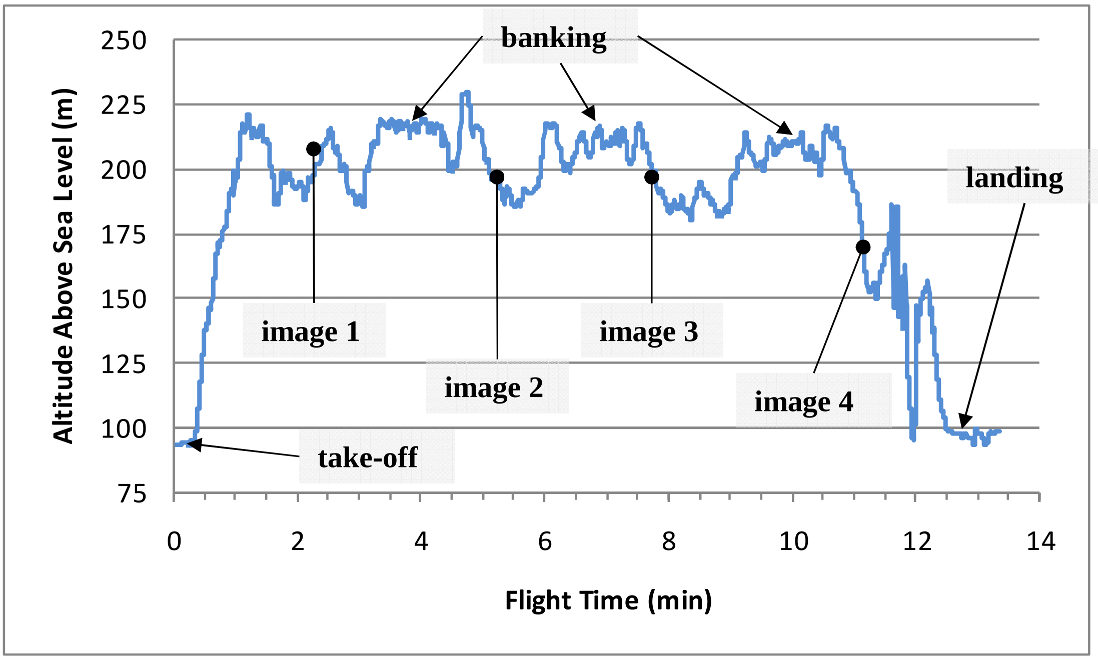

Figure 6.46 Altitude details for flight 4 (note the UAV reduced altitude to acquire images).

Figure 6.46 shows the relatively steep climb of the UAV after take-off. Also evident is the loss of altitude, and then correction, due to the banking of the aircraft when manoeuvring to align to the next waypoint. The saw-toothed nature of the plot, due to the banking, indicates that the feedback loops to the autopilot to control the flight surfaces are not finely tuned enough to optimise performance and ensure stable flight.

This study documents the accuracy of an autopiloted UAV to fly on a predetermined path and capture images, something that has not been published in the literature (excluding confidential military documents). For the use of this system to be expanded in the ‘real world,’ these limitations would have to be overcome. However, this study provides proof-of-concept that autopiloted UAV can fly on a predetermined path and take images. This autonomous system has the potential to be a highly suitable platform, but needs further development.

6.5 Synthesis of Findings

The ability of a low-cost low-altitude remote sensing system to detect variations in a growing crop has been documented by the research detailed in this thesis. The system, which started as surveillance video cameras on a hobbyist remotely controlled aircraft, provided proof-of-concept. The development of the system has progressed into a dual 1.0 megapixel digital camera system suspended beneath a helium balloon. This configuration found application in many and varied circumstances: predicting yield and protein, discriminating crop types, quantifying hail damage, detailing wet areas in cattle feedlots, spatially referencing pineapples, to assessing turf health in football stadium. Using dual 5 megapixel cameras found enhanced application in assessing crop maturity, quantifying lettuce growth rates and also as a measure of autopilot accuracy.

The system developed in this research is ideal where the entire area-of-interest or investigation can be captured in only a few images, as the system does not have the capacity to allow automatic registering and mosaicing of the acquired images. This however, may become a possibility with the further development of the autopiloted UAV remote sensing system.

6.5.1 Sensor

This research offers proof-of-concept that digital cameras can provide relatively cheap and useful data layers that are highly correlated with plant features, such as at-harvest parameters (yield and protein) and crop maturity, as well as to discriminate between different crop types.

6.5.2 Platform

Several differing platforms were utilised during this research with each having a particular niche. For trial sites, the balloon is the ideal platform as it is stable and can acquire many images in a short period of time over the same target. It is also very easy to alter the pixel resolution of the image by altering the acquisition height. However, the utility of the system to broader-scale applications is limited. An autonomous UAV (the final platform tested) holds great promise for extensive use as an LCLA remote sensing platform in broadacre agriculture. A 10 m mast system was also found useful for repeated weekly acquisitions in horticultural crops, but lacked application with cereal cropping.

6.6 Conclusions

Low-cost low-altitude remote sensing system can predict the yield and protein of a wheat crop with a single image acquired at flowering, and established relationships that equalled or were better than any other reported relationships in the literature. The excellent ability of this system to differentiate nutritional status of a growing crop was also demonstrated.

Statistical methods used to evaluate the potential of the system to differentiate between species of cereal crops showed an accuracy of 86%. Traditional image analysis methods (per-pixel approach) performed well (66% accuracy), but the capacity of object-orientated analysis to take into consideration other non-spectral information (e.g. texture and other spatial considerations) greatly increased the accuracy to 81%.

The capacity of the system to assess crop maturity was demonstrated by the accuracy of determining the primary growth stages of a barley crop, with 84% of the cases correctly classified. Further research is needed to fully investigate the potential.

Finally, preliminary testing of an autonomous UAV, where the autopilot controlled the flightpath and the image acquisition, demonstrated the feasibility of using such a system as an imaging platform. With the addition of other sensors, this system has great potential to be utilised in broader agricultural applications.

Chapter 7

Conclusions and Recommendations

7.1 Introduction

This study dealt with spectral discrimination, mapping and monitoring variations in agricultural crops. Its primary aim was to develop and evaluate a low-cost low-altitude (LCLA) remote sensing system that can be applied in precision agriculture. There were three specific objectives detailed in Chapter 1.3 that were addressed in Chapters 3 through 6, to meet this research goal. This last chapter presents a summary of the major findings of this research, and offers conclusions and recommendations for future research.

7.2 Summary of Findings

This study has provided new knowledge and insights on the use of off-the-shelf consumer technologies and a low-cost platform, as a remote sensing system, that has the ability to provide information for use in agriculture. It yields fresh information on how a low-cost low altitude remote sensing system can be applied to discriminate, map and monitor agricultural crops, with a spatial resolution that had not been possible with conventional remotely sensed imagery.

Chapter 3 scoped the technologies that had potential to be incorporated into a low-cost low-altitude remote sensing system. The range of imaging techniques that can be utilised as a sensor in the system was also investigated. Also investigated were various methods of mobilising the sensor that enabled the capture of images over a target area. The major findings are as follows:

- Video cameras, with their low resolution, provided useful images for positioning the sensing system over the target.
- Low-end 1.0 megapixel digital cameras are capable of capturing suitable colour images, generally without blur, when mounted under a remotely controlled aircraft.
- Removing the NIR blocking filter increased the digital camera's sensitivity to near-infrared light. This provided much higher shutter speed that overcome the blurring hurdles.
- Hobbyist remotely controlled aircraft provided a reliable and stable platform that had sufficient additional payload capacity to carry the dual camera sensor.
- The dual camera sensor could be successfully triggered using standard radio control equipment, without interfering with the UAV operations.

In ***Chapter 4***, the development of the low-cost low-altitude remote sensing system was detailed. The following are the major findings:

- A dual digital camera sensor system is capable of and was used to capture colour and near infrared images simultaneously. The sensor could be externally powered and remotely triggered.
- A 1.7 m diameter helium balloon has sufficient lift for the 2-camera system of about 1.0 kg. Sensor movement on the balloon platform can be overcome by a stabilising bar and dual tether-lines.
- The 2-camera system possessed sufficient spatial resolution to record very fine detail (6 cm pixel resolution) from a moving platform.

The methods used in evaluating the low-cost low-altitude remote sensing system to map cereal grain attributes are described in ***Chapter 5.*** Several different types of platforms were developed and evaluated during this work and have met all the needs of the desired applications. The notable findings are:

- Helium balloons provided a relatively inexpensive and easy-to-set-up and deploy platform that could be constrained to acquire imagery at various altitudes. This type of platform was particularly useful where the site was accessible and the area to be imaged is relatively small. The skill level to deploy this platform was low.
- Hobbyist remotely controlled aircraft provided the solution for broader scale imagery requirements. The initial purchase cost was higher (still within the targeted capital cost of AUD$2000 for platform and sensor), however the running costs were lower than the He balloon platform. The skill level to deploy this platform was considerably greater than the He balloon, but not beyond the average remote control hobbyist or for an agronomist to learn.
- Sensors installed atop a 10 m mast were only suitable to acquire repeated (weekly) images of specific small trial plots, with little application to broader scale agriculture.
- The updated 5.0 megapixel 2-cameras sensor provided the same functionality as the previous 1.0 megapixel 2-camera sensor but with better resolution that allowed finer detailed to be viewed, or larger areas to be imaged.
- The capacity of an autonomous unmanned aerial vehicle (UAV) to fly a set path and trigger the 2-camera sensor over a predetermined location was demonstrated. Although exceeding the cost constraints detailed earlier, the system showed considerable utility and development potential, especially for broadacre applications.

The analysis of the collected data resulted in the following major findings:

- The relationships derived for yield (R^2=0.90) from a single date acquisition was equal to, or exceeded all other studies reported in the literature.
- The relationship developed with grain protein (R^2=0.66) was comparable to other more sophisticated studies involving multiple acquisitions, complex sensors and crop modelling. As a one-off acquisition system, the relationship established using the LCLA gave superior results compared to all other reported studies.
- The LCLA system developed in this study proved to be very effective at discriminating between different species of cereal crops. Performing traditional statistical methods (per-pixel approach) on the images acquired by the low-cost low-altitude system enabled species to be clearly distinguished (with an accuracy of 66%) in a cereal crop trial. Additional rigour was added to the crop-type discrimination ability by the incorporation of textural considerations into the object-based image classification (81% accuracy).
- A crop maturity investigation was undertaken and showed great promise (an accuracy of 84%) when predicting primary growth stages of a cereal crop. Further investigations are needed to refine the method due to timing issues with the collection of the datasets.

7.3 Conclusions

This research proved the hypothesis that "*An off-the-shelf consumer camera technologies and low-cost low-altitude platforms can provide selected sets of information appropriate for use in precision agriculture*"

The system successfully acquired images that enabled relationships to be determined between imagery and the following cereal crop parameters: a) yield, b) protein, c) crop-type, and d) growth stage. The relationships derived for yield from a single date acquisition was equal too, or exceeded all other studies reported in the literature.

The relationship developed with protein was comparable to other more sophisticated studies involving multiple acquisitions, complex sensors and crop modelling. As a one-off acquisition, the relationship exceeds all other reported studies.

The LCLA system developed in this study proved to be very effective at discriminating between different species of cereal crops. Performing the traditional per-pixel approach on the images acquired by the low-cost low-altitude system enabled species to be clearly distinguished in a cereal crop trial. However, the use of texture-related information, through the object-based approach, produced better classification accuracy results. Similarly, the study on crop maturity discrimination using the spectral data obtained by the LCLA system showed great promise, particularly when a range of growth stages was evident. However, further investigations are needed to refine the method due to timing issues with the collection of the datasets.

Several different types of platforms were used during this work with all meeting the needs for the purpose to which they were applied. Helium balloons were relatively easy to set up and deploy but could be constrained to acquire imagery at various altitudes. However, this type of platform was particularly useful when the site was accessible and the area to be imaged is relatively small. The sensors were also installed atop a 10 m mast that was utilised to acquire repeated (weekly) images of specific small trial plots in a horticultural application. For broader scale imagery requirements, and for the ability to image areas that are not readily accessible, the hobbyist remotely controlled plane and the sophisticated autonomous unmanned aerial vehicle were the platforms of choice.

The LCLA remote sensing system is a simple and inexpensive system to set up that is relatively easy-to-deploy with low on-going operational cost. It has shown great utility for agricultural applications.

7.4 Recommendations for Future Work

Image extent is constrained by the altitude of the low-cost low-altitude remote sensing system. The higher the platform, the greater the extent but the lower the ground pixel resolution. The helium balloon has to be physically moved over the area of interest, so areas larger than several hectares are difficult to image. The UAV is limited by the ability of the operator to take-off and land, and to position it above the target area. Additionally, it was constrained to line-of-sight flight. The majority of these constraints were removed in early 2008 when tests were performed on an autonomous unmanned aerial vehicle (UAV) using the autopilot to trigger the low-cost low-altitude sensor when at predetermined locations. An operator was still required for take-off and landing, but the autopilot had the capacity to control the UAV beyond the conventional line-of-sight range. The testing proved the capacity of the system to be used as a platform that has applications to broader scale agriculture. However, incorporating additional instrumentation and refining the autopilot system will be necessary before the full potential of this system can be realised.

From an agricultural perspective, the degree of variation that can be managed is relatively coarse. A farmer is not going to modify management decisions for a 5–10% change in a particular variable being considered (e.g. yield, protein, maturity, fertiliser requirement). Due to the scale being considered, no attempt was made to compensate for vignetting or to perform other radiometric corrections on the images that were acquired. Should the detection of finer increments of change, or change over time be the focus of the investigation, then these issues will need to be addressed.

References

ABARE 2006, *Australian Grains 06.1*, Australian Bureau of Agriculture and Resource Economics, viewed 16 August 2008, <http://www.abareconomics.com/publications_html/crops/crops_06/ag06_april.pdf>.

Aber, JS, Zupancic, J & Aber, SW 2003, 'Applications of Kite Aerial Photography: Golf Course Management', *Transactions of the Kansas Academy of Science*, vol. 106, no. 3/4, pp. 211-4.

Algerbo, PA & Thylén, L 1998, 'Variable nitrogen application: effects on crop yield and quality.' paper presented to Proceedings of the Fourth International Conference on Precision Agriculture, American Society of Agronomy, Madison USA, 19-22 July 1998.

Allan, JA 1982, 'Remote sensing techniques for monitoring and managing irrigated lands', *Advances in Space Research*, vol. 2, no. 8, pp. 131-4.

Apan, A, Held, A, Phinn, S & Markley, J 2004, 'Detecting sugarcane "orange rust" disease using EO-1 Hyperion hyperspectral imagery', *International Journal of Remote Sensing*, vol. 25, no. 2, pp. 489-98.

Apan, A, Jensen, T, Kelly, R, Strong, W, Butler, D & Basnet, B 2002, 'Spectral Discrimination and Separability Analysis of Agricultural Crops, Soil and Related Land Cover Types Using ASTER Imagery', paper presented to The 11th Australasian Remote Sensing and Photogrammetry Association Conference, Brisbane, Australia, 2-6 August 2002.

Apan, A, Kelly, R, Phinn, S, Strong, W, Lester, D, Butler, D & Robson, A 2006, 'Predicting grain protein content in wheat using hyperspectral sensing of in-season crop canopies and partial least squares regression', *International Journal of Geoinformatics*, vol. 2, no. 1, pp. 93-108.

Asner, GP, Wessman, CA, Bateson, CA & Privette, JL 2000, 'Impact of Tissue, Canopy, and Landscape Factors on the Hyperspectral Reflectance Variability of Arid Ecosystems', *Remote Sensing of Environment*, vol. 74, no. 1, pp. 69-84.

Atkinson, PM & Curran, PJ 1997, 'Choosing an appropriate spatial resolution for remote sensing investigations', *Photogrammetric Engineering and Remote Sensing*, vol. 63, no. 12, pp. 1345-51.

Baker, AKM, Fitzpatrick, RW & Koehne, SR 2004, 'High resolution low altitude aerial photography for recording temporal changes in dynamic surficial environments', in IC Roach (ed.), *Regolith 2004.*, CRC LEME, pp. 21-5.

Baron, RJ, Crowe, TG & Wolf, TM 2002, 'Dual Camera Measurement of Crop Canopy Using Reflectance', paper presented to AIC 2002 Meeting CSAE/SCGR Program, Saskatoon, Canada, 2002.

Basnet, B, Apan, A, Kelly, R, Jensen, T, Strong , W & Butler, D 2003, 'Relating Satellite Imagery with Grain Protein Content', paper presented to Spatial Science 2003, Canberra, Australia, 22 – 27 September 2003.

Beavers, RL, Hammermeister, AM, Frick, B, Astatkie, T & Martin, RC 2008, 'Spring wheat yield response to variable seeding rates in organic farming systems at different fertility regimes', *Canadian Journal of Plant Science*, vol. 88, no. 1, pp. 43-52.

Bhanu, B, Symosek, P & Das, S 1997, 'Analysis of terrain using multispectral images', *Pattern Recognition*, vol. 30, no. 2, pp. 197-215.

Blackmer, TM, Schepers, JS, Varvel, GE & Meyer, GE 1996, 'Analysis of aerial photography for nitrogen stress within corn fields', *Agronomy Journal*, vol. 88, no. 5, pp. 729-33.

Blackmore, S, Godwin, RJ & Fountas, S 2003, 'The Analysis of Spatial and Temporal Trends in Yield Map Data over Six Years', *Biosystems Engineering*, vol. 84, no. 4, pp. 455-66.

Blaschke, T, Lang, S, Lorup, E, Strobl, J & Zeil, P 2000, 'Object-oriented image processing in an integrated GIS/remote sensing environment and perspectives for environmental applications', in A Cremers & K Greve (eds), *Environmental Information for Planning, Politics and the Public*, Metropolis Verlag, Marburg, vol. 2, pp. 555–70.

Boegh, E, Soegaard, H, Broge, N, Hasager, CB, Jensen, NO, Schelde, K & Thomsen, A 2002, 'Airborne multispectral data for quantifying leaf area index, nitrogen concentration, and photosynthetic efficiency in agriculture', *Remote Sensing of Environment*, vol. 81, no. 2-3, pp. 179-93.

Boike, J & Yoshikawa, K 2003, 'Mapping of periglacial geomorphology using kite/balloon aerial photography', *Permafrost and Periglacial Processes*, vol. 14, no. 1, pp. 81-5.

BOM 2008, *Dalby climate statistics*, Bureau of Meteorology, 5 May 2008 <http://www.bom.gov.au/climate/averages/tables/cw_041023.shtml>.

Borgelt, SC & Sudduth, KA 1992, 'Grain flow monitoring for in-field yield mapping.' paper presented to 1992 International Summer Meeting, American Society of Agricultural Engineers, Charlotte, USA, 21-24 June 1992.

Brivio, PA, Pepe, M & Tomasoni, R 2000, 'Multispectral and multiscale remote sensing data for archaeological prospecting in an alpine alluvial plain', *Journal of Cultural Heritage*, vol. 1, no. 2, pp. 155-64.

Brooner, WG & Simonett, DS 1971, 'Crop discrimination with color infrared photography: A study in Douglas County, Kansas', *Remote Sensing of Environment*, vol. 2, pp. 21-35.

CAMO 2004, *Unscrambler 9.1*, 9.1 edn, CAMO Process AS, Oslo.

Campbell, JB 2002, *Introduction to Remote Sensing*, Third edn, Taylor and Francis, London.

CASA 2003, *Civil Aviation Safety Regulations 1998 (CASR) - PART 101 - Unmanned aircraft and rocket*, Civil Aviation Safety Authority, viewed 20 August 2008, <http://www.casa.gov.au/rules/1998casr/101/101casr.pdf>.

Chapman, L 2007, 'Potential applications of near infra-red hemispherical imagery in forest environments', *Agricultural and Forest Meteorology*, vol. 143, no. 1-2, pp. 151-6.

Chen, JM, Pavlic, G, Brown, L, Cihlar, J, Leblanc, SG, White, HP, Hall, RJ, Peddle, DR, King, DJ & Trofymow, JA 2002, 'Derivation and validation of Canada-wide coarse-resolution leaf area index maps using high-resolution satellite imagery and ground measurements', *Remote Sensing of Environment*, vol. 80, no. 1, pp. 165-84.

Chubey, MS, Franklin, SE & Wulder, MA 2006, 'Object-based analysis of ikonos-2 imagery for extraction of forest inventory parameters', *Photogrammetric Engineering and Remote Sensing*, vol. 72, no. 4, pp. 383-94.

Clark, RL & McGuckin, RL 1996, 'Variable rate application technology: an overview', paper presented to Precision Agriculture - Proceedings of the 3rd International Conference, ASA/CSSA/SSSA, Minneapolis, USA, 23-26 June 1996.

Clevers, JGPW 1988, 'Multispectral aerial photography as a new method in agricultural field trial analysis', *International Journal of Remote Sensing*, vol. 9, no. 2, pp. 319-32.

Cohen, J 1960, 'A coefficient of agreement for nominal scales', *Educational and Psychological Measurement*, vol. 20, pp. 37-46.

Congalton, RG 1991, 'A review of assessing the accuracy of classifications of remotely sensed data', *Remote Sensing of Environment*, vol. 37, no. 1, pp. 35-46.

Cook, CG, Escobar, DE, Everitt, JH, Cavazos, I, Robinson, AF & Davis, MR 1999, 'Utilizing airborne video imagery in kenaf management and production', *Industrial Crops and Products*, vol. 19, pp. 205-10.

Cook, SE & Bramley, RGV 1998, 'Precision agriculture - opportunities, benefits and pitfalls of site-specific crop management in Australia', *Australian Journal of Experimental Agriculture*, vol. 38, no. 7, pp. 753-63.

Cook, SE, Adams, ML & Bramley, RGV 2000, 'What is obstructing the wider adoption of precision agriculture technology', paper presented to 5th International Conference on Precision Agriculture, American Society of Agronomy, Bloomington, USA, 16-19 July 2000.

Dammer, KH, Wollny, J & Giebel, A 2008, 'Estimation of the Leaf Area Index in cereal crops for variable rate fungicide spraying', *European Journal of Agronomy*, vol. 28, no. 3, pp. 351-60.

Dare, P 2005, 'The Use of Small Environmental Research Aircraft (SERAs) for Environmental Remote Sensing', *International Journal of Geoinformatics*, vol. 1, no. 3

Dean, C, Warner, TA & McGraw, JB 2000, 'Suitability of the DCS460c colour digital camera for quantitative remote sensing analysis of vegetation', *ISPRS Journal of Photogrammetry and Remote Sensing*, vol. 55, no. 2, pp. 105-18.

Definiens 2007, *Definiens Professional 5*, München, Germany.

Deguise, JC, McNairn, H, Staenz, K & McGovern, M 1998, 'Spatial high resolution crop measurements with airborne hyperspectral remote sensing', paper presented to 4th International Conference on Precision Agriculture, American Society of Agronomy/CSSA/SSSA, St Paul, USA, 19-22 July 1998.

Delin, S 2004, 'Within-field variations in grain protein content - Relationships to yield and soil nitrogen and consistency in maps between years', *Precision Agriculture*, vol. 5, no. 6, pp. 565-77.

Delin, S, Linden, B & Berglund, K 2005, 'Yield and protein response to fertilizer nitrogen in different parts of a cereal field: potential of site-specific fertilization', *European Journal of Agronomy*, vol. 22, no. 3, pp. 325-36.

Enclona, EA, Thenkabail, PS, Celis, D & Diekmann, J 2004, 'Within-field wheat yield prediction from IKONOS data: A new matrix approach', *International Journal of Remote Sensing*, vol. 25, no. 2, pp. 377-88.

ERDAS 1999, *ERDAS Field Guide*, Fifth edn, ERDAS Inc, Atlanta, Georgia.

ERDAS 2002, *ERDAS IMAGINE*, 8.6 edn, Leica Geosystems, Atlanta, GA, USA, <http://www.erdas.com/>.

ERDAS 2003, *ERDAS IMAGINE*, 8.7 edn, Leica Geosystems GIS & Mapping LLC, Atlanta, GA, USA, <http://www.erdas.com/>.

Esbensen, K 2002, *Multivariate Data Analysis - in practice*, CAMO Process AS, Oslo.

Escobar, DE, Everitt, JH, Noriega, JR, Cavazos, I & Davis, MR 1998, 'A Twelve-Band Airborne Digital Video Imaging System (ADVIS)', *Journal of Remote Sensing of Environment*, vol. 66, pp. 122-8.

Espinar, V & Wiese, D 2006, 'An Extreme Makeover - Scientists Upgrade a Toy Plane with Robotic Technologies', *GPS World*, vol. February 2006, pp. 20-7.

Everitt, JH, Escobar, DE, Cavazos, I, Noriega, JR & Davis, MR 1995, 'A Three-Camera Multispectral Digital Video Imaging System', *Journal of Remote Sensing of Environment*, vol. 54, pp. 333-7.

Fairfield Smith, H 1938, 'An Empirical Law Describing Hetrogeneity in the Yields of Agricultural Crops', *Journal of Agricultural Science*, vol. 28, pp. 1-23.

Filella, I, Serrano, L, Serra, J & Penuelas, J 1995, 'Evaluating wheat nitrogen status with canopy reflectance indices and discriminant analysis', *Crop Science*, vol. 35, no. 5, pp. 1400-5.

Foody, GM 2002, 'Status of land cover classification accuracy assessment', *Remote Sensing of Environment*, vol. 80, no. 1, pp. 185-201.

Frazier, BE, Walters, CS & Perry, EM 1997, 'Role of remote sensing in site-specific management', in *The state of site specific management for agriculture*, American Society of Agronomy, Madison USA, pp. 149-60.

Furfaro, R, Ganapol, BD, Johnson, LF & Herwitz, SR 2007, 'Neural network algorithm for coffee ripeness evaluation using airborne images', *Applied Engineering in Agriculture*, vol. 23, no. 3, pp. 379-87.

Galvao, LS, Formaggio, AR & Tisot, DA 2005, 'Discrimination of sugarcane varieties in Southeastern Brazil with EO-1 Hyperion data', *Remote Sensing of Environment*, vol. 94, no. 4, pp. 523-34.

Geoimage 2005, *Brochure - Satellite Imagery applications for the real world*, 10 August 2008, <http://www.geoimage.com.au/>.

Gianinetti, A, Toffoli, F, Cavallero, A, Delogu, G & Stanca, AM 2005, 'Improving discrimination for malting quality in barley breeding programmes', *Field Crops Research*, vol. 94, no. 2-3, pp. 189-200.

Gitelson, AA, Kaufman, YJ & Merzlyak, MN 1996, 'Use of a green channel in remote sensing of global vegetation from EOS-MODIS', *Remote Sensing of Environment*, vol. 58, no. 3, pp. 289-98.

Godwin, RJ, Richards, TE, Wood, GA, Welsh, JP & Knight, SM 2003a, 'An Economic Analysis of the Potential for Precision Farming in UK Cereal Production', *Biosystems Engineering*, vol. 84, no. 4, pp. 533-45.

Godwin, RJ, Wood, GA, Taylor, JC, Knight, SM & Welsh, JP 2003b, 'Precision Farming of Cereal Crops: a Review of a Six Year Experiment to develop Management Guidelines', *Biosystems Engineering*, vol. 84, no. 4, pp. 375-91.

Goodrich, MA, Morse, BS, Gerhardt, D, Cooper, JL, Quigley, M, Adams, JA & Humphrey, C 2008, 'Supporting wilderness search and rescue using a camera-equipped mini UAV', *Journal of Field Robotics*, vol. 25, no. 1-2, pp. 89-110.

Gopalapillai, S & Tian, L 1999, 'In-field variability detection and spatial yield modeling for corn using digital aerial imaging', *Transactions of the ASAE*, vol. 42, no. 6, pp. 1911-20.

Hansen, PM, Jørgensen, JR & Thomsen, A 2002, 'Predicting grain yield and protein content in winter wheat and spring barley using repeated canopy reflectance measurements and partial least squares regression', *Journal of Agricultural Science*, vol. 139, no. 3, pp. 307-18.

Hardin, PJ & Jackson, MW 2005, 'An unmanned aerial vehicle for rangeland photography', *Rangeland Ecology and Management*, vol. 58, no. 4, pp. 439-42.

Harris, PS, Biggs, AJW & Stone, BJ 1999, *Central Darling Downs Land Management Manual*, DNRQ990102 edn, The State of Queensland, Brisbane, Queensland.

Hausamann, D, Zirnig, W, Schreier, G & Strobl, P 2005, 'Monitoring of gas pipelines - A civil UAV application', *Aircraft Engineering and Aerospace Technology*, vol. 77, no. 5, pp. 352-60.

Herwitz, SR, Johnson, LF, Dunagan, SE, Higgins, RG, Sullivan, DV, Zheng, J, Lobitz, BM, Leung, JG, Gallmeyer, BA & Aoyagi, M 2004, 'Imaging from an unmanned aerial vehicle: agricultural surveillance and decision support', *Computers and Electronics in Agriculture*, vol. 44, no. 1, pp. 49-61.

Hinckley, TK & Walker, JW 1993, 'Obtaining and using low-altitude/large-scale imagery', *Photogrammetric Engineering & Remote Sensing*, vol. 59, no. 3, pp. 310-8.

HOYA 2005, *Infrared Transmitting Filter : R72*, viewed 7 February 2005 <http://www.hoyaoptics.com/pdf/R72.pdf>.

Huete, A, Didan, K, Miura, T, Rodriguez, EP, Gao, X & Ferreira, LG 2002, 'Overview of the radiometric and biophysical performance of the MODIS vegetation indices', *Remote Sensing of Environment*, vol. 83, no. 1-2, pp. 195-213.

Huete, AR 1988, 'A soil-adjusted vegetation index (SAVI)', *Remote Sensing of Environment*, vol. 25, no. 3, pp. 295-309.

Hummel, JW, Gaultney, LD & Sudduth, KA 1996, 'Soil property sensing for site-specific crop management', *Computers and Electronics in Agriculture*, vol. 14, no. 2-3 SPEC. ISS., pp. 121-36.

Hunt Jr, ER, Everitt, JH, Ritchie, JC, Moran, MS, Booth, DT, Anderson, GL, Clark, PE & Seyfried, MS 2003, 'Applications and research using remote sensing for rangeland management', *Photogrammetric Engineering and Remote Sensing*, vol. 69, no. 6, pp. 675-93.

Hunt Jr., ER, Cavigelli, M, Daughtry, CST, McMurtrey III, JE & Walthall, CL 2005, 'Evaluation of digital photography from model aircraft for remote sensing of crop biomass and nitrogen status', *Precision Agriculture*, vol. 6, no. 4, pp. 359-78.

Hussain, A, Raine, SR, Henderson, CW & Jensen, TA 2008, 'Evaluation of a proximal vision data acquisition system for measuring spatial variability in lettuce growth', paper presented to Global Issues, Paddock Action - 14th Australian Agronomy Conference, Adelaide, Australia, 21-25 September 2008.

Inman, D, Khosla, R, Reich, R & Westfall, D 2007, 'Active remote sensing and grain yield in irrigated maize', *Precision Agriculture*, vol. 8, no. 4, pp. 241-52.

Inoue, Y, Morinaga, S & Tomita, A 2000, 'A blimp-based remote sensing system for low-altitude monitoring of plant variables: a preliminary experiment for agricultural and ecological applications.' *International Journal of Remote Sensing*, vol. 21, no. 2, pp. 379-85.

Isbell, RF 1996, *The Australian Soil Classification - Australian Soil and Land Survey Handbook.*, vol. 4, CSIRO Publishing, Collingwood.

Jensen, JR 2007, *Remote Sensing of the Environment: - an earth resource perspective*, Second edn, Pearson Prentice Hall, Upper Saddle River, NJ.

Jensen, TA, Kelly, R & Strong, W 2001a, 'Using protein mapping to define yield-limiting factors', paper presented to Third European Conference on Precision Agriculture, agro Montpellier, Montpellier, France, 18-20 June 2001.

Jensen, TA, Powell, G & Neale, T 2001b, 'How does protein and yield vary within a planter width?' paper presented to Third European Conference on Precision Agriculture, agro Montpellier, Montpellier, France, 18-20 June 2001.

Jensen, TA, Zeller, L, Fox, G, Town, W & Kelly, R 2005, 'Real-time protein monitoring – Australian experiences', paper presented to 5th European Conference on Precision Agriculture, Uppsala, Sweden, 9-12 June 2005.

Jia, L, Buerkert, A, Chen, X, Roemheld, V & Zhang, F 2004, 'Low-altitude aerial photography for optimum N fertilization of winter wheat on the North China Plain', *Field Crops Research*, vol. 89, no. 2-3, pp. 389-95.

Jochinke, DC, Noonon, BJ, Wachsmann, NG & Norton, RM 2007, 'The adoption of precision agriculture in an Australian broadacre cropping system-Challenges and opportunities', *Field Crops Research*, vol. 104, no. 1-3, pp. 68-76.

Joernsgaard, B & Halmoe, S 2003, 'Intra-field yield variation over crops and years', *European Journal of Agronomy*, vol. 19, no. 1, pp. 23-33.

Johnson, DE 1998, *Applied Multivariate Methods for Data Analysts*, Duxbury Press, Pacific Grove, CA.

Johnson, LF, Herwitz, SR, Lobitz, BM & Dunagan, SE 2004, 'Feasibility of monitoring coffee field ripeness with airborne multispectral imagery', *Applied Engineering in Agriculture*, vol. 20, no. 6, pp. 845-9.

Jordan, CF 1969, 'Derivation of leaf area index from quality of light on the forest floor', *Ecology*, vol. 50, no. 4, pp. 663-6.

Jørgensen, JR & Jørgensen, RN 2007, 'Uniformity of wheat yield and quality using sensor assisted application of nitrogen', *Precision Agriculture*, vol. 8, no. 1-2, pp. 63-73.

Keen, BA & Haines, WB 1925, 'Studies in Soil Cultivation II. Test of soil uniformity by means of dynamometer and plough', *Journal of Agricultural Science*, vol. 15, pp. 387-94.

Kelly, RM, Strong, WM, Jensen, TA & Butler, D 2004, 'Application of probability analysis to assess nitrogen supply to grain crops in northern Australia', *Precision Agriculture*, vol. 5, no. 2, pp. 95-110.

King, D, Walsh, P & Ciuffreda, F 1994, 'Airborne digital frame camera imaging for elevation determination', *Photogrammetric Engineering & Remote Sensing*, vol. 60, no. 11, pp. 1321-6.

Kinnear, PR & Gray, CD 2004, *SPSS 12 Made Simple*, Psychology Press, New York.

Kodak 2004, *User's Guide - CX7525*, Eastman Kodak Company, Rochester NY.

Kodak 2008, *Kodak KAI-0340 Image Sensor - device performance specifications*, viewed 12 June 2008 <http://www.kodak.com/ezpres/business/ccd/global/plugins/acrobat/en/datasheet/interline/KAI-0340LongSpec.pdf>.

Krüger, G, Springer, R & Lechner, W 1994, 'Global Navigation Satellite Systems (GNSS)', *Computers and Electronics in Agriculture*, vol. 11, no. 1, pp. 3-21.

Lamb, DW & Brown, RB 2001, 'Remote-Sensing and Mapping of Weeds in Crops', *Journal of Agricultural Engineering Research*, vol. 78, no. 2, pp. 117-25.

Lamb, DW 2000, 'The use of qualitative airborne multispectral imaging for managing agricultural crops - A case study in south-eastern Australia', *Australian Journal of Experimental Agriculture*, vol. 40, no. 5, pp. 725-38.

Landis, JR & Koch, GG 1977, 'The measurement of observer agreement for categorical data', *Biometrics*, vol. 33, no. 1, pp. 159-74.

Layrol, L, Hedoin, E, Lepoutre, D & Francois, O 2000, 'Matching multitemporal yield and images data', paper presented to 5th International Conference on Precision Agriculture, American Society of Agronomy, Bloomington, USA, 16-19 July 2000.

Legg, BJ & Stafford, JV 1998, 'Precision agriculture - new technologies', paper presented to Brighton Crop Protection Conference: Pests and Diseases, British Crop Protection Council, Brighton, UK, 16-19 November 1998.

Leica 2005, *ERDAS Field Guide*, Leica Geosystems Geospatial Imaging, LLC.

Leica 2007, *ERDAS IMAGINE*, 9.1 edn, Leica Geosystems Geospatial Imaging LLC, Norcross GA.

Lévesque, J & King, DJ 1999, 'Airborne Digital Camera Image Semivariance for Evaluation of Forest Structural Damage at an Acid Mine Site', *Remote Sensing of Environment*, vol. 68, no. 2, pp. 112-24.

Li, F, Gnyp, ML, Jia, L, Miao, Y, Yu, Z, Koppe, W, Bareth, G, Chen, X & Zhang, F 2008, 'Estimating N status of winter wheat using a handheld spectrometer in the North China Plain', *Field Crops Research*, vol. 106, no. 1, pp. 77-85.

Light, DL 1996, 'Film cameras or digital sensors? The challenge ahead for aerial imaging', *Photogrammetric Engineering and Remote Sensing*, vol. 62, no. 3, pp. 285-91.

Lillesand, TM, Kieffer, RW & Chipman, JW 2004, *Remote Sensing and Image Interpretation*, 5th edn, John Wiley and Sons, New York.

Liu, L, Wang, J, Bao, Y, Huang, W, Ma, Z & Zhao, C 2006, 'Predicting winter wheat condition, grain yield and protein content using multi-temporal EnviSat-ASAR and Landsat TM satellite images', *International Journal of Remote Sensing*, vol. 27, no. 4, pp. 737-53.

Maas, SJ & Rajan, N 2008, 'Estimating ground cover of field crops using medium-resolution multispectral satellite imagery', *Agronomy Journal*, vol. 100, no. 2, pp. 320-7.

Martínez-Val, R & Hernández, C 1999, 'Preliminary design of a low speed, long endurance remote piloted vehicles (RPV) for civil applications', *Aircraft Design*, vol. 2, no. 3, pp. 167-82.

Mason, S, Ruther, H & Smit, J 1997, 'Investigation of the Kodak DCS460 digital camera for small-area mapping', *Journal of Photogrammetry and Remote Sensing*, vol. 52, pp. 202-14.

Mather, PM 2004, *Computer Processing of Remotely-Sensed Images*, 3rd edn, John Wiley and Sons, Chichester, UK.

Mausel, PW, Everitt, JH, Escobar, DE & King, DJ 1992, 'Airborne Videography - Current Status and Future Perspectives', *Photogrammetric Engineering and Remote Sensing*, vol. 58, no. 8, pp. 1189-95.

McBratney, A & Whelan, B 2001, 'Precision Ag. - Oz style', paper presented to First Australian Geospatial Information and Agriculture Conference, , Sydney, Australia, 17-19 July 2001.

Merzlyak, MN, Gitelson, AA, Chivkunova, OB & Rakitin, VY 1999, 'Non-destructive optical detection of pigment changes during leaf senescence and fruit ripening', *Physiologia Plantarum*, vol. 106, no. 1, pp. 135-41.

Moran, S, Fitzgerald, G, Rango, A, Walthall, C, Barnes, E, Bausch, W, Clarke, T, Daughtry, C, Everitt, J, Escobar, D, Hatfield, J, Havstad, K, Jackson, T, Kitchen, N, Kustas, W, McGuire, M, Pinter Jr, P, Sudduth, K, Schepers, J, Schmugge, T, Starks, P & Upchurch, D 2003, 'Sensor development and radiometric correction for agricultural applications', *Photogrammetric Engineering and Remote Sensing*, vol. 69, no. 6, pp. 705-18.

Murden, SB & Risenhoover, KL 2000, 'A blimp system to obtain high-resolution, low-altitude aerial photography and videography', *Wildlife Society Bulletin*, vol. 28, no. 4, pp. 958-62.

Murphy, RR, Steimle, E, Griffin, C, Cullins, C, Hall, M & Pratt, K 2008, 'Cooperative use of unmanned sea surface and micro aerial vehicles at Hurricane Wilma', *Journal of Field Robotics*, vol. 25, no. 3, pp. 164-80.

Navulur, K 2007, *Multispectral Image Analysis Using the Object-Orientated Paradigm*, CRC Press, Taylor and Francis Group, Boca Raton, FL.

Nice, K, Wilson, TV & Gurevich, G 2006, *How Digital Cameras Work*, HowStuffWorks.com, 2 October 2008, <http://electronics.howstuffworks.com/digital-camera.htm>.

Nixon, PR, Escobar, DE & Menges, RM 1985, 'A multiband video system for quick assessment of vegetal condition and discrimination of plant species', *Remote Sensing of Environment*, vol. 17, no. 2, pp. 203-8.

Norng, S, Pettitt, AN, Kelly, RM, Butler, DG & Strong, WM 2005, 'Investigating the relationship between site-specific yield and protein of cereal crops', *Precision Agriculture*, vol. 6, no. 1, pp. 41-51.

NRC 1997, *Precision Agriculture in the 21st Century: Geospatial and Information Technologies in Crop Management*, National Research Council (US) Committee on Assessing Crop Yield: Site-Specific Farming, Information Systems, and Research Opportunities, The National Academies Press, Washington DC.

Oliver, Y, Wong, M, Robertson, M & Wittwer, K 2006, 'PAWC determines spatial variability in grain yield and nitrogen requirement by interacting with rainfall on northern WA sandplain', paper presented to 13th Agronomy Conference Australian Society of Agronomy, Perth, Australia, 10-14 September 2006.

Pearson, R, Grace, J & May, G 1994, 'Real-time airborne agricultural monitoring', *Remote Sensing of Environment*, vol. 49, no. 3, pp. 304-10.

Perry, C, Pocknee, S & Hansen, O 2003, 'Variable-rate irrigation', *Resource: Engineering and Technology for Sustainable World*, vol. 10, no. 1, pp. 11-2.

Pettersson, CG & Eckersten, H 2007, 'Prediction of grain protein in spring malting barley grown in northern Europe', *European Journal of Agronomy*, vol. 27, no. 2-4, pp. 205-14.

Pierce, FJ & Nowak, P 1999, 'Aspects of Precision Agriculture', *Advances in Agronomy*, vol. 67, pp. 1-85.

Piron, A, Leemans, V, Kleynen, O, Lebeau, F & Destain, MF 2008, 'Selection of the most efficient wavelength bands for discriminating weeds from crop', *Computers and Electronics in Agriculture*, vol. 62, no. 2, pp. 141-8.

Plant, RE 2001, 'Site-specific Management: the Application of Information Technology to Crop Production', *Computers and Electronics in Agriculture*, vol. 30, pp. 9-29.

Price, JC & Bausch, WC 1995, 'Leaf Area Index Estimation from Visible and Near-Infrared Reflectance Data', *Journal of Remote Sensing of Environment*, vol. 52, pp. 55-65.

Price, JC 1998, 'An approach for analysis of reflectance spectra', *Remote Sensing of Environment*, vol. 64, no. 3, pp. 316-30.

Price, KP, Guo, X & Stiles, JM 2002, 'Optimal landsat TM band combinations and vegetation indices for discrimination of six grassland types in eastern Kansas', *International Journal of Remote Sensing*, vol. 23, no. 23, pp. 5031-42.

Qiu, W, Watkins, GA, Sobolik, CJ & Shearer, SA 1998, 'A feasibility study of direct injection for variable-rate herbicide application', *Transactions of the ASAE*, vol. 41, no. 2, pp. 291-9.

Quilter, MC & Anderson, VJ 2000, 'Low Altitude/Large Scale Aerial Photographs: A Tool for Range and Resource Managers', *Rangelands*, vol. 22, no. 2, pp. 13-7.

Quilter, MC & Anderson, VJ 2001, 'A proposed method for determining shrub utilization using (LA/LS) imagery', *Journal of Range Management*, vol. 54, no. 4, pp. 378-81.

Rango, A, Laliberte, A, Steele, C, Herrick, JE, Bestelmeyer, B, Schmugge, T, Roanhorse, A & Jenkins, V 2006, 'Using unmanned aerial vehicles for rangelands: Current applications and future potentials', *Environmental Practice*, vol. 8, no. 3, pp. 159-68.

Reitz, P & Kutzbach, HD 1996, 'Investigations on a particular yield mapping system for combine harvesters', *Computers and Electronics in Agriculture*, vol. 14, no. 2-3, pp. 137-50.

Reyns, P, De Baerdemaeker, J & Ramon, H 1999, 'Site-specific relationship between grain quality and yield', paper presented to 2nd European Conference on Precision Agriculture, Sheffield Academic Press, Odense Conference Centre, Denmark, 11-15 July 1999.

Reyns, P, Spaepen, P & De Baerdemaeker, J 2001, 'Site-specific relationship between grain quality and yield', *Precision Agriculture*, vol. 2, no. 3, pp. 231-46.

Richardson, AJ, Menges, RM & Nixon, PR 1985, 'Distinguishing weed from crop plants using video remote sensing', *Photogrammetric Engineering & Remote Sensing*, vol. 51, no. 11, pp. 1785-90.

Ries, JB & Marzolff, I 2003, 'Monitoring of gully erosion in the Central Ebro Basin by large-scale aerial photography taken from a remotely controlled blimp', *CATENA*, vol. 50, no. 2-4, pp. 309-28.

Rodriguez, D, Sadras, VO, Christensen, LK & Belford, R 2005, 'Spatial assessment of the physiological status of wheat crops as affected by water and nitrogen supply using infrared thermal imagery', *Australian Journal of Agricultural Research*, vol. 56, no. 9, pp. 983-93.

Roth, GW 1993, 'Agronomic Measurements to Validate Airborne Video Imagery for Irrigated Cotton Management', Masters of Applied Science thesis, University of Canberra.

Rouse, JW, Haas, RH, Schell, JA & Deering, DW 1974, 'Monitoring vegetation systems in the Great Plains with ERTS', paper presented to NASA SP-351, Third ERTS Symposium, NASA Washington DC.

Scharf, PC & Lory, JA 2000, 'Calibration of remotely-sensed corn color to predict nitrogen need', paper presented to 5th International Conference on Precision Agriculture, American Society of Agronomy, Bloomington, USA, 16-19 July 2000.

Schmale III, DG, Dingus, BR & Reinholtz, C 2008, 'Development and application of an autonomous unmanned aerial vehicle for precise aerobiological sampling above agricultural fields', *Journal of Field Robotics*, vol. 25, no. 3, pp. 133-47.

Schmidt, JP, Taylor, RK & Gehl, RJ 2003, 'Developing topographic maps using a sub-meter accuracy global positioning receiver', *Applied Engineering in Agriculture*, vol. 19, no. 3, pp. 291-300.

Schoonmaker, J, Wells, T, Gilbert, G, Podobna, Y, Petrosyuk, I & Dirbas, J 2008, 'Spectral detection and monitoring of marine mammals', paper presented to Airborne Intelligence, Surveillance, Reconnaissance (ISR) Systems and Applications V, SPIE, Orlando, USA, 17-20 March 2008.

Simpson, AD, Stombaugh, TS, Wells, LG & Jacob, JD 2003, 'Imaging Techniques and Applications for UAV’s in Agriculture ', paper presented to 2003 ASAE Annual International Meeting, American Society of Agricultural and Biological Engineers, Las Vegas, USA 27- 30 July 2003

SPSS 2003, *SPSS 12.0.1 for Windows*, Version 12.0.1 edn, SPSS Inc, Chicago, Illinois.

SST 2000, *FieldRover II*, 7.1 edn, SST Development Group Inc, Stillwater, OK, <http://www.sstsoftware.com/>.

Stafford, JV 1996, 'Essential technology for precision agriculture', paper presented to Precision agriculture - Proceedings of the 3rd International Conference, Minneapolis, USA, 23-26 June 1996.

Stafford, JV 1999, 'An investigation into the within-field spatial variability of grain quality', paper presented to 2nd European Conference on Precision Agriculture, Sheffield Academic Press, Odense Conference Centre, Denmark, 11-15 July 1999.

Stafford, JV 2000, 'Implementing Precision Agriculture in the 21st Century', *Journal of Agricultural Engineering Research*, vol. 76, no. 3, pp. 267-75.

Stafford, JV, Ambler, B, Lark, RM & Catt, J 1996, 'Mapping and interpreting the yield variation in cereal crops', *Computers and Electronics in Agriculture*, vol. 14, no. 2-3, pp. 101-19.

Staggenborg, SA & Taylor, RK 2000, 'Predicting grain yield variability with infrared images', paper presented to 5th International Conference on Precision Agriculture, American Society of Agronomy, Bloomington, USA, 16-19 July 2000.

Stewart, CM, McBratney, AB & Skerritt, J 2002, 'Site-specific durum wheat quality and its relationship to soil properties in a single field in northern New South Wales', *Precision Agriculture*, vol. 3, no. 2, pp. 155-68.

Stombaugh, TS, Simpson, AD, Jacob, JD & Mueller, T 2003, 'A low cost platform for obtaining remote sensed imagery', paper presented to 4th European Conference on Precision Agriculture, Berlin Germany, 16-18 June 2003.

Stone, ML, Solie, JB, Raun, WR, Whitney, RW, Taylor, SL & Ringer, JD 1996, 'Use of Spectral Radiance for Correcting In-season Fertilizer Nitrogen Deficiencies in Winter Wheat', *Transactions of the ASAE*, vol. 39, pp. 1623-31.

St-Onge, BA & Cavayas, F 1997, 'Automated forest structure mapping from high resolution imagery based on directional semivariogram estimates', *Remote Sensing of Environment*, vol. 61, no. 1, pp. 82-95.

Story, M & Congalton, RG 1986, 'Accuracy assessment: a user's perspective', *Photogrammetric Engineering & Remote Sensing*, vol. 52, no. 3, pp. 397-9.

Strachan, IB, Pattey, E & Boisvert, JB 2002, 'Impact of nitrogen and environmental conditions on corn as detected by hyperspectral reflectance', *Remote Sensing of Environment*, vol. 80, no. 2, pp. 213-24.

Strong , W & Holford, IC 1997, 'Fertiliser and Manures', in AL Clarke & PB Wylie (eds), *Sustainable Crop Production in the Subtropics*, QDPI, Brisbane, Australia, pp. 214-34.

Sudduth, KA, Drummond, ST, Birrell, SJ & Kitchen, NR 1996, 'Analysis of spatial factors influencing crop yield', paper presented to Precision Agriculture - Proceedings of the 3rd International Conference on ASA/CSSA/SSSA, Bloomington, Minnesota, 23-26 June 1996.

Sugiura, R, Noguchi, N & Ishii, K 2005, 'Remote-sensing Technology for Vegetation Monitoring using an Unmanned Helicopter', *Biosystems Engineering*, vol. 90, no. 4, pp. 369-79.

Sullivan, DG, Fulton, JP, Shaw, JN & Bland, GL 2007, 'Evaluating the sensitivity of an unmanned thermal infrared aerial system to detect water stress in a cotton canopy', *Transactions of the ASABE*, vol. 50, no. 6, pp. 1955-62.

Swain, KC, Jayasuriya, HPW & Salokhe, VM 2007, 'Low-Altitude Remote Sensing with Unmanned Radio-Controlled Helicopter Platforms: A Potential Substitution to Satellite-based Systems for Precision Agriculture Adoption under Farming Conditions in Developing Countries', *International Commission of Agricultural Engineering (CIGR, Commission Internationale du Genie Rural) E-Journal*, vol. Vol. IX, no. September.

Taylor, J, Whelan, BM, Thylen, L, Gilbertsson, M & Hassall, J 2005, 'Monitoring wheat protein content on-harvester - Australian experiences', paper presented to 5th European Conference on Precision Agriculture, Wageningen Academic, Uppsala Sweden, 9-12 June 2005.

Thenkabail, PS, Enclona, EA, Ashton, MS, Legg, C & De Dieu, MJ 2004, 'Hyperion, IKONOS, ALI, and ETM+ sensors in the study of African rainforests', *Remote Sensing of Environment*, vol. 90, no. 1, pp. 23-43.

Thenkabail, PS, Smith, RB & De Pauw, E 2002, 'Evaluation of narrowband and broadband vegetation indices for determining optimal hyperspectral wavebands for agricultural crop characterization', *Photogrammetric Engineering and Remote Sensing*, vol. 68, no. 6, pp. 607-21.

Thomas, GA, Dalal, RC, Weston, EJ, Chicken, CJ, Lehane, KJ, King, AJ, Orange, D, N. & McNamara, GT 1998, 'A farming systems study at Nindigully, southwest Queensland', paper presented to 9th Australian Agronomy Conference-Growing a Greener Future, Wagga Wagga, Australia, 20-23 July 1998.

Thorp, KR & Tian, LF 2004, 'A review on remote sensing of weeds in agriculture', *Precision Agriculture*, vol. 5, no. 5, pp. 477-508.

Thylen, L, Algerbo, PA & Pettersson, CG 1999, 'Grain quality variations within fields of malting barley', paper presented to Precision Agriculture '99. 2nd European Conference on Precision Agriculture, Sheffield Academic Press, Odense Conference Centre, Denmark, 11-15 July 1999.

Thylén, L, Gilbertsson, M, Rosenthal, T & Wrenn, S 2002, 'An on-line protein sensor - from research to product.' paper presented to Proceedings of the 6th International Conference on Precision Agriculture and Other Precision Resources Management, American Society of Agronomy, Minneapolis, USA, 14-17 July 2002.

Tucker, CJ 1979, 'Red and photographic infrared linear combinations for monitoring vegetation', *Remote Sensing of Environment*, vol. 8, no. 2, pp. 127-50.

US, HoR 1997, *To reform, extend, and repeal certain agricultural research, extension, and education programs, and for other purposes*, H.R.2534, 13 November 1997, <http://thomas.loc.gov/cgi-bin/query/F?c105:4:./temp/~c105NHTC2E:e80477:>.

Vaytek 2003, *Spectral response* 5 April 2003, <http://www.vaytek.com/specDVC.htm .>.

Vellidis, G, Tucker, MA, Perry, CD, Thomas, DL, Wells, N & Kvien, CK 2004, 'Predicting cotton lint yield maps from aerial photographs', *Precision Agriculture*, vol. 5, no. 6, pp. 547-64.

Vierling, LA, Fersdahl, M, Chen, X, Li, Z & Zimmerman, P 2006, 'The Short Wave Aerostat-Mounted Imager (SWAMI): A novel platform for acquiring remotely sensed data from a tethered balloon', *Remote Sensing of Environment*, vol. 103, no. 3, pp. 255-64.

Wang, J, Sammis, TW, Andales, AA, Simmons, LJ, Gutschick, VP & Miller, DR 2007, 'Crop coefficients of open-canopy pecan orchards', *Agricultural Water Management*, vol. 88, no. 1-3, pp. 253-62.

Wang, ZJ, Wang, JH, Liu, LY, Huang, WJ, Zhao, CJ & Wang, CZ 2004, 'Prediction of grain protein content in winter wheat (Triticum aestivum L.) using plant pigment ratio (PPR)', *Field Crops Research*, vol. 90, no. 2-3, pp. 311-21.

Wanjura, DF & Hatfield, JL 1986, 'Par and IR reflectance, Transmittance, and Absorptance of Four Crop Canopies', vol. 29, no. 1, pp. 143-50.

Whelan, B 2007, 'Current status and future directions of PA in Australia', paper presented to 2nd Asian Conference on Precision Agriculture, Pyeongtaek, Korea, 2-4 August 2007.

Willis, PR, Carter, PG & Johannsen, CJ 1998, 'Accessing yield parameters by remote sensing techniques', paper presented to 4th International Conference on Precision Agriculture, ASA/CSSA/SSSA, Bloomington, USA, 19-22 July 1998.

Wooten, J 2003, *Removing the IR blocking filter in the Nikon 950 and 990*, viewed 26 March 2003 <http://www.abe.msstate.edu/~jwooten/camera/lense.html>.

Wright, G & Mills, G 2002, 'Remote sensing applications for irrigated peanuts', paper presented to The 11th Australasian Remote Sensing and Photogrammetry Association Conference, Brisbane, Australia, 2-6 August 2002.

Wright, GG, Matthews, KB, Cadell, WM & Milne, R 2003, 'Reducing the cost of multi-spectral remote sensing: combining near-infrared video imagery with colour aerial photography', *Computers and Electronics in Agriculture*, vol. 38, no. 3, pp. 175-98.

Xue, L, Cao, W, Luo, W, Dai, T & Zhu, Y 2004, 'Monitoring Leaf Nitrogen Status in Rice with Canopy Spectral Reflectance', *Agronomy Journal*, vol. 96, no. 1, pp. 135-42.

Xue, L-H, Cao, W-X & Yang, L-Z 2007, 'Predicting Grain Yield and Protein Content in Winter Wheat at Different N Supply Levels Using Canopy Reflectance Spectra', *Pedosphere*, vol. 17, no. 5, pp. 646-53.

Yang, C & Anderson, GL 1999, 'Airborne Videography to Identify Spatial Plant Growth Variability for Grain Sorghum', *Precision Agriculture*, vol. 1, no. 1, pp. 67-79.

Yang, C & Anderson, GL 2000, 'Mapping Grain Sorghum Yield Variability Using Airborne Digital Videography', *Precision Agriculture*, vol. 2 (1), pp. 7-23.

Yang, C & Everitt, JH 2002, 'Relationships between yield monitor data and airborne multidate multispectral digital imagery for grain sorghum', *Precision Agriculture*, vol. 3, no. 4, pp. 373-88.

Yang, C 2001, 'A variable rate applicator for controlling rates of two liquid fertilizers', *Applied Engineering in Agriculture*, vol. 17, no. 3, pp. 409-17.

Yang, C, Bradford, JM & Wiegand, CL 2001, 'Airborne multispectral imagery for mapping vartable growing conditions and yields of cotton, grain sorghum, and corn', *Transactions of the ASAE*, vol. 44, no. 6, pp. 1983-94.

Yang, C, Everitt, JH, Bradford, JM & Escobar, DE 2000, 'Mapping Grain Sorghum Growth and Yield Variations Using Airborne Multispectral Digital Imagery', *Transactions of theASAE*, vol. 43, no. 6, pp. 1927-38.

Yang, C-C, Prasher, SO, Landry, J-A & Kok, R 2002, 'AE--Automation and Emerging Technologies: A Vegetation Localization Algorithm for Precision Farming', *Biosystems Engineering*, vol. 81, no. 2, pp. 137-46.

Zadoks, JC, Chang, TT & Konzak, CF 1974, 'A decimal code for the growth stages of cereals', *Weed Research*, vol. 14, no. 6, pp. 415-21.

Zhang, N, Wang, M & Wang, N 2002, 'Precision agriculture--a worldwide overview', *Computers and Electronics in Agriculture*, vol. 36, no. 2-3, pp. 113-32.

Zhao, C, Jiang, A, Huang, W, Liu, K, Liu, L & Wang, J 2007, 'Evaluation of variable-rate nitrogen recommendation of winter wheat based on SPAD chlorophyll meter measurement', *New Zealand Journal of Agricultural Research*, vol. 50, no. 5, pp. 735-41.

Zhao, C, Liu, L, Wang, J, Huang, W, Song, X & Li, C 2005, 'Predicting grain protein content of winter wheat using remote sensing data based on nitrogen status and water stress', *International Journal of Applied Earth Observation and Geoinformation*, vol. 7, no. 1, pp. 1-9.

Zhou, Q & Robson, M 2001, 'Automated rangeland vegetation cover and density estimation using ground digital images and a spectral-contextual classifier.' *International Journal of Remote Sensing*, vol. 22, no. 17, pp. 3457-70.

Appendices

Appendix 1 Summary of SPSS output–Colonsay

Tests of Equality of Group Means

	Wilks' Lambda	F	df1	df2	Sig.
RED	.588	26.892	3	115	.000
GREEN	.677	18.311	3	115	.000
BLUE	.481	41.403	3	115	.000
NIRR	.435	49.706	3	115	.000
NIRG	.418	53.387	3	115	.000
NIRB	.393	59.303	3	115	.000

Pooled Within-Groups Matrices[a]

		RED	GREEN	BLUE	NIRR	NIRG	NIRB
Covariance	RED	107.478	97.176	79.804	55.675	24.968	26.310
	GREEN	97.176	89.931	71.856	60.448	27.705	29.160
	BLUE	79.804	71.856	64.662	29.638	12.761	13.699
	NIRR	55.675	60.448	29.638	112.508	54.825	56.544
	NIRG	24.968	27.705	12.761	54.825	27.057	27.753
	NIRB	26.310	29.160	13.699	56.544	27.753	28.682
Correlation	RED	1.000	.988	.957	.506	.463	.474
	GREEN	.988	1.000	.942	.601	.562	.574
	BLUE	.957	.942	1.000	.347	.305	.318
	NIRR	.506	.601	.347	1.000	.994	.995
	NIRG	.463	.562	.305	.994	1.000	.996
	NIRB	.474	.574	.318	.995	.996	1.000

a. The covariance matrix has 115 degrees of freedom.

Summary of Canonical Discriminant Functions

Eigenvalues

Function	Eigenvalue	% of Variance	Cumulative %	Canonical Correlation
1	7.342[a]	95.2	95.2	.938
2	.298[a]	3.9	99.0	.479
3	.073[a]	1.0	100.0	.261

a. First 3 canonical discriminant functions were used in the analysis.

Wilks' Lambda

Test of Function(s)	Wilks' Lambda	Chi-square	df	Sig.
1 through 3	.086	277.170	18	.000
2 through 3	.718	37.464	10	.000
3	.932	7.995	4	.092

Standardized Canonical Discriminant Function Coefficients

	Function		
	1	2	3
RED	5.108	-.496	1.178
GREEN	-8.472	-1.320	2.290
BLUE	1.987	2.096	-2.457
NIRR	-1.701	-8.984	-6.538
NIRG	-4.811	7.478	-3.355
NIRB	8.755	1.821	9.152

Structure Matrix

	Function		
	1	2	3
NIRB	.457*	.002	.393
NIRG	.434*	.033	.348
NIRR	.419*	-.057	.357
GREEN	-.248	.011	.581*
RED	-.304	-.018	.563*
BLUE	-.380	.116	.445*

Pooled within-groups correlations between discriminating variables and standardized canonical discriminant functions
Variables ordered by absolute size of correlation within function.

*. Largest absolute correlation between each variable and any discriminant function

Functions at Group Centroids

N APPLIED	Function 1	2	3
0	-4.639	.495	-.073
40	-1.199	-.867	.285
80	1.625	-.132	-.279
120	2.655	.630	.335

Unstandardized canonical discriminant functions evaluated at group means

Canonical Discriminant Functions

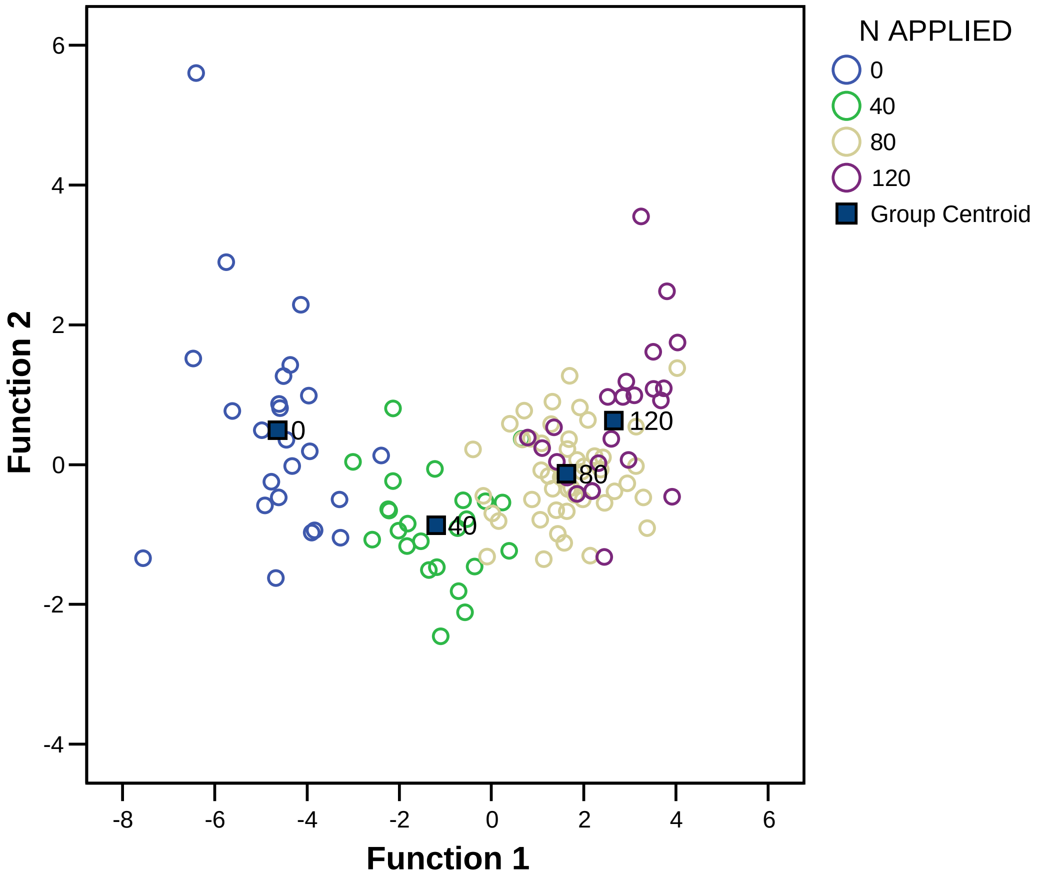

Classification Results[a]

		N APPLIED	Predicted Group Membership 0	40	80	120	Total
Original	Count	0	22	2	0	0	24
		40	1	22	1	0	24
		80	0	5	32	10	47
		120	0	0	10	14	24
	%	0	91.7	8.3	.0	.0	100.0
		40	4.2	91.7	4.2	.0	100.0
		80	.0	10.6	68.1	21.3	100.0
		120	.0	.0	41.7	58.3	100.0

a. 75.6% of original grouped cases correctly classified.

Appendix 2 Summary of SPSS output–Nindigully

N = 50

Tests of Equality of Group Means

	Wilks' Lambda	F	df1	df2	Sig.
BLUE	.447	8.850	6	43	.000
GREEN	.304	16.425	6	43	.000
RED	.341	13.879	6	43	.000
NIRB	.196	29.310	6	43	.000
NIRG	.161	37.415	6	43	.000
NIRR	.140	44.039	6	43	.000

Pooled Within-Groups Matrices[a]

		BLUE	GREEN	RED	NIRB	NIRG	NIRR
Covariance	BLUE	54.343	60.781	65.052	14.239	12.990	29.982
	GREEN	60.781	69.815	74.157	17.317	15.795	37.025
	RED	65.052	74.157	80.916	15.553	14.707	34.228
	NIRB	14.239	17.317	15.553	9.508	7.988	19.217
	NIRG	12.990	15.795	14.707	7.988	6.977	16.836
	NIRR	29.982	37.025	34.228	19.217	16.836	41.055
Correlation	BLUE	1.000	.987	.981	.626	.667	.635
	GREEN	.987	1.000	.987	.672	.716	.692
	RED	.981	.987	1.000	.561	.619	.594
	NIRB	.626	.672	.561	1.000	.981	.973
	NIRG	.667	.716	.619	.981	1.000	.995
	NIRR	.635	.692	.594	.973	.995	1.000

a. The covariance matrix has 43 degrees of freedom.

Eigenvalues

Function	Eigenvalue	% of Variance	Cumulative %	Canonical Correlation
1	13.825[a]	55.3	55.3	.966
2	7.256[a]	29.0	84.4	.937
3	3.272[a]	13.1	97.5	.875
4	.553[a]	2.2	99.7	.597
5	.055[a]	.2	99.9	.229
6	.029[a]	.1	100.0	.167

a. First 6 canonical discriminant functions were used in the analysis.

Wilks' Lambda

Test of Function(s)	Wilks' Lambda	Chi-square	df	Sig.
1 through 6	.001	288.216	36	.000
2 through 6	.017	173.623	25	.000
3 through 6	.139	83.906	16	.000
4 through 6	.593	22.189	9	.008
5 through 6	.921	3.483	4	.480
6	.972	1.195	1	.274

Standardized Canonical Discriminant Function Coefficients

	Function					
	1	2	3	4	5	6
BLUE	-.663	-5.582	-.688	2.930	-.349	4.286
GREEN	7.964	1.902	-7.883	-9.894	2.113	-2.116
RED	-6.683	4.281	7.595	6.395	-1.290	-.971
NIRB	-3.160	2.827	-.541	5.267	2.137	-1.116
NIRG	-2.230	-3.206	4.709	-12.234	2.676	-4.732
NIRR	4.793	.064	-2.291	8.453	-4.644	5.101

Structure Matrix

	Function					
	1	2	3	4	5	6
NIRR	.619*	-.062	.489	.221	.571	-.011
NIRB	.504	-.074	.378	.261	.723*	-.077
BLUE	.215	.167	.332	-.056	.647*	.628
GREEN	.311	.267	.354	-.063	.636*	.547
NIRG	.559	-.083	.500	.172	.634*	-.008
RED	.218	.320	.393	-.092	.550	.621*

Pooled within-groups correlations between discriminating variables and standardized canonical discriminant functions

Variables ordered by absolute size of correlation within function.

*. Largest absolute correlation between each variable and any discriminant function

Functions at Group Centroids

	Function					
CROP	1	2	3	4	5	6
1	-4.157	3.153	.755	-.471	-.102	-.040
2	5.623	.692	-2.400	-1.058	.060	-.209
3	4.330	3.243	-1.159	.868	-.217	.257
4	2.864	-1.799	2.728	-.214	-.011	.034
5	-1.175	.136	-.330	.581	.386	-.007
6	-1.460	-2.709	-.658	1.093	-.317	-.265
7	-3.557	-4.204	-2.089	-.694	-.072	.244

Unstandardized canonical discriminant functions evaluated at group means

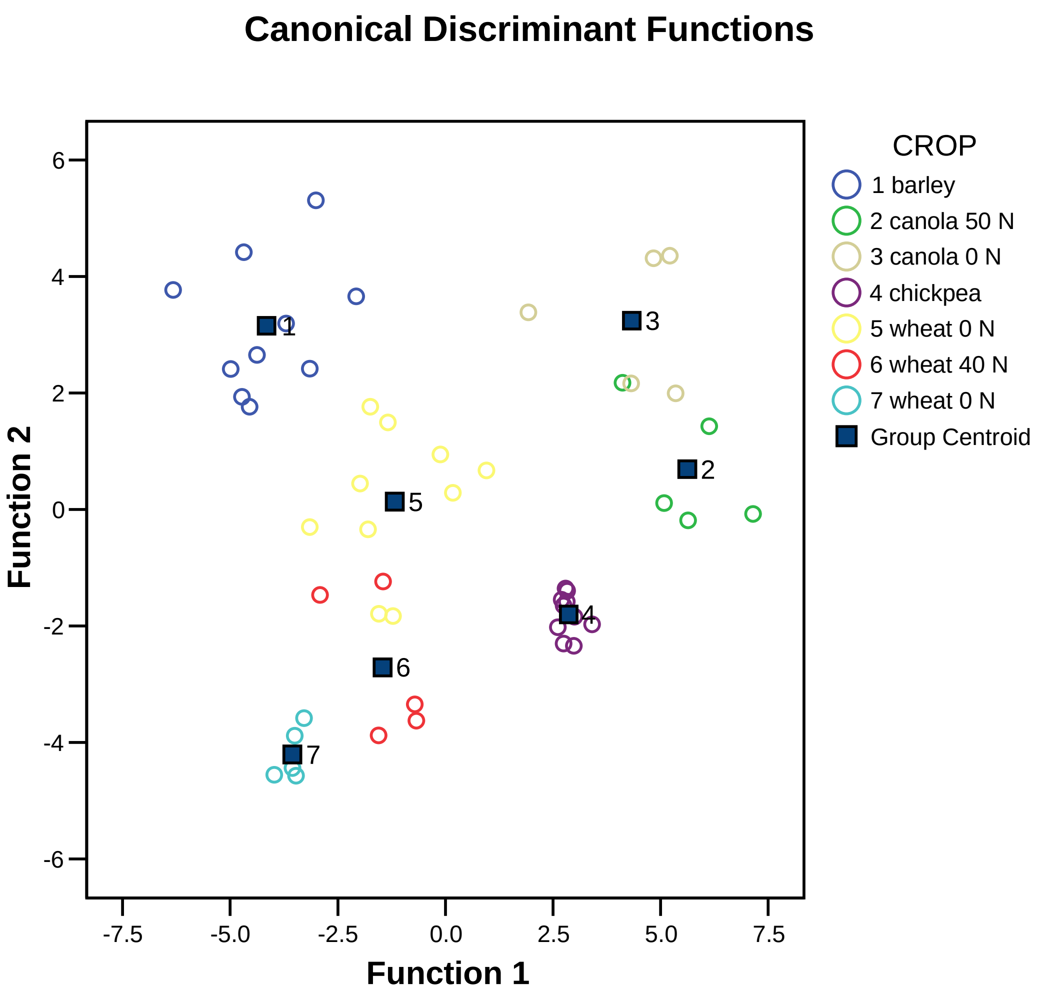
Canonical Discriminant Functions
CROP
1 barley
2 canola 50 N
3 canola 0 N
4 chickpea
5 wheat 0 N
6 wheat 40 N
7 wheat 0 N
Group Centroid
Function 1
Function 2
-7.5
-5.0
-2.5
0.0
2.5
5.0
7.5
6
4
2
0
-2
-4
-6

Classification Results[b,c]

		CROP	Predicted Group Membership 1	2	3	4	5	6	7	Total
Original	Count	1	10	0	0	0	0	0	0	10
		2	0	5	0	0	0	0	0	5
		3	0	0	5	0	0	0	0	5
		4	0	0	0	10	0	0	0	10
		5	0	0	0	0	8	2	0	10
		6	0	0	0	0	0	5	0	5
		7	0	0	0	0	0	0	5	5
	%	1	100.0	.0	.0	.0	.0	.0	.0	100.0
		2	.0	100.0	.0	.0	.0	.0	.0	100.0
		3	.0	.0	100.0	.0	.0	.0	.0	100.0
		4	.0	.0	.0	100.0	.0	.0	.0	100.0
		5	.0	.0	.0	.0	80.0	20.0	.0	100.0
		6	.0	.0	.0	.0	.0	100.0	.0	100.0
		7	.0	.0	.0	.0	.0	.0	100.0	100.0
Cross-validated[a]	Count	1	9	0	0	0	1	0	0	10
		2	0	5	0	0	0	0	0	5
		3	0	1	3	0	1	0	0	5
		4	0	0	0	10	0	0	0	10
		5	0	0	0	0	6	4	0	10
		6	0	0	0	0	2	3	0	5
		7	0	0	0	0	0	2	3	5
	%	1	90.0	.0	.0	.0	10.0	.0	.0	100.0
		2	.0	100.0	.0	.0	.0	.0	.0	100.0
		3	.0	20.0	60.0	.0	20.0	.0	.0	100.0
		4	.0	.0	.0	100.0	.0	.0	.0	100.0
		5	.0	.0	.0	.0	60.0	40.0	.0	100.0
		6	.0	.0	.0	.0	40.0	60.0	.0	100.0
		7	.0	.0	.0	.0	.0	40.0	60.0	100.0

a. Cross validation is done only for those cases in the analysis. In cross validation, each case is classified by the functions derived from all cases other than that case.

b. 96.0% of original grouped cases correctly classified.

c. 78.0% of cross-validated grouped cases correctly classified.

N = 80

Tests of Equality of Group Means

	Wilks' Lambda	F	df1	df2	Sig.
BLUE	.416	17.104	6	73	.000
GREEN	.257	35.089	6	73	.000
RED	.290	29.796	6	73	.000
NIRB	.269	33.096	6	73	.000
NIRG	.224	42.106	6	73	.000
NIRR	.200	48.778	6	73	.000

Pooled Within-Groups Matrices[a]

		BLUE	GREEN	RED	NIRB	NIRG	NIRR
Covariance	BLUE	46.986	50.756	55.328	11.354	10.182	23.402
	GREEN	50.756	57.762	61.739	15.100	13.502	32.045
	RED	55.328	61.739	69.222	11.474	10.873	25.349
	NIRB	11.354	15.100	11.474	12.736	10.578	26.009
	NIRG	10.182	13.502	10.873	10.578	9.073	22.369
	NIRR	23.402	32.045	25.349	26.009	22.369	55.708
Correlation	BLUE	1.000	.974	.970	.464	.493	.457
	GREEN	.974	1.000	.976	.557	.590	.565
	RED	.970	.976	1.000	.386	.434	.408
	NIRB	.464	.557	.386	1.000	.984	.976
	NIRG	.493	.590	.434	.984	1.000	.995
	NIRR	.457	.565	.408	.976	.995	1.000

a. The covariance matrix has 73 degrees of freedom.

Eigenvalues

Function	Eigenvalue	% of Variance	Cumulative %	Canonical Correlation
1	11.583[a]	56.7	56.7	.959
2	6.252[a]	30.6	87.4	.928
3	2.020[a]	9.9	97.3	.818
4	.505[a]	2.5	99.7	.579
5	.034[a]	.2	99.9	.182
6	.019[a]	.1	100.0	.138

a. First 6 canonical discriminant functions were used in the analysis.

Wilks' Lambda

Test of Function(s)	Wilks' Lambda	Chi-square	df	Sig.
1 through 6	.002	440.837	36	.000
2 through 6	.029	257.241	25	.000
3 through 6	.209	113.602	16	.000
4 through 6	.630	33.480	9	.000
5 through 6	.948	3.840	4	.428
6	.981	1.395	1	.238

Standardized Canonical Discriminant Function Coefficients

	Function					
	1	2	3	4	5	6
BLUE	.716	-4.280	.431	2.028	.712	3.331
GREEN	-8.065	-.499	-5.236	-7.440	.946	-2.019
RED	6.459	5.112	4.255	5.014	-1.030	-.435
NIRB	3.621	2.933	-1.982	5.054	2.453	-1.371
NIRG	1.880	-1.201	5.575	-12.621	1.099	-4.930
NIRR	-4.348	-1.574	-2.033	9.187	-3.499	5.712

Structure Matrix

	Function					
	1	2	3	4	5	6
NIRG	-.485	-.067	.572*	.281	.494	-.333
NIRR	-.534	-.057	.554*	.336	.430	-.327
BLUE	-.256	.243	.357	-.032	.714*	.488
GREEN	-.392	.358	.374	-.008	.671*	.358
RED	-.280	.443	.384	-.055	.580*	.489
NIRB	-.437	-.074	.448	.343	.577*	-.391

Pooled within-groups correlations between discriminating variables and standardized canonical discriminant functions
Variables ordered by absolute size of correlation within function.

*. Largest absolute correlation between each variable and any discriminant function

Functions at Group Centroids

	Function					
CROP	1	2	3	4	5	6
1	3.031	3.134	.109	-.327	-.069	-.018
2	-5.233	-.484	-1.449	-.940	-.015	-.152
3	-4.353	1.816	-.748	.953	-.076	.196
4	-2.333	-1.312	3.279	-.334	-.001	.043
5	.861	.040	-.157	.493	.440	-.061
6	1.726	-2.567	-.012	1.019	-.204	-.188
7	3.270	-3.761	-1.131	-.537	-.006	.197

Unstandardized canonical discriminant functions evaluated at group means

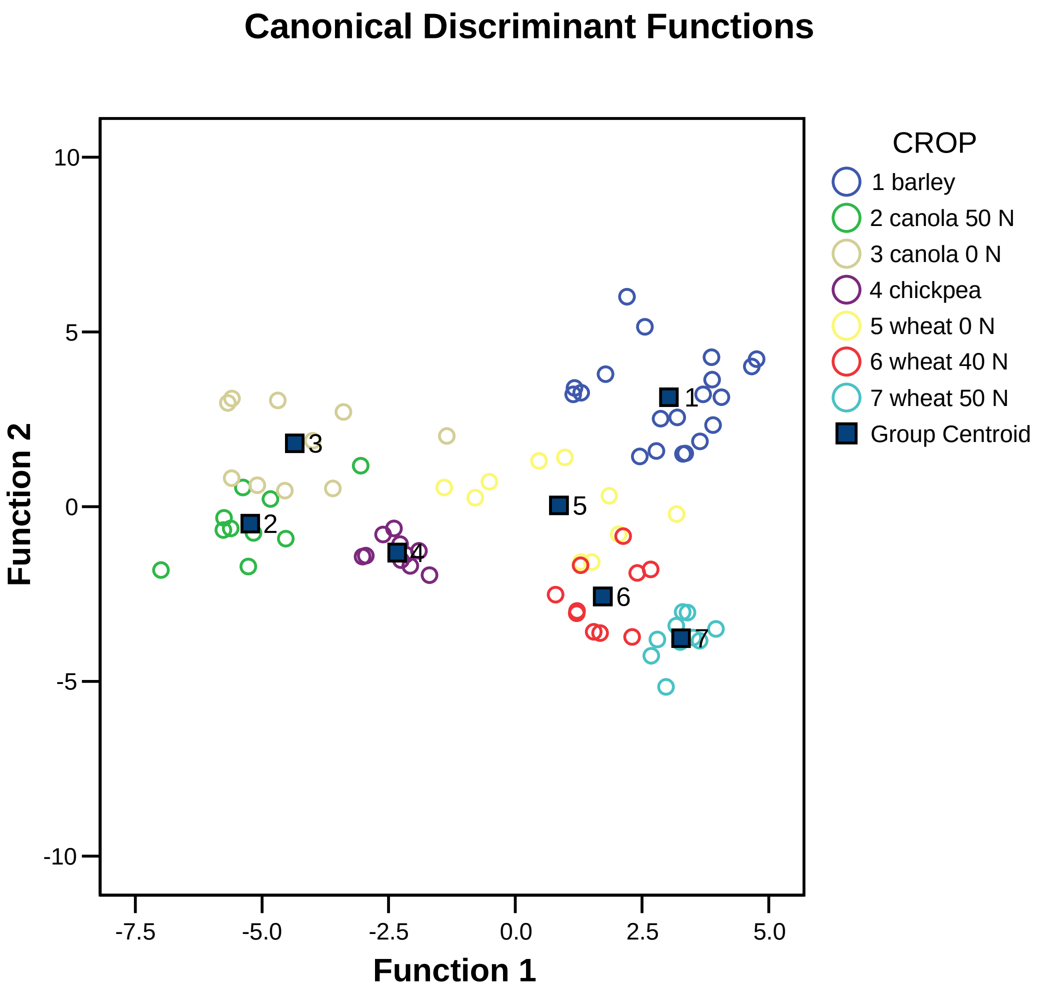
Canonical Discriminant Functions
CROP
1 barley
2 canola 50 N
3 canola 0 N
4 chickpea
5 wheat 0 N
6 wheat 40 N
7 wheat 50 N
Group Centroid
Function 2
Function 1
10
5
0
-5
-10
-7.5
-5.0
-2.5
0.0
2.5
5.0
1
2
3
4
5
6
7

Classification Results[b,c]

		CROP	Predicted Group Membership 1	2	3	4	5	6	7	Total
Original	Count	1	20	0	0	0	0	0	0	20
		2	0	10	0	0	0	0	0	10
		3	0	0	9	0	1	0	0	10
		4	0	0	0	10	0	0	0	10
		5	0	0	0	0	8	2	0	10
		6	0	0	0	0	0	10	0	10
		7	0	0	0	0	0	0	10	10
	%	1	100.0	.0	.0	.0	.0	.0	.0	100.0
		2	.0	100.0	.0	.0	.0	.0	.0	100.0
		3	.0	.0	90.0	.0	10.0	.0	.0	100.0
		4	.0	.0	.0	100.0	.0	.0	.0	100.0
		5	.0	.0	.0	.0	80.0	20.0	.0	100.0
		6	.0	.0	.0	.0	.0	100.0	.0	100.0
		7	.0	.0	.0	.0	.0	.0	100.0	100.0
Cross-validated[a]	Count	1	19	0	0	0	1	0	0	20
		2	0	10	0	0	0	0	0	10
		3	0	1	8	0	1	0	0	10
		4	0	0	0	10	0	0	0	10
		5	0	0	0	1	5	4	0	10
		6	0	0	0	0	1	9	0	10
		7	0	0	0	0	0	2	8	10
	%	1	95.0	.0	.0	.0	5.0	.0	.0	100.0
		2	.0	100.0	.0	.0	.0	.0	.0	100.0
		3	.0	10.0	80.0	.0	10.0	.0	.0	100.0
		4	.0	.0	.0	100.0	.0	.0	.0	100.0
		5	.0	.0	.0	10.0	50.0	40.0	.0	100.0
		6	.0	.0	.0	.0	10.0	90.0	.0	100.0
		7	.0	.0	.0	.0	.0	20.0	80.0	100.0

a. Cross validation is done only for those cases in the analysis. In cross validation, each case is classified by the functions derived from all cases other than that case.

b. 96.3% of original grouped cases correctly classified.

c. 86.3% of cross-validated grouped cases correctly classified.

Appendix 3 Summary of SPSS output–Lundavra

14 Zadok classes

Tests of Equality of Group Means

	Wilks' Lambda	F	df1	df2	Sig.
RED	.526	4.511	13	65	.000
GREEN	.534	4.355	13	65	.000
BLUE	.525	4.530	13	65	.000
NIR	.831	1.017	13	65	.446

Pooled Within-Groups Matrices[a]

		RED	GREEN	BLUE	NIR
Covariance	RED	102.511	76.896	96.894	-2.721
	GREEN	76.896	79.998	91.403	13.383
	BLUE	96.894	91.403	121.002	9.447
	NIR	-2.721	13.383	9.447	25.651
Correlation	RED	1.000	.849	.870	-.053
	GREEN	.849	1.000	.929	.295
	BLUE	.870	.929	1.000	.170
	NIR	-.053	.295	.170	1.000

a. The covariance matrix has 65 degrees of freedom.

Eigenvalues

Function	Eigenvalue	% of Variance	Cumulative %	Canonical Correlation
1	.906[a]	100.0	100.0	.689

a. First 1 canonical discriminant functions were used in the analysis.

Wilks' Lambda

Test of Function(s)	Wilks' Lambda	Chi-square	df	Sig.
1	.525	45.475	13	.000

Standardized Canonical Discriminant Function Coefficients

	Function
	1
BLUE	1.000

Structure Matrix

	Function
	1
BLUE	1.000
GREEN[a]	.929
RED[a]	.870
NIR[a]	.170

Pooled within-groups correlations between discriminating variables and standardized canonical discriminant functions
Variables ordered by absolute size of correlation within function.

a. This variable not used in the analysis.

Functions at Group Centroids

	Function
ZADOK	1
43.0	-2.050
47.0	-2.177
48.0	-.820
49.0	.234
50.0	.138
51.0	-.588
52.0	.162
53.0	-.223
54.0	.531
55.0	.948
56.0	1.209
57.0	1.125
58.0	-.239
59.0	1.787

Unstandardized canonical discriminant functions evaluated at group means

Classification Results[b,c]

		ZADOK	Predicted Group Membership 43.0	47.0	48.0	49.0	50.0	51.0	52.0	53.0	54.0	55.0	56.0	57.0	58.0	59.0	Total
Original	Count	43.0	0	1	1	0	0	0	0	0	0	0	0	0	0	0	2
		47.0	0	3	1	0	0	0	0	0	0	0	0	0	0	0	4
		48.0	0	2	1	0	0	0	1	2	0	0	0	1	0	0	7
		49.0	0	0	0	0	0	0	7	1	0	0	0	0	0	0	8
		50.0	0	0	0	0	0	0	4	1	0	0	0	0	0	0	5
		51.0	0	0	2	0	0	0	2	3	0	0	0	0	0	0	7
		52.0	0	0	1	0	0	0	9	1	1	0	0	0	0	0	12
		53.0	0	0	1	0	0	0	7	2	0	0	0	0	0	0	10
		54.0	0	0	1	0	0	0	4	1	0	0	0	1	0	1	8
		55.0	0	0	0	0	0	0	1	1	1	0	0	1	0	0	4
		56.0	0	0	0	0	0	0	1	0	0	0	0	2	0	0	3
		57.0	0	0	0	0	0	0	2	0	1	0	0	2	0	0	5
		58.0	0	0	0	0	0	0	1	1	0	0	0	0	0	0	2
		59.0	0	0	0	0	0	0	1	0	0	0	0	0	0	1	2
	%	43.0	.0	50.0	50.0	.0	.0	.0	.0	.0	.0	.0	.0	.0	.0	.0	100.0
		47.0	.0	75.0	25.0	.0	.0	.0	.0	.0	.0	.0	.0	.0	.0	.0	100.0
		48.0	.0	28.6	14.3	.0	.0	.0	14.3	28.6	.0	.0	.0	14.3	.0	.0	100.0
		49.0	.0	.0	.0	.0	.0	.0	87.5	12.5	.0	.0	.0	.0	.0	.0	100.0
		50.0	.0	.0	.0	.0	.0	.0	80.0	20.0	.0	.0	.0	.0	.0	.0	100.0
		51.0	.0	.0	28.6	.0	.0	.0	28.6	42.9	.0	.0	.0	.0	.0	.0	100.0
		52.0	.0	.0	8.3	.0	.0	.0	75.0	8.3	8.3	.0	.0	.0	.0	.0	100.0
		53.0	.0	.0	10.0	.0	.0	.0	70.0	20.0	.0	.0	.0	.0	.0	.0	100.0
		54.0	.0	.0	12.5	.0	.0	.0	50.0	12.5	.0	.0	.0	12.5	.0	12.5	100.0
		55.0	.0	.0	.0	.0	.0	.0	25.0	25.0	25.0	.0	.0	25.0	.0	.0	100.0
		56.0	.0	.0	.0	.0	.0	.0	33.3	.0	.0	.0	.0	66.7	.0	.0	100.0
		57.0	.0	.0	.0	.0	.0	.0	40.0	.0	20.0	.0	.0	40.0	.0	.0	100.0
		58.0	.0	.0	.0	.0	.0	.0	50.0	50.0	.0	.0	.0	.0	.0	.0	100.0
		59.0	.0	.0	.0	.0	.0	.0	50.0	.0	.0	.0	.0	.0	.0	50.0	100.0
Cross-validated[a]	Count	43.0	0	1	1	0	0	0	0	0	0	0	0	0	0	0	2
		47.0	0	3	1	0	0	0	0	0	0	0	0	0	0	0	4
		48.0	0	3	0	0	0	0	1	2	0	0	0	1	0	0	7
		49.0	0	0	0	0	0	0	7	1	0	0	0	0	0	0	8
		50.0	0	0	0	0	0	0	4	1	0	0	0	0	0	0	5
		51.0	0	0	2	0	0	0	2	3	0	0	0	0	0	0	7
		52.0	0	0	0	0	0	0	6	4	2	0	0	0	0	0	12
		53.0	0	0	1	0	0	0	7	2	0	0	0	0	0	0	10
		54.0	0	0	1	0	0	0	4	1	0	0	0	1	0	1	8
		55.0	0	0	0	0	0	0	1	1	1	0	0	1	0	0	4
		56.0	0	0	0	0	0	0	1	0	1	0	0	1	0	0	3
		57.0	0	0	0	0	0	0	2	0	3	0	0	0	0	0	5
		58.0	0	0	0	0	0	0	1	1	0	0	0	0	0	0	2
		59.0	0	0	0	0	0	0	1	0	0	0	0	1	0	0	2
	%	43.0	.0	50.0	50.0	.0	.0	.0	.0	.0	.0	.0	.0	.0	.0	.0	100.0
		47.0	.0	75.0	25.0	.0	.0	.0	.0	.0	.0	.0	.0	.0	.0	.0	100.0
		48.0	.0	42.9	.0	.0	.0	.0	14.3	28.6	.0	.0	.0	14.3	.0	.0	100.0
		49.0	.0	.0	.0	.0	.0	.0	87.5	12.5	.0	.0	.0	.0	.0	.0	100.0
		50.0	.0	.0	.0	.0	.0	.0	80.0	20.0	.0	.0	.0	.0	.0	.0	100.0
		51.0	.0	.0	28.6	.0	.0	.0	28.6	42.9	.0	.0	.0	.0	.0	.0	100.0
		52.0	.0	.0	.0	.0	.0	.0	50.0	33.3	16.7	.0	.0	.0	.0	.0	100.0
		53.0	.0	.0	10.0	.0	.0	.0	70.0	20.0	.0	.0	.0	.0	.0	.0	100.0
		54.0	.0	.0	12.5	.0	.0	.0	50.0	12.5	.0	.0	.0	12.5	.0	12.5	100.0
		55.0	.0	.0	.0	.0	.0	.0	25.0	25.0	25.0	.0	.0	25.0	.0	.0	100.0
		56.0	.0	.0	.0	.0	.0	.0	33.3	.0	33.3	.0	.0	33.3	.0	.0	100.0
		57.0	.0	.0	.0	.0	.0	.0	40.0	.0	60.0	.0	.0	.0	.0	.0	100.0
		58.0	.0	.0	.0	.0	.0	.0	50.0	50.0	.0	.0	.0	.0	.0	.0	100.0
		59.0	.0	.0	.0	.0	.0	.0	50.0	.0	.0	.0	.0	50.0	.0	.0	100.0

a. Cross validation is done only for those cases in the analysis. In cross validation, each case is classified by the functions derived from all cases other than that case.

b. 22.8% of original grouped cases correctly classified.

c. 13.9% of cross-validated grouped cases correctly classified.

Primary classes

Tests of Equality of Group Means

	Wilks' Lambda	F	df1	df2	Sig.
RED	.809	18.126	1	77	.000
GREEN	.863	12.272	1	77	.001
BLUE	.854	13.121	1	77	.001
NIR	.997	.224	1	77	.638

Pooled Within-Groups Matrices[a]

		RED	GREEN	BLUE	NIR
Covariance	RED	133.235	106.190	134.425	-1.902
	GREEN	106.190	108.978	127.617	14.762
	BLUE	134.425	127.617	166.347	10.845
	NIR	-1.902	14.762	10.845	25.983
Correlation	RED	1.000	.881	.903	-.032
	GREEN	.881	1.000	.948	.277
	BLUE	.903	.948	1.000	.165
	NIR	-.032	.277	.165	1.000

a. The covariance matrix has 77 degrees of freedom.

Eigenvalues

Function	Eigenvalue	% of Variance	Cumulative %	Canonical Correlation
1	.235[a]	100.0	100.0	.437

a. First 1 canonical discriminant functions were used in the analysis.

Wilks' Lambda

Test of Function(s)	Wilks' Lambda	Chi-square	df	Sig.
1	.809	16.172	1	.000

Standardized Canonical Discriminant Function Coefficients

	Function
	1
RED	1.000

Structure Matrix

	Function
	1
RED	1.000
BLUE[a]	.903
GREEN[a]	.881
NIR[a]	-.032

Pooled within-groups correlations between discriminating variables and standardized canonical discriminant functions
Variables ordered by absolute size of correlation within function.

a. This variable not used in the analysis.

Functions at Group Centroids

prim_growth	Function 1
1	-.796
2	.288

Unstandardized canonical discriminant functions evaluated at group means

Classification Results[b,c]

		prim_growth	Predicted Group Membership 1	2	Total
Original	Count	1	10	11	21
		2	2	56	58
	%	1	47.6	52.4	100.0
		2	3.4	96.6	100.0
Cross-validated[a]	Count	1	10	11	21
		2	2	56	58
	%	1	47.6	52.4	100.0
		2	3.4	96.6	100.0

a. Cross validation is done only for those cases in the analysis. In cross validation, each case is classified by the functions derived from all cases other than that case.

b. 83.5% of original grouped cases correctly classified.

c. 83.5% of cross-validated grouped cases correctly classified.